

## Quantifying and modelling the effect of external and internal vegetation water dynamics on radar data

Khabbazan, S.

**DOI**

[10.4233/uuid:0efc4707-eceb-49bc-9f9d-52027ec82673](https://doi.org/10.4233/uuid:0efc4707-eceb-49bc-9f9d-52027ec82673)

**Publication date**

2024

**Document Version**

Final published version

**Citation (APA)**

Khabbazan, S. (2024). *Quantifying and modelling the effect of external and internal vegetation water dynamics on radar data*. [Dissertation (TU Delft), Delft University of Technology].  
<https://doi.org/10.4233/uuid:0efc4707-eceb-49bc-9f9d-52027ec82673>

**Important note**

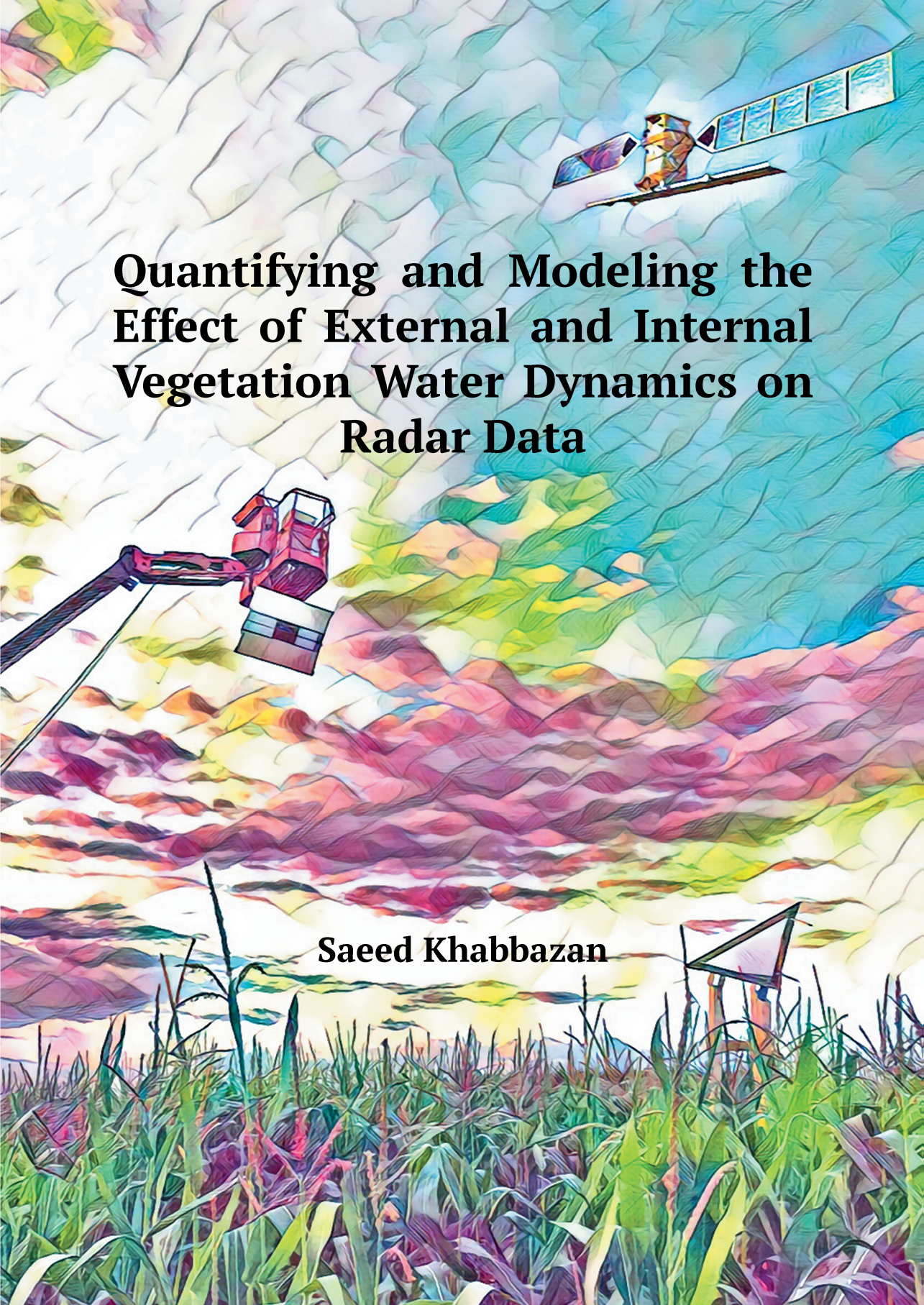
To cite this publication, please use the final published version (if applicable).  
Please check the document version above.

**Copyright**

Other than for strictly personal use, it is not permitted to download, forward or distribute the text or part of it, without the consent of the author(s) and/or copyright holder(s), unless the work is under an open content license such as Creative Commons.

**Takedown policy**

Please contact us and provide details if you believe this document breaches copyrights.  
We will remove access to the work immediately and investigate your claim.

The background is a vibrant, abstract illustration. At the top, a satellite is shown in orbit against a blue and white sky. Below it, a red crane-like structure extends from the left, holding a white sensor or camera. The middle ground features a landscape of rolling hills and fields in shades of green, yellow, and pink. At the bottom, a field of tall, green crops is visible, with a small white structure on the right. The overall style is painterly and colorful.

# **Quantifying and Modeling the Effect of External and Internal Vegetation Water Dynamics on Radar Data**

**Saeed Khabbazan**



**QUANTIFYING AND MODELING THE EFFECT OF  
EXTERNAL AND INTERNAL VEGETATION WATER  
DYNAMICS ON RADAR DATA**



# **QUANTIFYING AND MODELING THE EFFECT OF EXTERNAL AND INTERNAL VEGETATION WATER DYNAMICS ON RADAR DATA**

## **Dissertation**

for the purpose of obtaining the degree of doctor  
at Delft University of Technology  
by the authority of the Rector Magnificus, prof. dr. ir. T.H.J.J. van der Hagen,  
chair of the Board for Doctorates  
to be defended publicly on  
Monday 22, January 2024 at 17:30 o'clock

by

**Saeed Khabbazan**

Master of Science in Remote Sensing,  
Department of Surveying and Geomatics Engineering,  
University of Tehran, Iran,  
born in Mashhad, Iran.

This dissertation has been approved by the

promotor: Prof.dr. ir. S. C. Steele-Dunne  
copromotor: Dr. ir. P. Lopez-Dekker

Composition of the doctoral committee:

Rector Magnificus,  
prof. dr. ir. S. C. Steele-Dunne  
Dr. ir. P. Lopez-Dekker

chairperson  
Delft University of Technology, *promotor*  
Delft University of Technology, *copromotor*

*Independent members:*

Prof. dr. J. M. Lopez-Sanchez  
Dr. H. McNairn  
Prof. dr. J. Judge  
Prof. dr. ir. H.W.J. Russchenberg  
Prof. dr. ir. R. Uijlenhoet

Universidad de Alicante, Spain  
Agriculture and Agri-Food Canada, Canada  
University of Florida, USA  
Delft University of Technology  
Delft University of Technology



*Keywords:* Active Microwave Remote Sensing, SAR, Dew, Interception, Agriculture, Vegetation water content, VOD, SCW, Scatterometer, Sentinel-1, L-band, Soil Moisture

*Printed by:* <http://www.proefschriftspecialist.nl>

*Cover by:* Saeed Khabbazan

Copyright © 2023 by S. Khabbazan

ISBN 978-94-93330-50-4

An electronic copy of this dissertation is available at  
<https://repository.tudelft.nl/>.

*To my family and my wife.*





# CONTENTS

<b>Summary</b>	<b>xi</b>
<b>Samenvatting</b>	<b>xv</b>
<b>Preface</b>	<b>xix</b>
<b>1. Introduction</b>	<b>1</b>
1.1. Using Synthetic Aperture Radar (SAR) data for agricultural monitoring . . .	2
1.2. The importance of surface canopy water . . . . .	4
1.3. The effect of surface canopy water on SAR data . . . . .	5
1.4. Modeling the effect of surface canopy water dynamics on radar data . . . . .	6
1.5. Research gap and objectives . . . . .	6
1.6. Research Outline . . . . .	7
<b>2. Florida field campaign and data</b>	<b>9</b>
2.1. Study area . . . . .	10
2.2. UF-LARS Radar . . . . .	11
2.3. Ground measurements . . . . .	11
2.3.1. Meteorological data . . . . .	11
2.3.2. Soil data . . . . .	12
2.3.3. Surface Canopy Water data . . . . .	13
2.3.4. Ground vegetation sampling and vegetation data . . . . .	15
<b>3. Crop monitoring using Sentinel-1 SAR Data: A case study from the Netherlands</b>	<b>17</b>
3.1. Introduction . . . . .	18
3.2. Data and Methods . . . . .	18
3.2.1. Study area . . . . .	18
3.2.2. Hydrometeorological ground data . . . . .	19
3.2.3. Ground data at 24 parcels . . . . .	20
3.2.4. Sentinel-1 data . . . . .	20
3.3. Results and Discussion . . . . .	23
3.3.1. Hydrometeorological data . . . . .	23
3.3.2. Sentinel-1 time series . . . . .	27
3.3.3. Mapping key dates . . . . .	36
3.4. Conclusions . . . . .	41
<b>4. The influence of surface canopy water on the relationship between L-band backscatter and biophysical variables in agricultural monitoring</b>	<b>43</b>
4.1. Introduction . . . . .	44

4.2.	Data and Methods	45
4.2.1.	Field experiment	45
4.2.2.	Radar data	45
4.3.	Methodology	45
4.3.1.	Radar data	45
4.3.2.	Vegetation Optical Depth (VOD) estimation	46
4.4.	Results	48
4.4.1.	Hydrometeorological data	48
4.4.2.	Crop development	50
4.4.3.	Time series of L-band backscatter and derived indices	52
4.4.4.	Effect of surface canopy water on morning radar backscatter	53
4.4.5.	VOD Time series retrieved from dry and wet vegetation	55
4.4.6.	Effect of surface canopy water on the relation between radar backscatter data and crop biophysical variables	59
4.4.7.	Effect of surface canopy water on relation between VOD and vegetation water content	61
4.5.	Discussion	61
4.6.	Conclusions	64
<b>5.</b>	<b>Toward modeling the influence of sub-seasonal variation in vegetation on radar backscatter using a Radiative Transfer Model</b>	<b>67</b>
5.1.	Introduction	68
5.2.	Materials and Method	68
5.2.1.	Radiative Transfer Model	68
5.2.2.	Experimental data	69
5.2.3.	RT model calibration method	71
5.2.4.	Multi Linear Regression method	72
5.3.	Results and Discussions	73
5.3.1.	Field measurements	73
5.3.2.	Effect of small cylinders size as a function of frequency	73
5.3.3.	Optimal small cylinder radius (SCR)	77
5.3.4.	Factors controlling optimum small cylinders radius	80
5.4.	Summary and Conclusion	81
<b>6.</b>	<b>The Influence of Surface Canopy Water on L-, C-, and X-Band Backscatter: A Study Combining Detailed <i>In situ</i> Data and the Tor Vergata Radiative Transfer Model</b>	<b>85</b>
6.1.	Introduction	86
6.2.	Data and Methods	86
6.2.1.	Experimental site	86
6.2.2.	Field measurements	87
6.2.3.	Radiative Transfer Model	87
6.2.4.	Accounting for SCW in the Tor Vergata Model	89
6.3.	Results and Discussions	90
6.3.1.	Field measurements	90
6.3.2.	Representing the effect of SCW in the Tor Vergata model	92

6.3.3. The effect of dew on soil . . . . .	94
6.3.4. Effect of SCW on scattering mechanisms . . . . .	98
6.3.5. The effect of SCW alone on backscatter at L-, C-, and X-band . . . . .	101
6.4. Conclusions . . . . .	109
<b>7. Conclusion . . . . .</b>	<b>113</b>
7.1. Knowledge generated and implications . . . . .	114
7.1.1. Crop monitoring using Sentinel-1 SAR Data . . . . .	114
7.1.2. Influence of SCW on the relationship between L-band backscatter and biophysical variables . . . . .	115
7.1.3. Modeling the influence of SCW on L-, C-, and X-band backscatter . . . . .	116
7.2. Directions for future research . . . . .	117
7.2.1. Using Sentinel-1 for agricultural monitoring . . . . .	117
7.2.2. Surface canopy water validation data . . . . .	119
7.2.3. Validation campaigns for microwave remote sensing of vegetation . . . . .	121
7.2.4. Radiative Transfer Modeling . . . . .	122
7.3. Concluding remarks . . . . .	124
<b>A. Appendix-A: The importance of overpass time in agricultural applications of radar . . . . .</b>	<b>145</b>
A.1. Introduction . . . . .	146
A.2. DATA AND METHODS . . . . .	146
A.2.1. Study area . . . . .	146
A.2.2. Hydrometeorology . . . . .	146
A.2.3. Microwave scattering system . . . . .	147
A.3. RESULTS . . . . .	147
A.3.1. Meteorological data . . . . .	147
A.3.2. Factors influencing L-band backscatter . . . . .	147
A.3.3. Diurnal cycles of water content and backscatter . . . . .	149
A.3.4. Impact of SCW on L-band backscatter . . . . .	149
A.3.5. Effect of Surface canopy water on relationship between backscatter and biophysical variables . . . . .	150
A.4. CONCLUSION . . . . .	151
<b>B. Appendix-B: Supplementary Material . . . . .</b>	<b>155</b>
B.1. Supplementary Material for Chapter 3 . . . . .	156
B.2. Supplementary Material for Chapter 5 . . . . .	159
B.3. Supplementary Material for Chapter 6 . . . . .	162
<b>Acknowledgements . . . . .</b>	<b>163</b>
<b>Curriculum Vitæ . . . . .</b>	<b>165</b>
<b>List of Publications . . . . .</b>	<b>167</b>



# SUMMARY

Agriculture plays a critical role in the economy and environment worldwide, and the provision of real-time, reliable information on large-scale agricultural activity is essential for precision agriculture and global economic prosperity. In this context, remote sensing, especially through Synthetic Aperture Radar (SAR), can play an important role by offering accurate estimation of crop biophysical parameters such as Leaf Area Index (LAI), crop height, dry biomass, and Vegetation Water Content (VWC). Unlike traditional high-resolution optical imagery, which is often undermined by cloud cover, SAR microwave remote sensing overcomes these limitations by generating and transmitting longer wavelengths (300 MHz – 10 GHz) that penetrate clouds and aerosols and allowing data acquisition both day and night. However, SAR data is influenced by various factors such as sensor characteristics such as frequency, polarization, and incidence angle, as well as target characteristics like the size and shape distribution of crop constituents, and more importantly, the water content of crop constituents. In the path towards precision farming and more sustainable and efficient farming using SAR data, understanding the role of these factors, particularly the dynamics of external and internal vegetation water content on radar backscatter, is vital.

To date, however, the potentially confounding effects of both internal and, particularly, external water dynamics in vegetation on radar backscatter have not been adequately addressed. Existing studies have indeed illustrated the effects of SCW on radar backscatter, but the degree to which it influences different frequencies and polarizations, and the subsequent impact on crop bio-geophysical parameters remains unclear. Therefore, the main goal of this thesis is to expand our knowledge of the relationship between radar backscatter, vegetation dynamics, and surface canopy water (SCW) in agricultural monitoring. In this thesis we utilized statistical analysis and radiative transfer modeling in combination with fully polarimetric L-band data from a truck-mounted scatterometer and C-band data from Sentinel-1, along with extensive field data.

This thesis begins by investigating the promising potential of Sentinel-1 SAR backscatter for crop monitoring and the identification of critical dates in crop phenological stages (Chapter 3). This chapter focuses on five key crop types: sugar beet, potato, maize, wheat, and English rye grass in the Flevopolder, the Netherlands. It presents a comprehensive analysis of the radar backscatter time series, alongside an exploration of interferometric coherence data from Sentinel-1. The results highlight the guaranteed availability of data even in cloudy conditions, thus ensuring real-time, reliable, and continuous information on crop growth and development, and emphasizing the significant potential of radar data for crop monitoring.

A significant objective of this thesis is to improve the understanding of the effect of SCW on total backscatter, considering frequency, polarization, and growth stage. This involves delving into the complexities of the interaction between SCW and radar backscat-

ter and adapting and validating the radiative transfer model for the first time to account for SCW on vegetation and soil surfaces. Therefore, Chapters 4 to 6 of this thesis will comprehensively investigate this effect by utilizing fully polarimetric L-band data from a truck-mounted scatterometer along with extensive field data.

Chapter 4 deepens the analysis by investigating the influence of Surface Canopy Water (SCW) on the relationship between radar backscatter and crop biophysical parameters. The results from this chapter show that the presence of SCW can significantly affect radar backscatter, with an increase of up to 2-3 dB in the L-band. Furthermore, the findings illustrate how SCW impacts the relation between L-band observations and biophysical variables such as dry biomass, vegetation water content (VWC), plant height, and leaf area index (LAI) across all polarization, RVI, and cross ratios (CR). By examining the effect of SCW on VOD estimation, the research in this chapter suggests that while VOD and VWC typically exhibit a linear relationship, this relationship changes substantially in the presence or absence of SCW. These findings emphasize the importance of understanding daily patterns in SCW on radar backscatter and its implications for current and future SAR missions in agricultural monitoring.

Building on the insights from Chapter 4, Chapters 5 and 6 aim to improve our understanding of how Surface Canopy Water (SCW) influences total backscatter and the underlying mechanisms across various frequencies and polarizations, by employing a radiative transfer model. For this thesis, the radiative transfer model developed by Tor Vergata University (Tor Vergata model) is used. Recognizing existing challenges related to the Tor Vergata model with handling high temporal dynamics in backscatter data, Chapter 5 introduces a calibration technique to simulate these dynamics related to soil moisture and internal vegetation water. This helps to capture sub-daily cycle, which is necessary to study the influence of SCW. In Chapter 6, the calibrated version of the Tor Vergata model is used to quantify and also improve our understanding of the effect of SCW on backscatter as a function of frequency and polarization, and to better understand the underlying mechanisms.

The results of this chapter demonstrate that accounting for SCW by including additional water in the vegetation improves the correlation between simulated and observed backscatter at the L-band, especially when vegetation substantially influences the total backscatter. Concerning the influence of SCW on L-band backscatter mechanisms, the presence of SCW increases the vegetation volume contribution and reduces contributions from double bounce and direct scattering from the ground. A comparison of the effects of SCW at different frequencies revealed that the increase in total backscatter is more prominent at lower frequencies and it decreases with increasing frequency. The modeling results suggest that the impact of SCW on backscatter could reach up to 2.5 dB in the L-band, emphasizing its relevance for low-frequency data. The isolated effect of dew on backscatter could be up to 3.8 dB across all bands, making its consideration vital during bare soil and low vegetation cover stages across all frequencies. These findings provide novel insights into the effects of SCW on radar backscatter, underscoring the significance of dew and interception at microwave frequencies.

Together, these chapters try to underscore how changes in SCW can influence radar backscatter and show why this is important for monitoring agriculture. The results of this thesis highlight the potential value of current and future SAR missions, including

but not limited to Sentinel-1, ROSE-L, NISAR, SAOCOM, ALOS, CosmoSkyMed, and constellations such as those from ICEYE and Capella, which have dawn/dusk overpasses or multiple overpasses per day, for improving radar-based agricultural monitoring.





# SAMENVATTING

dutch

Landbouw speelt een cruciale rol in de economie en het milieu wereldwijd. Het verstreken van real-time, betrouwbare informatie over grootschalige landbouwactiviteiten is essentieel voor precisielandbouw en wereldwijde economische welvaart. In deze context kunnen satellietwaarnemingen, zoals observaties van Synthetic Aperture Radar (SAR), een belangrijke rol spelen. SAR observaties kunnen een nauwkeurige schatting geven van biofysische parameters zoals Leaf Area Index (LAI), gewashoogte, droge biomassa, en Vegetation Water Content (VWC).

In tegenstelling tot traditionele hoge resolutie optische beelden, die vaak worden ondermijnd door bewolking, overwint SAR observaties deze beperkingen. SAR observatie-technieken gebruiken namelijk langere golflengtes (300 MHz - 10 GHz), deze golflengtes doordringen wolken en aerosolen en zijn zowel overdag als 's nachts inzetbaar. De data van SAR observaties wordt echter beïnvloed door verschillende factoren zoals sensor karakteristieken, waarbij frequentie, polarisatie en invalshoek een rol spelen, evenals doelkarakteristieken zoals de grootte en vormverdeling van gewasbestanddelen, en belangrijker nog, het watergehalte van gewasbestanddelen.

Op weg naar precisielandbouw en duurzamere en efficiëntere landbouw met behulp van SAR-data is het begrijpen van de rol van deze factoren, en met name de dynamiek van extern en intern vegetatiewatergehalte op radarobservaties, van vitaal belang. Tot op heden zijn de potentieel verwarrende effecten van zowel intern als, met name, externe waterdynamieken in vegetatie op radarobservaties echter niet voldoende bestudeert. Bestaande studies hebben de effecten van Surface Canopy Water (SCW) op radar terugkaatsing geïllustreerd, maar de mate waarin het verschillende frequenties en polarisaties beïnvloedt, en de daaropvolgende impact op het meten van bio-geofysische gewasparameters blijft onduidelijk. Daarom is het hoofddoel van dit proefschrift om onze kennis van de relatie tussen radarwaarnemingen, vegetatiedynamiek en SCW in landbouwmonitoring uit te breiden. In dit proefschrift hebben we statistische analyse en *Radiative Transfer Modeling* gecombineerd met polarimetrische L-bandwaarnemingen van een truck-mounted scatterometer, en C-bandwaarnemingen van Sentinel-1 samen met uitgebreide veldgegevens en observaties.

Dit proefschrift begint met het onderzoeken van de veelbelovende Sentinel-1 SAR-waarnemingen voor gewasmonitoren en het identificeren van kritieke momenten in de fenologische stadia van verschillende gewassen (Hoofdstuk 3). Dit hoofdstuk richt zich op vijf belangrijke gewas types: suikerbiet, aardappel, maïs, tarwe en Engels raaigras in de Flevopolder, Nederland. Een uitgebreide tijdreeks analyse van de radar waarnemingen wordt gepresenteerd, en daarnaast een verkenning van interferometrische coherentiegegevens van Sentinel-1. De resultaten benadrukken het voordeel van de gegarandeerde beschikbaarheid van radarwaarnemingen. Zelfs in bewolkte omstandigheden is

er betrouwbare en continue informatie beschikbaar over gewasgroei.

Een belangrijk doel van dit proefschrift is om kennis te vergroten over het effect van SCW op de SAR waarnemingen, waarbij frequentie, polarisatie en groeistadium in acht moeten worden genomen. Dit houdt in dat we ons verdiepen in de complexiteiten van de interactie tussen SCW en radarwaarnemingen en een Radiative Transfer Model aanpassen en valideren om voor het eerst rekening te houden met SCW op het vegetatie- en bodemoppervlak. Daarom zullen de hoofdstukken 4 tot 6 van dit proefschrift het effect van SCW uitgebreid onderzoeken door polarimetrische L-bandobservaties van een truck-mounted scatterometer te gebruiken samen met veldgegevens.

In Hoofdstuk 4 wordt de analyse verder uitgebreid door het onderzoek van de invloed van SCW op de relatie tussen radarwaarnemingen en biofysische parameters. De resultaten van dit hoofdstuk tonen aan dat de aanwezigheid van SCW de radarwaarnemingen aanzienlijk kan beïnvloeden, met een toename van maximaal 2-3 dB in de L-band observaties. Bovendien illustreren de bevindingen hoe SCW de relatie beïnvloedt tussen L-bandobservaties en biofysische variabelen zoals droge biomassa, vegetatie watergehalte (VWC), planthoogte, en bladoppervlakte-index (LAI) in alle polarisaties, RVI en CR. Door het effect van SCW op VOD-berekeningen te onderzoeken, suggereert het onderzoek in dit hoofdstuk dat hoewel VOD en VWC doorgaans een lineaire relatie vertonen, deze relatie aanzienlijk verandert in aan- of afwezigheid van SCW. Deze bevindingen benadrukken het belang van het begrijpen van dagelijkse patronen in SCW op radarwaarnemingen en de implicaties ervan voor het gebruik van huidige en toekomstige SAR-observaties in landbouwmonitoring.

Voortbouwend op de inzichten uit Hoofdstuk 4, hebben Hoofdstukken 5 en 6 tot doel onze kennis te vergroten over hoe SCW de totale terugkaatsing en de onderliggende mechanismen beïnvloedt bij verschillende frequenties en polarisaties, door gebruik te maken van een Radiative Transfer Model. Voor dit proefschrift wordt het Radiative Transfer Model, Tor Vergata-model, ontwikkeld door Tor Vergata University, gebruikt. Met erkenning van bestaande uitdagingen met betrekking tot het Tor Vergata-model bij het gebruik met hoge temporele dynamiek in radarwaarnemingen, introduceert Hoofdstuk 5 een kalibratietechniek om deze dynamiek te simuleren met betrekking tot bodemvochtigheid en intern vegetatiewater. Deze techniek zal helpen de subdagelijkse cyclus vast te leggen, wat nodig is om de invloed van SCW te bestuderen. In Hoofdstuk 6 wordt de gekalibreerde versie van het Tor Vergata-model gebruikt om het effect van SCW op radarwaarnemingen te kwantificeren en ook om onze kennis van het effect van SCW op terugkaatsing als functie van frequentie en polarisatie te verbeteren, om zodoende de onderliggende mechanismen beter te begrijpen.

De resultaten van dit hoofdstuk tonen aan dat het rekening houden met SCW door extra water in de vegetatie op te nemen de correlatie verbetert tussen gesimuleerde en waargenomen terugkaatsing in de L-band, vooral wanneer de vegetatie de totale terugkaatsingsmechanismen, verhoogt de aanwezigheid van SCW de bijdrage van het vegetatievolume en vermindert het bijdragen van dubbele sprong en directe verstrooiing van de grond. Een vergelijking van de effecten van SCW bij verschillende frequenties toonde aan dat de toename van de totale terugkaatsing prominenter is bij lagere frequenties en afneemt met toenemende frequentie. De modelresultaten suggereren dat de impact van

SCW op de radarwaarnemingen tot 2,5 dB in L-band observaties kan bereiken, waardoor het belang van SCW voor laagfrequente observaties wordt benadrukt. Het geïsoleerde effect van dauw op terugkaatsing kan tot 3,8 dB bedragen over alle banden, waardoor het in acht nemen van SCW essentieel is tijdens kale bodem- en lage vegetatiebedekkingsfasen over alle frequenties. Deze bevindingen bieden nieuwe inzichten in de effecten van SCW op radar terugkaatsing, en onderstrepen het belang van dauw en interceptie bij radarwaarnemingen.

Samen proberen deze hoofdstukken te onderstrepen hoe veranderingen in SCW radar waarnemingen kunnen beïnvloeden en tonen aan waarom dit belangrijk is voor het monitoren van de landbouwgewassen. De resultaten van dit proefschrift benadrukken de potentiële waarde van huidige en toekomstige SAR-missies, waaronder maar niet beperkt tot Sentinel-1, ROSE-L, NISAR, SAOCOM, ALOS, CosmoSkyMed, en constellaties zoals die van ICEYE en Capella, die tijdens dageraad / schemering overvliegen of meerdere keren per dag overvliegen, om daarmee radar-gebaseerde landbouwmonitoring te verbeteren.



# PREFACE

The journey to complete this Ph.D. thesis in the field of Remote Sensing has been both challenging and rewarding, filled with endless discovery, personal growth, and exciting exploration. My fascination with space and astronomy began in high school when I became captivated by the mysteries of the cosmos and nurtured a dream of becoming a scientist at NASA. I chose the Remote Sensing field to be able to achieve it. That teenage aspiration has now become a reality, as I am currently working as a scientist at NASA-Harvest. This achievement was made possible by pursuing my Ph.D. in this complex field under the wise and supportive guidance of my esteemed supervisor and promotor, Prof. Dr. Ir. Susan Steele-Dunne. I must express my profound gratitude to Susan for her unwavering support, guidance, and encouragement throughout this process. Her expertise and passion have not only shaped this work but have also greatly contributed to my personal and professional development.

This thesis does not merely represent a turning point in my academic career; it stands as a milestone on a lifelong journey towards achieving my childhood dreams. Through careful research, creative thinking, and hard work, this research has brought me one step closer to fulfilling my ambition to use data from space to make a tangible impact on Earth. This thesis, focusing on the role of vegetation water dynamic on radar data for agricultural monitoring, is a step towards fulfilling that ambition, with the potential to aid more accurate agricultural management and contribute to the betterment of human life. I would also like to thank my fellow researchers and colleagues at TU Delft for their collaboration and insights, and my family, my lovely wife and friends for their enduring support and belief in me.

The following chapters present the research, findings, and contributions of this thesis. It is my hope that this work will serve as a valuable resource for future research in monitoring agricultural activity using SAR data and inspire others to explore these fascinating and critical issues.

*Saeed Khabbazan  
Delft, August 2023*



# 1

## INTRODUCTION

*“The scientist is not a person who gives the right answers,  
he’s one who asks the right questions.”*

Claude Levi-Strauss



## 1.1. USING SYNTHETIC APERTURE RADAR (SAR) DATA FOR AGRICULTURAL MONITORING

Agricultural monitoring using Synthetic Aperture Radar (SAR) plays an important role in precision agriculture and economic prosperity worldwide. The ability to estimate crop biophysical parameters such as Leaf Area Index (LAI), crop height, dry biomass, and Vegetation Water Content (VWC) using SAR data is important for various applications including yield forecasting, crop health monitoring, and soil moisture estimation [1–7]. By providing real-time, reliable, and accurate crop information, these remote sensing techniques enable timely interventions, allow for optimal resource usage, and increases in crop yields. The use of remote sensing data not only supports the sustainability and growth of the agriculture sector but also helps to mitigate global food security challenges by reducing famine risk and enhancing food production efficiency [8, 9]. The transition towards precision agriculture also promises lower environmental impact, transparent production, and smarter production methods, ushering in an era of sustainable and efficient farming [9–11].

The current abundance of high-resolution optical and SAR data offers unprecedented opportunities for agricultural monitoring. Satellite imagery can be used for many applications as mentioned. However, the reliability of optical imagery is severely undermined by cloud cover worldwide, posing a significant challenge for capturing clear and cloud-free images. For example, van der Wal *et al.* [12] used 20 years of data from a KNMI weather station data at Eelde (the Netherlands) and showed that there is about a 20 % chance of obtaining a clear (< 2 Oktas) satellite acquisition during the growing season.

On the other hand, microwave remote sensing stands out for its unique advantages compared to optical remote sensing methods. The key advantage is the use of longer wavelengths (300 MHz – 300 GHz) compared to other techniques. The longer wavelengths enable the microwave signals to penetrate through clouds and aerosols without significant disturbance. Data can be acquired during both day and night, eliminating the temporal restrictions inherent in other remote sensing techniques [13]. Therefore microwave remote sensing can ensure timely observations for agricultural applications [5, 14–20]. Another advantage of the microwave signals is their distinctive ability to penetrate through canopies and soils, thereby providing information that is typically unattainable through alternative techniques. However, in the microwave domain the penetration is not equal for all range of frequencies and generally by increasing in frequency the penetration depth decreases [13, 21]. In general, observations at shorter wavelengths, such as X-band and C-band, are primarily influenced by the uppermost layers of the canopy. Observations at longer wavelengths, like L-band, have a larger sensing depth and can interact with the entire crop canopy [17, 21, 22].

The depth of this penetration is controlled by the bio-physical properties of the scatters within the vegetative layer, such as the water content of the canopy and the size and shape of its constituents [23]. Moreover the received backscatter from agricultural area is dependent upon both the sensor configuration such as

frequency, polarization and incidence angle and target characteristics such as the size and shape distribution of crop constituents, their orientation, the roughness and dielectric constant of the underlying surface, and the canopy cover [5, 6, 16, 24].

To date, many ground-based experiments and campaigns based on scatterometer, airborne and satellite data (SAR data) have conducted to demonstrate the value of low frequency radar data in agricultural applications such as crop monitoring and classification, soil moisture estimation, and extracting bio- and geo-physical parameters from radar data [5, 17, 22, 25–30]. Ground-based scatterometers campaigns enable high temporal resolution collection of datasets, very suitable for plot scale observations, but they are limited to measure a single field or, at best, can be moved with a mechanical system to observe multiple fields. This greatly limits the diversity of fields and conditions that can be observed in a single campaign [5, 15, 17]. In contrast, air borne sensors, although typically limited to a few flights, can capture data across many fields with different characteristics. The other option for large scale monitoring can be use space borne scatterometer observations which have a very coarse resolution [21, 31–34]. In the context of microwave instruments, passive systems like radiometers provide coarse resolutions ( $> 10$  km) and observe naturally emitted radiation from the land surface, whereas active radar systems, especially synthetic aperture radars (SAR), can yield significantly higher resolutions (meter-scale) [19, 35].

Active microwave systems like SAR enable a more detailed analysis of vegetation constituents, including absorption, scattering and their sensitivity to water content [15, 22, 36]. Therefore, in many ways data from SAR system can overcome the problems found in ground-based, airborne, and passive systems by giving high spatial resolution with large coverage of land surfaces. This makes SAR a key tool with great potential for new developments in the field of microwave remote sensing. Several studies have focused on specifically used of the SAR data for agricultural application and the sensitivity SAR data to biophysical parameters of crops [13, 26, 28, 37–47]. Despite these advantages, SAR data had not been used as extensively or operationally as optical data until 2015. Reasons for this have included the traditionally high cost of SAR data acquisition and the relatively complex and specialized processing methods [21].

The launch of the European commission's Sentinel-1 Mission in 2015 generated unique opportunities in terms of the operational use of radar observations for agricultural monitoring for two reasons: (1) its revisit time is unprecedented, and (2) the imagery are freely distributed. Temporal coverage of this data varies across the globe, but combining ascending and descending tracks from both Sentinel-1A and Sentinel-1B yields observations every 1-2 days in the central Europe. This considerable improvement in revisit time and availability of imagery by the Sentinel-1 Mission represented a significant improvement over RADARSAT-2, which, prior to the launch of the Canada three-satellite RADARSAT Constellation Mission (RCM) in 2018, provided observations with a 24 days repeat cycle [17, 21]. Since the launch of the first Sentinel-1 satellite in 2015, numerous studies have leveraged this data for providing insight into the temporal variability of vegetation, monitoring the phenological stages of crops, crop classification and crop type map generation, soil

moisture estimation, monitoring and detecting important agricultural practice such as tillage, sowing and harvest date and retrieving biophysical parameter of crops such as leaf area index (LAI), biomass and vegetation optical depth (VOD). [3, 13, 29, 30, 40, 41, 44–46, 48–64]. Having data from two different times of the day from ascending/descending tracks means that the condition of the agricultural target such as internal and external water content can be different. However, little attention has been paid to the potentially confounding effect of internal, and especially external, vegetation water dynamics on radar backscatters.

## 1.2. THE IMPORTANCE OF SURFACE CANOPY WATER

Surface canopy water (SCW), i.e. external vegetation water, refers to the presence of water in a form of dew or interception from irrigation and precipitation on the canopy surface. This water is retained as tiny droplets or as a thin water film upon the surface of the canopy or top layer of soil. The presence, duration, amount, and distribution of the SCW is relevant in agriculture itself, as well in microwave remote sensing for agricultural applications [65–76].

The presence of SCW can play an important role in the recovery of the water content in plants after a heavy water loss or can be an important source of moisture for plants in an arid area during the dry season [65, 70]. SCW can also benefit crops by reducing the vapor pressure deficit and thus allowing stomatal opening and photosynthesis [70–72]. Formation and accumulation of dew on topsoil can help recharge the soil moisture and decrease evaporation from the soil layer if the moisture is not evaporated before it can infiltrate [77]. On the other hand, leaf wetness can contribute to the development of diseases in many crops [66, 70, 74]. The duration and amount of SCW can influence fungal diseases, expansion of bacteria and fungal pathogens, and germination of spores on many crops [74]. Therefore, information about the duration and amount of SCW can be valuable to support crop management decisions such as the optimal scheduling of fungicide applications.

In addition to the direct effect of SCW on plant biology, SCW can directly affect microwave data and influence retrieval of e.g. soil moisture, VOD, biophysical variables, canopy fuel load, and crop classifications [66–69, 75, 76]. As explained in the previous section, active microwave observations from agricultural land are highly sensitive to the dielectric and structural properties of the crops and soil, depending on system properties. The presence of SCW increases the water content, and hence the dielectric constant of the vegetation, leading to an increase in the observed backscatter and can have a confound influence on retrieval of crop bio-geophysical variables of interest [78, 79]. However, it remains challenging to understand the influence of SCW on the retrieval of crop bio-geophysical variables and estimates of vegetation optical depth.

### 1.3. THE EFFECT OF SURFACE CANOPY WATER ON SAR DATA

Dew is often present on vegetation in temperate regions during the early morning [66, 80]. Kabela *et al.* [66] found that dew was present on more than 80 % of days during the SMEX-05 experiment in Ames, Iowa, with dew accumulating on corn and soybean fields between 00:30 and 6:30 Central Standard Time (CST). As most satellites carrying radar instruments are in a near-polar, sun-synchronous orbit with local overpass times between 4:00 AM/PM and 10:00 AM/PM, the effect of dew on the radar backscatter needs to be considered. Several early experimental studies have reported an increase in radar backscatter at different frequencies due to the presence of SCW caused by dew and interception.

In an early study conducted by Gillespie *et al.* [79] over a wheat field, it was found that radar backscatter increased by 4 dB in C-band and 1 dB in the L- and Ku-band during dew events. It was found that an incidence angle of 20 degrees had the highest sensitivity to the presence of dew compared with incidence angles of 40 and 60 degrees. They found lower sensitivity of a signal to dew event by increasing the incidence angle from the nadir. However, Herold, Pathe, and Schmillius [81] reported no significant effect from SCW on radar backscatter at X-band and a modest increase of up to 1 dB in C-band for forest and non-cereal crops with heterogeneous surface structure (i.e. corn and potato). They found that L-band observations were less sensitive to SCW than C-band.

A series of experiments conducted by Riedel *et al.* [76, 82, 83] used polarimetric data at L-, C-, and X-band from E-SAR over different crop types to investigate the effect of SCW on radar observations, scattering mechanisms, and crop classification. At L-band, they found that the effect of SCW was less dependent on plant structure and a strong influence of SCW was observed on cross-pol data while no impact was observed on VV-pol data. At C-band, they observed that the impact on backscatter depended on vegetation structure and growth stages. At X-band, no significant influence was observed from dew events. They found an increase of about 2 dB in volume scattering in cross-pol under wet conditions. They also found a significant decline (4 dB) in surface scattering and double bounce in the presence of SCW. They also reported that the impact of dew on the signal was independent of vegetation type. In case of classification, they found that generally the accuracy increased by a decrease in SCW amount, and the crop separability was affected by SCW.

Wood *et al.* [75], compared RADARSAT-1 data from ascending and descending passes to understand the effect of SCW on crop separability. They found that the difference in backscatter between ascending and descending passes was similar among various crop types and that C-band backscatter was on average 1.7 to 2.5 dB higher during the dawn acquisition (6 AM) compared to the dusk acquisition (6 PM). Contrary to Riedel and Schmillius [76], they concluded that the overall crop separability is not affected by choice of overpass time but that the choice of overpass time should be considered for retrieval of crop bio-geophysical variables of interest since the presence of dew increase the radar backscatter during dawn acquisitions.

These studies provide valuable insight into the potential impact of SCW on radar observables but very limited and temporarily sparse data were used to investigate

the effect of SCW. Moreover, in some studies, the presence of SCW was not measured directly but was predicted using meteorological data. This may contribute to the occasionally contradictory conclusions. Furthermore, it remains challenging to explain the observed difference between the frequencies and polarizations because the widely-used radiative transfer models have mostly been developed to account for the influence of internal water content on the various contributions to total backscatter, and do not currently account for the presence of the SCW on vegetation.

#### 1.4. MODELING THE EFFECT OF SURFACE CANOPY WATER DYNAMICS ON RADAR DATA

Several widely-used radiative transfer models have been developed to better understand and simulate backscattering from agricultural crops [36, 84–87]. The most commonly used model among these models is semi-empirical Water Cloud Model (WCM) which considers the vegetation as a cloud containing identical water droplets randomly distributed within the canopy [84]. The WCM is a zero-order radiative transfer solution in which the power backscattered by the entire canopy is modeled as the incoherent sum of the contributions from the canopy (as a whole) as well as the underlying soil. This model is widely used due to its simplicity. However, it does not consider higher order scattering mechanisms. To obtain a more detailed understanding of scattering from vegetation surfaces, more advanced models based on energy and the wave approaches such as Michigan Microwave Canopy Scattering Model (MIMICS) [36], Multi-static Interferometric and Polarimetric Electromagnetic mode for Remote Sensing (MIPERS) [87], and the Tor Vergata model [85] have been proposed. The “Tor Vergata model” is a fully polarimetric model developed at the Tor Vergata university in Rome [85] and has been used in multiple studies for the simulation of radar backscatter across various crop types and frequencies, ranging from P- to X-band [18, 88–101].

Previous studies using the Tor Vergata model showed the high sensitivity of the model to crop growth and good agreement between the model and observed backscatter [18, 88–101]. However, these studies relied on temporally sparse data (i.e. ranging from every 3 days to every 12 days) for the input parameters and the simulations were primarily capturing the seasonal growth cycle. Moreover, this model has mostly been developed to account for the influence of internal water content on the various contributions to total backscatter and does not currently account for the presence of the SCW on vegetation.

#### 1.5. RESEARCH GAP AND OBJECTIVES

As argued in previous sections, active microwave data offer substantial advantages over optical data in agricultural monitoring. However, the potentially confounding effects of both internal and, particularly, external water dynamics in vegetation on radar backscatters have not been adequately addressed. Previous sections have highlighted several research gaps, mainly regarding our understanding of the impact

of internal water, specifically surface canopy water (SCW), on radar backscatter, and subsequently, on the interpretation of radar data for agricultural monitoring.

As mentioned, past studies have uncovered the influence of SCW on radar backscatter [66–68, 75, 76, 79, 81–83]. Despite this knowledge, understanding of the extent to which SCW affects radar backscatter across different frequencies and polarizations, and how it impacts the relationship between radar observables and crop bio-geophysical variables of interest, is limited. Additionally, current radiative transfer models, such as the Water Cloud Model (WCM), Michigan Microwave Canopy Scattering model (MIMICS) and the Tor Vergata model are primarily focused on the influence of internal water content on total backscatter, neglecting the potential presence of SCW [36, 84–87]. Therefore, to date, the full extent and mechanisms through which SCW affects radar backscatter and its influence on the relationship between radar observables and crop bio-geophysical variables have not been thoroughly investigated. This research gap motivates this research and we try to answer main question regarding the extent of the effect of SCW on radar data particularly across frequencies and polarization in this thesis.

Taking into account the aforementioned research gap, this research proposes several key objectives:

- 1- Demonstrate the significant potential of Sentinel-1 SAR backscatter and interferometric coherence for crop monitoring and the identification of key dates in crop phenological stages.

- 2- Enhance our understanding of the quantitative influence of SCW on radar observables and their relationship with various geophysical variables.

- 3- Broaden our understanding of the impact of SCW on total backscatter as a function of frequency, polarization, and growth stage and to comprehend the underlying mechanisms. This objective seeks to delve deeper into the complexities of the interaction between SCW and radar backscatter by adapting and validating the radiative transfer model for the first time to account for the presence of SCW on vegetation and soil surfaces.

## 1.6. RESEARCH OUTLINE

The main goal of this PhD research is to expand our knowledge of the relationship between radar backscatter, vegetation dynamics, and surface canopy water (SCW) in agricultural monitoring.

Chapter 2 provides a comprehensive overview of the experimental setup used during the campaigns in Citra, Florida, USA. It includes essential details about the instrumentation and methodologies employed

Chapter 3 explores the capability of using Sentinel-1 in monitoring the important crops in Netherlands, namely sugarbeet, potato, maize, winter wheat, and English ryegrass. The time series of Sentinel-1 backscatter and cross-ratio have been analyzed to understand the effect of structural and biomass change of crop and environmental conditions during the whole season on the radar backscatter. Then the possibility of detecting the key phenological stages such as crop emergence, closure, and harvest date was tested by utilizing curve fitting and statistical analysis

methods over time series of both backscatter and interferometric coherence.

Chapter 4 examines the influence of surface canopy water on the radar backscatter, on the relationship between the radar observables and geophysical variables of interest such as vegetation water content, dry biomass, leaf area index, and plant height, and on the vegetation optical depth estimation. In this chapter, all analyses are based on data collected from a fully polarimetric, L-band scatterometer, and intensive ground measurements during a field experiment in Florida, USA.

Chapters 5 and 6 focus on modeling the effect of diurnal variation in both SCW and internal water on radar backscatter as a function of frequency and polarization to understand its effect on the underlying mechanisms. The radiative transfer model developed by Tor Vergata University is used to simulate and investigate the effects. This model can accurately simulate the seasonal evolution of radar backscatter in response to crop growth. In Chapter 5, this model is calibrated at a sub-seasonal scale to improve the simulation of daily and sub-daily variations in radar backscatter.

In Chapter 6, the calibrated version of the model is adapted to investigate the effect of SCW on backscatter as a function of frequency, polarization, and growth stage and to understand the underlying mechanisms.

Finally, Chapter 7 presents the conclusion of this thesis, along with implications and recommendations for further research.

# 2

## FLORIDA FIELD CAMPAIGN AND DATA

*This section of the dissertation describes detailed experiments conducted in Florida during the spring of 2018. It provides an in-depth explanation of how the experiments were set up. The primary goal of this experiment was to gather essential data to help us understand the relationship between internal and external water dynamics and radar backscatter. To achieve this, various ground measurements were taken, and time-series analyses of backscatter coefficients were performed using a ground-based scatterometer. The information presented in this chapter will be referenced in Chapters 4, 5, and 6 of this thesis. In those chapters, the data will not be repeated; instead, there will only be references to the information in this chapter.*

---

This chapter is based on:

Khabbazan, Saeed et al., "The influence of surface canopy water on the relationship between L-band backscatter and biophysical variables in agricultural monitoring." *Remote Sensing of Environment* 268 (2022): 112789. [102]

Khabbazan, Saeed et al., "The Influence of Surface Canopy Water on L-, C-, and X-Band Backscatter: A Study Combining Detailed *In situ* Data and the Tor Vergata Radiative Transfer Model." *Science of Remote Sensing* (2023): Under revision



## 2.1. STUDY AREA

The field camping was carried out at the University of Florida Institute of Food and Agricultural Sciences (UF/IFAS) Plant Science Research and Education Unit (PSREU) near Citra, Florida, USA (29.4° N, 82.17° W) during the spring of 2018. This field campaign lasted for a whole growing season of corn (i.e., 70-day), starting during the bare soil period in early April and continuing until the harvest in mid-June. The site's climate is classified as *Cfa* under the Köppen Geiger Climate classification [103], characterized as a humid subtropical climate with hot and humid summers, and cold to mild winters. The rainy season mostly runs from around May to November [104], and this study period encountered a dry period in the early season and heavy rainy period after mid May.

The corn field measured 250 m by 150 m, with the soil comprising over > 90% by volume fine sand [105]. Sweet corn (*Zea mays L. var. rugosa*) was planted on April 13th at a row spacing of 92.5 cm and an average density of 7.9 plants  $m^{-2}$ . The crop was harvested before the start of the senescence stage on June 18. Irrigation was applied several times during the early season using a center-pivot irrigation system. Irrigation was applied close to midnight to control the soil moisture content and minimize evaporation losses. The Schematic representation of the experimental setup is presented in Fig. 2.1.

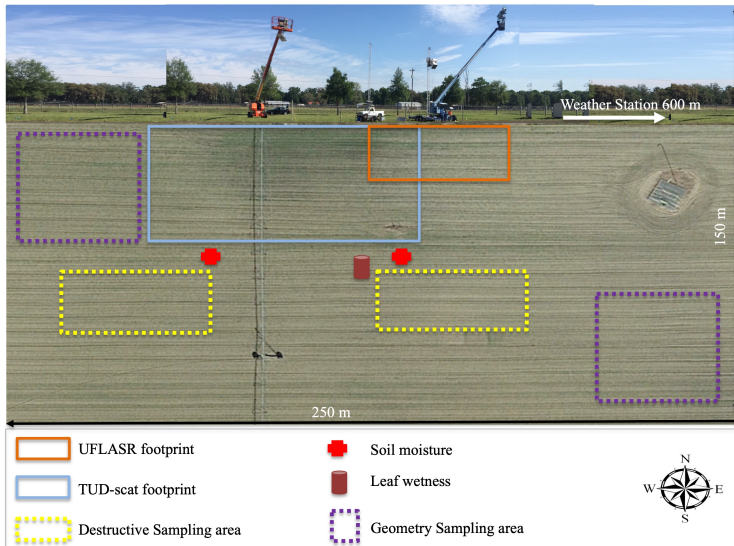


Figure 2.1.: Schematic representation of the experimental setup: corn field layout, instruments, and sensor locations during the Florida campaign. (i.e. Not to scale)

## 2.2. UF-LARS RADAR

Radar backscatter was measured using the truck-mounted University of Florida L-band Automated Radar System (UF-LARS) [106] (Table 2.1). Radar data were acquired at four polarization combinations (VV, HH, VH, and HV) using a dual polarization horn antenna. The VH and HV data were very similar so, following previous studies [107], they were averaged and are referred to here as the cross-polarized backscatter  $\sigma_{XP}$ . The system was installed on a Genie platform with an antenna height of 14 meter from the soil surface. UF-LARS scanned the corn field with a fixed elevation angle of  $40^\circ$ . In this research, samples at three azimuth scans at  $-9^\circ$ ,  $0^\circ$  and  $+9^\circ$  were used. At each azimuth scan, nine samples were taken at 30 MHz increments from 1130 to 1370 MHz which resulted in 27 independent samples. Individual samples are prone to noise due to fading, i.e. the noise arising from interference between returns from multiple ground targets [108]. The average of 27 samples were used in order to account for variations in row direction, and to increase the signal-to-noise ratio, which for a single sample is lowered by fading [107].

Internal calibration was applied during each acquisition to account (among others) for the effect of temperature on the electronics. External calibration was conducted using a trihedral corner reflector of known radar cross section several times during the growing season. The Single Target Calibration Technique (STCT) [109] was used to calculate the backscatter coefficient  $\sigma^\circ$  from the received signal. The total systematic error and random error were estimated as 1.49 and 0.85 dB, respectively [106, 107]. The ground range and azimuth range for each polarization combination were determined using the 3 dB antenna beamwidth of  $14.7^\circ$  and  $19.7^\circ$  in E-plane and H-plane, respectively as shown in Table 2.1. Scanning the corn field over 3 azimuth angles resulted in the total footprint area of 120, 119 and  $87.5 \text{ m}^2$  in HH, VV and XP polarization, respectively. Vegetation samples were collected outside, but adjacent, to the radar footprint to avoid introducing patches and heterogeneity within the radar footprint, and to prevent any changes in roughness due to foot traffic. All sensors and hardware are installed outside the footprint to avoid any influence of metal structures or cables on the radar backscatter. The UF-LARS system was programmed to automatically acquire 32 measurements per day during the growing season. During the last 7 days, this was reduced to 16 measurements per day to avoid any radio frequency interference with other microwave sensors.

## 2.3. GROUND MEASUREMENTS

### 2.3.1. METEOROLOGICAL DATA

Meteorological data were obtained from the nearby weather station from the Florida Automated Weather Network (FAWN). The station was located <600 m from the experimental site. 15-min observations of rainfall, relative humidity, temperature, solar radiation, and wind speed were obtained from the Report Generator (<https://fawn.ifas.ufl.edu/data/reports/>). The timing and amount of irrigation was provided by UF/IFAS.

Table 2.1.: UF-LARS system specifications

Parameter		UF_LARS
Frequency (GHz)		1.25
3dB Beam-width (deg)	E-Plane	14.7
	H-plane	19.7
Bandwidth (MHz)		300
Antenna Type		Dual-polarization horn
Range resolution (m)	HH/VV/XP	8.5 / 6.2 / 6.2
Azimuth Resolution (m)	HH/VV/XP	4.7 / 6.4 / 4.7
$NE\sigma^\circ$ (dB)	HH/VV/XP	-23.43/ -25.58/ -48.12
Error in $\sigma^\circ$ (dB)	Systematic	1.49
	Random	0.85
Incidence Angle (deg)		40
Platform height (m)		14



Figure 2.2.: The University of Florida L-band Automated Radar System (UF-LARS) is mounted on the blue crane

### 2.3.2. SOIL DATA

Surface to root zone soil moisture was measured every 15 minutes using 10 Decagon EC-5 sensors [110] installed at 5, 10, 20, 40, and 80 cm depth in two pits located 40 m apart, adjacent to the radar footprint (Fig. 2.3 (b)). The averaged measurement at 5 cm depth was used as surface soil moisture, and this average was used in this thesis. A site-specific calibration was conducted before the installation of sensors, both in the laboratory and using soil samples from the field. Soil moisture was measured using EC-5 sensors, and the gravimetric sampling method was applied for saturated to dry soil. The goodness of fit for the linear regression between soil

moisture estimates from the EC-5 sensors and values from gravimetric sampling was 0.993, and the RMSE was  $0.028 \text{ m}^3 \text{ m}^{-3}$ . Although the two profiles were 40 m apart, the observations of the two pits closely matched.

Surface roughness was characterized in the period between sowing and the crop emergence using a 2-meter long grid board (Fig. 2.3 (a)). The roughness profiles were acquired along, and perpendicular to the row direction. In each direction, the grid board was moved twice to build a synthetic 6-meter roughness profile. These profiles were digitized at 1 cm intervals, and the digitized profiles were used to compute the root mean square (RMS) height and the correlation length (L) following the procedure described in [111]. The averaged RMS height and correlation length was found to be 0.92 and 9.17 cm, respectively. In general, measuring the correlation length accurately is difficult because it is extremely variable [112]. Previous studies conducted by [112–114] suggested calibrating the correlation length by finding the value that gives the best fit between simulated and observed backscatter during the bare soil period. For this research, we try to calibrate the correlation length; however, we decided to use the measured value of correlation length (i.e. 9.17 cm) since the optimum value of the correlation length which gave the best fit in both polarization was not found.

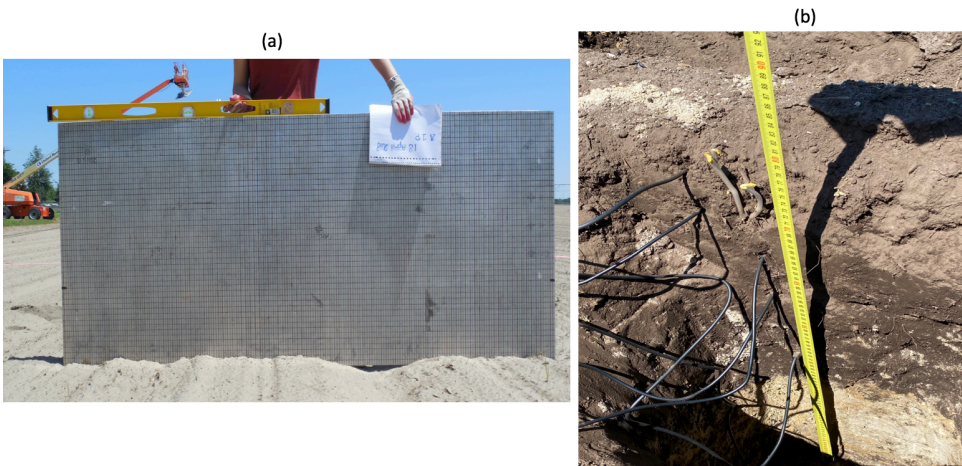


Figure 2.3.: Using a 2-meter long grid board to measure soil roughness (a), soil moisture sensors installation at depths of 5, 10, 20, 40, and 80 cm (b)

### 2.3.3. SURFACE CANOPY WATER DATA

The presence, frequency, duration, and amount of the surface canopy water (SCW) caused by dew or interception were measured using three dielectric leaf wetness sensors (Pythos31) [115] every 15 minutes during the whole growing season (Fig. 2.4). These sensors are designed to mimic the thermodynamic and match the radiative properties of real leaves. The three sensors were installed at three different

heights after plant emergence. The height of the sensors was adjusted as the canopy grew to ensure they were evenly distributed along the height of the plants and could capture the vertical distribution of the wetness on the canopy. The angle of the sensors was also adjusted to mimic the angle of neighboring leaves. The surface coating of the PHYTOS 31 is hydrophobic, similar to a leaf with a hydrophobic cuticle, and unlike conventional leaf wetness sensors, its resistance grid does not use salt-laced latex paint which resulted in extra sensitivity to avoid false positives.



Figure 2.4.: 3 leaf wetness sensors installed at a wooden pole at early stage.

The primary output of these sensors is a voltage (in mV) proportional to the dielectric constant of a zone approximately 1 cm from the upper surface of the sensor which is proportional to the amount of water on the sensor's surface. The EM50 data logger [116] converts the voltage output to a scale in terms of "counts." The factory calibration of this sensor indicated consistency in output data, and the outputs for the dry PHYTOS 31 approximately 435 raw counts when read with METER data loggers. When the sensor is totally wet, as in heavy rain, the signal can range up to around 1,100 counts.

The mass of water ( $M_w$ ) deposits on the sensor surface ( $g\ m^{-2}$ ) is calculated using an empirical formula reported by the factory and Cobos et al. [117, 118]:

$$M_w = 1.54 \times \exp(5.8 \times 10^{-3} \times \text{counts}) \quad (2.1)$$

Following [119], two assumptions were made to convert the mass of water on sensors to SCW. First, the area of each corn leaf ( $A_L$ ) in  $m^2$  was calculated from leaf length

(l) and width (w) assuming that corn leaves were elliptical:

$$A_L = \frac{\pi}{4} \times l \times w \quad (2.2)$$

Second, it was assumed that the wetness on a leaf at any height was similar to the wetness on the sensor closest to that leaf. Then the SCW could be calculated as follows:

$$SCW = \rho_{plant} \times \sum_{i=1}^n A_{L_i} \times M_{w_i} \quad (2.3)$$

where SCW is the amount of surface canopy water on the corn leaves per square meter of ground ( $kg\ m^{-2}$ ),  $n$  is the average number of leaves per plant,  $M_{w_i}$  is the water mass on the sensor closest to leaf  $i$  ( $kg\ m^{-2}$ ),  $A_{L_i}$  is the area of leaf  $i$  ( $m^2$ ), and  $\rho_{plant}$  is the average number of plants  $m^{-2}$ .

#### 2.3.4. GROUND VEGETATION SAMPLING AND VEGETATION DATA

Predawn destructive vegetation sampling was conducted every 2-3 days during the entire growing season to measure Vegetation Water Content (VWC) and dry biomass ( $m_d$ ), as well as gravimetric water content ( $M_g$ ). Four rectangular sampling areas with average dimensions of 30 by 35  $m^2$  were delineated outside, but adjacent, to the radar footprint at the beginning of the season. For each sampling event, eight field-representative plants were chosen from the four sampling areas.

From the eight samples, all constituents (leaves, stems, ears, tassel, and tillers) of these plants were separated, paper towel-dried to remove any surface water, weighed, and oven dried at 60° C for 4 to 8 days, with 5 to 7 days being typical. The dry samples were weighed again to estimate field-average VWC,  $m_d$ , and  $M_g$  using the following equations [119]:

$$VWC = (W_f - W_d) \times \rho_{plant} \quad (2.4)$$

$$m_d = W_d \times \rho_{plant} \quad (2.5)$$

$$M_g = \frac{W_f - W_d}{W_f} \quad (2.6)$$

where  $W_f$  and  $W_d$  are the average fresh and dry weight of the eight samples ( $kg$ ), respectively, and  $\rho_{plant}$  is the average number of plants per square meter ( $m^{-2}$ ).

The samples were also used to estimate field-average plant height and stem height using measuring tapes. The number of leaves per plant were counted on each sampling date. Detailed vegetation geometry measurements, including leaf length, width, diameter, and angles, were conducted weekly. These measurements were used to determine Leaf Area Index (LAI) on seven dates during the growing season. Leaf length and width were measured and used to estimate the leaf area, assuming that corn leaves are elliptical. Then, the leaf area for one plant was summed and multiplied by plant density to obtain LAI. Visual identification of growth stages was performed on sampling days using the *Biologische Bundesanstalt, Bundessortenamt, and Chemical industry* (BBCH) scale for corn [120].



# 3

## CROP MONITORING USING SENTINEL-1 SAR DATA: A CASE STUDY FROM THE NETHERLANDS

*Agriculture is of huge economic significance in the Netherlands where the provision of real-time, reliable information on crop development is essential to support the transition towards precision agriculture. While the optical data often can be severely hampered by cloud cover, the SAR data can be a solution for consistent monitoring. This chapter introduces a case study from Flevopolder, illustrating the potential of Sentinel-1 C-band SAR for monitoring five major crops in the Netherlands. We present a comprehensive analysis of the radar backscatter time series from the European Space Agency's Sentinel-1 Mission, alongside an exploration of interferometric coherence data.*

---

This chapter is based on:

Khabbazan, Saeed, et al., "Crop monitoring using Sentinel-1 data: A case study from The Netherlands." *Remote Sensing* 11.16 (2019): 1887. [121]



### 3.1. INTRODUCTION

The Netherlands is the second largest exporter of food and agricultural products in the world, exporting 65 billion euros of agricultural produce annually. These exports represent 17.7 % of total Dutch exports [122] and the sector is expected to grow further in the next 15 years [123]. The provision of timely, reliable, accurate, and high-resolution satellite remote sensing data is essential to facilitate a transition from parcel-level decision-making towards precision agriculture [124, 125]. This transition towards precision agriculture is expected to yield increased productivity, lower environmental impact, transparent production, and more intelligent production methods. Furthermore, the commercialization of remote sensing data processing and added-value product generation has the potential to become a valuable export commodity. Satellite remote sensing provides valuable information for many users from individual farmers to food producers, as well as national and international governmental agencies.

This chapter is focused on one of the most productive agricultural areas in the Netherlands to explore the value of Sentinel-1 in monitoring regionally important crops, namely sugar beet, potato, maize, winter wheat and English rye grass. By comparing Sentinel-1 imagery to hydrometeorological data and ground measurements of phenological stage, and vegetation height it is shown that the time series of Sentinel-1 backscatter data reflects moisture and structural changes associated with phenological development of crops during the growing season in this region. It is shown that key dates of interest (emergence and closure dates) can be mapped using Sentinel-1 backscatter data. Finally, it is shown that, in addition to backscatter data, the coherence between consecutive Sentinel-1 images is influenced by the structural changes associated with (potato) haulming and harvest.

### 3.2. DATA AND METHODS

#### 3.2.1. STUDY AREA

The study was conducted in the Flevopolder, a region of reclaimed land with an area of 970 km<sup>2</sup> which was drained in 1957 with the main purpose of agriculture. Fig. 3.1 shows the location of the Flevopolder in the Netherlands, as well as the spatial distribution of the five crops considered. Parcel boundaries and crop types were determined from the Basisregistratie Gewaspercelen (BRP) [126]. The land surface in this region is flat and lies  $\pm 3$  m below sea level. Soil at the surface is clay overlaying a sand layer at about 2 m depth. Capillary rise from the shallow groundwater is a major stabilizing control on soil moisture. The average minimum temperature during winter is  $-3.3^{\circ}\text{C}$ , the average maximum temperature during summer is  $22^{\circ}\text{C}$  and the mean annual precipitation is 797 mm per year [57]. Weekly crop growth stage, crop height and soil moisture data were collected in 24 agricultural parcels on the Flevopolder. The crop types were sugar beet (5 parcels), potato (4 parcels), maize (5 parcels), wheat (5 parcels) and English rye grass (5 parcels).

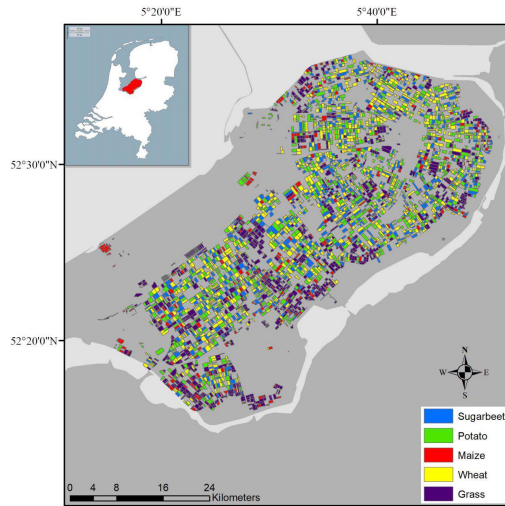


Figure 3.1.: Location of study area and map of crop types in Flevopolder.

### 3.2.2. HYDROMETEOROLOGICAL GROUND DATA

Hydrometeorological sensors were installed at a silage maize parcel at the Aeres Practijkcentrum in Dronten (52.53N, 5.66E) for continuous ground measurements. The growing season of this parcel lasted from May to the end of September 2017. A weather station was installed on the 24<sup>th</sup> of May, adjacent to the maize parcel. A Decagon ECH2O Rain Model ECRN-100 tipping bucket was mounted on the station, however it failed and was replaced on 23 June. Precipitation data from the KNMI station at Dronten (Station Number 364) were used in the interim [127]. The weather station also included an Apogee SP-212 pyranometer (solar radiation), a Davis Cup anemometer (wind and gust speed, and wind direction), and a HOBO Temperature/RH Smart Sensor Model S-THB-M008 (temperature and relative humidity).

Radar backscatter, particularly at C-band, is sensitive to the presence of water on the canopy [47, 79, 81, 82, 128]. Therefore, three Decagon Dielectric Leaf Wetness Sensors were installed in the maize parcel in Dronten to measure the presence and duration of interception or dew on the leaf. To investigate the wetting and drying at different levels, the sensors were installed on three heights in the canopy: 27.5, 42.5, and 145 cm from the ground. Precipitation data were used to determine whether water droplets on the sensor were likely to be interception or dew.

Root zone soil moisture was monitored by installing five Decagon ECH2O EC-5 soil moisture sensors between two rows in the middle of the parcel, at five different depths: -5, -10, -20, -40, -80 cm. The accuracy of the factory generic calibration is approximately 3 to 4 % [129]. Results from the sensor at 20 cm were excluded from the analysis because the sensor produced spurious values throughout the study period.

### 3.2.3. GROUND DATA AT 24 PARCELS

In each of the 24 parcels, two sampling locations were identified and marked at the start of the growing season. The sampling locations were located 20 m from the parcel boundary to avoid edge effects. These sites were visited approximately once per week, weather permitting.

Soil surface roughness parameters (root mean square (rms) height and correlation length (L)) were determined using digital photos of a grid board during the bare soil period for the maize, sugar beet, potato and wheat parcels. Surface soil moisture at each sampling point was measured using ML3 ThetaProbe Soil Moisture Sensors [130]. The parcel soil moisture was estimated as the average of eight measurements, four at each sampling location. In potato parcels, soil moisture measurements were made at the crest and trough of the soil mounds. Crop growth stage was determined by visual inspection, based on the BBCH scale [120, 131]. Where the BBCH stage differed across parcels, the average value is indicated in the following sections. Crop height was measured, and a photo archive was generated to document the development stage.

### 3.2.4. SENTINEL-1 DATA

Sentinel-1 includes C-band Synthetic Aperture Radar (SAR) operating at a centre frequency of 5.405 GHz. The observation mode over (non-polar) land is the Interferometric Wide mode (IW) providing dual polarization (VV and VH) imagery over a 250 km swath at a 5 x 20 m spatial resolution.

Combining data from Sentinel-1A and 1B, the Flevopolder is covered by 4-5 tracks (See Table 1). Track 110 was not considered because it only covers part of the domain. This potentially provides an average of 20-25 acquisitions per month. This research uses 60 images from Sentinel-1A and 1B from relative orbit 88 between January 2017 and January 2018. An evening overpass time was chosen to minimize the influence of dew on the vegetation (See Section 3.3.1). GRD data were obtained via Google Earth Engine, and SLC products for the coherence analysis were downloaded from the Sentinel Hub [35, 132].

Table 3.1.: Sentinel-1 IW data available over the study area.

Relative Orbit	Pass	Local Time	Min. Inc. Angle [°]	Max. Inc. Angle [°]
37	DESC	06:49	38.9	41.9
161	ASC	18:32	44.7	46.1
88	ASC	18:24	36.6	40.4
15	ASC	18:15	30.0	31.5
110	DESC	06:58	30.0	33.7

Time series of co-polarized (VV) and cross-polarized (VH) normalized cross

section ( $\sigma^\circ$ ) were extracted from the GRD products for all parcels shown in Fig. 3.1. The number of parcels for each crop type is shown in Table 3.2. Pre-processing steps including radiometric calibration, removal of thermal noise offset and orthorectification with radiometric correction for residual slope effects had been done by Google Earth Engine using Sentinel-1 Toolbox [133].

Spatial multilooking was performed by averaging across all pixels within each parcel polygon. Hence, the radiometric resolution, or precision, for a single parcel depends on the parcel area. Typically, about 100 independent looks are available per hectare, resulting in a radiometric precision  $n$  of 0.5 dB for a parcel of 1 ha.

Table 3.2.: Number of parcels for each of five crop types in the study area.

Crop type	Number of parcels
Maize	335
Potato	886
Sugar beet	763
Wheat	1048
English Rye	1286
Grass	

Interferometric coherence can be defined as the amplitude of the complex correlation coefficient between two radar acquisitions. Given two interferometric complex SAR images  $s_1$  and  $s_2$  (Sentinel-1 SLC products), the coherence amplitude is described as:

$$\gamma = \frac{|\langle s_1 s_2^* \rangle|}{\sqrt{\langle s_1 s_1^* \rangle \langle s_2 s_2^* \rangle}} \quad (3.1)$$

Where  $|\cdot|$  indicates the absolute value,  $\langle \cdot \rangle$  indicates an ensemble averaging operation, and  $*$  denotes the complex conjugate product.

A time series of interferometric coherence was obtained by processing Sentinel-1 IW mode images with a temporal base line of 6 days using the SNAP tool (version 6.0.0) [134, 135], and the SNAP Graph Processing Tool (GPT) for batch processing. A flow chart of the processing steps for each pair of images is shown in Fig. 3.2. The relevant sub-swath, bursts and polarization (VV) were extracted from the original Sentinel-1 SLC product. This was done separately, but with the same parameters, for each pair of images. The Sentinel-1 precise orbit files were then applied to both images separately. In the Back-Geocoding step, the orbital and DEM information was used to geometrically co-register the SLCs. The Enhanced Spectral Diversity (ESD) function was used to correct for both range and azimuth shifts over the burst overlap regions of the TOPS data. After the interferogram was generated, the TOPSAR-Deburst function was used to generate a spatially continuous product, the Flat Earth phase term was removed using the TopoPhaseRemoval function, and phase adaptive filtering (Goldstein Phase filtering) was applied to improve visualization

and aid the subsequent unwrapping step. Finally, terrain-based geocoding was performed to produce the final product in geographical coordinates so that it could be combined with the parcel boundary information.

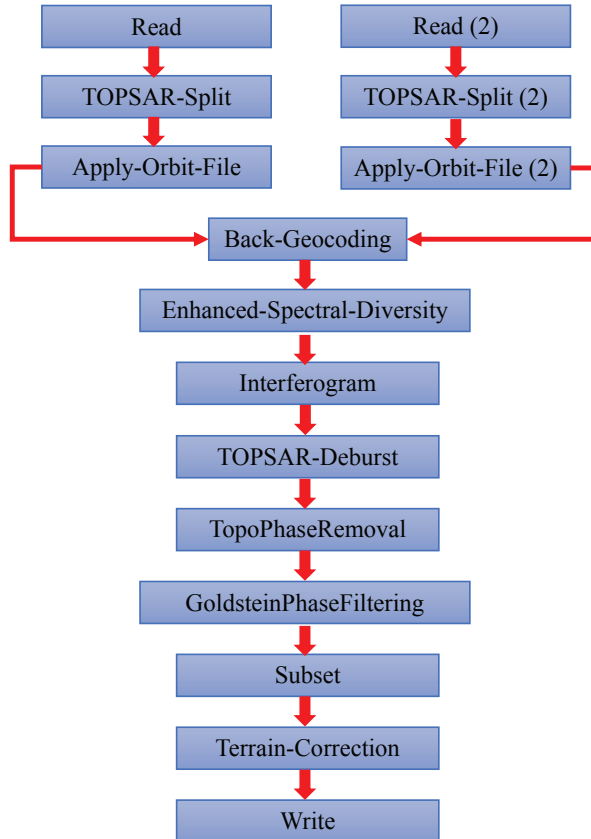


Figure 3.2.: Flow chart of procedure to map interferometric coherence from a pair of images of Sentinel-1 using SNAP software.

#### DETECTING EMERGENCE, CLOSURE AND HARVEST DATE

Emergence refers to the appearance of the first shoots and leaves above the ground. After emergence, VH backscatter is expected to increase as leaf development results in an increase in volumetric scattering. Therefore, emergence will be estimated as the time at which the slope of the VH backscatter becomes positive. Closure is defined as the moment when leaves from adjacent rows meet. It is a key input for crop growth models currently used for harvest forecasting and planning. For example, the SUIkerbieten Model (SUMO) has been in operational use in the Netherlands since 1996 to provide bi-weekly forecasts of sugar beet yields, sugar

content, and refined sugar yield [136]. These estimates are essential to provide timely advice to growers and to plan for the transport and processing of harvested beets to processing plants. Later closure dates generally correspond to lower yields [137]. A previous proof-of-concept study found the slowing down of leaf production around the closure date caused the VH backscatter to stabilize [57]. Hence, the closure date could be estimated as the time at which the slope in the VH backscatter becomes zero.

To estimate the emergence and closure dates, a curve is first fit to the time series of VH backscatter from 1 April to 1 July. This period is assumed to encompass the vegetative stages for sugar beet, potato and maize. The minimum and maximum points of this curve are determined and assumed to correspond to the emergence and closure dates. The estimated dates were validated visually using photos from the monitored parcels.

In Section 3.3.2 it will become clear that backscatter alone is not always sufficient to detect harvest in some crops. It will also be demonstrated that the disturbance to soil and vegetation properties and structure during harvest produce a change in coherence that can be used to detect harvest. In particular, it will be illustrated that when the crop is harvested, the scene becomes more static and the coherence increases. A rule-based classification will be applied to identify harvest at a parcel level.

## 3.3. RESULTS AND DISCUSSION

### 3.3.1. HYDROMETEOROLOGICAL DATA

#### WEATHER STATION DATA

Daily precipitation, average daily temperature and solar radiation, and 15-minute relative humidity and wind speed are shown in Fig. 3.3. Total precipitation in the period between May 27 and September 19 was 468.6 mm. The start of this period was characterized by two dry intervals of about two weeks with maximum daily average temperatures reaching up to 24 °C. More than one third of all rain fell between September 8 and 19. The highest peaks of solar radiation and temperature were found in June and July, while August was relatively moderate. In September, both solar radiation and temperature decreased substantially.

#### INTERCEPTION AND DEW

Fig. 3.4 shows the presence of water on the sensors at three different heights in the canopy. Most periods during which water was detected coincide with rain events, and are indicated as 'interception'. Water detection in periods without rain are indicated as 'suspected dew'. The lower, middle, and upper sensor were wet 20.5, 15.4, and 25.7 percent of their measuring time respectively. The upper sensor (Fig. 3.4 (a)) detected water more frequently than the lower sensors, particularly during periods of low-intensity rainfall, e.g. July 22-25 and August 17-20. During high-intensity rainfall, e.g. on September 8, some interception was detected on all sensors.

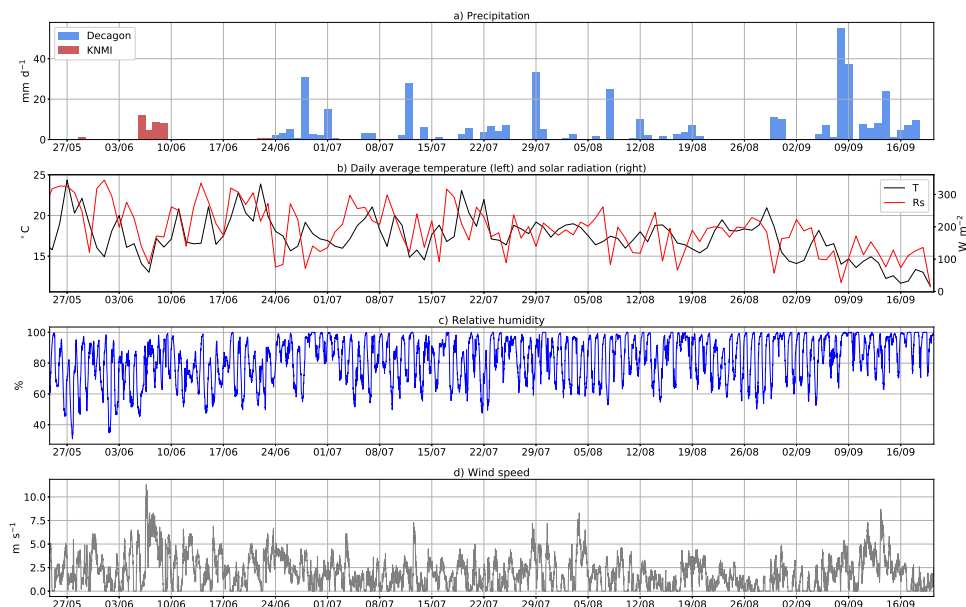


Figure 3.3.: Meteorological data collected at the Aeres Praktijkcentrum, Dronten (52.53N, 5.67E): **(a)** Precipitation data [ $\text{mm day}^{-1}$ ] **(b)** Daily Average Temperature [ $^{\circ}\text{C}$ ] and solar radiation [ $\text{W m}^{-2}$ ] **(c)** Relative Humidity [%] **(d)** Wind Speed [ $\text{m s}^{-1}$ ].

Table 3.3.: Percentage of days with water on canopy at morning and evening overpass times.

Sensor	AM (%)	PM (%)
upper	45.6	19.1
middle	26.1	8.0
lower	35.2	11.4

Table 3.3 shows the percentages of days with water on the canopy at times coinciding with satellite overpasses (Table 1). Moisture was detected on the canopy almost three times more often during the morning (descending) than the evening (ascending) passes. In the following analysis, only data from the ascending pass (Relative Orbit 88) will be used to avoid the confounding effect of vegetation surface water on backscatter.

### SOIL MOISTURE

Fig. 3.5 shows the volumetric soil moisture ( $\theta$ ) measured at four depths at the Aeres Practijkcentrum from June 13 to September 20. In general, the season was

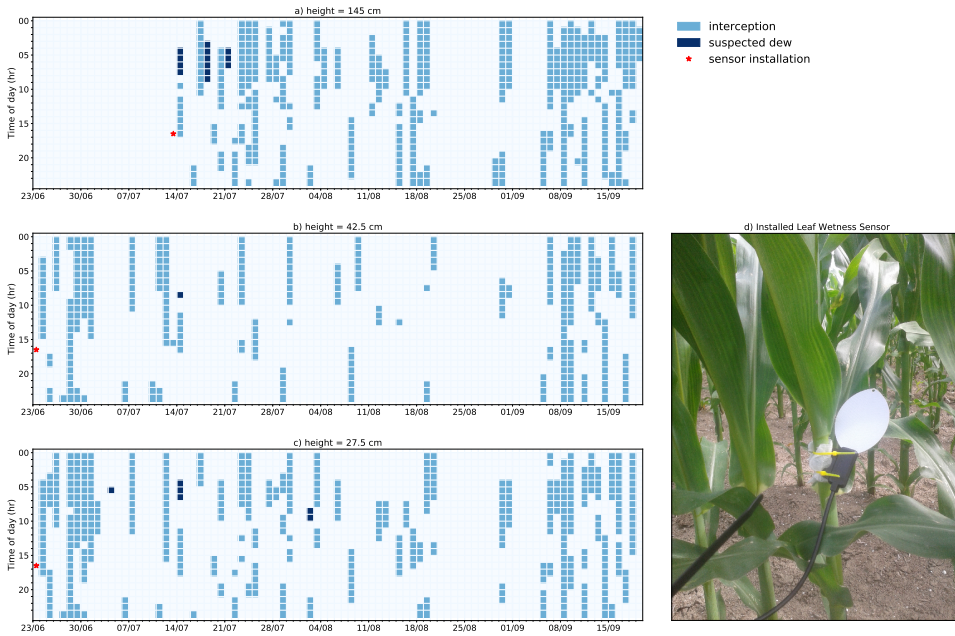


Figure 3.4.: Interception and dew measurements in the maize parcel at the Aeres Practijkcentrum (52.53N, 5.66E) at (a) 145 cm (b) 42.5 cm and (c) 27.5 cm. Coloured squares represent detection of water on the sensor for at least 15 minutes during that hour. A distinction is made between interception (light-blue), and suspected dew (dark-blue). Installation date for the lowest sensors was June 23, and for the upper sensor July 13. The picture shows the middle sensor.

characterized by well-watered growing conditions. From Fig. 3.5, the soil moisture at 40 cm and 80 cm saturate close to 0.5 and  $0.52 \text{ m}^3/\text{m}^3$  respectively. Porosity values higher than 0.5 are not uncommon in this clay soil, with higher values likely at depth [138]. The soil moisture values at 80 cm remain close to saturation throughout the study period due to precipitation and the availability of moisture from shallow groundwater. The frequent rain events in July and August allow the soil moisture at 5 cm and 10 cm to rise continuously, reaching near saturation by 9 September.

Fig. 3.6 shows the surface soil moisture measured in each crop type throughout the growing season. Warm temperatures and limited precipitation in late-May and June are reflected in the relatively dry surface soil moisture values before June 30. After that date, regular precipitation ensures that the surface soil moisture in all crop types remained relatively high. Temporal variations are similar across the different crop types due to the limited spatial extent and soil texture homogeneity of the study domain. Spatial variations are largest in the potato parcels due to differences between the crests (drier) and troughs (wetter) of the ridges. This is particularly clear during the drier period in late-May. Surface soil moisture in the grass parcels



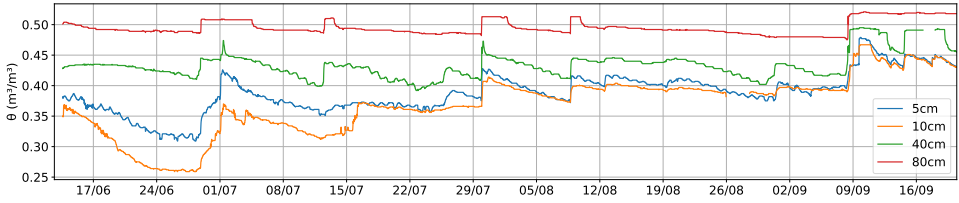


Figure 3.5.: Volumetric soil moisture ( $\text{m}^3 \text{m}^{-3}$ ) in the maize parcel in Dronten (52.53N, 5.66E) on different depths (5, 10, 40 and 80 cm). The sensors measured from the 13 June onwards.

3

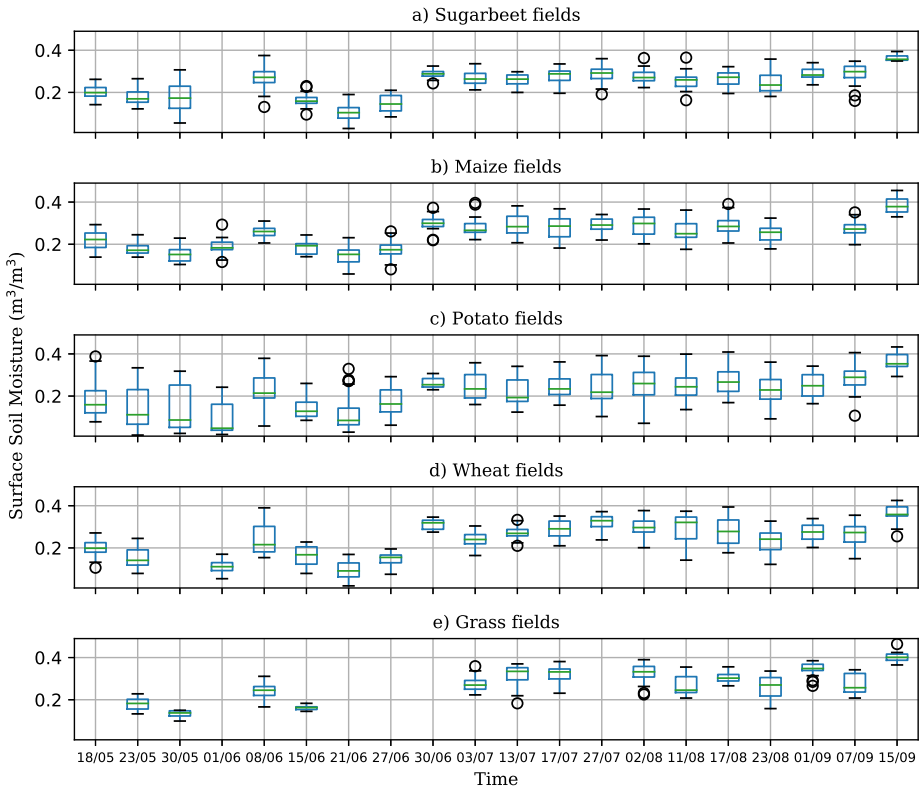


Figure 3.6.: Surface volumetric soil moisture ( $\text{m}^3 \text{m}^{-3}$ ) for different crop types using Theta Probe soil moisture sensor. For a given date, the box plot displays the minimum, maximum, median and first and third quartiles of four samples at two locations at each parcel of the given crop type.

exhibits limited spatial variability. In the remaining crops, the variability is limited following large precipitation events or persistent precipitation (e.g. 30 June and 15

September).

### 3.3.2. SENTINEL-1 TIME SERIES

#### MAIZE

The time series of Sentinel-1 backscatter (VV, VH and VH/VV), as well as phenological development stages and measured crop height for maize parcels are shown in Fig. 3.7. The crop height measurements indicate that the maize plants emerged around mid-May. In this region, maize is typically left to ripen in the field and harvested from mid-September onwards. Weekly phenological stage monitoring therefore covered the development from the early vegetative stages (BBCH=12) to fully ripe (BBCH=89).

From January 1 to mid-May, VH backscatter is around 12 dB lower than VV backscatter but the temporal variations in both are quite similar. These are dominated by the surface soil moisture. Variations in space can be attributed to variations in roughness, soil texture and row orientation/geometry. The three sharp decreases in VV and VH on 22 January, 9 February and 12 December 2017 are the result of frost and snow cover respectively [58] and are observed in the other crops too (Fig. 3.8 to 3.11). The increase of VV and VH before 5 March is caused by melting snow and precipitation on 26 February and 5 March. A heavy rain event on 16 April caused an abrupt increase in both VV and VH. It is noteworthy that these events have little or no influence on the VH/VV ratio. This reflects its reduced sensitivity to soil moisture variations compared to the individual VV and VH backscatter [45].

During the leaf development stage (BBCH 12 to 30) from 17 May to 8 June, the VH backscatter and VH/VV ratio increased by 7 and 3.5 dB respectively. This is mainly due to an increase in volume scattering as the newly formed leaves unfold. From stem elongation (BBCH 31 to 39), through to the beginning of tassel emergence (BBCH 51), the maize height increased from 40 cm to 2 m. This rapid accumulation of above ground biomass, from 8 June to 10 July, resulted in increases in the VH backscatter and VH/VV ratio of 4.0 and 2.43 dB.

In general, VV backscatter also increases slightly during the leaf development and stem elongation phases. This can be explained by an increase in the double bounce between the vertical stalks and the soil [139, 140]. While some studies report an increase in VV backscatter associated with maize biomass [140, 141], others have reported no correlation or even an inverse relation between maize biomass and VV backscatter intensity [13, 142]. The VV and VH backscatter start to plateau as the maize reaches its maximum height and the grain begins to develop (BBCH 71). This is consistent with previous studies showing that radar backscatter from maize parcels tends to saturate around the tasseling stage (BBCH 51) as the LAI reaches values of 2-3 [45, 143, 144].

During the late fruit development (BBCH 75) and ripening stages (BBCH 89) from 23 August until mid September (BBCH 85 to 89), VH backscatter is relatively constant with an average of -16.2 dB. At the same time, the VV backscatter increased slightly from -9.5 to -7.5 dB. The combined effect is a decrease in VH/VV ratio consistent with the conclusion of Vreugdenhil et al. that the dynamics VH/VV reflect changes in vegetation water content [45].

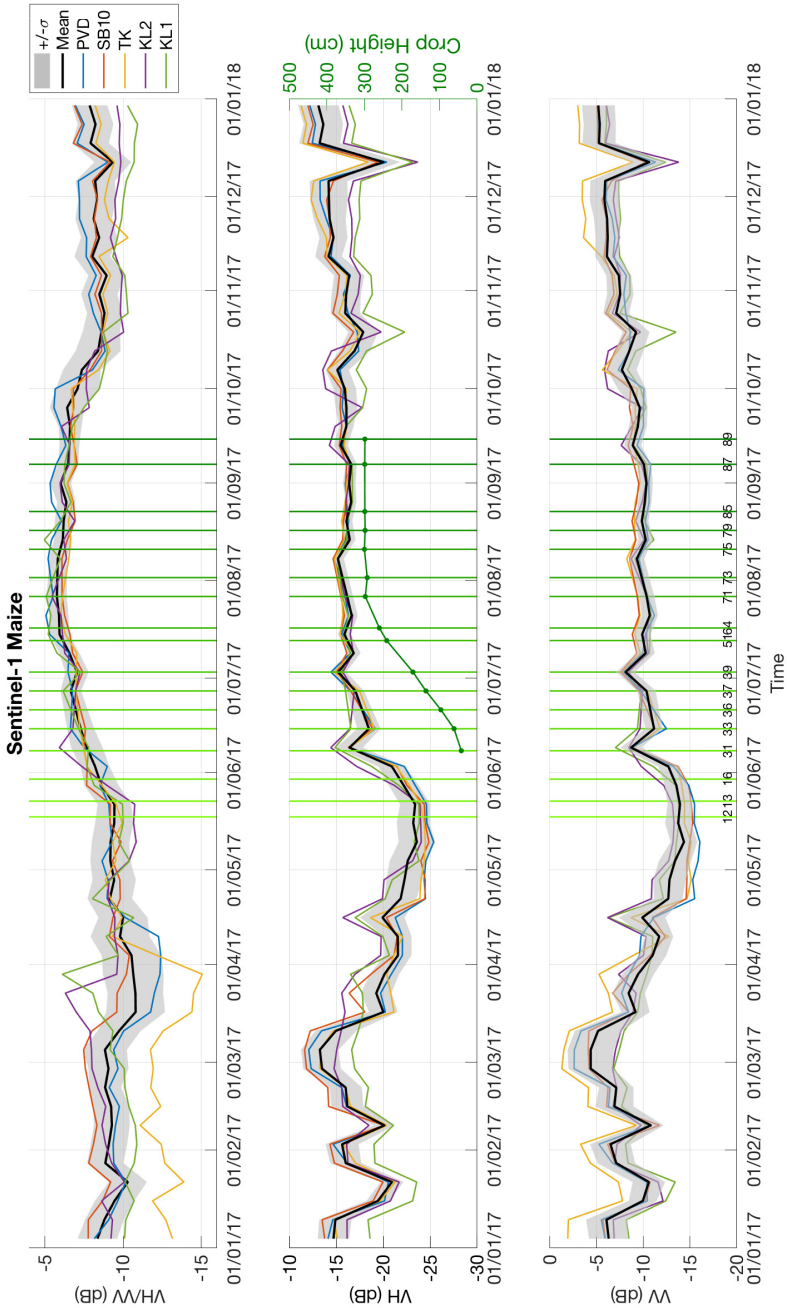


Figure 3.7.: Sentinel-1 backscatter data for all maize parcels in the Flevopolder; (a) VH/VV [dB] (b) VH [dB] and crop height [cm], (c) VV [dB]. The black line and shaded gray areas indicates the mean and +/- one standard deviation across all maize parcels in the domain. The colored data series correspond to individually monitored parcels. Green vertical lines indicate the growth stage according to the BBCH scale [131].

Abrupt decreases in backscatter are observed in the individual parcels on various dates between mid-September and mid-October as maize is harvested. Harvesting reduces the backscatter, particularly in VH, and increases the spread in VV, VH, and VH/VV backscatter among the parcels. Harvesting the vegetation removes the dense maize canopy which reduced the sensitivity of both VV and VH backscatter to soil moisture signal during the growing season [13, 141, 145]. From mid-October onwards, the variability between the parcels remains relatively constant and fluctuations due to precipitation (25 of October and 12 of November 2017) and snowfall (12 of December 2017) are observed.

### POTATO

Fig. 3.8 shows the Sentinel-1 and in-situ data from January 2017 until January 2018 from 886 potato parcels in the Flevopolder. From November to March, the soil is bare so the dynamics in VV and VH backscatter are due to surface soil moisture variations and land management practices (tillage). Similar to the maize time series, the drops in backscatter associated with snow/frozen soil events on 22 of January, 9 February and 12 December 2017 are observed in the potato parcels. The increase in standard deviation of backscatter in both polarizations from mid-March is due to the formation of ridges for potato cultivation. Differences in the orientation of the ridges with respect to the radar look direction results in variations in the backscatter from bare soil.

By the start of the phenological monitoring, the potatoes had already reached BBCH 61 (the beginning of flowering). The rapid increase in both VH and VV backscatter from May 22 onwards corresponds to the period of leaf formation and stem elongation. During this time in the potato plants enters a stage of exponential growth until the ground cover reaches a maximum in the middle of flowering stage at BBCH 63. Above ground biomass stabilizes during the flowering stage (BBCH 63, 27 June). The backscatter stays relatively constant, with only slight variations in VH due to heavy rain on 3 and 15 July and 8 August.

During the fruit development (BBCH 71 to 79) and ripening of fruit and seeds (BBCH 81 to 90) stages, the average height of the plants decreases. Variations in planting date, and field management practices (e.g. ridge structure and nutrient application) mean that the amount of above ground biomass can vary between parcels. Also, the rate at which the plants reach the yellowing and brownish stages varies. Moreover, the reduction in vegetation water content increases sensitivity of the backscatter to the underlying soil layer. Therefore variability in radar backscatter in VV and VH polarizations increase during this time. This is clear from the the increasing standard deviation in backscatter from 10 August to mid-September, particularly in the VH backscatter.

The abrupt decrease in VH backscatter from 13 to 28 September is related to haulming, the process of destroying the haulms (i.e. stalks or stems) prior to harvesting. In the Netherlands, chemical haulming is typically carried out 10-20 days before the intended harvest date to facilitate an equally ripening crop so that all tubers form resilient skin. Destruction of the above-ground plant reduces volumetric scattering and increases sensitivity to surface soil moisture and roughness. Hence the

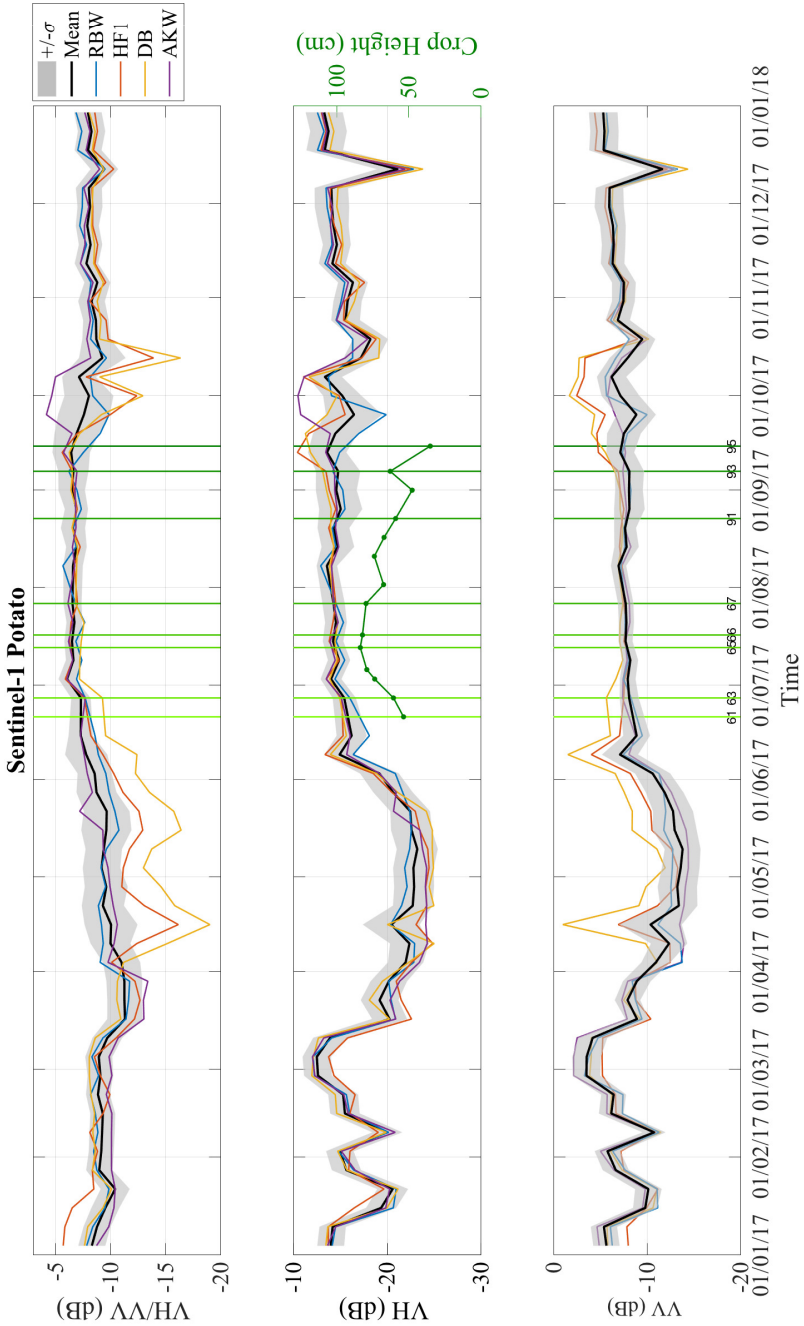


Figure 3.8.: Sentinel-1 backscatter data for all potato parcels in the Flevopolder; (a) VH/VV [dB] (b) VH [dB] and crop height [cm], (c) VV [dB]. The black line and shaded gray areas indicates the mean and  $\pm$  one standard deviation across all potato parcels in the domain. The colored data series correspond to individually monitored parcels. Green vertical lines indicate the growth stage according to the BBCH scale [131].

subsequent increase in variability among the parcels. The rise in radar backscatter from 1 to 10 of October was caused by a rainy period from 29 September until 11 of October during which 67.4 mm of precipitation was observed at the KNMI station at Dronten [127].

The reduction in standard deviation in the VV, VH and VH/VV data after mid-October suggests that harvesting has been completed by that time. The main effect of mechanical harvesting is a perturbation in surface roughness after which the backscatter dynamics are primarily sensitive to soil moisture. This could explain the decrease in backscatter around this time. The combined influence of the changing roughness and increased sensitivity to soil moisture make it difficult to pinpoint the exact harvest time in the backscatter data. In Section 3.3.3 it will be shown that harvest is more readily identifiable using coherence data.

### SUGAR BEET

Fig. 3.9 shows the Sentinel-1 and in-situ data from January 2017 until January 2018 based on 763 sugar beet parcels in the Flevopolder. There are just three BBCH stages noted for sugar beets. The first BBCH stage measurement was during the rosette growth period and the last was when the crop cover was complete (BBCH 39), so the difference observed was primarily a change in ground cover from 60% to 90%. The later stages concern the development of harvestable beet root, and cannot be evaluated from visual inspection of the above-ground plant. Crop height was measured through to September 2017.

During March and April, the standard deviation across the parcels is high due to variations in sowing date, soil roughness and row orientation. The backscatter values start to converge in late May during the leaf development stages. This coincides with a rapid increase in backscatter, particularly in VH as the development of new leaves increases the plant's above-ground biomass. The sugar plant produces broad leaves in both horizontal and vertical direction which leads to an increase in volume scattering. The backscatter in both VV and VH stabilizes in mid-June and remains relatively constant until mid-August, with the exception of the influence of precipitation on 9 June and 8 August. Leaves cover 90% of the ground by 10 July (BBCH 39), so this stability in backscatter is due to stability in the structure and moisture content of the above-ground vegetation. There is limited sensitivity to increases in soil moisture due to smaller precipitation events during this period as the canopy is attenuating the signal from the soil completely. The influence of the larger events on 9 June and 8 August is clear in the VV and VH backscatter but is barely discernible in the VH/VV ratio.

From August to mid-September, there is a noticeable decrease in the average VH/VV, and the standard deviation across parcels increases. This is due to the combined effect of very slight increases in backscatter, particularly in VV. This increase may be due to the increase in soil moisture (Fig. 3.6), and an increased sensitivity to the surface soil moisture as the leaves lose moisture at the end of the summer. The standard deviation across parcels increases considerably from September to December coinciding with the harvest period. Sugar beet is harvested throughout this period. Hence, a sudden drop in the mean backscatter across all

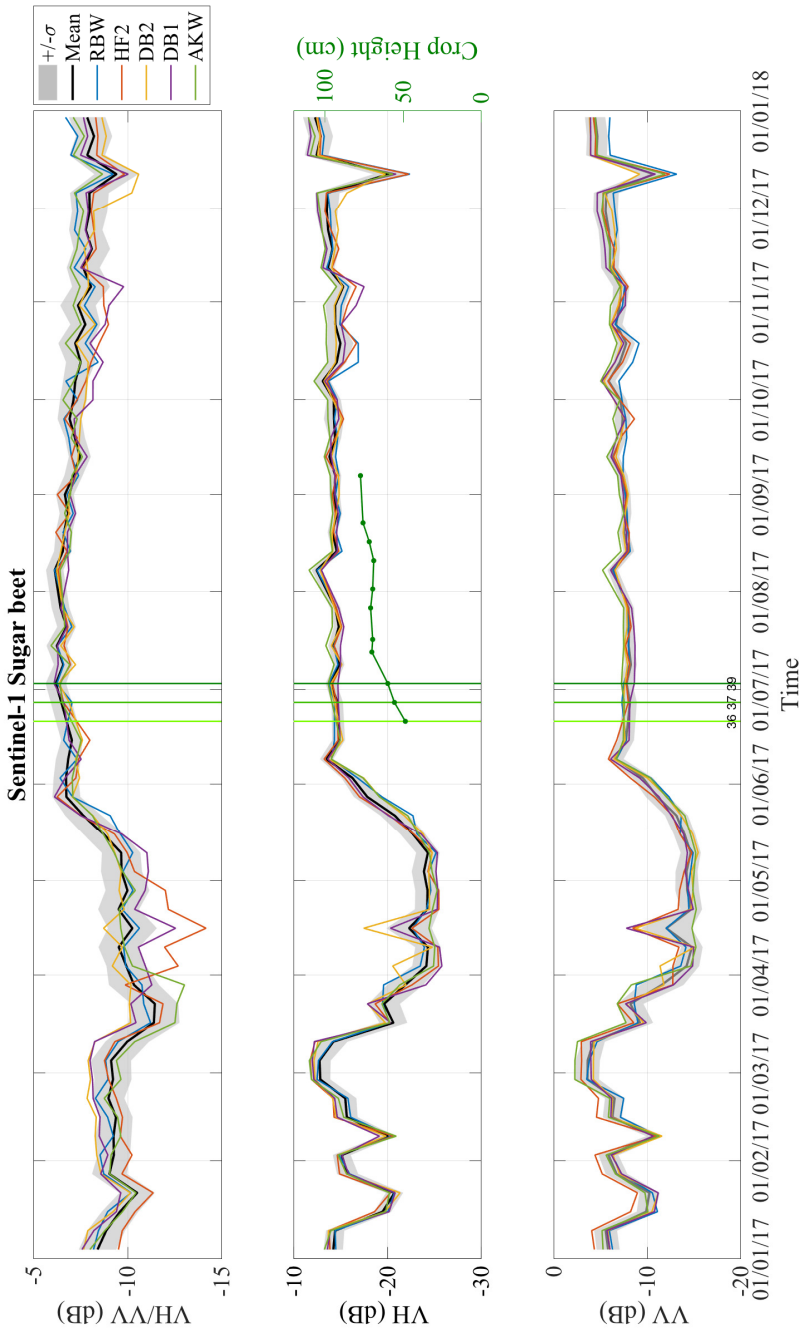


Figure 3.9.: Sentinel-1 backscatter data for all sugar beet parcels in the Flevopolder; (a) VH/VV [dB] (b) VH [dB] and crop height [cm], (c) VV [dB]. The black line and shaded gray areas indicates the mean and  $\pm$  one standard deviation across all potato parcels in the domain. The colored data series correspond to individually monitored parcels. Green vertical lines indicate the growth stage according to the BBCH scale [131].

parcels is not expected. At an individual parcel scale, backscatter may decrease due to harvest. However, in Fig. 3.9 these are difficult to distinguish from fluctuations due to precipitation/soil moisture.

#### WINTER WHEAT

The time series of Sentinel-1 backscatter (VV, VH and VH/VV) and in-situ measurements of crop height and phenological growth stages for 1048 wheat parcels are shown in Fig. 3.10. The wheat was sown from mid-October to mid-November 2016 and harvested in August 2017. Four distinct periods can be identified in the backscatter time series.

From mid-March to mid-May, both VV and VH decrease due to the increase in biomass during the tillering and stem elongation period. VV backscatter is dominated by the direct ground and canopy contributions. The decrease in VV during the stem elongation is therefore attributed to the increasing attenuation due to the predominantly vertical structure of the wheat [13, 45, 146–149]. The decrease observed in VH is less severe than in VV. VH backscatter is influenced by double-bounce between the wheat stems and the ground [31, 146] as well as a volume scattering component [140]. During the tillering and stem elongation periods, the increased attenuation of the double-bounce is countered by an increase in volume scattering from the new biomass [13, 140]. The net effect is an increase in the VH/VV ratio, affirming its suitability as a measure of fresh biomass [45].

From mid-May to 1 June, during the booting and heading periods, VH backscatter remains stable while the VV backscatter starts to increase as the flag leaf opens and the inflorescences emerge. Brown *et al.* [146] found that the C-band VV backscatter during this period was primarily generated by the flag leaves and/or ears when they conducted detailed 3-D imaging of wheat during this growth stage. The booting stage is therefore identifiable as the time at which the increase in backscatter due to stem elongation tapers off, but the VV backscatter increases due to the moisture content of the flag leaves and emerging ears.

From 1 June to 8 August, both VV and VH backscatter increase steadily by 8-9 dB as the winter wheat goes through the flowering, fruit development and ripening stages. This is due to the increased sensitivity to the ground contribution (both direct and double-bounce) as the vegetation loses internal moisture. Mattia *et al.* [147] emphasized the significance of the heading period as a turning point at which the radar backscatter becomes primarily sensitive to soil moisture rather than above ground biomass variations. The VH/VV increases by just 2dB during this period.

Finally, the sudden drop in both VV and VH backscatter between 8 and 14 August is due to the harvest period. After this date, the standard deviation in backscatter between parcels increases. This is due to the diversity in post-harvest land management practices and the sensitivity to surface soil moisture and roughness which varies between parcels.

#### ENGLISH RYE GRASS

Fig. 3.11 shows the Sentinel-1 and in-situ data from January 2017 until January 2018 for 1286 English Rye Grass parcels in the study area. The snow/frozen soil events



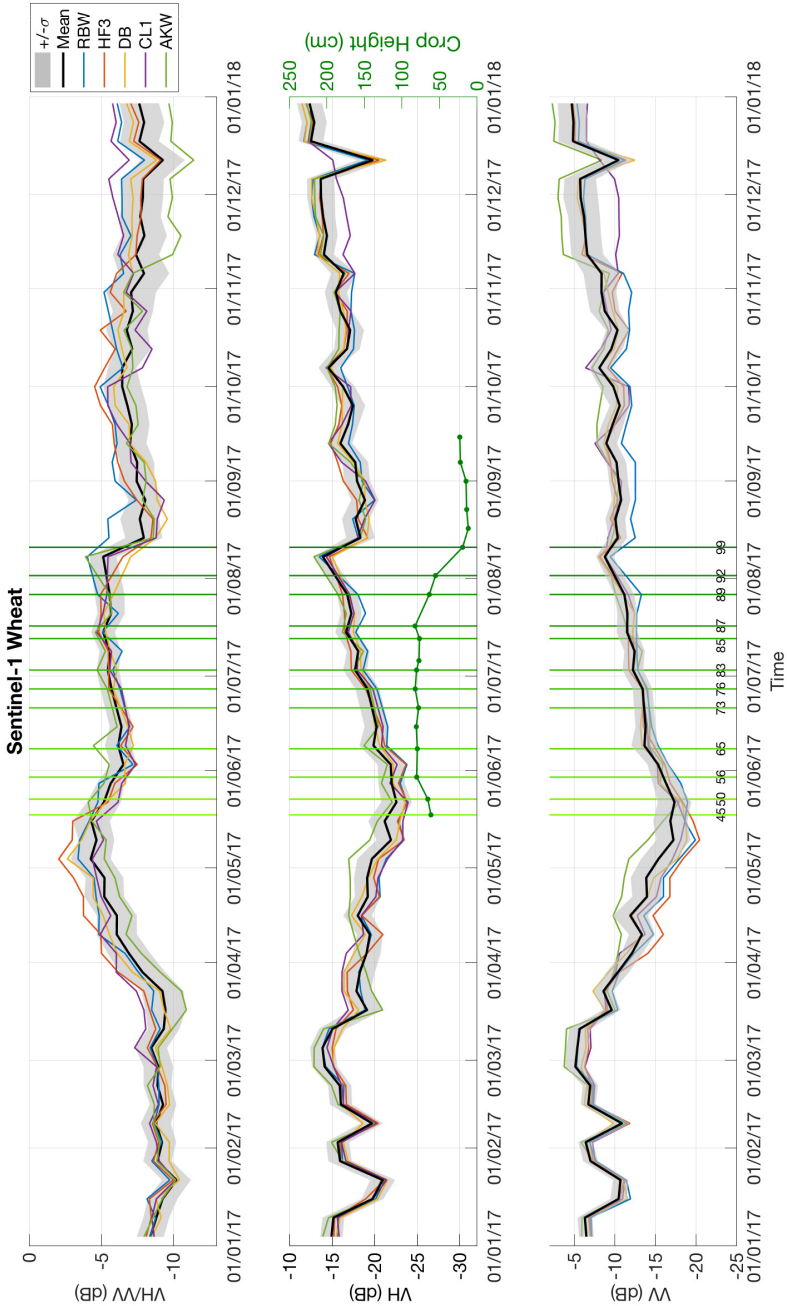


Figure 3.10.: Sentinel-1 backscatter data for all winter wheat parcels in the Flevopolder; **(a)** VH/VV [dB] **(b)** VH [dB] and crop height [cm], **(c)** VV [dB]. The black line and shaded gray areas indicates the mean and +/- one standard deviation across all winter wheat parcels in the domain. The colored data series correspond to individually monitored parcels. Green vertical lines indicate the growth stage according to the BBCH scale [131].

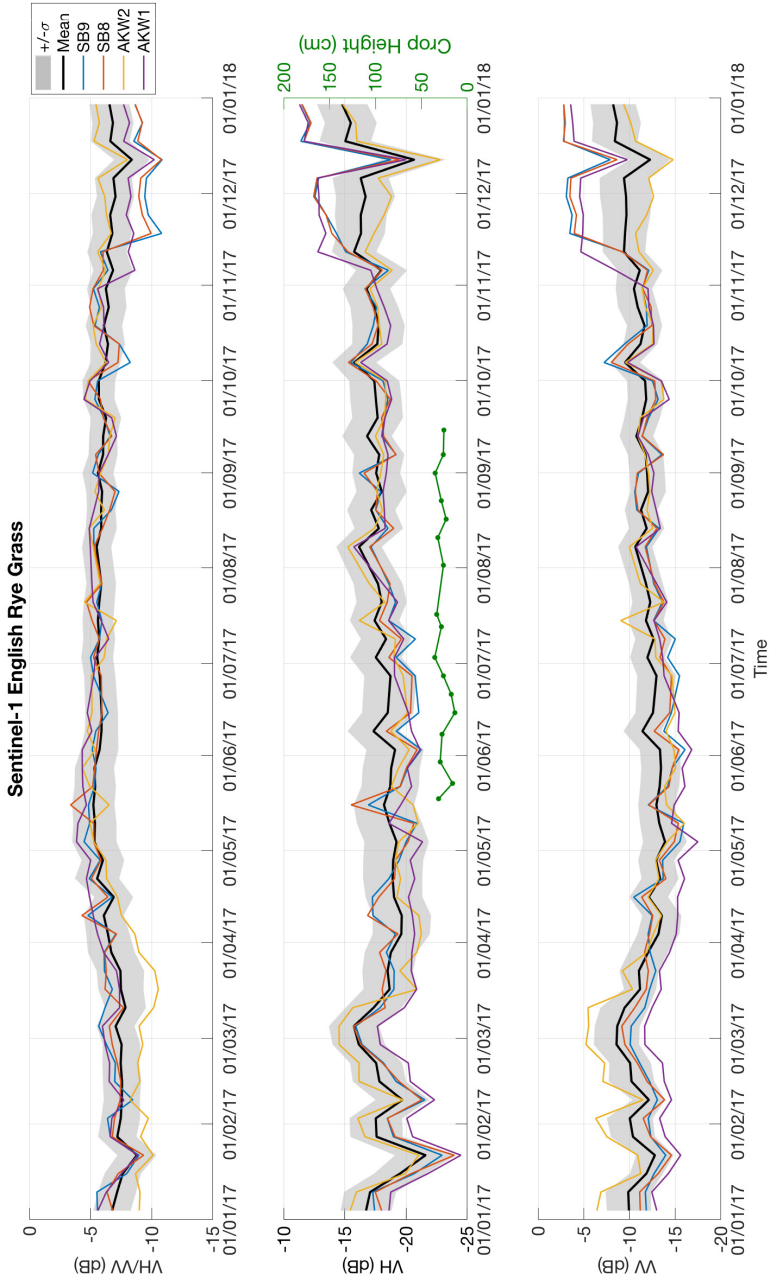


Figure 3.11.: Sentinel-1 backscatter data for all English Rye Grass parcels in the Flevopolder; (a) VH/VV [dB] (b) VH [dB] and crop height [cm], (c) VV [dB]. The black line and shaded gray areas indicates the mean and +/- one standard deviation across all grass parcels in the domain. The colored data series correspond to individually monitored parcels.

on 22 January, 9 February and 12 December 2017 result in dips in the VV and VH backscatter in the grass parcels. The heavy rain events on 9 June, 3 July, 8 August, 13 September and 7 October result in peaks of similar magnitudes in both VV and VH backscatter. The effect of precipitation/soil moisture on the VH/VV ratio is therefore limited, confirming that VH/VV is a good indicator of fresh biomass and vegetation water content [13, 45].

The VH/VV ratio has a limited seasonal cycle due to the presence of grass cover throughout the year. A slight increase is observed in the summer months as the grass responds to increased solar radiation and warmer temperatures. This increase is due to a decrease in both VV and VH backscatter as the increasing fresh biomass attenuates the backscatter from the soil. The decrease in VV is larger than that observed in VH resulting in an increase in VH/VV during this time. Conversely, the lower temperatures from August onwards result in a decrease in biomass and an increase in sensitivity to soil moisture.

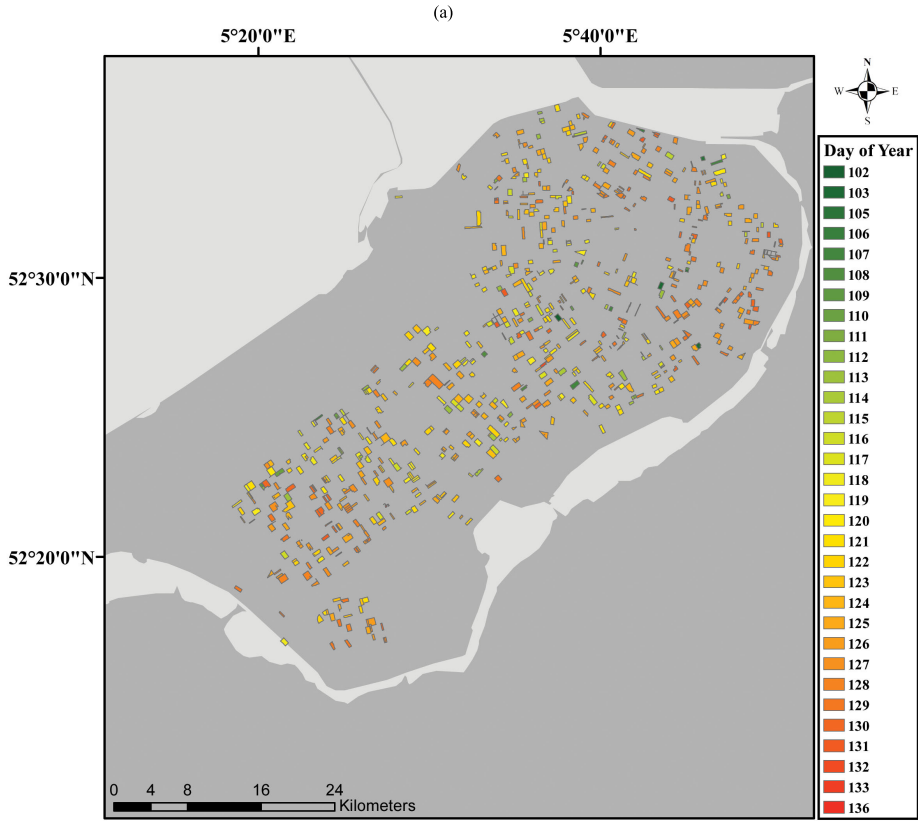
Dips in the grass height observations suggest that mowing occurred around 23 May, 15 June, 13 July, 17 August and 7 September. Slight decreases in VH backscatter are detected after these events. However, backscatter during this period is also influenced by precipitation and soil moisture variations which makes it difficult to distinguish mowing events from soil moisture changes [150].

### 3.3.3. MAPPING KEY DATES

#### EMERGENCE DATE

The sugar beet emergence date was estimated as the point at which the emergence of the first leaves resulted in an increase in volumetric scattering from the vegetation, and hence an increase in VH backscatter. Several relationships were fit to the 6-day Sentinel-1 VH backscatter data from 1 April to 1 July, a period assumed to contain the vegetative stages. The highest goodness of fit (coefficient of determination) was obtained using a third order polynomial. The average goodness of fit across all parcels was  $R^2 = 0.97$ . For each parcel, the emergence date was determined as the minimum of the fitted curve. Results for the entire study area are mapped in Fig. 3.12 (a). The estimated emergence date for 93 % of parcels occurred between day 115 (25 April) and day 130 (10 May) with the remainder emerging either one week earlier or one week later.

The first available photos of the sugar beet parcels are shown in Fig. 3.12 (b) to (e), along with the estimated emergence date. For the RBW parcel in Fig. 3.12 (b), the first pair of leaves is visible (BBCH 12). Therefore it is plausible that shoot emergence (BBCH 9) occurred four days previously. For the other three monitored parcels, the first photo is 10 to 14 days after the estimated emergence date. However, visual inspection of Fig. 3.12 (c) to (e) indicates that these sugar beets were already at BBCH 17 to 19 by the time there were first photographed. The consistency in estimated emergence date across all parcels, together with this limited photo validation suggest that the estimated emergence dates are credible. Similar results obtained for potato and maize are provided in the Fig. B1 to B3 in the Appendix-B.



Field Name:	RBW	HF	AKW	DB
Photo Date:	12/5/2017	18/5/2017	18/5/2017	17/5/2017
Estimated Date:	8/5/2017	4/5/2017	6/5/2017	7/5/2017

Figure 3.12.: Estimated emergence date for sugar beet parcels in Flevopolder; (a) Map of emergence date; (b-e) Photos from monitored parcels in the closest time to emergence date.

### CLOSURE DATE

The closure date was estimated as the date of the maximum of the third order polynomial fit to the data. Results for sugar beet are mapped in Fig. 3.13 (a). The closure date for 93% percent of parcels (710 parcels) was estimated to be between Day 166 (15/06/2017) and Day 171 (20/06/2017). Photos taken from five monitored parcels around the estimated closure dates are shown in Fig. 3.13 (b) to (k). For each of the five monitored parcels, it is clear that closure date occurred between the dates of the photos in the top and bottom rows. The leaves from adjacent rows are several centimetres apart in Fig. 3.13 (b), (c) and (d), but are clearly touching in Fig. 3.13 (g) and (i). In Fig. 3.13 (e), the leaves appear to be almost touching and the estimated closure date is two days later. In the next photo at that location (Fig. 3.13 (j)), the leaves are providing almost full ground cover, so it is plausible that closure is closer in time to the first photograph.

In practice, closure date is also determined by visual inspection and is an inherently subjective measure. Additional photos around the expected closure date, and a larger number of photos distributed across the study domain are essential to draw a more robust conclusion. However, the limited range of estimated closure dates, their timing and the agreement with photographs from the field suggest that this method provides a reasonable estimate of the closure date.

### SUGAR BEET HARVEST DATE

Fig. 3.14(a) shows an example of parcel-averaged NDVI from 6 August to 30 November 2017 estimated from Sentinel-2 imagery. This parcel is chosen because it is known that it was harvested before 15 September. The parcel-averaged coherence between pairs of Sentinel-1 VV images is shown in blue for the same period. The coherence reported for a given date indicates the coherence between the image on that date and its predecessor.

The NDVI is greater than 0.7 until 3 September and decreases to around 0.1 by 15 September. This is consistent with the parcel being harvested between these dates. The coherence between images is low ( $< 0.3$ ) in the period when the NDVI is high. This is to be expected in a vegetated field where movement of leaves, fluctuations in water content and structure, and variations in soil moisture or leaf surface water result in phase differences between consecutive images. Conversely, in October and November when the NDVI is close to zero, the coherence is generally above 0.6 as the scene is comparatively stable. Therefore, harvest is associated with a significant increase in coherence. Occasionally, the coherence decreases when soil moisture variations result in phase differences between consecutive images.

The high coherence on 19 September suggests that the phase differences were small between 13 and 19 September, i.e. that harvest occurred between 7 and 13 September.

Fig. 3.14 (b) shows a box plot of the parcel-averaged coherence for all 763 sugar beet parcels in the study area during the same period. The coherence is generally below 0.4 until 13 September, suggesting that all parcels are covered in vegetation. From 7 October onwards, the median slowly increases until it reaches almost 0.9 by 30 November and the interquartile range (IQR) gradually shifts towards higher

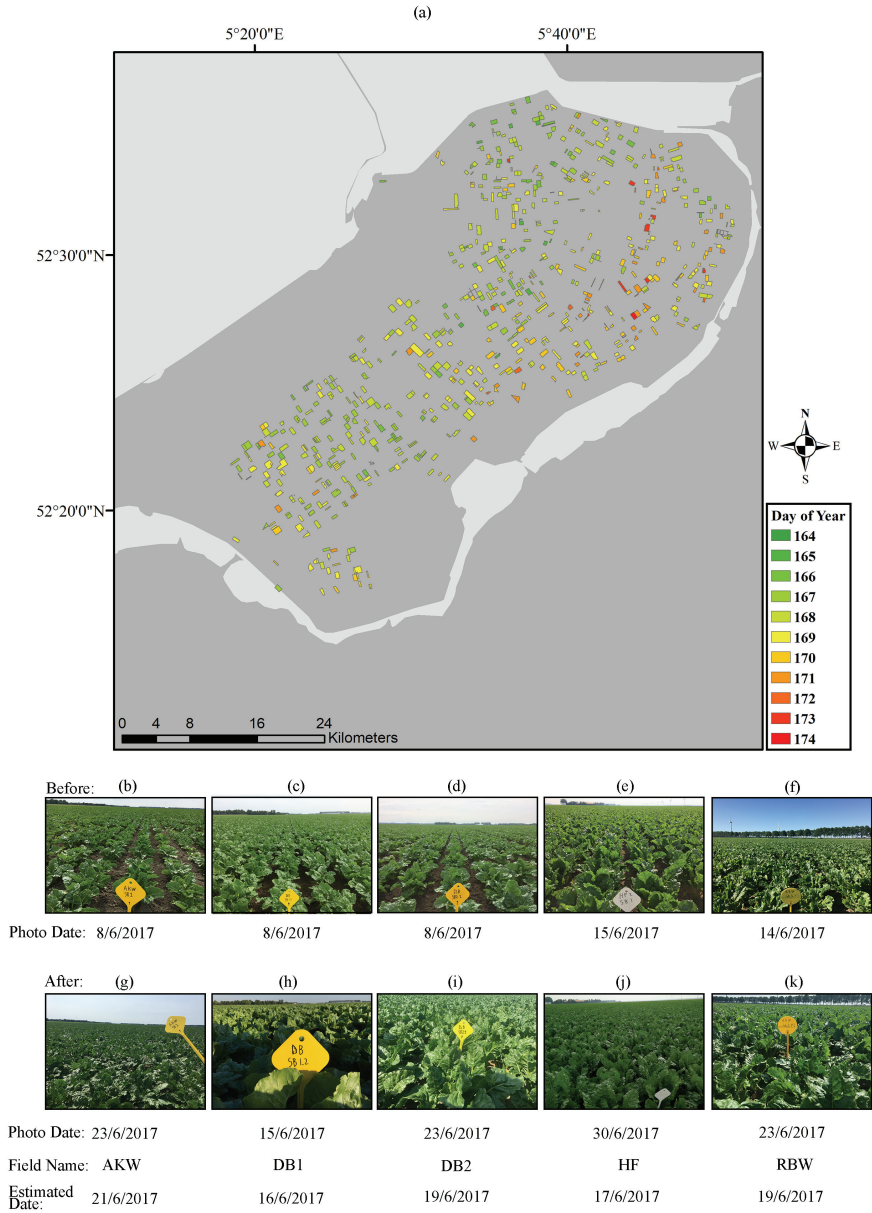


Figure 3.13.: Estimated closure date for sugar beet parcels in Flevopolder; (a) Map of closure date; (b-f) Photos from monitored parcels in the closest time before closure date; (g-k) Photos from monitored parcels in the closest time after closure date.

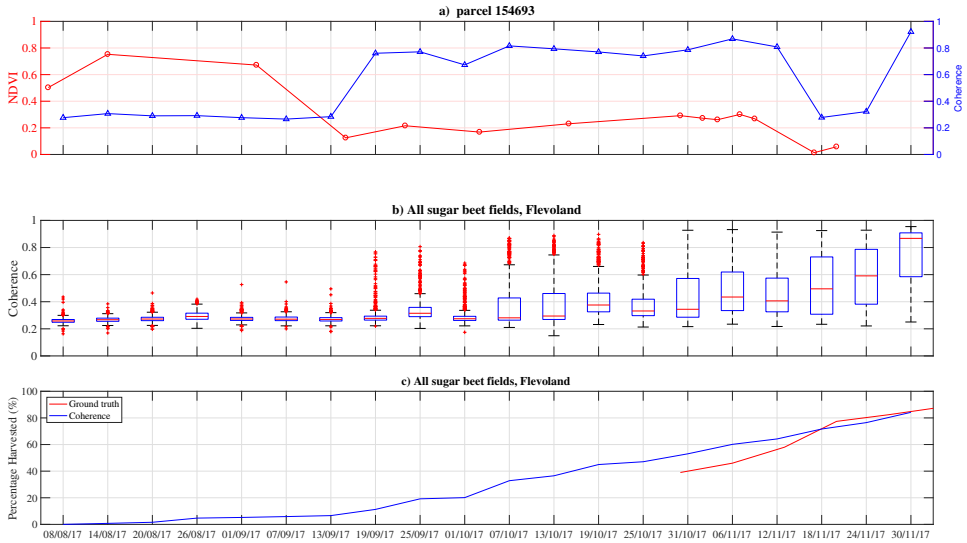


Figure 3.14.: Harvest date for Sugar beet parcels in Flevopolder; (a) NDVI and Coherence time series for monitored parcel 154693; (b) Box plot time series of mean coherence for all 763 sugar beet parcels; The central mark indicates the median, and the bottom and top edges of the box indicate the 25th and 75th percentiles, respectively. (c) percentage of all sugar beet harvested parcels.

values. From 19 September to 25 October, there are so few parcels with high coherence that they are considered outliers of the distribution. By 30 November, the entire IQR has a coherence greater than 0.6 suggesting that most of the parcels have been harvested.

Fig. 3.14 (c) shows the results from a simple rule-based classification formulated based on the results in Fig. 3.14 (a) and (b). An increase in coherence is considered significant if it is greater than 1.5 times the standard deviation of coherence during the reference vegetated period (6 August - 6 September). Coherence values of 0.5 are considered "high". In Fig. 3.14 (c), a parcel is considered harvested when the coherence undergoes a significant increase and reaches a "high" coherence value.

The red curve is the percentage of harvested parcel observed estimated by field agents/SuikerUnie. The two estimates converge after 18 November, and both suggest that 85 % of parcels have been harvested by 30 November. Prior to that date, the rule-based approach estimates a higher percentage of harvested parcels. One contribution to the mismatch in Fig. 3.14 (c) is that the coherence is averaged to parcel level before the rule-based classification. This leads to ambiguities if the parcel is not all harvested at once, something quite common in this study area.

### POTATO HAULMING AND HARVEST DATE

Fig. 3.15 shows a box plot similar to Fig. 3.14 (b) for all potato parcels in the study area. The median coherence is less than 0.3 throughout August during the ripening and senescence stages as the loss in moisture content and associated changes in structure cause phase differences between consecutive images. The median coherence between images on 13 and 19 September is 0.5, suggesting that a transition to a more stable scene occurred between 7 and 13 September. Recall from Fig. 3.8 that there was a decrease in mean backscatter from mid-September and an increase in the standard deviation of backscatter across the potato parcels. Together, Fig. 3.8 and 3.15 suggest that haulming occurred during this period. Harvesting can typically be expected around 10-20 days later. However, frequent rainfall in September and October produced some decreases in coherence during these months. This precipitation also possibly delayed harvest to longer than 20 days after haulming. Nonetheless, increases in coherence generally increase during October. Coherence values greater than 0.6 from 31 October onwards suggest that most parcels were harvested before 25 October.

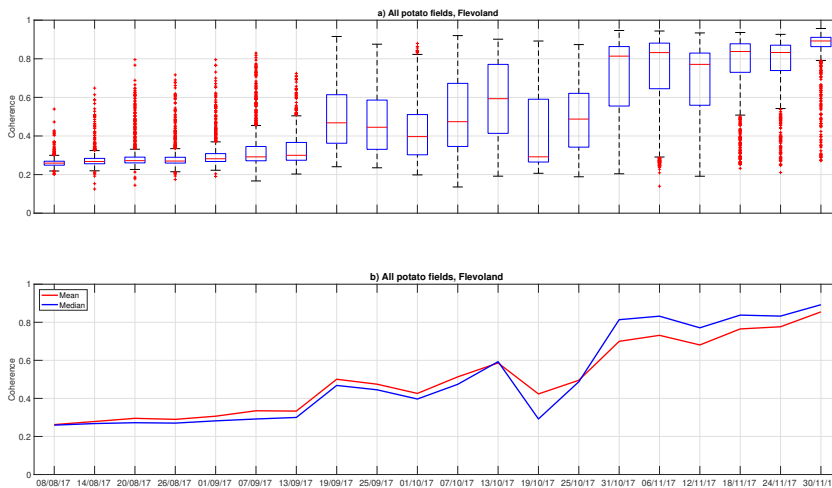


Figure 3.15.: Haulming and harvest date for Potato parcels in Flevopolder.

## 3.4. CONCLUSIONS

Results presented here illustrate the potential of Sentinel-1 SAR backscatter and interferometric coherence for crop monitoring and the detection of key dates for important agricultural crops in the Netherlands. Furthermore, the prevalence of rainy (and cloudy) conditions during this growing season underscore the need to use Sentinel-1 data by itself, or combined with optical data to provide timely and reliable information on crop monitoring in the Netherlands.



Time series analyses showed that, for each of the crops considered, structural and biomass changes associated with crop development influenced the backscatter throughout the season. Similar to the results of Vreugdenhil (2018) and Veloso (2017), the VH/VV ratio proved to be particularly useful as it reduces the influence of soil moisture. It is particularly sensitive to the increase in fresh biomass during the vegetative stages, and decreases during senescence as the vegetation water content decreases.

Key dates such as emergence and closure dates were estimated by fitting polynomials to the time series of backscatter, and were validated using field photos. Harvest detection proved to be more difficult in all crops apart from wheat. For sugar beet and potato, coherence data were needed to detect the harvest date.

# 4

## THE INFLUENCE OF SURFACE CANOPY WATER ON THE RELATIONSHIP BETWEEN L-BAND BACKSCATTER AND BIOPHYSICAL VARIABLES IN AGRICULTURAL MONITORING

*Chapter 3 illustrates the capability of radar data for monitoring agricultural activity throughout an entire growing season. Radar data, while unaffected by atmospheric conditions and capable of cloud penetration, is sensitive to the presence of water on the surface of the canopy. Despite this, the influence of surface canopy water (SCW) on the relationship between radar backscatter and crop biophysical parameters remains unexplored. Therefore, the aim of this chapter is to quantify the influence of SCW on the relationship between L-band radar backscatter and biophysical variables of interest in agricultural monitoring. Results indicate that the presence of SCW can increase radar backscatter by up to 2-3 dB and affect the relationship between radar observations and crop biophysical variables. The findings presented underscore the necessity of considering the influence of SCW when retrieving biophysical variables relevant to agricultural monitoring. They particularly emphasize the significance of overpass time, as well as the impact that daily patterns in dew and interception, can have on the retrieval of such variables.*

---

This chapter is based on:

Khabbazan, Saeed et al., "The influence of surface canopy water on the relationship between L-band backscatter and biophysical variables in agricultural monitoring." *Remote Sensing of Environment* 268 (2022): 112789. [102]

## 4.1. INTRODUCTION

Quantification of crop biophysical parameters is essential for many applications including agricultural management, yield forecasting, crop health monitoring and soil moisture estimation. Providing continuous and reliable crop information enables farmers and food producers to implement timely interventions to maximize yields and make optimal use of resources. Satellite data are increasingly used to estimate crop biophysical parameters such as Leaf Area Index (LAI) [26, 43, 151–153], crop height [42, 43, 154], dry biomass [43, 144, 151, 153, 155] and Vegetation Water Content (VWC) [5, 156, 157]. LAI is related to crop productivity and growth [1] and is a vital input parameter for crop growth and yield forecasting models [26, 158]. Crop height and dry biomass are also important indicators for crop development [154], crop identification and crop yield estimation [17]. VWC can provide information to support irrigation management [159, 160] and drought assessment [161, 162], and is an essential parameter in soil moisture retrieval [38, 84, 163]. Vegetation Optical Depth (VOD) is increasingly used for vegetation monitoring in agricultural applications and natural ecosystems [30, 164, 165].

Low frequency (1-10 GHz) radar data are not affected by atmospheric conditions, can penetrate clouds and can acquire data during day and night. Radar observations are sensitive to dielectric and geometric properties of crops such as vegetation water content, leaf size, stem density, as well as the moisture and roughness of the underlying soil. Furthermore, microwaves penetrate the canopy, with lower frequencies penetrating deeper into the canopy and the underlying soil. As a result, radar data are well suited to monitor soil and vegetation in agricultural applications [5, 17]. Many ground-based experiments and campaigns based on airborne and satellite data have demonstrated the value of low frequency radar data in agricultural applications such as crop monitoring and classification, soil moisture estimation, and extracting bio- and geo-physical parameters from radar data [5, 17, 124]. Several studies have investigated the sensitivity of radar backscatter to biophysical parameters of crops (e.g. [26, 27, 166]). Others have shown that L-band backscatter coefficients and RVI are highly correlated with VWC [167–170], LAI [152, 171, 172] and the fresh weight of various crops [168, 171]. The launch of ESA's Sentinel-1 mission in 2014 and Radarsat Constellation Mission (RCM) in 2019 provide high temporal resolution SAR data with revisit time of 6-12 days and 4 days respectively. This unprecedented revisit time has accelerated the use of radar observation for monitoring temporal variability in agricultural areas [13, 28–30, 37, 44–46, 64, 121]. However, little attention has been paid to the potentially confounding influence of surface canopy water (SCW) on retrieval of crop biophysical parameters. The SCW is generally referred to the presence of water in a form of dew or interception on the canopy surface.

The aim of this chapter, therefore, was to quantify the influence of SCW on the relationship between radar observables and geophysical variables. The analysis was based on L-band data collected in an intensive field campaign during an entire growing season of corn. L-band data are particularly relevant in the context of the future availability of L-band SAR data from NISAR [173] and ROSE-L [174]. In this chapter, first the effect of SCW on different radar observables

such as co- and cross-polarization data ( $\sigma_{VV}$ ,  $\sigma_{HH}$ ,  $\sigma_{XP}$ ), polarimetric ratio data ( $\sigma_{VH}/\sigma_{VV}$  and  $\sigma_{HV}/\sigma_{HH}$ ), and Radar Vegetation Index (RVI) was investigated. Then, correlation analyses were conducted between these radar observables and dry biomass, Vegetation Water Content (VWC), plant height and Leaf Area Index (LAI) at different growth stages of the corn plant. Finally, Vegetation Optical Depth (VOD) was estimated in each polarization, and the effect of SCW on VOD estimation from L-band radar data was investigated.

## 4.2. DATA AND METHODS

### 4.2.1. FIELD EXPERIMENT

#### STUDY AREA

This research conducted over corn field during a field campaign near Citra, Florida at the Plant Science Research and Education Unit (PSREU) of the University of Florida and the Institute of Food and Agricultural Sciences (UF|IFAS). For detailed information regarding the study area specific to this part of the research, please refer to section 2.1 of this thesis.

#### HYDROMETEOROLOGY

For detailed information regarding the hydrometeorology data specific to this part of the research, please refer to sections 2.3.1 to 2.3.3 of this thesis.

#### GROUND VEGETATION SAMPLING

For detailed information regarding the ground vegetation sampling data specific to this part of the research, please refer to section 2.3.4 of this thesis.

### 4.2.2. RADAR DATA

Radar backscatter was measured using the truck-mounted University of Florida L-band Automated Radar System (UF-LARS) [106]. For detailed information regarding the radar data specific to this part of the research, please refer to section 2.2 of this thesis.

## 4.3. METHODOLOGY

### 4.3.1. RADAR DATA

In addition to analyzing the radar backscatter itself, time series of Radar Vegetation Index and Cross Ratio were also considered. The RVI is calculated using:

$$RVI = \frac{8\sigma_{VH}}{\sigma_{HH} + \sigma_{VV} + 2\sigma_{VH}} \quad (4.1)$$

where  $\sigma_{HH}$ ,  $\sigma_{VV}$  and  $\sigma_{VH}$  are the observed linear backscatter intensities [-]. Here,  $\sigma_{XP}$  which is the average of  $\sigma_{VH}$  and  $\sigma_{HV}$  is used instead of  $\sigma_{VH}$ .

The RVI was first introduced by Kim and van Zyl [175] and is often used to monitor vegetation growth [39, 64, 167, 176], map vegetation cover [39, 177], and monitor crop development [167, 178]. RVI is a (dimensionless) normalized index that ideally varies between zero (bare soil) and one [179].

The cross ratios  $CR_H$  and  $CR_V$  are defined as  $\sigma_{XP}/\sigma_{HH}$  and  $\sigma_{XP}/\sigma_{VV}$  in the linear domain respectively [45]. Recall that the average of  $\sigma_{VH}$  and  $\sigma_{HV}$  is used as the cross-polarized backscatter ( $\sigma_{XP}$ ) here. Hence, the only difference between the  $CR_H$  and  $CR_V$  here is in the denominator. CRs and RVI are less sensitive to surface soil moisture variations [13, 45, 121] and are considered useful indicators of crop growth [13, 26, 45, 121, 167].

The influence of SCW on radar observables was quantified by comparing radar observations from early morning (6 am) to the first observations after SCW had dissipated. Generally this occurred at around 10 am. Spearman's rank correlation coefficient ( $\rho$ ) was used to quantify the effect of SCW on the relationship between six radar observables and four plant biophysical parameters.

#### 4.3.2. VEGETATION OPTICAL DEPTH (VOD) ESTIMATION

The VOD estimation approach is based on that of Vreugdenhil *et al.* [33], where the VOD can be estimated from the decrease in sensitivity of backscatter over bare soils as a result of vegetation. Fig. 4.1 shows an illustrative time series of backscatter in a vegetated area. The upper and lower limits of the backscatter time series are referred to as the wet reference ( $\sigma_{wet}^0$ ) and dry reference ( $\sigma_{dry}^0$ ) respectively. The wet reference corresponds to the backscatter values one would obtain under saturated soil conditions. The dry reference at some time  $t$  ( $\sigma_{dry}^0(t)$ ) is the value corresponding to backscatter from a completely dry soil. It is a combination of a static component ( $\sigma_{s,dry}^0$  e.g. due to soil texture, roughness etc.) and a dynamic component due to vegetation phenology. Vegetation growth leads to an increase in the dry reference, which indicates that the change in backscatter in response to a given change of soil moisture is assumed to be less than that during the bare soil period [180]. Note that this implicitly assumes that any change in the sensitivity to soil moisture is entirely due to the change in attenuation, and neglects any changes in double bounce or multiple-scattering.

The vegetation optical depth (VOD) is a measure of the degree to which the vegetation attenuates backscatter from the soil, and is a parameter of the Water Cloud Model [84]. Vreugdenhil *et al.* [33] showed that the VOD can be expressed at any time step as the difference between the sensitivity of backscatter to soil moisture changes in bare soils and the observed sensitivity attenuated by the vegetation in terms of the dry and wet reference as follows:

$$VOD(t) = \frac{-\cos\theta}{2} \ln\left(\frac{\sigma_{wet}^0 - \sigma_{dry}^0(t)}{\sigma_{wet}^0 - \sigma_{s,dry}^0}\right) \quad (4.2)$$

The value of  $\sigma_{wet}^0$  was determined by averaging the highest backscatter values observed during the soil moisture peaks throughout the season. Vreugdenhil *et al.* [33] used the Integral Equation Method to model backscatter and, in particular, to

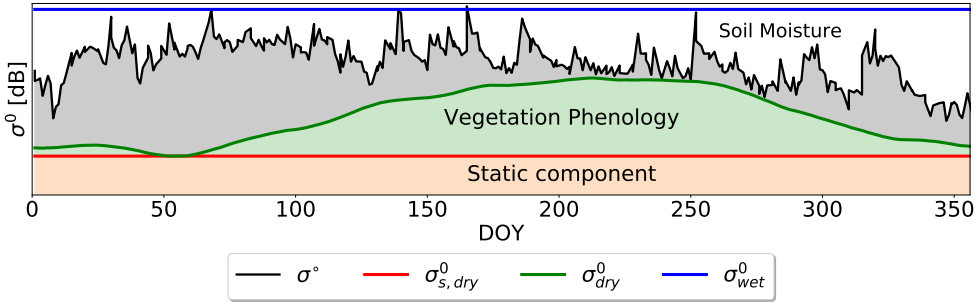


Figure 4.1.: Illustration of the wet reference ( $\sigma_{wet}^0$ ), and static components ( $\sigma_{s,dry}^0$ ) and dynamic components of the dry reference ( $\sigma_{dry}^0$ ) as three components of the TU Wien soil moisture retrieval method along with radar backscatter coefficient [34].

estimate  $\sigma_{s,dry}^0$ . In this research, the tower-based measurements of radar backscatter are combined with in situ soil moisture data to estimate the dry reference. Following Wagner, Lemoine, and Rott [180] and Attema and Ulaby [84], it is assumed that for a given vegetation water content, radar backscatter and soil moisture are linearly related. VWC influences the slope of this linear relationship. Therefore, a linear fit is obtained for a dynamic window (1-3 days) during which it is assumed that VWC is relatively constant. The dry reference  $\sigma_{dry}^0(t)$  varies in time due to vegetation growth, so it was obtained by fitting a linear model between backscatter and soil moisture during a moving window, and extrapolating to determine the backscatter that would correspond to a completely dry soil. The static component of the dry reference ( $\sigma_{s,dry}^0$ ) was estimated based on the backscatter data from 1 to 3 May. This corresponds to the period after planting (April 13) and during the formation of the first leaves (see Table 2). Estimating  $\sigma_{s,dry}^0$  during this period, rather than the bare soil period directly after planting, ensures that the soil surface has been smoothed by several irrigation events (see Fig. 4.4 (b) and (c)), and that the roughness controlling  $\sigma_{s,dry}^0$  is as close as possible to roughness under the growing canopy. The length of the dynamic window for the estimation of  $\sigma_{dry}^0(t)$  was obtained using a rule-based decision tree. The window should be as short as possible to minimize the variations in vegetation water content. However, it needs to be long enough to ensure that there is some variation in soil moisture (and backscatter), and that sufficient data are included to obtain a reasonable goodness of fit, defined here as  $R^2 > 0.7$  and  $P < 0.05$ . The leaf wetness sensor data were used to distinguish between backscatter data obtained in the presence (wet) or absence (dry) of SCW due to dew or interception. The dry reference was determined separately for these two conditions. Hence, two time series of VOD were obtained.  $VOD_{dry}$  indicates the attenuation due to internal vegetation water content alone. It is the estimate of VOD obtained in the absence of any SCW.  $VOD_{wet}$  is the estimate of VOD based on observations obtained when SCW was present due to dew or interception.

## 4.4. RESULTS

### 4.4.1. HYDROMETEOROLOGICAL DATA

#### WEATHER DATA

Daily precipitation and irrigation and 15-minute air temperature, relative humidity, and solar radiation are presented in Fig. 4.2. The early season (26 April to 18 May) was hot and dry with strong daily cycles in air temperature and relative humidity. Irrigation was applied at midnight on 8 occasions to ensure moisture availability for plant growth. During the mid-season (19 May to 30 May), rainfall occurred on most days with three particularly heavy rainfall events on 21, 27 and 30 May. Nighttime temperatures were generally warmer than in the early season, so the amplitude of the daily temperature cycle was less than during the early season. The late-season was dry and warm with high temperatures and solar radiation and a few small rain events.

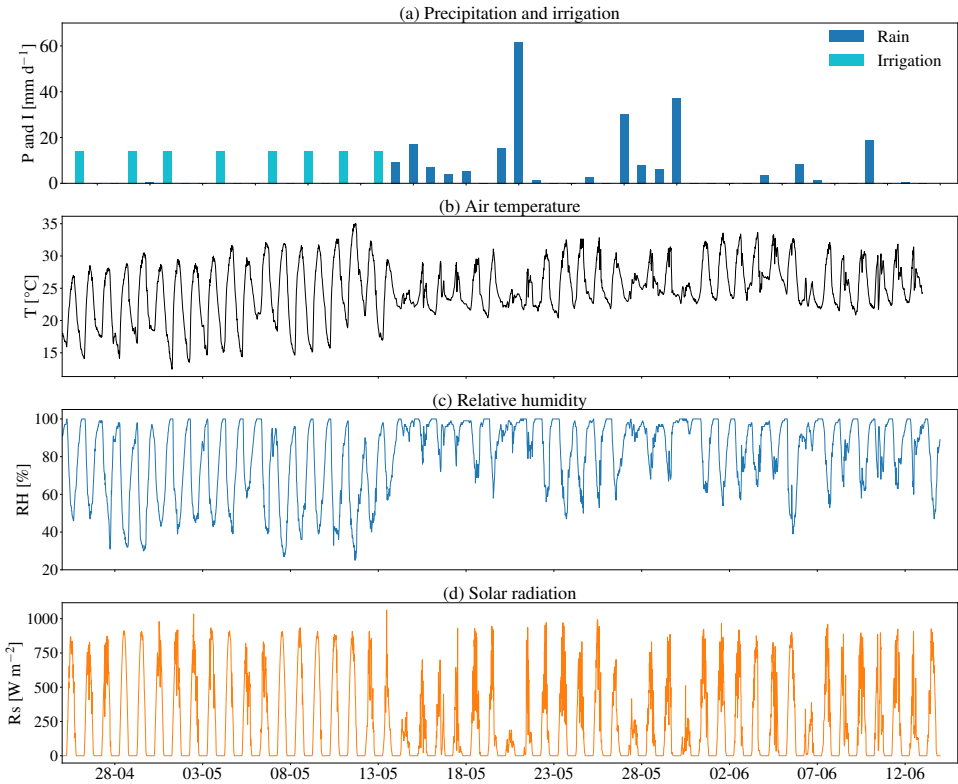


Figure 4.2.: Time series of meteorological data collected by Florida Automated Weather Network: a) daily rainfall and irrigation ( $mm d^{-1}$ ), b) air Temperature at 2-meter height ( $^{\circ}C$ ), c) relative humidity at 2-meter height (%) and d) solar radiation at 2-meter height ( $W m^{-2}$ ).

### ROOT ZONE SOIL MOISTURE

Fig. 4.3 shows the volumetric soil moisture ( $\theta$ ) at five depths. In general, soil moisture at 5 and 10 cm were highly affected by irrigation and precipitation events, while the soil moisture content was mostly stable at 20, 40, and 80 cm depth. The soil moisture at 80 cm depth was only affected by very heavy rainfall events. The effect of midnight irrigation during the early season can be seen as a rapid increase in 5 cm and 10 cm soil moisture, followed by a clear dry down. The soil moisture at 20 cm was slightly affected by irrigation events, but the water did not infiltrate to the sensors at 40 and 80 cm. During the mid-season, heavy rain events led to several abrupt increases throughout the root zone. Three intense rain events from 21 May to 1 June resulted in higher soil moisture content at 10 and 20 centimeters compared with soil moisture at 5 centimeters. The dry period from 2 June to 11 June resulted in a significant decrease in soil moisture at all depths. The minimum soil moisture observed in situ was  $0.107 \text{ m}^3 \text{ m}^{-3}$ . This value will be considered as "dry soil" for the estimation of the dry reference.

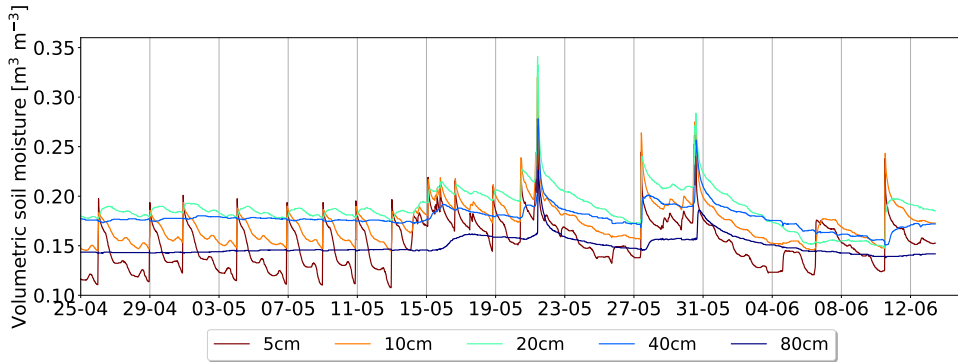


Figure 4.3.: Averaged volumetric soil moisture ( $\text{m}^3 \text{m}^{-3}$ ) from two pits on different depths (5, 10, 40, and 80 cm).

### INTERCEPTION AND DEW DATA

Fig. 4.4 shows the presence and duration of water on the leaf wetness sensors at three different heights. Fig. 4.4 (a), (b), and (c) show results from the sensor installed at the upper, middle and lower canopy respectively.

During the early season, the canopy surface wetness was related to the presence of dew and midnight irrigation practices. During the mid-season, the surface of the canopy was mostly wet due to the frequent rain events. Fig. 4.4 (d) shows the number of days on which SCW (dew or interception of precipitation/irrigation) was present as a function of time of day. Dew is almost always present from midnight until around 10 am. The presence of SCW is 3.05 times more likely between 12 AM and 10 AM than between 11 AM and 11 PM.



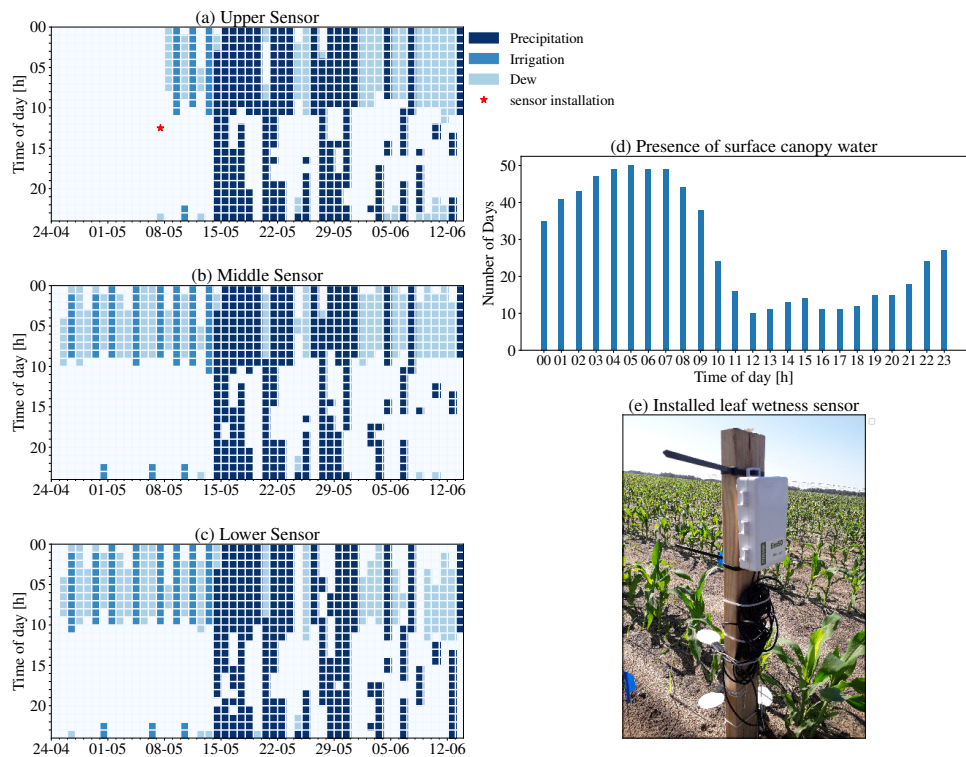


Figure 4.4.: Presence of SCW resulted from precipitation, irrigation, and dew on detected from a) upper sensor, b) middle sensor c) lower sensor. The red star on 7 May shows the installation date for the upper sensor. Colored squares represent detection of water in the sensors for at least 15 min during that hour. d) The percent of days that SCW was presented at each hour of the day. e) The picture of leaf wetness sensors at early stage.

#### 4.4.2. CROP DEVELOPMENT

Data on crop development are shown in Fig. 4.5 and Table 4.1. While corn height continued to increase until the end of the season, the LAI reached its maximum value around 23 May. Slight variations in LAI are observed after this date due to variability within the field. However, leaf VWC (Fig. 4.5 (a)) and leaf dry biomass (Fig. 4.5 (b)) suggest that leaf formation stabilized after this date. On 23 May, the dry biomass of both stems and leaves was almost equal but the stems account for 65% of the total VWC. The formation of corn ears at the start of June is clear from the increase in both dry biomass and ear water content. The stem VWC decreases by around 30% ( $-0.8 \text{ kg m}^{-2}$ ) from 1 to 8 June due to a combination of ear formation and separation, the decline in root zone soil moisture due to warm and dry weather conditions, and the start of senescence.

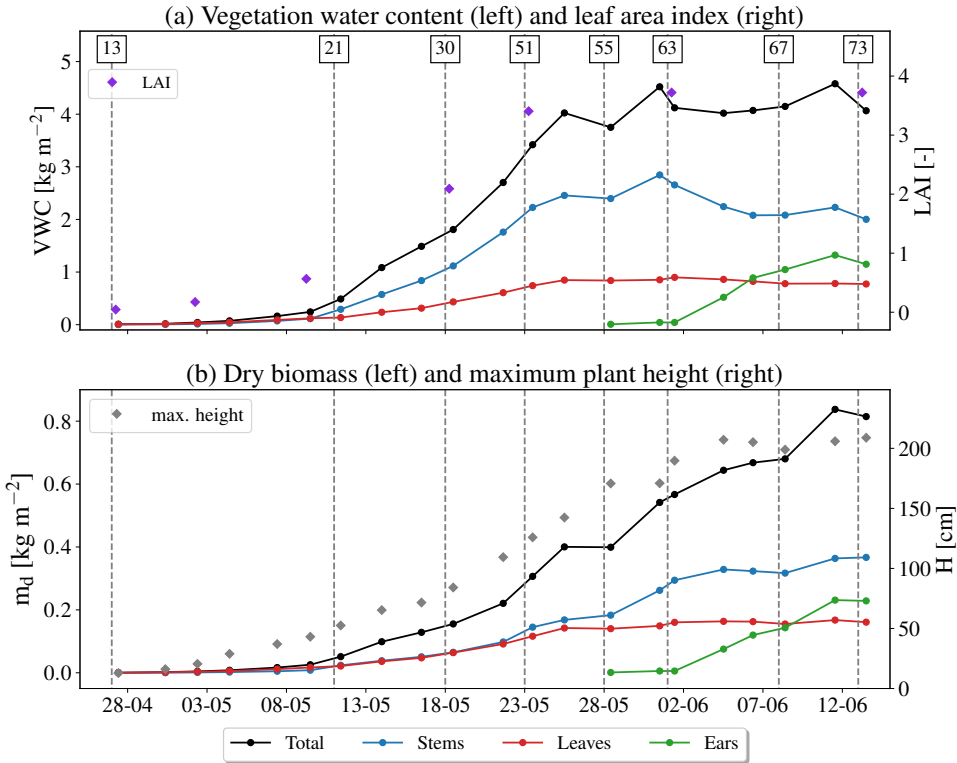


Figure 4.5.: Seasonal pattern of (a) vegetation water content ( $kg\ m^{-2}$ ) per constituents and leaf area index, and (b) dry biomass ( $kg\ m^{-2}$ ) per constituents and canopy height (cm). Phenological stages are shown by BBCH codes, which are explained in Table 4.1.

Table 4.1.: Description of BBCH codes and growth stages of sweet corn

Period	Date	DAP	BBCH	Description
2*Early Season	Apr 27	14	13	Leaf development - 3 leaves (V)
	May 11	28	21	Beginning of tiller formation (V)
3*Mid Season	May 18	35	30	Beginning of stem elongation (V)
	May 23	40	51	Beginning of tassel emergence (V)
	May 28	45	55	Middle of tassel emergence (V)
4*Late Season	2*Jun 1	2*49	2*63	Male: Beginning of pollen shedding (R) Female: tips of stigmata visible (R)
	Jun 8	56	69	End of flowering (R)
	Jun 13	61	73	Development of suit - Early milk (R)

V = Vegetative stage ; R = Reproductive stage.

#### 4.4.3. TIME SERIES OF L-BAND BACKSCATTER AND DERIVED INDICES

Fig. 4.6 (a) shows the seasonal variation in the observed radar backscatter. The increasing trend in backscatter during the early stage (27 April to 18 May) is due to crop growth. It is particularly clear in XP and VV, which are less sensitive than HH backscatter to soil moisture. Fluctuations of up to 5 dB are observed in all polarizations after irrigation events. The influence of biomass accumulation on backscatter dynamics during the mid-season (19 - 31 May) is limited because the soil and vegetation are both wet for much of this period, resulting in persistently high backscatter. The lack of precipitation or irrigation from June 1 (Fig. 4.2) results in a drydown in the root zone (Fig. 4.3), and decrease in stem VWC (Fig. 4.5), which result in a decrease in cross-pol backscatter from -16 dB to -21 dB. Ear development from 2 to 12 June coincides with an overall increasing trend in XP- and VV-pol backscatter, with short-term variations corresponding to the precipitation events on 5 and 11 June.

In a previous study [119], the Tor Vergata Model [85, 98] was used to simulate the observed backscatter using the soil moisture and vegetation data discussed in Section 2.1. In addition to providing the total backscatter, the Tor Vergata model simulations also provide some insight into the relative importance of different scattering mechanisms to total backscatter and how this changes throughout the growing season. Direct scattering from the ground dominates co-polarized backscatter in the early season. Increasing biomass leads to attenuation of direct scattering and increased double-bounce and multiple scattering between the vegetation and ground in both HH and VV. Direct scattering from vegetation dominates after mid-May, with double-bounce as the second largest contribution. This term is more significant in HH than VV and ensures some sensitivity to soil moisture throughout the growing season. In contrast,  $\sigma_{XP}^{\circ}$  is dominated by direct vegetation scattering as soon as the vegetation emerges, with limited influence of soil moisture due to multiple scattering between the vegetation and ground.

In Fig. 4.6 (b), CRs and RVI data clearly follow plant development, increasing steadily from 27 April to 28 May. The steady decrease in both CRs and RVI data from 28 May to 5 June coincides with the general decrease in stem VWC in response to high evaporative demand and decreasing root zone soil moisture availability (Fig. 4.2). The differences among the two CRs and RVI are greatest in the early season, i.e. before 18 May. The difference between the V-pol and H-pol CRs, in particular, can be attributed to the difference between HH and VV-pol backscatter during the early season due to the difference in their sensitivities to soil moisture and vegetation. The presence of system noise in the HH data partly explains higher variability in the  $CR_H$  at this time. The  $CR_V$  and  $CR_H$  converge after 18 May when backscatter is dominated by vegetation scattering. The divergence from 5 to 10 June may be attributed to the difference in sensitivity of VV and HH to changes in ear and stem VWC.

Fig. 4.7 shows the mean daily cycle of the radar backscatter for the period from June 1 to June 13. This specific period was chosen because the limited precipitation means that the SCW is primarily due to the presence of dew, and the corn has reached maximum biomass. There is clear daily cycle in radar backscatter in

response to accumulation and dissipation of dew (shown in Fig. 4.4) and variations in internal water content (VWC). The maximum value is observed at the acquisition of 7:30 am in VV and cross-pol, coinciding with the maximum dew accumulation. The minimum backscatter occurs in the late afternoon in all polarizations when the VWC reaches its minimum value. The increase in backscatter between 13:00 and 15:00 is due to the influence of rain events on 6 and 11 June. The range of the mean daily cycle in backscatter during this period is 0.78, 1.02, and 0.96 dB in HH, VV and cross-pol respectively. In Section 4.4, it will be shown that even larger variations are observed in the early and mid-season. A detailed discussion about the daily cycle of backscatter can be found in Vermunt *et al.* [119].

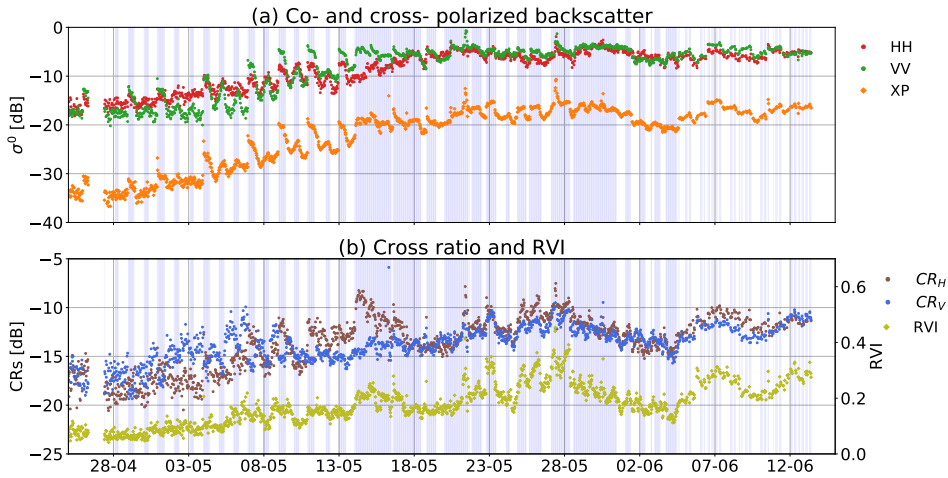


Figure 4.6.: Complete time series of L-band (a) HH, VV, and cross-polarized (XP) radar backscatter, and (b) CRs ( $CR_V$ , and  $CR_H$ ) and Radar Vegetation Index (RVI). Light blue vertical lines indicate the presence of SCW during the radar acquisition.

#### 4.4.4. EFFECT OF SURFACE CANOPY WATER ON MORNING RADAR BACKSCATTER

Fig. 4.8 shows the difference in radar observables acquired during early and late morning, i.e. in the presence and absence of SCW. Dawson and Goldsmith [73] found that the presence of SCW influenced cellular, leaf and whole-plant water relations through its role in suppressing transpiration and changing water potential. It is also assumed that the plant water potential has finished equilibrating with the soil by 6 am and will not continue to rise during the mid-morning period [72]. Therefore, it is assumed here that the presence of SCW limits transpiration, so that the change in internal water content between the 6 am and late morning observations is limited.

Note from Fig. 4.8 (a), that the coincident difference in soil moisture is less than  $0.01 \text{ m}^3 \text{ m}^{-3}$ . However, it is important to note that variations in backscatter in

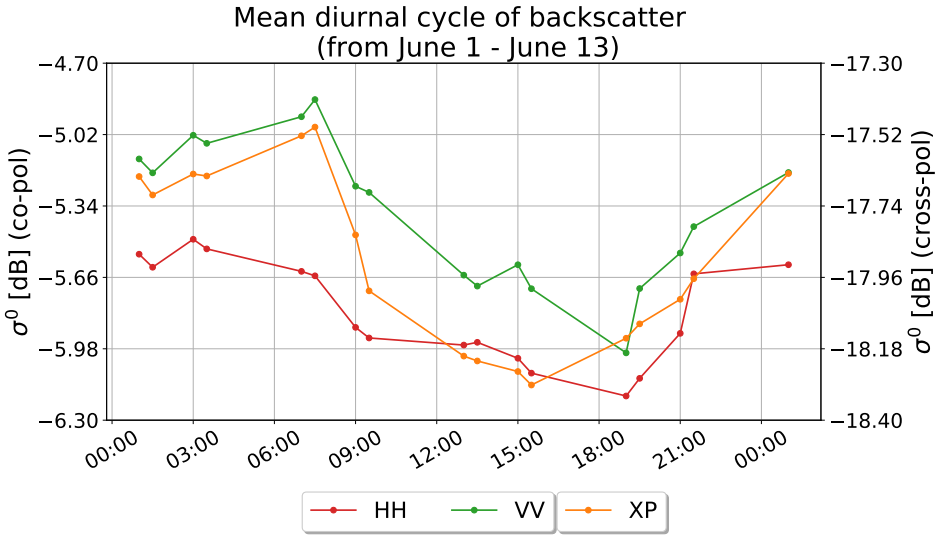


Figure 4.7.: Mean daily cycle of co- and cross-polarized backscatter for a 13 day period from June 1 to June 13.

the early season may be affected by dew formation on the soil surface [119]. The formation and dissipation of dew on the soil surface will not influence the observed 5 cm soil moisture, but will affect backscatter.

Fig. 4.8 (a) shows that early morning backscatter is higher than late morning backscatter by up to 1.02 dB for co-pol and 1.27 dB for cross-pol, and can reach up to 3.56 dB ( $\sigma_{VV}$  on 9 May). Note that these differences are not negligible while the dynamic range for HH, VV and XP during the growing season was around 11.36, 8.19 and 12.93 dB respectively. The magnitude of the difference varies considerably during the growing season. Large differences, particularly in VV and XP are observed in the early season. However the low fractional cover during this period means that this is also influenced by dew on the soil. During the mid-season, the growing vegetation results in an increase in direct scattering from the vegetation and increased attenuation of the return from the soil. Note that large differences of up to 2.77 dB in XP (23th May), and 1.49 dB in HH and VV (25th May) occur on days when SCW was due to dew rather than interception. Differences of around 1 dB are observed in all polarizations in the late season with a maximum value of 1.37 dB observed in  $\sigma_{VV}$  on 11th June.

Fig. 4.8 (b) shows the difference in early morning CRs and RVI due to the dissipation of SCW. On average, the difference between early- and late-morning CRs is 0.7 dB, and the average difference in RVI is 0.02. These are relatively small compared to the dynamic range of CRs and RVI observed in Fig. 4.6 (b). However, the observed sensitivity of XP backscatter to SCW (Fig. 4.8 (a)) means that both CRs and RVI are especially affected by SCW in the mid-season. Differences in this period

are consistently positive, and reach up to 2 dB and 0.125 in CRs and RVI respectively.

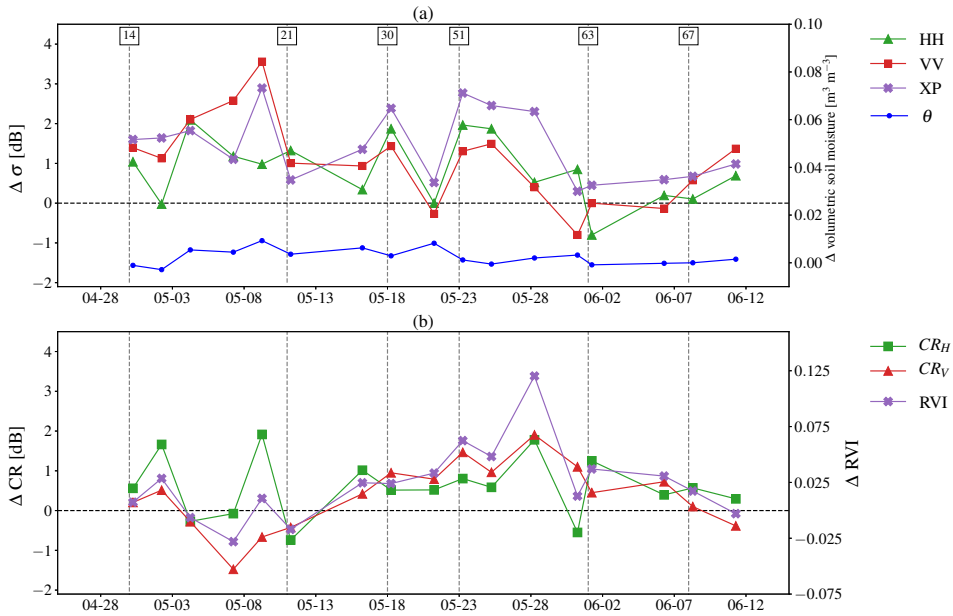


Figure 4.8.: Differences in early morning backscatter from wet and dry vegetation on destructive sampling dates. The difference is calculated between observations at 6am (wet vegetation) minus the first radar observation after the SCW has dissipated ( 10am - 12pm). Data are presented for (a) backscatter and soil moisture, and (b) CRs and RVI.

#### 4.4.5. VOD TIME SERIES RETRIEVED FROM DRY AND WET VEGETATION

Fig. 4.9 shows the dry reference, estimated separately for wet and dry vegetation. The annotation  $\sigma_{dry-PSCW}^0$  and  $\sigma_{dry-ASCW}^0$  indicates whether the dry reference was estimated from radar observations in the presence or absence of SCW. During the early season, sufficient data were available to estimate the dry reference for both wet and dry SCW conditions in VV and XP. Noise in the first few days of HH backscatter (Fig. 4.6 (a)) resulted in goodness of fit values lower than our threshold for the linear fit between soil moisture and backscatter. Hence it was not possible to estimate  $\sigma_{dry-ASCW}^0$  in HH reliably in the early season. Frequent rain events during the mid-season meant that there were not enough data to calculate  $\sigma_{dry-ASCW}^0$  from 18 May to 1 June.

Both  $\sigma_{dry-PSCW}^0$  and  $\sigma_{dry-ASCW}^0$  increase during the vegetative stages as the fresh biomass increases. Recall that  $\sigma_{wet}^0 - \sigma_{dry}^0$  corresponds to the range within which backscatter varies due to soil moisture, and is therefore an indication of the sensitivity of backscatter to soil moisture. As  $\sigma_{wet}^0$  has a constant value for the

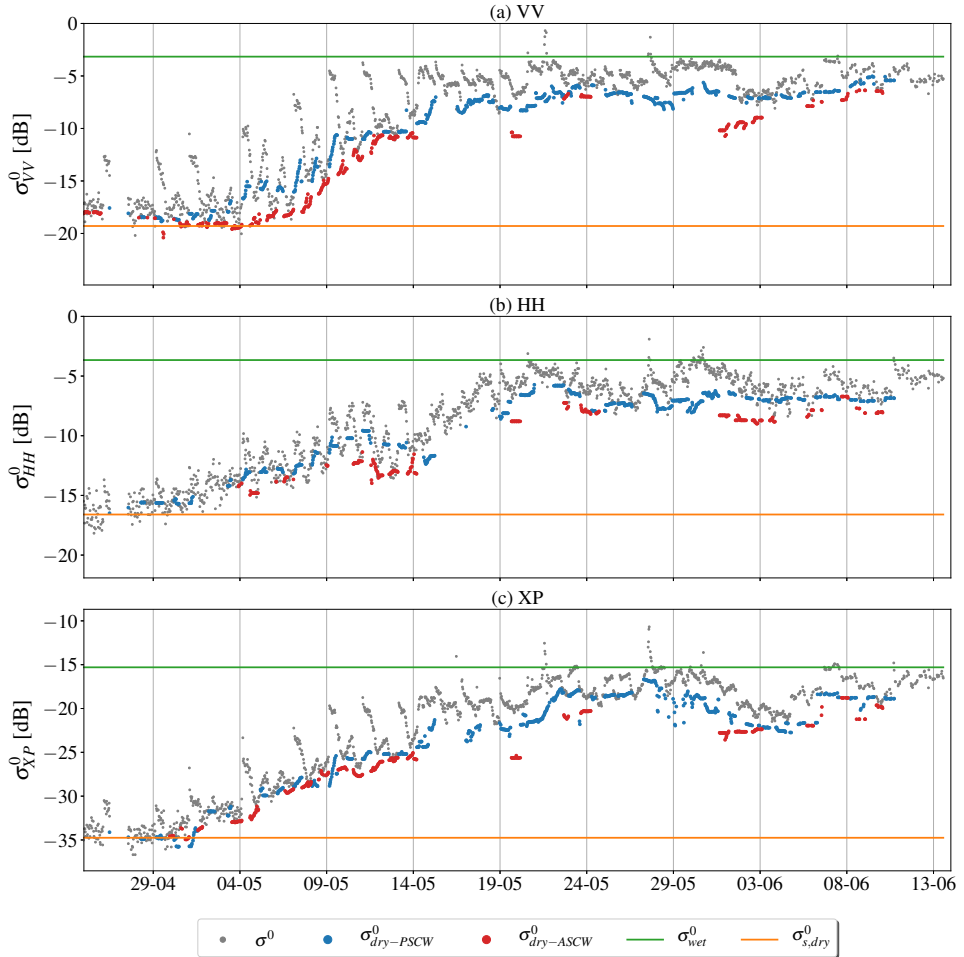


Figure 4.9.: Time series of radar backscatter along with the calculated static component ( $\sigma^0_{s,dry}$ ), the dry reference for wet vegetation ( $\sigma^0_{dry-PSCW}$ ) and dry vegetation ( $\sigma^0_{dry-ASCW}$ ), and the wet reference ( $\sigma^0_{wet}$ ) for co- and cross-polarization data. The green and orange horizontal lines on each plot indicate the wet reference and the static component, both of which are constant for the entire growing season.

growing season, an increase of  $\sigma^0_{dry}$  indicates a loss in sensitivity of backscatter to soil moisture as a result of vegetation attenuation. The rate of increase in  $\sigma^0_{dry}$  varies per polarization as backscatter in different polarizations is sensitive to different constituents of the canopy. The rapid increase in  $\sigma^0_{dry}$  in VV is due to stem elongation, while the more gradual increase in XP corresponds to the increase in LAI, which reaches a maximum around 23 May.

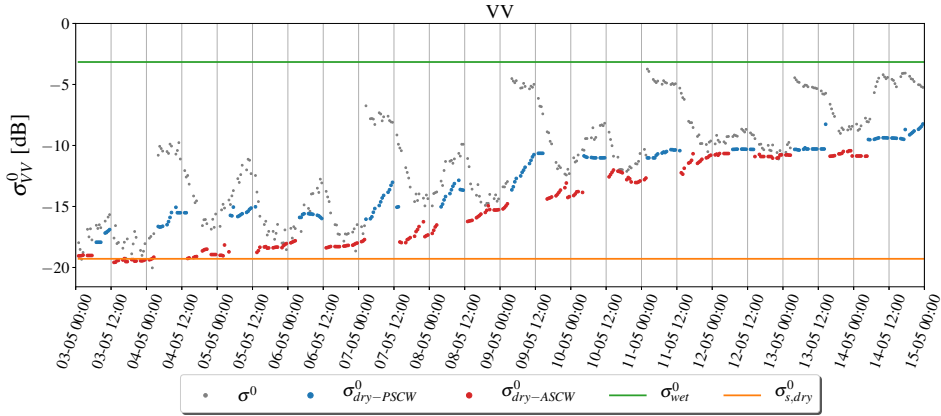


Figure 4.10.: Time series of radar backscatter along with the calculated static component ( $\sigma_{s,dry}^0$ ), the dry reference for wet vegetation ( $\sigma_{dry-PSCW}^0$ ) and dry vegetation ( $\sigma_{dry-ASCW}^0$ ), and the wet reference ( $\sigma_{wet}^0$ ) for VV-pol and period of 3 to 15 May.

In general,  $\sigma_{dry-PSCW}^0$  is higher than  $\sigma_{dry-ASCW}^0$ . In terms of Equation 4.2, this means that the estimated attenuating effect of vegetation is higher in the presence of SCW. The difference between  $\sigma_{dry-PSCW}^0$  and  $\sigma_{dry-ASCW}^0$ , depends on polarization, with a larger difference observed in VV than XP backscatter. In the absence of reliable data in the early season in HH, it is difficult to draw a conclusion about HH polarized data. In the late-season, drier weather ensured that sufficient data were available to estimate  $\sigma_{dry-PSCW}^0$  and  $\sigma_{dry-ASCW}^0$ . In both VV and HH,  $\sigma_{dry-PSCW}^0$  remains relatively flat in the late-season. Temporal variations in  $\sigma_{dry-ASCW}^0$  vary with polarization. The increase in VV, for example, coincides with the increase in ear water content, while HH and XP are more sensitive to the leaf water content. Fig. 4.10 provides a closer view of the estimated wet and dry references in VV polarization during the early stages. While  $\sigma_{dry-ASCW}^0$  increases relatively steadily during this period,  $\sigma_{dry-PSCW}^0$  is influenced by irrigation events and dew formation. As dew accumulates,  $\sigma_{dry-PSCW}^0$  increases, corresponding to a gradual reduction in sensitivity to soil moisture at 5 cm depth.

Fig. 4.11 shows the VOD for each polarization, estimated using equation 4.2. From 5 May onwards, the rapid increase in biomass of all plant constituents (Fig. 4.5) results in an increase in VOD. The rate at which it increases varies by polarization due to the sensitivity to different vegetation constituents. The sharpest increase is observed in VV due to the sensitivity to increasing biomass in the corn stems during the early stage.

Recall from Fig. 4.9 that  $\sigma_{dry-PSCW}^0$  was always greater than  $\sigma_{dry-ASCW}^0$ . As a result, VOD values estimated in the presence of SCW are always higher than those



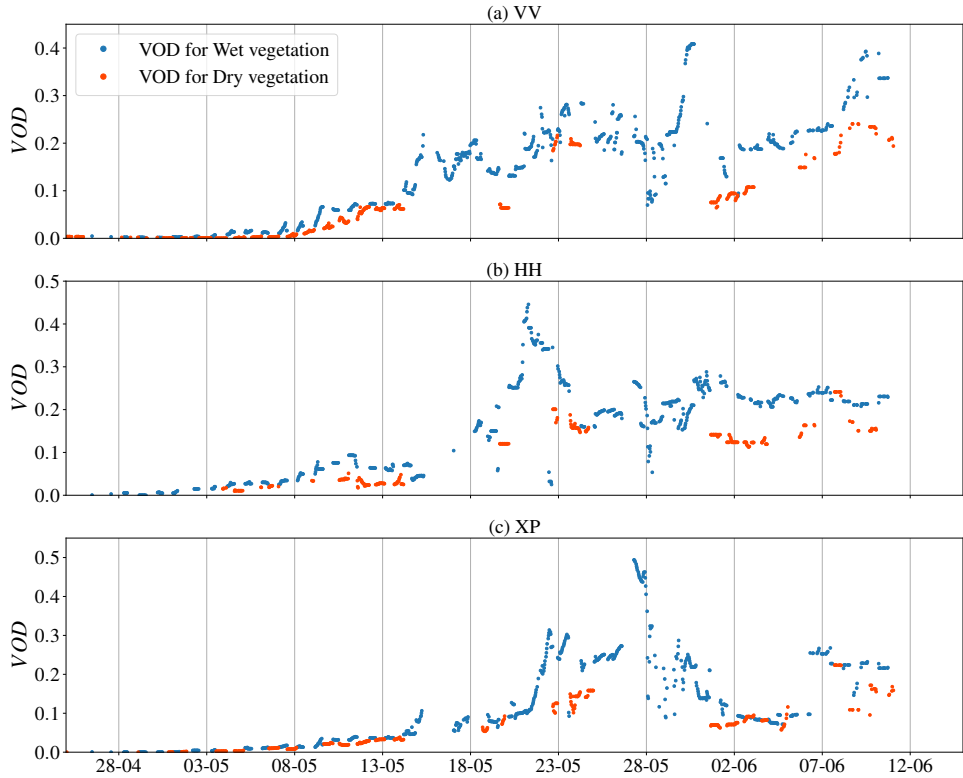


Figure 4.11.: Temporal pattern of VOD for wet and dry vegetation computed for a) VV polarization, b) HH polarization and c) XP polarization.

estimated in its absence. The difference is particularly striking in the mid-season when interception following several heavy rainfall events results in significant variations in VOD in all polarizations. Fig. 4.4 showed the persistent presence of SCW in this period. As a result, few data were available to estimate  $\sigma_{dry-ASCW}^0$  (Fig. 4.9) and hence VOD (Fig. 4.11) from dry vegetation during this period. Nonetheless, Fig. 4.11 shows that VOD in the presence of SCW reached up to 0.4 - 0.5, while that from dry vegetation was in the range 0.1 - 0.2. Three heavy rain events (Fig. 4.2) occurred on 21, 27, and 30 May. Their influence on the estimated VOD varies considerably with polarization due to the polarization-dependent sensitivity of backscatter to different constituents of the canopy (Fig. 4.9).

During the late-season (1 to 12 June), both VOD estimates in VV polarization increase steadily, coinciding with ear formation (Fig. 4.5). Between 1 and 8 June, the difference between VOD estimated in the presence and absence of SCW is around 0.1 for VV and HH, though barely any difference is discernible in XP.

#### 4.4.6. EFFECT OF SURFACE CANOPY WATER ON THE RELATION BETWEEN RADAR BACKSCATTER DATA AND CROP BIOPHYSICAL VARIABLES

Fig. 4.12 shows how each of the radar observables relates to the biophysical parameters of interest in the presence (blue) and absence (red) of SCW. The scatter plots and Spearman's rank correlation coefficient ( $\rho$ ) values in Fig. 4.12 show that cross-polarized backscatter, and the indices derived from it, are strongly related to each of the biophysical parameters of interest. In general,  $\rho$  is consistently lower (by around 0.2) when the backscatter data are collected in the presence of SCW. This is true for all radar observables and all biophysical parameters. It is also clear that increase in backscatter due to SCW (Fig. 4.6) results in a different relationship between the radar observables and the biophysical variables, so the presence of SCW potentially has a confounding effect on the retrieval of biophysical parameters from radar observables. On the other hand, the dynamic range of backscatter values is marginally larger when backscatter is acquired in the presence of SCW. So, while the relationship may be less well-defined, there is greater sensitivity to the biophysical variables. This is clear, for example, in Fig. 4.12 (m to p) where the sensitivity of the  $CR_V$  is higher for wet vegetation than for dry vegetation when BBCH < 55. The same is true in Fig. 4.12 (u to x) for the RVI, particularly for BBCH < 55.

Recall from Fig. 4.5 that the rapid changes in biophysical parameters, particularly in VWC and LAI, occur before BBCH = 55. These rapid changes result in a strong increasing trend in backscatter, particularly in cross-polarization (Fig. 4.6). In contrast, after BBCH = 55, VWC is quite stable and the backscatter is closer to saturation. There is no increasing trend after BBCH = 55, but backscatter still varies in response to changes in the structure (e.g. ear formation), as well as changes in stem and ear VWC, their influence on the relative importance of different contributions to total backscatter. The dominant contribution to backscatter in all polarizations at this time is direct scattering from vegetation. So, the variations are primarily due to vegetation, but some (limited) sensitivity to soil moisture remains due to the contribution of double-bounce. Consequently, the ability to relate biophysical parameters to radar observables is very different before and after BBCH = 55. This can also be observed in Fig. 4.12, where the relationship between the radar observables and biophysical parameters is not linear over the full range of biophysical parameter values.

Table 3 compares  $\rho$  between the radar observables and the biophysical parameters for  $\rho$  calculated using the whole season, or only the period before BBCH = 55. Due to the limited number of destructive sampling dates, note that this corresponding number of samples is 21 and 13 respectively.  $\rho$  values for which the corresponding P-value is greater than 0.01 are indicated in bold in Table 3. For BBCH < 55, the presence of SCW leads to similar or higher  $\rho$  values when cross-polarized data are used (e.g. in XP, RVI and  $CR_V$ ) and lower values of  $\rho$  when co-polarized data are used. When data from the whole season are used,  $\rho$  values are lower than those obtained using data for BBCH < 55 alone. The difference between the two is greater when the radar observables were acquired in the presence of SCW (i.e. "Wet").

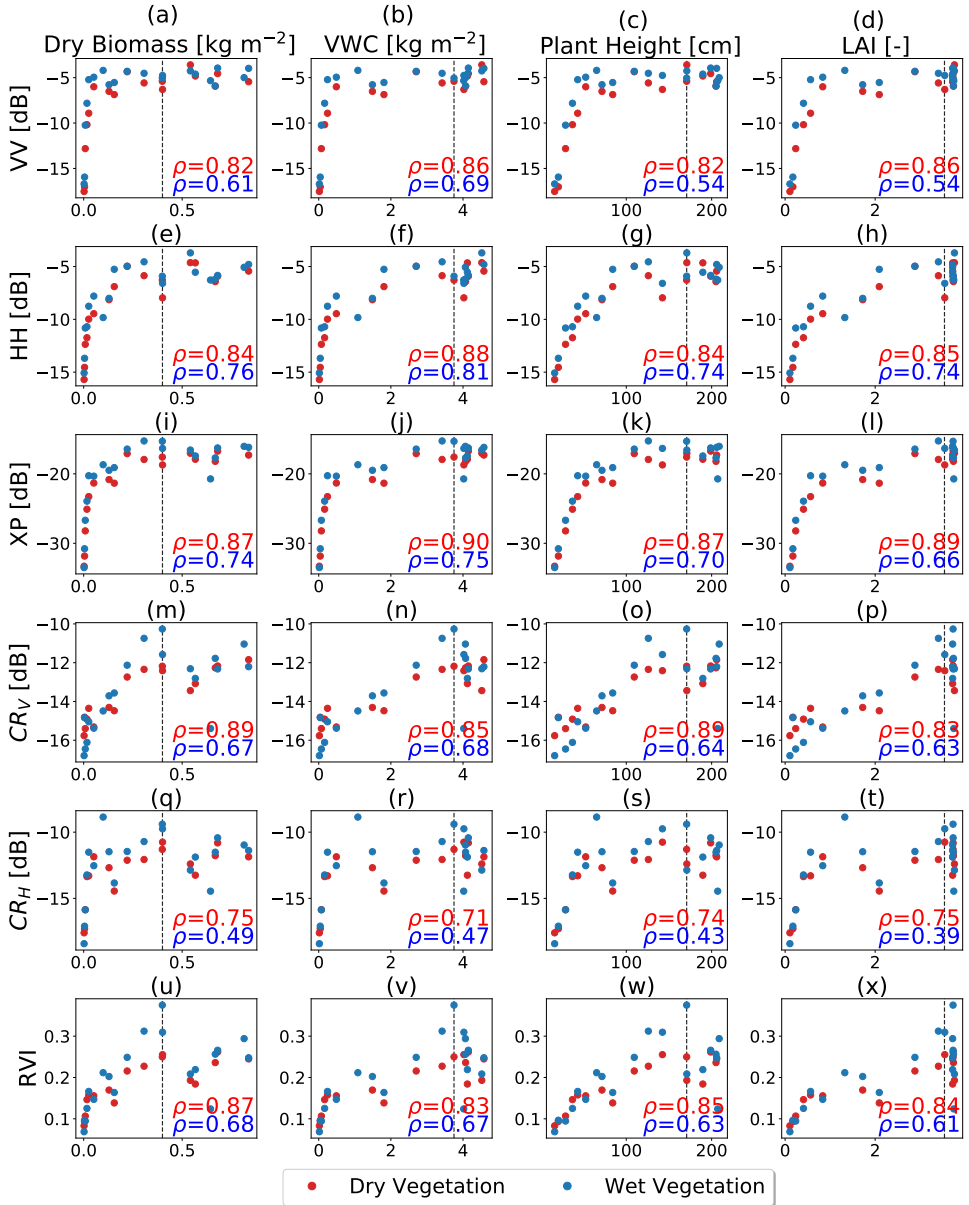


Figure 4.12.: The relationship between six radar observables and four key biophysical variables based on data from the full growing season. Blue and red indicate that the radar observables correspond to acquisitions from wet (including SCW) and dry (no SCW) vegetation. The corresponding Spearman's rank Correlation Coefficients ( $\rho$ ) are in the lower right corner. The vertical dashed line indicates BBCH = 55 (middle of heading stages and start of ear formation).

Table 4.2.: Spearman's rank correlation coefficients between four biophysical variables and the six radar parameters for dry and wet vegetation at two different growing stages.

	Dry Biomass				VWC				Plant Height				LAI			
	BBCH < 55		Whole season		BBCH < 55		Whole season		BBCH < 55		Whole season		BBCH < 55		Whole season	
	Dry	Wet	Dry	Wet	Dry	Wet	Dry	Wet	Dry	Wet	Dry	Wet	Dry	Wet	Dry	Wet
VV	0.87	0.75	0.82	0.61	0.87	0.75	0.86	0.70	0.89	0.74	0.82	<b>0.54*</b>	0.89	0.74	0.86	0.57
HH	0.90	0.89	0.84	0.76	0.90	0.89	0.86	0.80	0.92	0.89	0.84	0.74	0.92	0.89	0.85	0.74
XP	0.92	0.96	0.87	0.74	0.92	0.96	0.90	0.75	0.93	0.96	0.87	0.70	0.93	0.96	0.89	0.66
CRV	0.88	0.92	0.89	0.67	0.88	0.92	0.85	0.68	0.90	0.93	0.89	0.64	0.90	0.93	0.83	0.63
CRH	0.87	0.80	0.75	<b>0.49*</b>	0.87	0.80	0.71	<b>0.47*</b>	0.87	0.81	0.74	<b>0.44*</b>	0.87	0.81	0.75	<b>0.39*</b>
RVI	0.92	0.93	0.87	0.68	0.92	0.93	0.83	0.67	0.92	0.94	0.85	0.64	0.92	0.94	0.84	0.61

\* P-value of the Spearman's rank correlation coefficient is higher than 0.01.

#### 4.4.7. EFFECT OF SURFACE CANOPY WATER ON RELATION BETWEEN VOD AND VEGETATION WATER CONTENT

VOD is assumed to depend linearly on vegetation water content according to  $VOD = b * VWC$ . Fig. 4.13 shows the linear fit between VOD and total VWC for the whole season (a - c) and for the period with BBCH < 55. The goodness of fit ( $R^2$ ) is up to 0.34 higher when the linear fit is limited to BBCH < 55 (Fig. 4.13 (d - e)).

Recall from Fig. 4.5 that after BBCH = 55, the total VWC remains at around  $4 \text{ kg m}^{-2}$ , but the stem water content decreases and the ears form and separate from the stem. So, while VWC does not change, the internal moisture distribution changes and the canopy is undergoing structural changes which influence the backscatter (Fig. 4.6), and VOD (Fig. 4.5). Focusing on the relationship for BBCH < 55, the goodness of fit is  $> 0.94$  for both VV and XP in the presence and absence of SCW. Values are lower for HH polarization, though this may be due to limited data. Goodness of fit values are similar in the presence and absence of SCW, so the assumption that there is a linear relationship is reasonable in both scenarios. Note, however, that VOD values obtained in the presence of SCW (blue) are generally higher, than those obtained in its absence (red), and the difference increases with VWC. So, the linear regressions between VOD and VWC in the presence and absence of SCW are markedly different. The  $b$  parameters are generally much higher when estimated using VOD in the presence of SCW (Table 4.3). The difference occurs regardless of whether  $b$  is estimated using data from the entire season or the period where BBCH < 55.

## 4.5. DISCUSSION

Results in Fig. 4.4 demonstrated that L-band backscatter is influenced by the presence of SCW, in the form of both dew and interception. This is compatible with previous studies [67, 79, 119, 181]. Fig. 4.8 showed that the presence of early morning dew can contribute to a difference of up to 2 dB in L-band backscatter. This

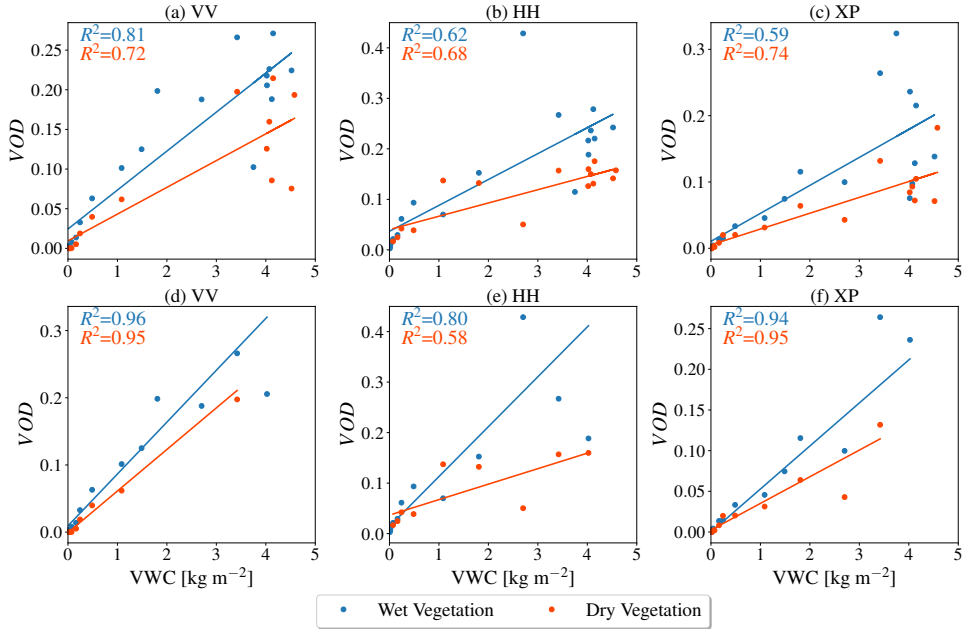


Figure 4.13.: Vegetation optical depth (VOD) calculated for VV- (left), HH- (middle) and cross-polarized backscatter (right), as a function of vegetation water content (VWC). Results are shown for the full growing season (a - c), and the period up to BBCH = 55 (d - f). The data, fitted linear regressions and goodness of fit ( $R^2$ ) values are shown in blue and red to indicate if they were obtained in the presence (blue) or absence (red) of SCW.

Table 4.3.: Regression coefficient ( $b$ -factor) for each linear regression between VWC and VOD retrieved from VV, HH and XP backscatter.

2*Channel	BBCH < 55		Whole season	
	Dry	Wet	Dry	Wet
VV	0.06	0.08	0.03	0.05
HH	0.03	0.10	0.03	0.05
XP	0.03	0.05	0.02	0.04

is consistent with previous studies [47, 80, 119, 181]. However, here the availability of high temporal resolution data from both leaf wetness sensors and tower-based radar throughout the entire season allowed us to show that the impact of SCW on backscatter varies with growth stage and with polarization. In the early season, while the fractional cover was low, the difference between SCW and no-SCW conditions were large due to the combined influence of dew on the canopy as well as the soil. In the mid-season, the amount of SCW is higher due to both interception and dew,

and the fact that LAI is much higher than the early-season. In the late-season, the LAI is still high, but the difference between SCW and no-SCW is lower than the early and mid-season because the high biomass means that radar backscatter is close to saturation and the SCW is almost entirely due to dew rather than a combination of dew and interception. It remains challenging to explain the differences observed between polarizations because there is a limited understanding of how the presence of droplets or a film of water affects the various contributions to total backscatter. Unfortunately, current models do not account for the presence of SCW [36, 85, 86, 181, 182].

In addition to backscatter, we also examined the influence of SCW on CRs and RVI. These are increasingly used to monitor vegetation because they are less influenced by soil moisture as they are normalized with co-polarized backscatter [13, 26, 45, 121, 167]. The difference between early morning and late morning values, i.e. in the presence and absence of dew, was not zero. In fact, the difference in morning values during the mid-season was around a quarter of the dynamic range. This suggests that while CRs and RVI may be useful in mitigating the influence of soil moisture, they are not immune to the influence of SCW.

The relationships between radar observables (backscatter, CRs, RVI) and biophysical variables are most meaningful during the vegetative stages as they all monotonically increased in response to the accumulation of fresh biomass. This is consistent with previous studies [26, 27, 42, 152, 178]. In the later stages the backscatter was closer to saturation, but it still varied in response to changes in the structure and internal distribution of moisture within and among constituents. This explains why the Spearman's rank correlation coefficient was lower when determined for the whole season rather than the stages where BBCH < 55.

Unlike previous studies, this thesis explicitly addressed the influence of time of day on the relationship between radar observables and biophysical parameters. Occasionally, rapid daytime growth can occur in the early vegetative stages when a dry spell ends. Generally though, LAI, dry biomass and plant height do not vary much on a single day. On the other hand, the impact of SCW on backscatter means that the timing of observations used to retrieve biophysical parameters matters. If we consider the entire growing season, results in Fig. 4.12 showed that the strength of the monotonic relationship between backscatter and the biophysical variables is higher (difference in  $\rho$  up to 0.25) when one uses backscatter collected in the absence of SCW. This is quite consistent with decades of research using destructive sampling of vegetation to prove that backscatter is sensitive to the dielectric constant of vegetation, which is primarily controlled by its water content. However, results in Table 4.2 showed that the lower  $\rho$  values were primarily due to the low sensitivity of backscatter to biophysical variables when BBCH > 55. During the vegetative stages, the  $\rho$  values were comparable in the presence and absence of SCW. Results for BBCH < 55 in the Table 4.2 suggests that stronger relationships (higher  $\rho$ ) were observed in the presence of SCW. This is consistent with the conclusions of earlier studies that argued that the presence of SCW made it easier to distinguish between crop types [79, 183]. This is likely due to the influence of vegetation geometry on the amount of water that can be held by the vegetation.

However, it is essential to note that the relationship between the radar observable and the biophysical parameter is just different due to the higher values of backscatter obtained in the presence of SCW. If ground data are used to calibrate relationships between radar observables and biophysical parameters it is essential, therefore, to calibrate the relationship for the situation likely to be observed. For example, if early morning dew is common, and morning satellite overpasses will be used, these relationships need to be determined for wet vegetation.

VOD estimated using radar backscatter data obtained in the presence of SCW was generally higher than that obtained in its absence. This was true for all polarizations. The largest differences were found in the mid- to late-season, but the dynamics (i.e., the difference between VOD obtained in the presence and absence of SCW) were found to vary by polarization. This may be related to the polarization-dependent response of radar backscatter to SCW, but the influence of data scarcity can not be overlooked.

VOD is often used as a proxy for vegetation water content as the two are assumed to be linearly related [164]. However, results presented here show that the linear regression coefficient  $b$  is very different when the backscatter data are obtained in the presence and absence of SCW. Higher backscatter values in the presence of SCW result in considerably higher  $b$  values. It is important to highlight that VOD is not a biophysical parameter, but a parameter of an electromagnetic model, in this case the Water Cloud Model. The VOD is assumed to be a measure of the degree to which the signal from the soil is attenuated by the vegetation. However, the VOD time series contain artifacts from the manner in which VOD is estimated from this model and the validity of any inherent assumptions. For example, multiple scattering is not considered. This assumption is particularly problematic in the presence of SCW as any enhancement of multiple scattering due the presence of droplets or a film of water on the leaves is not accounted for. In addition, the methodology involves fitting a relationship between backscatter and soil moisture within some time window. The length of this window must be long enough to ensure a reasonable fit, but this implies that the dry reference (hence VOD) is constant within this window. Data sparsity and noise in the data will influence the VOD estimate, as will any rapid changes in VOD during the window due to growth or water uptake.

## 4.6. CONCLUSIONS

Data from an intensive field campaign were used to investigate the influence of SCW on the relationship between L-band backscatter and biophysical variables in crop monitoring. Continuous leaf wetness sensor data, combined with precipitation and irrigation data were used to chart the accumulation and dissipation of dew and interception throughout the growing season. These were combined with data from an L-band fully polarimetric tower-based radar to quantify the effect of SCW on L-band radar observables (backscatter, RVI and CRs), as well as the relationship between these observables and biophysical parameters of a corn crop. In addition, VOD was estimated to consider the effect of SCW on VOD, and its relationship with VWC.

At the study site in Florida, dew was present on the canopy for most days from 12 am to 10 am and was found to have a substantial effect on backscatter in all polarizations and throughout the growing season. The cross-ratio and RVI, often used to mitigate the influence of soil moisture, were not immune to the influence of dew and interception. Furthermore, it was shown that the presence of SCW affected the relationship between L-band observables and biophysical variables. This means that it is important to consider daily patterns in SCW and overpass time when deciding to retrieve biophysical parameters from radar data. Sentinel-1 and RCM are in near-polar, sun-synchronous orbits with local overpass times at 18:00 and 06:00 hours. Future SAR missions, like NiSAR and ROSE-L, are likely to be in similar orbits [173, 174]. Daily patterns in SCW should be taken into consideration when choosing to retrieve biophysical parameters from ascending or descending passes, or by combining data from both. Further research exploring the influence of frequency and viewing geometry is strongly recommended to support agricultural applications using data from these and other current and future SAR missions.

Results presented here show that the VOD estimate in the presence of SCW was higher than those estimated in its absence. In some sense, it is acceptable to say that the higher values of VOD from wet vegetation indicate a reduced sensitivity to soil moisture. However, this reduced sensitivity is not entirely attributable to the attenuation. It is hypothesized that the presence of water on the canopy may be leading to an increase in direct scattering from the vegetation, which is also reducing the signal that reaches the soil surface. The influence of SCW on multiple scattering, and how it might affect sensitivity to soil moisture is entirely unknown. This suggests that if VOD is to be used as a proxy for internal vegetation water content, backscatter values affected by SCW should not be included in the VOD estimate. In areas with strong daily cycles in dew or interception, it would be prudent to limit the estimation of VOD to satellite radar acquisitions at overpass times less likely to be affected by SCW.

The conclusions drawn in this thesis are based on experimental data collected in a field experiment of limited duration, with a single crop type. Interestingly, similar conclusions were drawn in a recent study using VOD obtained from satellite passive microwave remote sensing, suggesting that the outcomes of this study are relevant for a wider range of cover types. Xu *et al.* [184] used VOD data derived from X-band (10.7 GHz) measurements by the Advanced Microwave Scanning Radiometer for the Earth Observing System (AMSR-E) in combination with a terrestrial biosphere model in order to evaluate the relationship between canopy water content (CWC) and leaf surface water ( $LW_s$ ) due to dew formation and rainfall interception with VOD at four tropical forest and savanna sites in Brazil. They found that  $LW_s$  accounts for >50% of diurnal variation in CWC at all four of the study sites that could make a large contribution to diurnal variation in CWC and AMSR-E VOD signals over tropical forests. Additional studies, over multiple locations, crop and land cover types are essential to characterize the impact of surface canopy water on retrievals of soil and vegetation states more generally from both active and passive microwave remote sensing.

All of the above point to an urgent need for an improved understanding



of microwave interactions with vegetation in the presence of SCW. Additional experiments are strongly recommended to examine the influence of SCW over a wider range of vegetation. The capacity of various crops to store water will depend on their structure and geometry (e.g. narrow-leaved or broad-leaved etc.). These data are needed to understand how droplets or a film of water on the vegetation influences microwave interactions with the vegetation and soil. Inclusion of SCW in radiative transfer models of vegetated surfaces is essential to account for its influence in retrieval of soil and vegetation states. Furthermore, the potential to observe and retrieve SCW using radar remote sensing offers many new opportunities in the context of hydrology [185], and plant physiology [73].

# 5

## TOWARD MODELING THE INFLUENCE OF SUB-SEASONAL VARIATION IN VEGETATION ON RADAR BACKSCATTER USING A RADIATIVE TRANSFER MODEL

*In Chapters 4 and Appendix A, we assessed the influence of surface canopy water (SCW) on backscatter, cross-ratio, RVI, and VOD at the L-band. We demonstrated that the presence of SCW impacts the relationships between radar observables and key biophysical variables. However, due to a limited understanding of how SCW affects the various components of total backscatter, we were unable to explain the observed differences between polarizations. This underscored a pressing need for a more in-depth understanding of how microwaves interact with vegetation in the presence of SCW.*

*In this chapter and the next, we aim to employ a radiative transfer model to enhance our understanding of how SCW affects the various components contributing to total backscatter. For this chapter, we utilize the radiative transfer model developed at Tor Vergata University. Although this model accurately simulates the seasonal evolution of the signal due to crop growth, it struggles with the simulation of fast temporal dynamics in the signal. Therefore, the objective of this chapter is to present a calibration technique that could augment the model's ability to simulate high temporal dynamics, specifically those due to soil moisture and internal vegetation water dynamics in the signal.*

## 5.1. INTRODUCTION

Several electromagnetic models have been developed to better understand and simulate backscattering from agricultural crops. Both semi-empirical and theoretical models have been developed to model the influence of the soil and vegetation on radar backscatter [36, 84–87]. Among these, the most commonly used is the semi-empirical Water Cloud Model (WCM), which considers the vegetation as a cloud containing identical water droplets randomly distributed within the canopy [84]. The WCM is a zero-order radiative transfer solution. This model, widely preferred due to its simplicity, does not consider higher-order scattering mechanisms. To obtain a more detailed understanding of scattering from vegetation surfaces, advanced models based on energy and wave approaches like the Michigan Microwave Canopy Scattering model (MIMICS) [36], Multi-static Interferometric and Polarimetric Electromagnetic Model for Remote Sensing (MIPERS) [87], and the Tor Vergata model [85] have been proposed.

Previous studies using the Tor Vergata model demonstrated the high sensitivity of the model to crop growth and good agreement between the model and observed backscatter. However, these studies relied on temporally sparse data (i.e., ranging from every 3 days to every 12 days) for the input parameters, with simulations primarily capturing the seasonal growth cycle. Vermunt *et al.* [119] combined daily input data (soil and vegetation water content) with data from a scatterometer to understand the contribution of different scattering mechanisms to total L-band backscatter during the corn-growing season. The results showed that, in general, the model could simulate the increase in backscatter due to crop growth with an average RMSE equal to 3.91 dB for the whole season. In all polarizations, the modeled total backscatter could not simulate the daily dynamics in observed backscatter, indicating that the Tor Vergata model cannot accurately simulate the higher temporal (i.e., daily and sub-daily) dynamics of the observed signal.

The goal of this chapter is to improve the ability of the Tor Vergata model to simulate higher temporal dynamics due to internal vegetation water and soil moisture dynamics in the signal. We will first show that the small cylinder radius (SCR) significantly impacts backscatter at L-band, in all polarizations, and argue that its influence is less noticeable at higher frequencies. We will then present an approach that allows for the calibration of SCR using hyper-temporal, ground-based L-band scatterometer data. Finally, we will investigate the factors that could drive the dynamics in the SCR.

## 5.2. MATERIALS AND METHOD

### 5.2.1. RADIATIVE TRANSFER MODEL

The model used in this research was developed at the University of Rome, Tor Vergata [85], and is therefore referred to as the “Tor Vergata model” throughout. This is a discrete microwave scattering model which simulates the backscattering coefficient of vegetated surfaces with an approach based on the radiative transfer theory and the matrix doubling algorithm. The model is able to simulate both scattering and extinction properties of vegetation elements and of the underlying soil by applying

the most suitable electromagnetic approximation, depending on the scatterers' size and shape and frequencies. For the soil, the permittivity was computed using Mironov's soil dielectric model [186, 187] and the Integral Equation Model (IEM) [188] was used to determine the backscattering coefficient. For maize, the model considers two layers, where the lower layer is a homogeneous half-space with rough interface, representing the soil, and the top layer contains the stems, leaves, and petioles (i.e. ribs) as shown in Fig 5.1. The ear is not considered in this version of the model since Della Vecchia *et al.* [98] showed that their inclusion has a limited effect on total simulated backscatter (<0.3 dB) even at L-band. Leaves are represented as dielectric discs while stems and petioles (i.e. ribs) are represented by big and small cylinders respectively. To compute the scattering matrices and the extinction vector, the Rayleigh-Gans approximation [189] is used for both leaves and petioles (i.e. ribs) for L-band. For C and X bands, the Physical Optics approximation is used for leaves and the infinite length approximation [190] is used for petioles (i.e. ribs). For the stem, the infinite length approximation is used for all frequencies. In order to combine contributions from the various scatterers, and between vegetation and soil, the matrix doubling algorithm [189] is used. This method enables including multiple scattering effects of any order in the calculation of the backscattering coefficient and it can separate contributions of different scatterers in the vegetation canopy. The simulated total backscattering coefficient is calculated as the combination of contributions due to four scattering mechanisms as shown in Fig. 5.1 and equation 6.1.

$$\sigma_{total}^0 = \sigma_{veg}^0 + \sigma_{veg-ground}^0 + \sigma_{double-bounce}^0 + \sigma_{soil}^0 \quad (5.1)$$

where  $\sigma_{total}^0$  is the total backscatter coefficient,  $\sigma_{veg}^0$  is the vegetation direct backscattering component (i.e. multiple scattering from the vegetation layer Fig. 5.1 (b)),  $\sigma_{veg-ground}^0$  is the vegetation-ground scattering (i.e. multiple scattering due to interactions between vegetation and ground Fig. 5.1 (c)),  $\sigma_{double-bounce}^0$  is the double bounce scattering between vegetation and soil or vice versa (Fig. 5.1 (d) and (e)), and  $\sigma_{soil}^0$  is the direct component from the soil surface attenuated by the canopy (Fig. 5.1 (b)). The required input parameters describing the dielectric and geometry of the vegetation and soil are listed in Table 5.1. These data were collected during a field campaign in Florida, USA, in 2018 (see section C). The reader is referred to Bracaglia, Ferrazzoli, and Guerriero [85] for a more detailed and comprehensive description of the model and its assumptions.

### 5.2.2. EXPERIMENTAL DATA

#### STUDY SITE

This research also conducted over corn field during a field campaign near Citra, Florida during spring 2018. For detailed information regarding the study site specific to this part of the research, please refer to section 2.1 of this thesis.

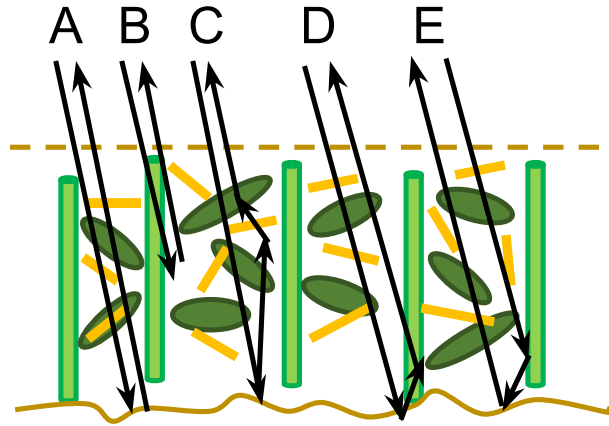


Figure 5.1.: Schematic representation of the radiative transfer model geometry for corn. The four components of rough soil, main stems, leaves, and ribs, and 5 scattering mechanisms of direct soil (A), Volume (B), Vegetation-ground (C), and double bounce (D, E) are shown.

Table 5.1.: List of input parameters for *Tor vergata* model simulation

Parameter	Value or Time series
Frequencies (GHz)	L=1.25 / C=5.405 / X=9.6
Incidence angle (degree)	40
Soil volumetric moisture content	Time series
Soil rms height (cm)	0.92
Soil correlation length (cm)	9.17
Plant density (plant/m <sup>2</sup> )	8
plant height (cm)	Time series
LAI	Time series
number of leaves per plant	Time series
Leaf area (cm <sup>2</sup> )	Time series
Leaf half width (cm)	Time series
Disc (leaf) thickness (cm)	0.03
Disc (leaf) gravimetric moisture	Time series
Stem height	Time series
Stem radius	Time series
Stem gravimetric moisture	Time series
small cylinder (ribs) length (cm)	70% of leaf length
small cylinder (ribs) maximum radius (cm)	0 - 0.4
small cylinder (ribs) gravimetric moisture	Time series

### FIELD MEASUREMENTS

**Soil** For detailed information regarding the soil data specific to this part of the research, please refer to section 2.3.2 of this thesis.

**Vegetation** For detailed information regarding the vegetation data specific to this part of the research, please refer to section 2.3.4 of this thesis.

**Surface Canopy Water** For detailed information regarding the surface canopy water data specific to this part of the research, please refer to section 2.3.3 of this thesis.

### GROUND-BASED RADAR OBSERVATIONS

Radar backscatter was measured using the truck-mounted University of Florida L-band Automated Radar System (UF-LARS) [106]. For detailed information regarding the ground-based radar observations data specific to this part of the research, please refer to section 2.3.4 of this thesis.

#### 5.2.3. RT MODEL CALIBRATION METHOD

In the Tor Vergata model, a leaf is described as a combination of a disc representing the leaf area and a small cylinder representing the rib, i.e. the relatively sturdy central spine of the leaf. The inclusion of small cylinders was necessary to improve the agreement between simulated and observed backscatter. The dielectric constant of the small cylinder is assumed to be the same as that for the whole leaf, and is obtained from the measured leaf moisture content. The length of the small cylinder is assumed to be 70% of the leaf length, and can therefore be determined from weekly field measurements. In the Tor Vergata model, the maximum radius of a small cylinder, measured in centimeters, is defined as "acylmax." In the original version of the model, this parameter was assumed to have a single value (i.e., 0.3 cm) throughout the growing season. The model also requires another parameter, the value of the small cylinder centimeters for each time, referred to as "acyl." It is calculated using the following equation:

$$acyl = acylmax \cdot (arealeaf/450)^{0.25} \quad (5.2)$$

Here, the value of the small cylinder radius (SCR) is determined based on the maximum radius for the small cylinder ("acylmax" in cm) and the average area of corn leaves ("arealeaf" in cm). Section 5.3.2 will demonstrate that the total backscatter is sensitive to SCR, and that allowing SCR to vary during the season leads to improved agreement between the modeled and observed backscatter.

Since the maximum radius of small cylinders was not directly measured in the field, we employed a calibration method to determine the optimal values for this parameter on a daily basis. The calibration started by running the model using all the measured data, with the only variable being modified being the maximum radius ("acylmax"), ranging from 0 to 0.4 cm in increments of 0.01 cm. This upper limit of 0.4 cm for "acylmax" was established based on measurements from previous studies

[182, 191, 192]. The main reason for changing the maximum radius (“acylmax”) instead of the SCR was to ensure that the calibrated SCR is always in a valid range defined by previous studies. Therefore, for the calibration of the model, we used the optimum “acylmax” value, which in turn provided us with the optimal SCR size based on the measured average leaf area of corn. In the following sections, we always refer to calibrating the SCR since this is the input of the model, and it is directly changed by “acylmax” values.

Next, we used dynamic windows ranging from 1 to 10 days, with each polarization being handled separately. Within each window, we determined the SCR that resulted in the lowest root mean square error (RMSE) between observed and simulated backscatter. The window was shifted with an increment of 24 hours across the data, to yield daily estimates of the optimal SCR value.

#### 5.2.4. MULTI LINEAR REGRESSION METHOD

In this section, understanding the factors that primarily impact SCR dynamics is important. Given the complex nature of SCR, characterized by its dependency on more than one parameter, the multiple linear regression (MLR) technique was selected over the simple linear regression method.

The MLR method allows for the analysis of the relationship between a dependent variable and two or more independent variables. Unlike simple linear regression, where the relationship between a dependent and a single independent variable is examined, MLR extends this concept to encompass multiple predictors. The general mathematical form of MLR can be expressed as [193]:

$$y = \beta_0 + \beta_1 x_1 + \beta_2 x_2 + \dots + \beta_n x_n + \epsilon \quad (5.3)$$

Here,  $y$  represents the dependent variable (in this case, SCR),  $\beta_0$  is the intercept,  $\beta_1, \beta_2, \dots, \beta_n$  are the coefficients of the independent variables  $x_1, x_2, \dots, x_n$ , and  $\epsilon$  denotes the error term.

The coefficients quantify the contribution of each independent variable to the prediction of the dependent variable. They are estimated using various techniques such as the least squares method, which aims to minimize the sum of the squared differences between the observed and predicted values.

The utilization of MLR in this context enables a more comprehensive investigation of SCR dynamics, allowing the simultaneous consideration of multiple factors.

In this chapter to use the MLR method, the time series of SCR at each polarization (Fig. 5.7 (a)-(c)) was considered as the dependent variable, and both soil moisture at a depth of 5cm and one of the vegetation water content constituents (Fig. 5.7 (d)) were considered as independent variables at each point in time. The corn growing season can be divided into two distinct periods: the vegetative stage (i.e., 28 April to 28 May) and the reproductive stage (28 May to 12 June). To better understand the factors controlling SCR dynamics, the analysis was performed separately for these two periods. To maintain comparable results, the number of data points used in the analysis for each period had to be similar. Because the reproductive stage had 11

data points, we had to choose the 11 data points in the vegetative stage. Therefore only data from 14 to 28 May were used as vegetative stage data.

## 5.3. RESULTS AND DISCUSSIONS

### 5.3.1. FIELD MEASUREMENTS

Seasonal variations in observed radar backscatter ( $\alpha$ ), volumetric soil moisture ( $\theta$ ) at a depth of 5 cm (b), and vegetation water content (VWC) per constituent (c) are shown in Fig. (5.2). The radar backscatter and soil moisture data are presented exclusively for dry vegetation conditions, meaning that they were acquired in the absence of surface canopy water (SCW). In the early season (28 April - 15 May), midnight irrigation was implemented on eight occasions, resulting in a sharp increase in soil moisture and fluctuations of up to 5 dB in backscatter across all polarizations. The upward trend in backscatter during this period can be attributed to crop growth and an increase in VWC, with a notable increase of  $1.81 \text{ (kg m}^{-2}\text{)}$ . Throughout the mid-season (17 - 31 May), radar backscatter remained consistently high, exhibiting limited dynamics, while the total VWC experienced a rise of approximately  $2.51 \text{ (kg m}^{-2}\text{)}$ . This was predominantly due to numerous rainfall events and the subsequent extended period of high moisture in both soil and vegetation. The late season (1-12 June) was characterized by the development and growth of ears, coinciding with limited precipitation and irrigation events. During this period, the water content of stems and leaves decreased, while ear water content increased. The simultaneous change in internal corn water content and soil moisture explained the dynamic in radar backscatter during this period. More details about the field measurements are described in [119] and [102], respectively.

### 5.3.2. EFFECT OF SMALL CYLINDERS SIZE AS A FUNCTION OF FREQUENCY

Fig. 5.3 illustrates the effect of small cylinder size on the time series of simulated L, C, and X band HH-polarized backscatter. Line color is varied from blue to red as the SCR is increased from 0 to the maximum SCR value of 0.4 cm. The top row shows total backscatter, and the rows below correspond to the contributions to total backscatter from direct vegetation scattering, vegetation-ground scattering, double-bounce scattering, and direct ground scattering.

Changing the SCR can significantly influence the simulated backscatter coefficients and the values of all scattering mechanisms. Increasing the SCR from 0 to 0.4 cm leads to an increase in total, direct vegetation, and vegetation-ground scattering in the L band, while causing a decrease in these quantities in C and X bands. Increasing SCR led to reductions in double-bounce and ground scattering at all three frequencies. Additionally, changes in the SCR influenced the relative dominance of the different contributions to total backscatter, particularly in the L-band.

In L-band, the dominant scattering mechanism differed between low and high SCR values. During the early season (18 April - 15 May), employing a lower SCR value (i.e.,  $\text{SCR} < 0.25 \text{ cm}$ ), means that direct ground scattering and direct vegetation scattering emerge as the first and second dominant contributions. However, using a



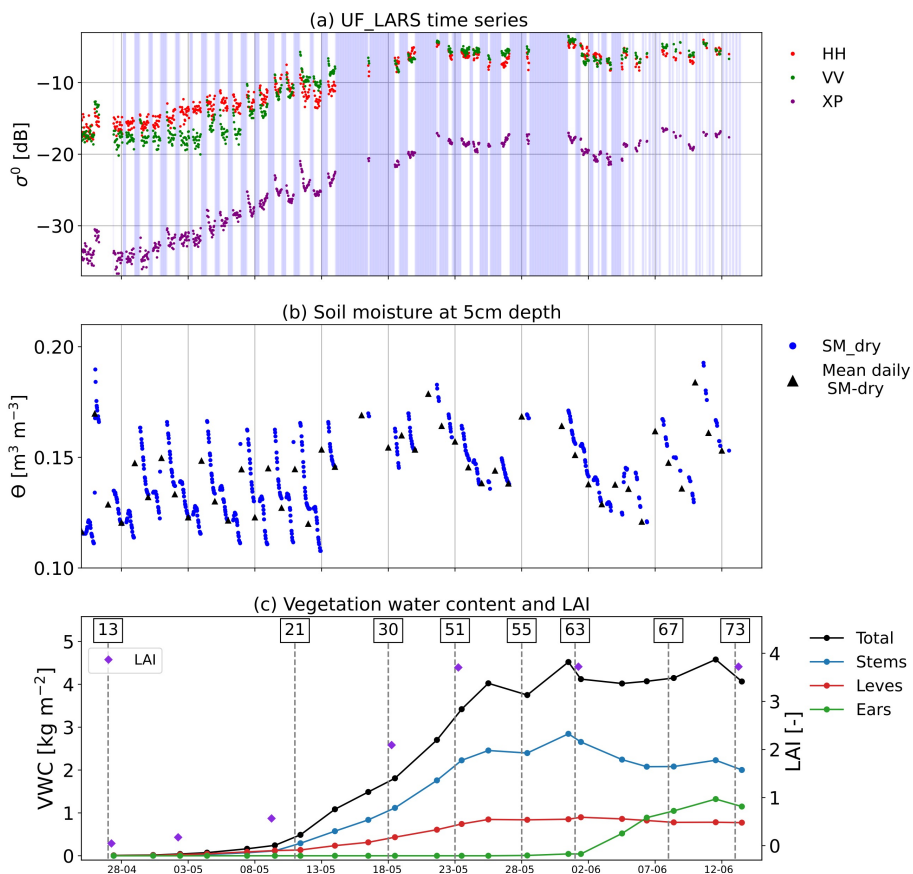


Figure 5.2.: Seasonal variation in (a) L band radar backscatter in HH, VV and cross-polarization (XP), (b) volumetric soil moisture ( $\text{m}^3 \text{m}^{-3}$ ) content at 5 cm depth with a 15 minutes resolution and the mean daily soil moisture ( $\text{m}^3 \text{m}^{-3}$ ) at 5 cm depth), and (c) vegetation water content ( $\text{kg m}^{-2}$ ) per constituents (the phenological stages are shown by BBCH codes). Figures (a) and (b) are only shown when surface canopy water are absence.

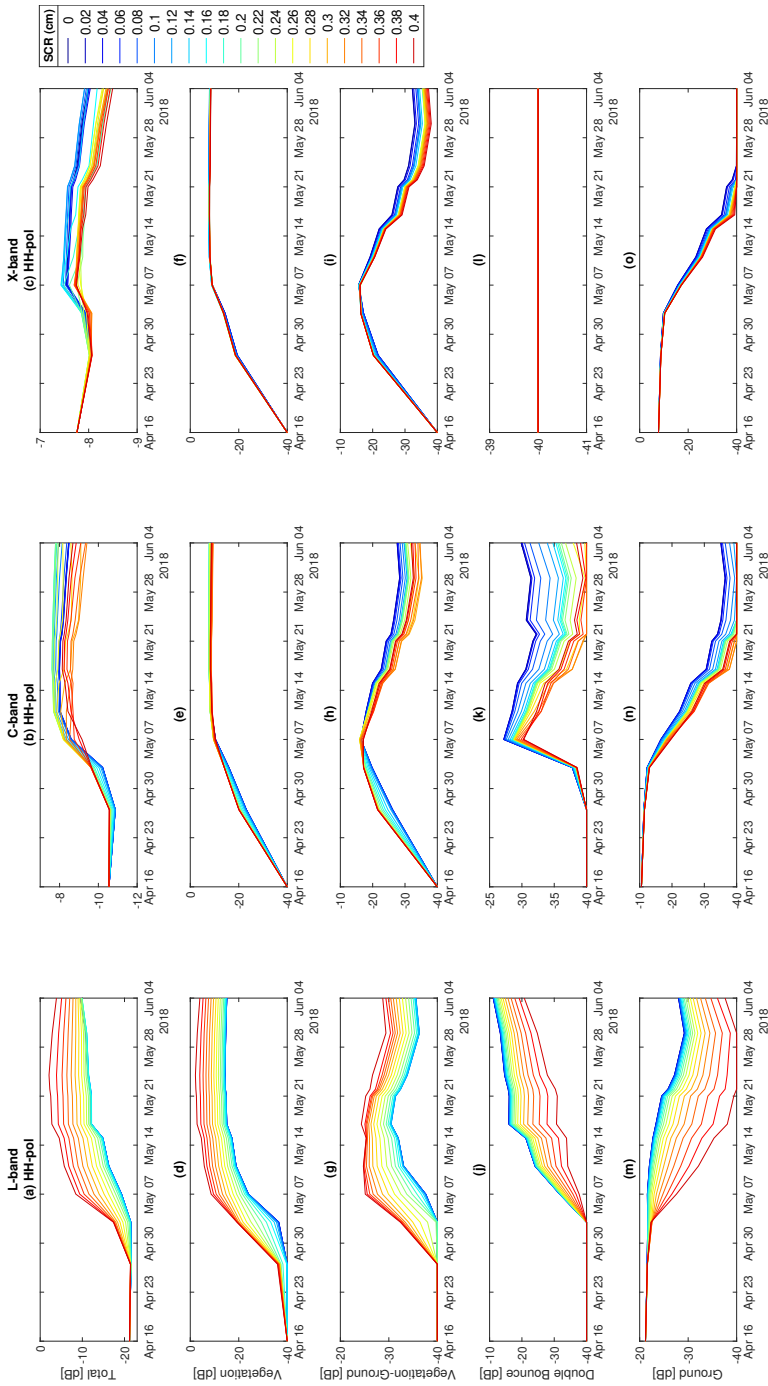


Figure 5.3.: Time series of total and contribution to total backscatter for Tor Vergata model simulations using different small cylinder radius (SCR) sizes for HH pol in L-band (left columns), C-band (middle columns), and X-band (right columns) for a whole growing season of corn.

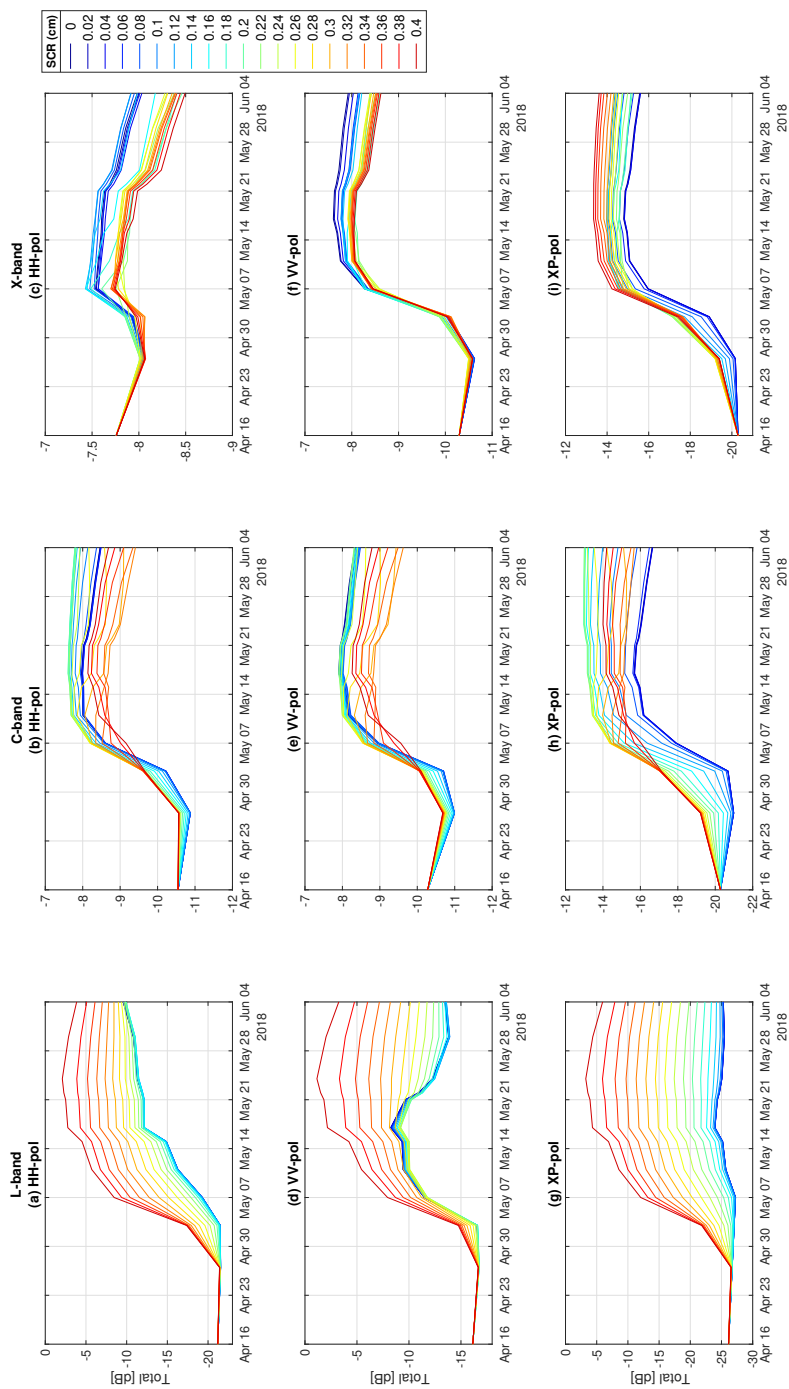


Figure 5.4.: Time series of Tor Vergata model simulations of the total backscatter using different small cylinder radius (SCR) sizes for L-band (left columns), C-band (middle column), and X-band (right columns) and HH, VV, and XP polarizations, during a whole growing season of corn.

larger SCR value (i.e.,  $SCR > 0.29$  cm) reduces direct ground scattering so that direct vegetation scattering and the vegetation-ground scattering becoming the first and second dominant contributions. During the mid and late season (15 May - 4 June), direct vegetation and double-bounce scattering were predominant with lower SCR values. However, an increase in SCR led to a reduction in double-bounce scattering and an increase in vegetation-ground scattering. Hence, for larger SCR values (i.e.,  $SCR > 0.29$  cm), direct vegetation and vegetation-ground scattering emerged as the dominant mechanisms. This shift was caused by increases in the size and water content of the corn leaves due to the increase in SCR, reducing the signal penetration depth and amplifying the interaction of the L band signal with the leafy part of the crop.

In C-band, increasing SCR reduced all ground-related scattering contributions after May 5 (the onset of tiller formation), resulting in a decrease of up to 5 dB in vegetation-ground, and direct ground and up to 10 dB in double-bounce scattering. Direct vegetation scattering remained stable and was unaffected by changes in SCR during this period, possibly due to the small wavelength of the C band compared to the size of corn leaves at this stage.

In X-band, the impact of increasing SCR was the least pronounced compared to the L and C bands. Similar to the C band, from May 5 onwards, direct vegetation scattering dominated, reaching a saturation point by the end of the early season (May 8) and resulting in near-monotonous and similar values across all SCRs. The most noticeable impact of SCR was on vegetation-ground scattering, causing a decrease of up to 4.2 dB. In X band, due to a very short wavelength, the radar signal could not penetrate through out the corn canopy, resulting in zero double-bounce scattering and very negligible direct soil effect during the mid and late season.

The results for VV and XP polarizations are similar to those from the HH polarization. To avoid redundancy, the detailed time series plots of model simulations for VV and XP polarizations can be found in Fig. B.4 and B.5) of Appendix B.2.

To examine the effect of SCR on simulated scattering coefficients across different polarizations, the total simulated backscatter for L, C, and X bands, and HH, VV, and XP polarizations for different SCRs are displayed in Fig 5.4. An increase in SCR from 0 to 0.4 cm led to a maximum increase of 9.38, 11.63, and 18.93 dB in the L band for HH, VV, and XP polarizations, respectively. In the C band, an increase in SCR resulted in decreases of -0.86 and -1.05 dB in HH and VV polarizations, respectively, and an increase of 2.45 dB in cross-pol. In the X band, trends resembled those in the C band, but with smaller backscatter changes of -0.49, -0.65, and 1.88 dB in HH, VV, and XP polarizations, respectively. These findings indicate that the SCR effect is considerable at L-band, but less substantial at C- and X-bands.

### 5.3.3. OPTIMAL SMALL CYLINDER RADIUS (SCR)

Fig. 5.5 shows (in blue) the optimal SCR values obtained using a window size of 1-day (left column) and 5 days (middle column). The right column shows the fixed value of SCR obtained by using all available data. The fixed value was calculated as 0.34 cm for co-pol channels and 0.23 for cross-pol channel. The

corresponding simulated total backscatter is shown in red, and compared to the observed backscatter in grey. The root mean square error (RMSE) between observed and simulated total backscatter for each case was calculated for the period from May 1 to June 12 (i.e the end of the season) and is shown in the lower right corner of each plot. This period was selected because the SCR had no effect on the simulated backscatter before May 1 across all polarizations.

The comparison of simulated backscatter using a fixed SCR and a dynamic SCR reveals that in the very early season (17 April - May 1), while corn leaves are small ( $LAI < 0.9$ ), changes in the SCR do not affect the simulated backscatter. The simulated backscatter is overestimated in VV polarization and underestimated in HH polarization during this period. This discrepancy is primarily linked to the measured roughness parameter, specifically the correlation length values. Accurate measurement of the correlation length is challenging due to its high variability[112]. Previous studies conducted by [112–114] recommend using a calibrated correlation length that provides the best fit between simulated and observed backscatter during the bare soil period. Although this method was attempted in this research, an optimum value for the correlation length yielding the best fit in both polarizations was not found. Hence, the measured value of the correlation length was used. Since the SCR does not influence the simulated backscatter in this period, the main focus is on the mid and late season period (15 May to 12 June), since the effect of SCR size on simulated backscatter is prominent during this period as corn grew and reach its maximum biomass (i.e  $LAI = 3.8$ ).

Simulated backscatter in all cases exhibits gradual changes related to crop growth and more rapid changes tied to SCR variations. The highest dynamic in SCR (blue line) can be seen in Fig 5.5 left column, when using the windows size of 1 day, which results in rapid changes in simulated backscatter. Despite the lowest RMSE values in this case, a very small window size could lead to overfitting of simulated backscatter. The simulated backscatter jumps rapidly and unrealistically, just to fit the observed backscatter better. These swift jumps in simulated backscatter lead to rapid changes in all scattering mechanisms, which cannot be realistic, as previous modeling studies showed gradual changes in scattering mechanisms during the growing season[86, 182].

In general, a fixed value of SCR is sufficient to capture the increase of backscatter in response to vegetation growth during the season, although the rate of increase in backscatter during the vegetative stages in early May differs between the observed and simulated. Using a dynamic SCR reduces the RMSE, as the simulated backscatter captures the finer scale temporal variability of that observed. However, one should be mindful of over-fitting as the smaller window size obviously incorporates fewer data.

Fig. 5.6 highlights the improved ability of the model with a dynamic SCR to simulate daily and sub-daily dynamics in observed backscatter. The observed backscatter is displayed in gray, while the simulated backscatter is shown in red (dynamic SCR) and blue (fixed SCR). In the early season (Fig. 5.6, left column), both simulations using either fixed or dynamic SCR can capture the increase in backscatter associated with plant growth. However, the use of a dynamic SCR

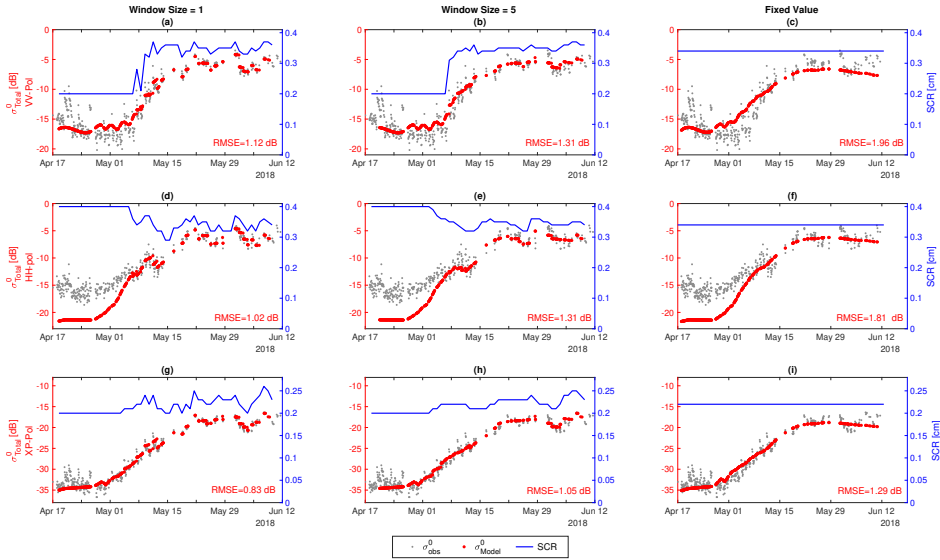


Figure 5.5.: Time series of observed and simulated total backscatter coefficients beside the optimum SCR for window size of 1 day (left column), window size of 5 days (middle column), and fixed SCR (right column) for VV, HH and XP polarization. The root mean square error (RMSE) between the observed radar backscatter and simulated total backscatter for the period of May 1 to end of the season was shown on the bottom of each plots.

improves the ability of the model to capture the diurnal dynamics of the observed backscatter, particularly in VV and XP polarization. Utilizing a dynamic SCR during this period results in RMSE value reductions of 1.16, 0.23, and 0.19 dB in VV, HH and XP respectively, compared to using a fixed SCR. Recall that the disparity between the modeled and observed data in VV and HH polarization for the period of 1 May until 5 May is mainly attributable to the roughness parameter.

In the mid-to-late season (Fig. 5.6, right column), the use of a fixed SCR means that the simulated backscatter lacks the daily and sub-daily dynamics of the observations. Using a dynamic SCR yields a simulated backscatter time series with more temporal variability, a reduced RMSE and a visibly improved agreement with the observations in all polarizations. Reductions of around 0.29, 0.37, and 0.76 dB were obtained using the dynamic SCR in VV, HH and XP polarization. Therefore, we conclude that dynamic calibration of SCR leads to better estimates of fine temporal variations in backscatter, e.g. those associated with soil moisture and vegetation water content changes and therefore a better agreement with observed backscatter in all polarizations.

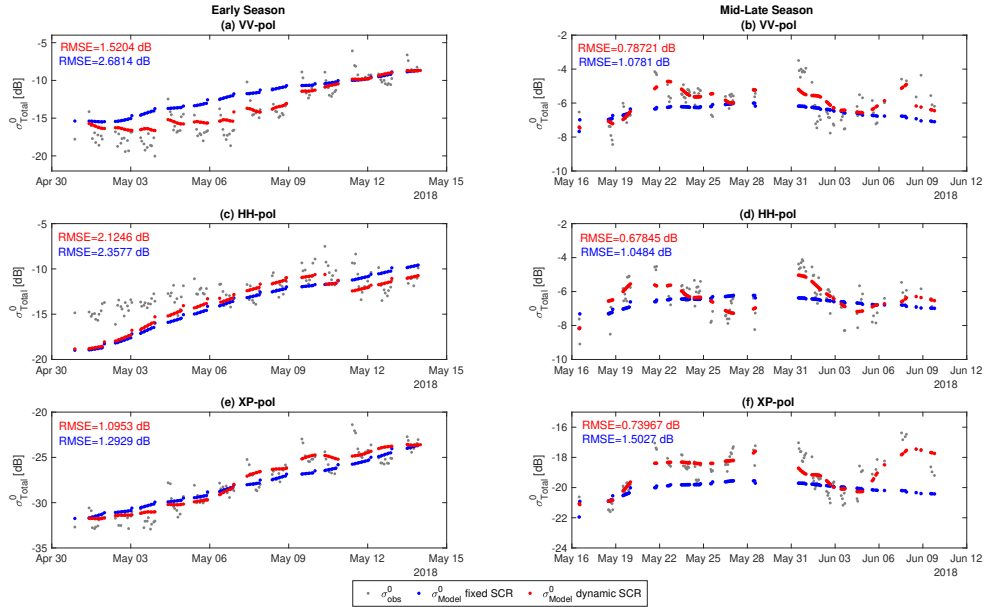


Figure 5.6.: Time series of observed and simulated total backscatter coefficients using the fixed SCR and dynamic SCR using window size of 5 day for two period of Early season (left column) and mid and late season (right column) in VV, HH and XP polarization respectively. The root mean square error (RMSE) between the observed radar backscatter and simulated total backscatter in each case was shown on the top of each plots.

### 5.3.4. FACTORS CONTROLLING OPTIMUM SMALL CYLINDERS RADIUS

The coefficient of determination ( $R^2$ ) of the MLR method for HH, VV, and XP polarization and the two growth stages is displayed in Table 5.2. This demonstrates the relationship between the modeled and calibrated SCR. The coefficient of determination ( $R^2$ ) in the MLR method can explain how much variability in one factor can be attributed to its relationship with other factors. A higher  $R^2$  signifies a stronger linear relationship.

Results in Table 5.2 indicate that the highest  $R^2$  occurred during the vegetative stage, when considering the vegetation water content of corn leaves and surface soil moisture. This suggests that SCR dynamics during this period were primarily affected by the simultaneous changes in corn leaf VWC and surface soil moisture. During the reproductive stage, the highest  $R^2$  values were observed when considering stem water content and surface soil moisture. This period corresponds with ear formation and development.

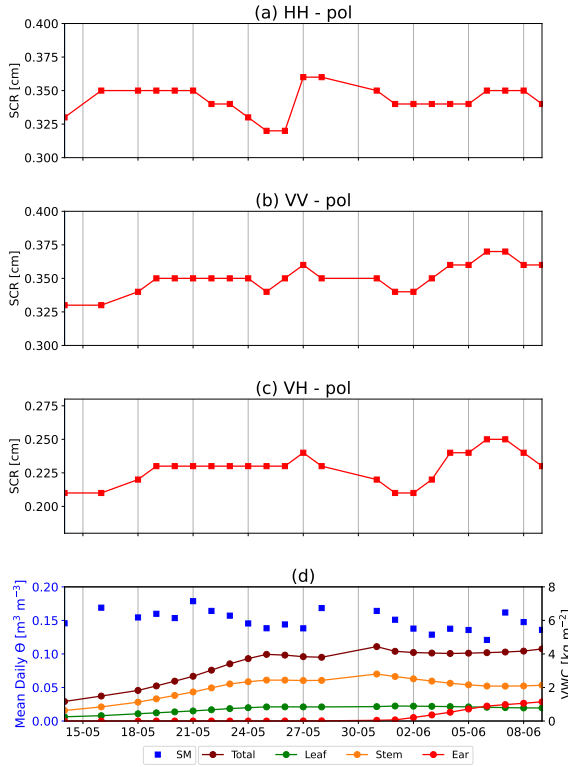


Figure 5.7.: Time series of optimum small cylinder radius (SCR) using the windows size of 5 days in (a) HH polarization, (b) VV polarization, (c) cross-polarization XP during mid and late season. (d) shows the seasonal variation in the same period for the mean daily soil moisture ( $\text{m}^3 \text{m}^{-3}$ ) at 5 cm depth, and vegetation water content ( $\text{kg m}^{-2}$ ) per constituents.

Table 5.2.: The coefficient of determination ( $R^2$ ) of the multi linear regression (MLR) method for HH, VV and XP polarization and two growth stages of vegetative and reproductive stage.

	HH		VV		XP	
	Vegetative stage	Reproductive stage	Vegetative stage	Reproductive stage	Vegetative stage	Reproductive stage
SM & $\text{VWC}_{total}$	0.8	0.44	0.53	0.05	0.71	0.05
SM & $\text{VWC}_{leaf}$	<b>0.81</b>	0.57	<b>0.6</b>	0.63	<b>0.77</b>	0.53
SM & $\text{VWC}_{stem}$	0.8	<b>0.62</b>	0.58	<b>0.71</b>	0.75	<b>0.75</b>
SM & $\text{VWC}_{ear}$		0.46		0.67		0.55

## 5.4. SUMMARY AND CONCLUSION

This research utilized high temporal resolution data from an L-band fully polarimetric tower-based radar, along with the geometrical and water content of corn constituents,



to study the effect of SCR on three frequencies (L-, C-, and X-band) and all polarizations (HH, VV, and XP) in the radiative transfer (RT) model developed by Tor Vergata University. A calibration technique was also presented to determine the optimum SCR for each polarization, with the goal of improving the model's ability to simulate sub-seasonal and daily dynamics in response to internal vegetation water content and soil moisture variations.

Results show that SCR can significantly affect total simulated backscatter across all polarizations and the three frequencies considered. The impact was most pronounced in the L-band (up to 18.93 dB) and diminished significantly for the C and X bands (up to 2.45 and 1.88 dB, respectively). This suggests that SCR selection is crucial for frequencies up to 5 GHz, while its impact is less significant at higher frequencies. Furthermore, it was demonstrated that the choice of SCR can directly affect the relative contribution of different scattering mechanisms to total simulated backscatter, and their relative importance throughout the growing season. This influence varied across different frequencies, indicating that the optimum SCR is frequency-dependent. Analysis of the trend and dynamic range of the optimal SCR in L-band during the mid- and late- seasons showed that the optimal SCR is also polarization-dependent. Therefore, the choice of optimal SCRs cannot be transferred across polarizations or frequencies. This implies that the calibration method presented in this thesis should be applied separately for each polarization and frequency.

In L-band, the use of a dynamic SCR improved model performance by better simulating the sub-seasonal and daily temporal dynamics in observed data, particularly during the mid and late seasons. By employing a dynamic SCR derived from a window size of five days instead of a fixed SCR, the root mean square error (RMSE) between the model and observation was reduced by around 0.64, 0.58, and 0.69 dB in VV, HH, and XP polarization, respectively. Multiple linear regression results show that the SCR dynamics are not arbitrary. MLR analysis suggests that during the vegetative stage, surface soil moisture and corn leaf water content drove the SCR dynamics in all polarizations. Conversely, during the reproductive stage, the simultaneous dynamics in surface soil moisture and corn stem water content drove the SCR dynamics in all polarizations.

The findings of this chapter underscore the potential importance of considering a dynamic SCR over a fixed SCR, particularly for frequencies up to 5 GHz, to improve model accuracy by better simulating the temporal dynamics in observed data. Nonetheless, the conclusions drawn in this thesis are confined to a single crop type and a fixed incidence angle, necessitating further experimental research to explore the performance of the calibration technique presented here using different viewing geometries and for different crop types.

The results presented in this chapter show that in order to capture sub-seasonal, daily and sub-daily dynamics in observed backscatter, we need to revisit the assumptions made in radiative transfer models. In particular, we need to revisit assumptions regarding parameters that are assumed to be constant for the growing season. While this assumption may be sufficient to capture the overall seasonal dynamics, it may not be sufficient to capture fine temporal variations associated

with water status rather than biomass changes. The dynamics observed in SCR and its influence on the total backscatter show that it is effectively controlling the relative importance of the ground-affected contributions. It is physically plausible that such a parameter would be directly related to vegetation water content which is known to influence both scattering and extinction. Nonetheless, additional research is recommended to explore this and other parameters used in the Tor Vergata model and other models to represent the distribution of moisture within the vegetation. The data presented by [23], for example, highlight that the vertical distribution is non-uniform, and highly dynamic over a range of timescales. As the microwave remote sensing community pays increasing attention to the use of radar (and radiometry) data to study water status as well as biomass, it is essential to ensure that models are parameterized in a way that allows us to account for the known spatial (vertical and among constituents) and temporal variations in water content.



# 6

## THE INFLUENCE OF SURFACE CANOPY WATER ON L-, C-, AND X-BAND BACKSCATTER: A STUDY COMBINING DETAILED *In situ* DATA AND THE TOR VERGATA RADIATIVE TRANSFER MODEL

*As explained in previous chapters, our current understanding of the impact of surface canopy water (SCW) on total backscatter and the underlying mechanisms is limited. To advance our understanding, we require a radiative transfer model capable of simulating the effect of SCW on the radar signal. To this end, we employed the radiative transfer model developed at Tor Vergata University.*

*In the previous chapter, we presented a calibration technique for this model, facilitating its simulation of high temporal dynamics in backscatter data. However, to explore the impact of surface canopy water (SCW) on backscatter across various frequencies and polarizations, there was still a need to develop a model that could accurately simulate the influence of SCW on radar backscatter.*

*In this chapter, the calibrated Tor Vergata model is used to simulate total backscatter at L-, C-, and X-bands and to study the relative contributions of various scattering mechanisms. In this chapter, we first compared simulations from the standard form of the calibrated Tor Vergata model to L-band observations from the fully-polarimetric UF-LARS tower-based scatterometer. Subsequently, we developed two additional implementations of the Tor Vergata model to account for the effects of SCW and the presence of water on the soil surface on radar backscatter. After comparing simulated and observed backscatter for the full growing season at the L-band, we used the three implementations to simulate backscatter at C- and X-bands for the same period.*

## 6.1. INTRODUCTION

Surface canopy water (SCW) refers to water present in the form of dew or interception from irrigation or precipitation on the canopy surface. Several studies have investigated the influence of the presence of water on the canopy surface. It has been shown that the presence of SCW can play an important role in the recovery of the water content in plants after heavy water loss, and that SCW can be an important source of moisture for plants in arid areas during the dry season [65, 70]. Therefore, The information about the duration and amount of SCW can be valuable to support crop management decisions such as the optimal scheduling of fungicide applications.

In addition to the direct effect of SCW on hydrology and plant biology, SCW can directly affect microwave observations and influence the retrieval and estimation of e.g. soil moisture, vegetation optical depth (VOD), biophysical variables, canopy fuel load, and crop classification [66–69, 75, 76, 102, 194].

Radar observations from agricultural land are highly sensitive to the dielectric and structural properties of the crops and soil depending on system properties (i.e. frequency, polarization, and incidence angle) [5, 6, 24, 139]. The presence of SCW increases the water content, and hence dielectric constant of the crop, leading to an increase in the observed backscatter [78, 79]. Several experimental studies have been conducted using different radar configurations over different crop types to understand the effect of SCW on radar data. However, the previous studies could not explain the differences observed between polarizations because there was limited understanding of how the presence surface canopy water affects the various contributions to total backscatter.

The aim of this chapter is to investigate the effect of SCW on backscatter as a function of frequency, polarization, and growth stage and to understand the influence of SCW on the contributions to total backscatter. The radiative transfer model developed at the Tor Vergata University is used to simulate the backscatter response as a function of frequency and polarization. The standard form of the Tor Vergata model does not consider the presence of SCW on leaves. Therefore, two additional implementations of the Tor Vergata model are considered in this chapter, whereby the standard model is adapted to account for the presence of water on the surface of the vegetation and soil by adjusting the leaves' internal water content and soil moisture respectively. Simulations at L-band from the three model implementations are first compared to the L-band observations from the UF-LARS scatterometer. Then the three model implementations are used to simulate backscatter at C- and X-band to explore the difference in sensitivity to SCW as a function of frequency and polarization.

---

This chapter is based on:

Khabbazan, Saeed et al., "The Influence of Surface Canopy Water on L-, C-, and X-Band Backscatter: A Study Combining Detailed *In situ* Data and the Tor Vergata Radative Transfer Model." *Science of Remote Sensing* (2023): Under revision

## 6.2. DATA AND METHODS

### 6.2.1. EXPERIMENTAL SITE

The data for this research were also collected during a field campaign near Citra, Florida during spring 2018. For detailed information regarding the Study site specific to this part of the research, please refer to section 2.1 of this thesis.

### 6.2.2. FIELD MEASUREMENTS

#### SURFACE CANOPY WATER

For detailed information regarding the surface canopy water data specific to this part of the research, please refer to section 2.3.3 of this thesis.

#### SOIL DATA

For detailed information regarding the soil data specific to this part of the research, please refer to section 2.3.2 of this thesis.

#### VEGETATION DATA

For detailed information regarding the vegetation data specific to this part of the research, please refer to section 2.3.4 of this thesis.

#### GROUND-BASED RADAR OBSERVATIONS

Radar backscatter was measured using the truck-mounted University of Florida L-band Automated Radar System (UF-LARS) [106]. For detailed information regarding the ground-based radar observations data specific to this part of the research, please refer to section 2.3.4 of this thesis.

### 6.2.3. RADIATIVE TRANSFER MODEL

In this research, the two-layer model developed at the University of Rome, Tor Vergata [85] specifically for corn was used, and is referred to as the "Tor Vergata model" throughout. This model has been used in multiple studies for the simulation of radar backscatter across various crop types and frequencies, ranging from P- to X-band [18, 88–101]. The model has therefore been validated at the frequencies (L-, C- and X-band) considered here. For instance, in the work of Della Vecchia *et al.* [89], the model was used to simulate the scattering from corn during the growing season for frequencies between 2.5 and 10.2 GHz for incidence angles between 20 and 50 degrees, across all linear polarizations. This chapter, compared model simulated data with experimental data collected by the Radio ScAtteroMeter (RASAM). The findings indicated that the RMS error between the simulated and actual data across five different frequencies ranged from 1.37 to 2.23 dB. In another study, Della Vecchia *et al.* [98] employed the model for maize and wheat backscatter simulation at C-band frequencies, comparing it with ground-based and ERS-2 data. The model performance demonstrated RMSE of 1.44 and 0.96 dB when comparing simulated and observed data in corn fields, and 1.78 and 2.23 dB in wheat fields.

The RMS errors of less than 2 dB in previous studies demonstrate the model performance matched observations, demonstrating its sensitivity to crop growth across various frequencies. Vermunt *et al.* [119] employed the Tor Vergata model to quantify the relative importance of soil and vegetation contributions to the total L-band backscatter of maize and how this changes during the growing season. Note that Vermunt *et al.* [119] used the same observations from UF LARS but did not account for the influence of surface canopy water (SCW) or the presence of water on top of the soil layer on backscatter or on the contributions to total backscatter.

This model is a discrete microwave scattering model based on radiative transfer theory. The model simulates both scattering and extinction properties of vegetation elements and of the underlying soil by applying the most appropriate electromagnetic approximation, based on the scatterer shape and the wavelength. The corn field is modeled as a homogeneous half-space with a rough interface, representing the soil, overlaid by a single layer made up of the stems, leaves, and petioles (i.e. ribs). This model does not consider ears because Della Vecchia *et al.* [98] found that including ears has a limited effect on total simulated backscatter from corn (<0.3 dB).

For the soil layer, the scattering coefficient of soil is computed by means of the original version of the Integral Equation Model (IEM) [188]. Input data for this model comprises the soil permittivity that was computed using Mironov's soil dielectric model [186, 187], soil roughness parameter such as root mean square (RMS) height ( $s$ ), correlation length ( $l$ ), and the exponential autocorrelation function. Álvarez-Mozos *et al.* [112], Baghdadi *et al.* [113], and Baghdadi, Holah, and Zribi [114] and others suggest calibrating the correlation length, selecting the value that yields the minimum RMSE between observed and simulated backscatter for the measured RMS height. This approach is generally a pragmatic solution to the difficulty in measuring accurate correlation length in the field. However, we measured both RMS height and correlation length (Section 2.2.2), and use the measured values directly here.

For the vegetation layer, leaves are represented by dielectric discs and stems, and ribs by dielectric cylinders. The permittivity of the vegetation constituents is computed using the model of Matzler [195]. The discs are described by their diameter and thickness while the cylinders are described by their diameter and length. Long leaves are subdivided into several discs, with the diameter equal to the leaf width. The orientation of leaves and ribs scatterers within the canopy layer was arranged randomly assuming a uniform distribution.

To compute the scattering matrices and the extinction vector, different approximations are used depending on the frequency. For frequencies up to 5 GHz, the Rayleigh-Gans approximation [189] is used for both leaves and ribs (i.e. L-band). For frequencies higher than 5 GHz, the Physical Optics approximation is used for leaves and the infinite length approximation [190] is used for ribs (i.e. C- and X-band). For stems, the infinite length approximation is used for all frequencies. The model utilizes the matrix doubling algorithm [189] to combine contributions from the various scatterers, and between vegetation and soil. This method allows for the inclusion of multiple scattering effects of any order in the calculation of the backscattering coefficient and it can separate contributions of different scatterers

in the vegetation canopy. In the Tor Vergata model, the total backscatter has four contributions:

$$\sigma_{total}^0 = \sigma_v^0 + \sigma_{vg}^0 + \sigma_{db}^0 + \sigma_g^0 \quad (6.1)$$

where  $\sigma_{total}^0$  is the total backscatter coefficient,  $\sigma_v^0$  is the vegetation scattering (i.e. volume scattering by the vegetation layer),  $\sigma_{vg}^0$  is the vegetation-ground scattering (i.e. multiple scattering effects due to interactions between the vegetation and ground),  $\sigma_{db}^0$  is the soil-stem double bounce specular reflection, and  $\sigma_g^0$  is the direct component solely from the soil surface attenuated by the canopy. In  $\sigma_{vg}^0$ , multiple interactions between the plant elements, and between the plant elements and the ground are considered, whereas in  $\sigma_{db}^0$ , only the corner reflection between the vertical stem and the ground is taken into account, as illustrated in Fig. 5.1.

A more detailed and comprehensive description of the model and its assumptions can be found in [85]. A list of the input variables provided to the Tor Vergata model is presented in Table 5.1. Moreover, the hourly values of vegetation geometry measurements for the input of the model were obtained by linear interpolation and is shown in Fig. B.6 in the Appendix-B. It should be noted that in this study the sub-daily cycles of Mg were not considered, because of the laborious nature of destructive sampling.

#### 6.2.4. ACCOUNTING FOR SCW IN THE TOR VERGATA MODEL

The presence of SCW increases the amount of water present in the vegetation layer above the soil. In reality, SCW consists of droplets of free water on the outside of the leaves. It is not trivial to introduce this into a model because it would require parameterization of the shape, size, and distribution of the water droplets and a model to account for their behavior in an electric field. As a first approximation, we account for the presence of water on the surface of the vegetation by adjusting the internal gravimetric water content for the disc and small cylinders so that the additional moisture due to SCW “appears” as extra leaf moisture. It implicitly assumes that water on the surface of the leaf behaves in the same way as water within the leaf, which may not be the case. Nonetheless, it at least includes the additional moisture, and ensures that it is distributed within the canopy using the canopy architecture. In the Tor Vergata model, the average gravimetric water content ( $M_g$ ) of all corn leaves is used as an input parameter for the disc (leaf) and small cylinders (ribs) gravimetric moisture to account for their internal water content. The adjusted internal gravimetric water content ( $M_{g+}$ ) for the disc and small cylinders is calculated as follows:

$$W_{f+} = W_f + \frac{SCW}{\rho_{plant}} \quad (6.2)$$

$$M_{g+} = \frac{W_{f+} - W_d}{W_{f+}} \quad (6.3)$$

where  $W_{f+}$  is the combination of the fresh weight and the amount of SCW of corn leaves ( $kg$ ) and the  $W_d$  is the dry weight of the corn leaves ( $kg$ ).



Vermunt *et al.* [119] and [102] observed increases in radar backscatter during the bare soil period that could not be explained by *in situ* soil moisture measurements at 5cm but coincided with non-zero measurements of the SCW sensors. They argued that these increases could be attributed to the presence of a thin layer of dew visually observed on the soil surface. Here, we account for the effect of the presence of dew on the soil surface by setting the soil moisture in the surface layer to the measured saturated value for sandy soil (i.e.  $0.37 \text{ m}^3 \text{ m}^{-3}$ ) when the leaf wetness sensor indicates the presence of water.

In the following analysis, we will consider three implementations to investigate the effect of SCW on the vegetation and the soil surface:

(1) In the “VWC” scenario, the presence of SCW is not taken into account and the measured  $M_g$  was used for disc and small cylinders. This corresponds to a standard implementation of the Tor Vergata model.

(2) In the “VWC+” scenario, the internal water content is adjusted so that the gravimetric water content used in the model is the ( $M_{g+}$ ) calculated using Eq. 6.3. In this scenario, the role of dew on the soil surface is not considered.

(3) In the “VWC+SM+” scenario, the internal water content is adjusted so that the gravimetric water content used in the model is the  $M_{g+}$  calculated using Eq. 6.3. In addition, the surface soil layer is assumed to be saturated when the presence of SCW is detected.

## 6.3. RESULTS AND DISCUSSIONS

### 6.3.1. FIELD MEASUREMENTS

#### HYDROMETEOROLOGICAL DATA

Fig. 6.1 shows the daily amount of irrigation and accumulated precipitation as well as the time series of volumetric soil moisture. The early season (28 April - 15 May) was dry, therefore irrigation was conducted every 8 days, close to midnight to minimize evaporation losses.

The mid-season (16 - 31 May) had frequent and heavy tropical rainfall with a cumulative precipitation amount of around 215 mm.

The late season (1-13 June) was almost dry with few rain events, and a cumulative precipitation amount of around 35 mm. A more detailed description of the hydrometeorological data is provided by Khabbazan *et al.* [102] and Vermunt *et al.* [119]

#### SCW DATA

Fig. 6.2 (a) illustrates that the average water mass ( $M_w$ ) deposited on the surface of the three leaf wetness sensors (LWS) due to dew was approximately one-third of that resulting from interception. In the early season, the water accumulation on the LWS and canopy was primarily due to dew and interception from irrigation, whereas, in the mid-season, it was predominantly from interception from frequent rain events. In the late season, dew was the main source of wetness.

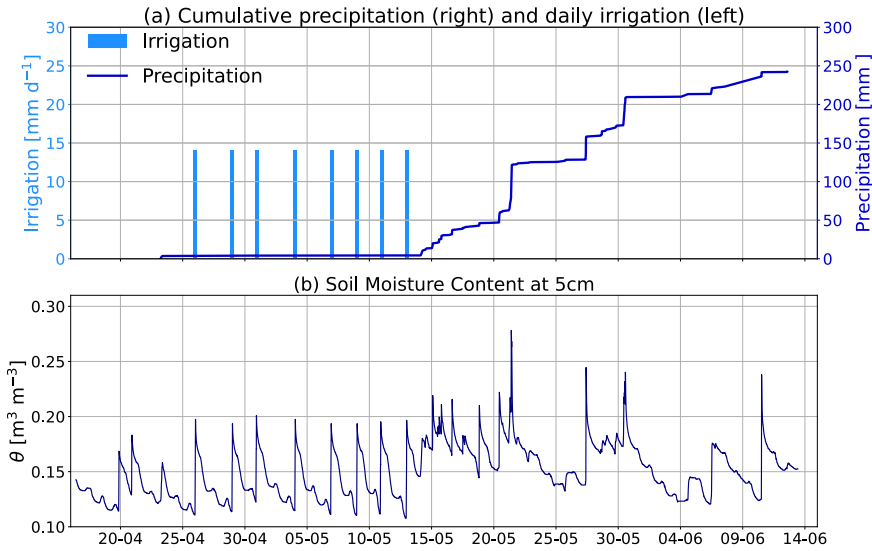


Figure 6.1.: Time series of (a) daily irrigation amounts mm per day and cumulative rainfall mm captured every 15 minutes by Florida Automated Weather Network, (b) averaged volumetric soil moisture  $m^3 m^{-3}$  from two pits at 5cm depth captured every 15 minutes.

The results from Fig. 6.2 (a) indicate variability in the water mass on the LWS caused by dew events during the early season, highlighting both moderate and high dew occurrences. For example, the dew event on 6 May was the heaviest of the season, resulting in a water deposition of  $125 \text{ g m}^{-2}$  on the LWS, while the following day event (7 May) led to only  $20 \text{ g m}^{-2}$ . In case of the interception events, early season irrigation resulted in lower water deposition on the LWS compared to the precipitation events during the mid and late seasons.

Fig. 6.2 (b) displays a time series of the surface canopy water (SCW) on the corn leaves, which is derived from the water mass data on the LWS (Fig. 6.2 (a)) by applying equations 2 and 3. The results show that the amount of SCW increased with biomass accumulation. During the early season, the SCW was relatively low for both dew and interception events, approximately  $0.04$  and  $0.09 \text{ kg m}^{-2}$  respectively. This increased up to  $0.47$  and  $1.28 \text{ kg m}^{-2}$  in the late season. Comparing results from Fig. 6.2 (a) and (b) for the early season reveals that although the water mass on the LWS exhibited significant variation due to dew and irrigation, the SCW remained relatively consistent. This consistency in SCW can be attributed to the small size of the corn leaves during this period. As the corn reached its maximum biomass in the late season, the SCW increased by up to 10 times compared to the early season, even though the water mass on the LWS remained almost similar throughout. These results highlight the impact of biomass accumulation on the amount of water on top of the canopy surface.

The frequency of the presence of SCW is shown in Fig. S2 (supplementary

material). SCW was present on more than 80 % of days after midnight and on more than 90 % of days after 3 AM until 10 AM. This is noteworthy because many polar-orbiting, sun-synchronized satellites have an overpass during this period.

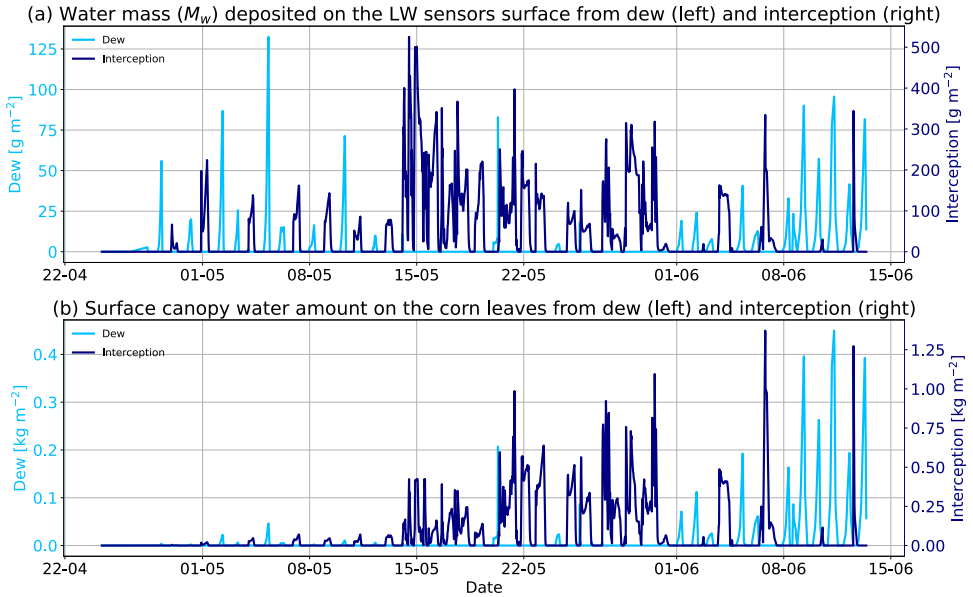


Figure 6.2.: Time series of (a) water mass ( $M_w$ ) deposited on the leaf wetness sensors surface from dew and interception and (b) the amount of SCW on corn leaves caused by dew or interception. Note: consider the magnitudes involved are very different for dew (left axis) and interception (right axis) events.

### VEGETATION DATA

Crop development and internal water content dynamics during the whole season are shown in Fig. 6.3. The corn leaves reached their maximum size around 25 May when LAI reached its maximum value of 3.8. Before 25 May, the gravimetric water content of both stems and leaves were almost stable. Tassel emergence occurred around 25 May, after which  $M_g$  of both stems and leaves decrease. A sharp decrease is observed after 1 June. Ear formation results in a significant decrease in the  $M_g$  of the stems. The hourly interpolated and the adjusted gravimetric water content of the leaves ( $M_g$ ) calculated using Eq. 6.3 are also shown in this figure. Note, that the adjusted gravimetric water content never exceeds 1.

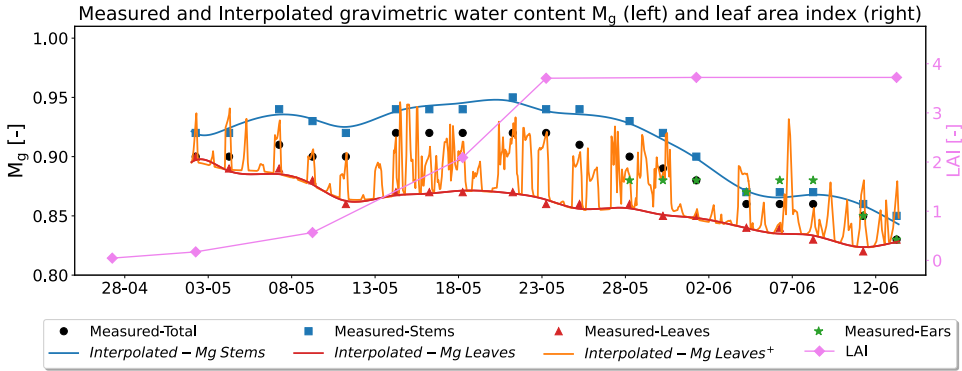


Figure 6.3.: Seasonal pattern of measured predawn gravimetric water content for total plant and per constituents and measured LAI, in addition with hourly interpolated gravimetric water content of stems and leaves and the adjusted gravimetric water content of corn leaves using the SCW amount ( $M_{g+}$ ).

### 6.3.2. REPRESENTING THE EFFECT OF SCW IN THE TOR VERGATA MODEL

Here, we compare the three implementations of the Tor Vergata model in terms of their capacity to simulate total L-band backscatter. The results for these three implementations at L-band for HH, VV, and XP polarizations are shown in Fig. 6.4, 6.5, and 6.6 respectively. Statistics describing the agreement between the model and L-band observations are provided in Table 6.1.

Fig. 6.4 - 6.6 (a) show that, in all three implementations, there is poor agreement between simulated and observed L-band backscatter during the bare soil and early vegetative stage (before 15 May). However, the model performance improves during the middle and late season (after 15 May) when the LAI is above 1.5. In Table 6.1, the RMSE values are always higher for the period before 15 May than the period after 15 May. This is primarily due to the performance of the IEM soil scattering model during the bare soil and early season period. Even for dry data (days without SCW), the IEM model does not capture the observed dynamics in radar backscatter due to the change in surface soil moisture. In addition, in HH polarization (Fig. 6.4), a significant bias occurs due to a well-documented challenge related to determining the surface roughness [112], our treatment of which is discussed in Section 2.3, and the presence of system noise in the first few days of this period in HH backscatter [102, 194]. It worth mentioning that, in the UF-LARS scatterometer, all channels are designed to be independent, which results in independent noise levels. During the first few days of the season, up to May 8th, the power ratios at HH polarization were closer to the noise floor compared to those at VV polarization. This noise led to variability in the sigma nought data obtained post-calibration. Despite extensive investigations, the primary reason for this noise remained undetermined and unresolved. These HH data are plotted for completeness but are not used in

any quantitative analyses.

In all three polarization (Fig. 6.4 - 6.6 (a)), in the presence of SCW (wet data), even when the surface layer is assumed to be fully saturated to represent the presence of SCW, the IEM model underestimates the backscatter dynamics from bare soil. In this period, the  $VWC^+$  implementation has a limited effect due to the small size of the corn leaves. However, the  $VWC^+SM^+$  implementation reduced the RMSE considerably. This will be discussed in detail in Section 3.3.

In the absence of SCW (dry data) the RMSE and ubRMSE values after 15 May are half of those obtained before 15 May. In addition, the bias is close to zero for dry data after 15 May. This can be easily seen by comparing Fig. 6.4 - 6.6 (b) to Fig. 6.4 - 6.6 (c). These results show that the standard Tor Vergata model can simulate the observed backscatter from corn in L-band, and in all polarizations (RMSE<0.85 dB) at the mid and late season (LAI>1.5) in the absence of SCW.

For wet data, the performance of all three Tor Vergata model implementations is better for the period after 15 May (mid to late season) compared with the period before 15 May (early season). This can be seen by comparing Fig. 6.4 - 6.6 (d) to Fig. 6.4 - 6.6 (e). Comparing the three implementations, the RMSE and bias values after 15 May are always highest for the standard VWC implementation. The reduction in RMSE, and particularly, bias values in the  $VWC^+$  implementation shows that representing the observed SCW as additional internal water content of leaves (Modeled  $VWC^+$ ) leads to some improvement in the agreement between modeled and simulated L-band backscatter. However, the bias is still higher than that observed for dry data, suggesting that there is considerable scope for improvement in how SCW on the vegetation can be represented. The additional value of  $VWC^+SM^+$  over  $VWC^+$  is limited after 15 May due to the limited sensitivity to the soil surface under the fully grown canopy.

### 6.3.3. THE EFFECT OF DEW ON SOIL

Fig. 6.7 provides a detailed view of the period before 15 May when the soil is transitioning from bare to light vegetation cover (LAI<1.5) for VV and XP pol. The HH pol is not included here due to a significant bias between observed and modeled data as a result of a well-documented challenge related to determining the surface roughness [112] and also the presence of system noise in the first few days of this period in this channel [102] as already explained in previous sections.

The gradual increase in the observed radar backscatter during this period is related to crop growth (Fig. 6.3). The daily cycles superimposed on this upward trend are due to dynamics in the soil moisture, internal vegetation water content, and the presence of interception or dew. Midnight irrigation (indicated by the blue background) led to a rapid increase of around  $0.1 \text{ m}^3/\text{m}^3$  in soil moisture at 5 cm depth which resulted in an increase of more than 5 dB in backscatter in both polarizations. On nights without irrigation, the accumulation of dew from midnight until sunrise (periods indicated by grey background) led to a gradual increase in backscatter of up to 2-3 dB, even though soil moisture (measured at 5 cm) was decreasing. While the corn leaves are small during this period, this increase can be related to the accumulation of dew on the soil surface as discussed by [102, 119].

Table 6.1.: Comparison of modeled and observed backscatter per polarization, where a distinction is made between early (before 15 May) and late (after 15 May) season, as well as between acquisitions obtained in the presence (Wet data) and absence (Dry data) of SCW.

Polarization		Assesment parameter		Modeled dataset conditions							
				Before 15 May				After 15 May			
				Dry data		Wet data		Dry data		Wet data	
		VWC	VWC	$VWC^+$	$VWC^+SM^+$	VWC	VWC	$VWC^+$	$VWC^+SM^+$		
VV	RMSE	1.63	3.18	3.07	2.72	0.85	1.58	1.49	1.46		
	UbrMSE	1.62	2.4	2.38	2.71	0.85	1.06	1.49	1.46		
	Bias	-0.17	2.09	1.93	-0.18	0.01	1.17	-0.05	-0.09		
HH	RMSE	4.24	3.84	3.96	3.06	0.78	1.14	1.05	1.05		
	UbrMSE	2.37	1.97	2.27	1.77	0.78	0.79	0.98	0.97		
	Bias	3.52	3.3	3.24	2.5	0.08	0.82	-0.37	-0.41		
XP	RMSE	1.34	1.84	2.27	2.51	0.73	1.94	1.29	1.25		
	UbrMSE	1.26	2.07	2.25	2.38	0.73	1.22	1.28	1.25		
	Bias	0.44	1.21	0.33	-0.8	-0.01	1.51	0.13	0.02		

In VV, simulated backscatter from the VWC and  $VWC^+$  implementations are virtually identical. With the exception of 9 and 11 May, the  $VWC^+$  results overlay the VWC results completely. Due to the limited vegetation cover, the total VV backscatter is primarily affected by the soil surface rather than the vegetation. Both implementations simulate the increase in the observed backscatter due to crop growth and biomass accumulation, and the variation in 5 cm soil moisture. But neither captures the observed sub-daily dynamics. The RMSE from the VWC and  $VWC^+$  implementations are 3.18 dB and 3.08 dB in VV. Part of the discrepancy is due to the limitations of the IEM model discussed earlier. However, our working hypothesis is that the failure to account for water on the soil surface explains the lack of sub-daily dynamics. In VV, the  $VWC^+SM^+$  implementation introduces a steep change in backscatter as soon as any SCW is detected on the leaf wetness sensor. The high values, during the dew and interception period, correspond to the VV backscatter from saturated soil. The value increases from -12 dB on 28 April to -9 dB on 12 May. While this introduces a response in backscatter at the right time, it is too high for dew events before 4 May, and too low for interception events after 4 May. The  $VWC^+SM^+$  leads to an increase in ubRMSE compared to  $VWC^+$  because it has limited variability, but it results in a significant reduction in absolute bias.

In cross-pol, the sensitivity of total backscatter to even a small amount of vegetation means that the VWC and  $VWC^+$  simulations can be distinguished during most dew and interception events. The inclusion of additional moisture in the leaves of these young crops is enough to increase backscatter and reduce the bias between simulated and observed XP backscatter. However, even the increase in  $VWC^+$  is not enough to explain the dynamics in backscatter during interception events from

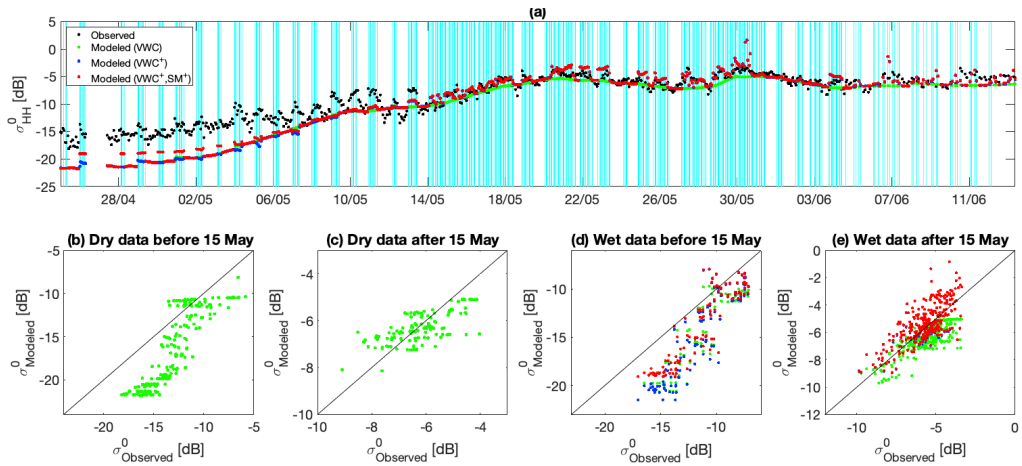


Figure 6.4.: The time series of observed backscatter and modeled backscatter for the three implementations at L-band and HH polarization. Light blue vertical lines indicate the presence of SCW during radar acquisition (a). The scatter plot between the observed and modeled backscatter for data when there was no SCW (dry data) for time periods before 15 May (bare soil and early season) (b), and after 15 May (mid- to late season) (c). The scatter plot between the observed and modeled backscatter for data when the SCW was presented (wet data) for time periods before 15 May (bare soil and early season) (d) and after 15 May (mid- to late season) (e).

6

4 May onwards. The effect of  $VWC^+SM^+$  is most significant in the first few days (before 4 May). Once the XP backscatter starts to increase due to plant growth, the limited difference between  $VWC^+$  and  $VWC^+SM^+$  suggests that the backscatter is primarily sensitive to the vegetation rather than the soil. Again, it seems that  $VWC^+SM^+$  is too wet for dew in the first few days but not wet enough to capture interception in the latter half of this period. Table 2 confirms that while there is an increase in the random errors through the inclusion of the extra moisture, there is a considerable reduction in bias in VV and XP using the  $VWC^+SM^+$  model.

These results illustrate that for low vegetation cover before 15 May ( $LAI < 1.5$ ), the presence of water on the soil surface during dew and interception events needs to be accounted for. Setting surface soil moisture to saturation in the presence of dew or interception is a pragmatic interim solution, but it provides a conservative estimate of the effect of interception in these conditions. Furthermore, the agreement between model and simulation is still not comparable to the agreement in the absence of SCW. This suggests that there is considerable scope for improvement in how the effect of dew on the soil surface could be represented in the model.

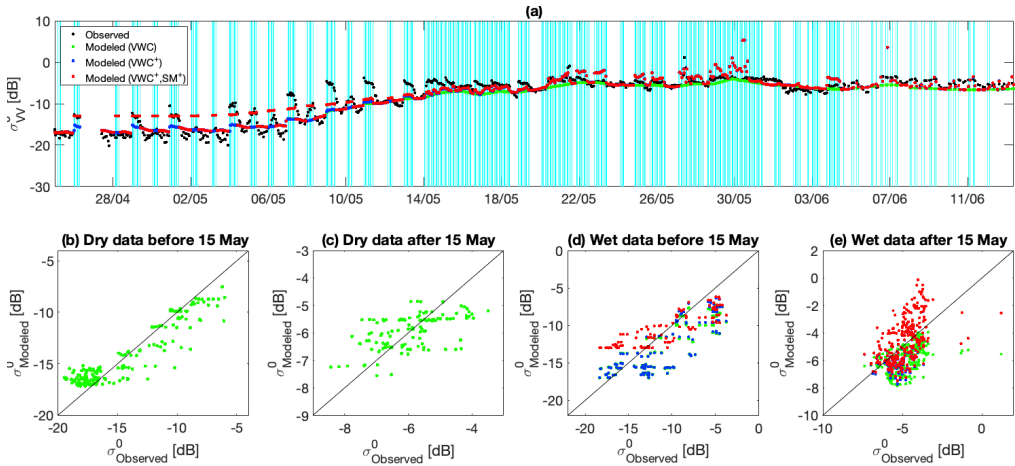


Figure 6.5.: The time series of observed and modeled backscatter for the three implementations at L-band and VV polarization. Light blue vertical lines indicate the presence of SCW during radar acquisition (a). The scatter plot between the observed and modeled backscatter for data when there was no SCW (dry data) for time periods before 15 May (bare soil and early season) (b), and after 15 May (mid- to late season) (c). The scatter plot between the observed and modeled backscatter for data when the SCW was presented (wet data) for time periods before 15 May (bare soil and early season) (d) and after 15 May (mid- to late season) (e).

### 6.3.4. EFFECT OF SCW ON SCATTERING MECHANISMS

Fig. 6.8 shows the simulated total backscatter as well as the contributions from each scattering mechanism for the three Tor Vergata model implementations at L-band. The (standard) VWC implementation (Fig. 6.8 left column) shows that the co-polarized backscatter was dominated by ground scattering until 4 May. From 4 to 15 May, increasing biomass resulted in attenuation of ground scattering and an increase in vegetation scattering, double bounce, and vegetation-ground scattering. After 15 May, when LAI > 1.5, the simulated backscatter is dominated by vegetation scattering with the double bounce term providing the second largest contribution. During this period, the contributions of ground, and vegetation-ground scattering were negligible in VV-pol (Fig. 6.8 (a)), while in HH-pol (Fig. 6.8 (b)) they had some limited effect. In cross-polarization (Fig. 6.8 (g)), ground scattering was dominant until 29 April. From 29 April (one week after crop emergence) onward, vegetation scattering dominated.

The inclusion of additional internal water in the VWC<sup>+</sup> implementation (Fig. 6.8 middle column), mainly has an effect after 15 May. The presence of SCW led to an increase in the total backscatter in all polarizations mainly due to the increase in the vegetation scattering term. The SCW also slightly increases the vegetation-ground scattering while it reduces the double bounce and ground scattering contributions to



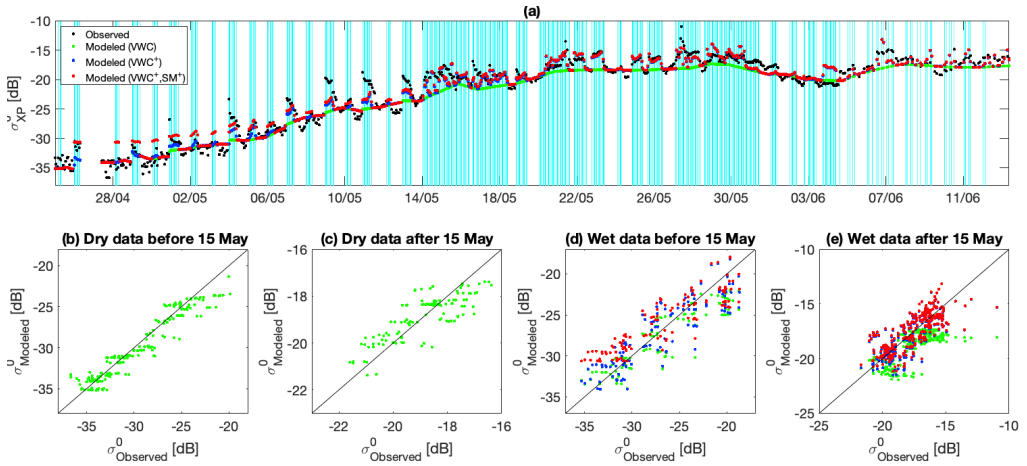


Figure 6.6.: The time series of observed backscatter and modeled backscatter for the three implementations at L-band and cross-polarization (XP). Light blue vertical lines indicate the presence of SCW during radar acquisition (a). The scatter plot between the observed and modeled backscatter for data when there was no SCW (dry data) for time periods of before 15 May (bare soil and early season) (b), and after 15 May (mid- to late season) (c). The scatter plot between the observed and modeled backscatter for data when the SCW was presented (wet data) for time periods before 15 May (bare soil and early season) (d) and after 15 May (mid- to late season) (e).

close to -40 dB in all polarizations. This illustrates that the presence of SCW affects penetration through the canopy layer, consistent with previous studies [102, 184].

Accounting for water on the soil surface using the  $VWC^+SM^+$  implementation during the dew and interception events (Fig. 6.8 right column) leads to an increase in all contributions except the vegetation scattering term before 15 May. This is mainly due to an increase in ground scattering and vegetation-ground scattering. After 15 May, the combined effect of SCW and dew on the soil surface led to a decrease in double bounce and ground scattering. Comparing the rows in Fig. 6.8, it is clear that the impact on total backscatter varies somewhat with polarization, depending on the relative importance of the vegetation and ground scattering.

In the case of higher frequencies of C and X bands, the effect of SCW and dew accumulation on the soil surface on the total simulated backscatter was first investigated. Fig. 6.9 shows the total simulated backscatter in C- and X-band for the three Tor Vergata model implementations. In the (standard) VWC implementation (green), backscatter increases in both frequencies and all polarizations until 15 May. This is due to crop growth. The magnitude of the increase is higher in cross-pol than co-pol in both C- and X-band due to higher sensitivity of the cross-pol data to biomass. After 15 May, the total modeled backscatter decreases gradually. The

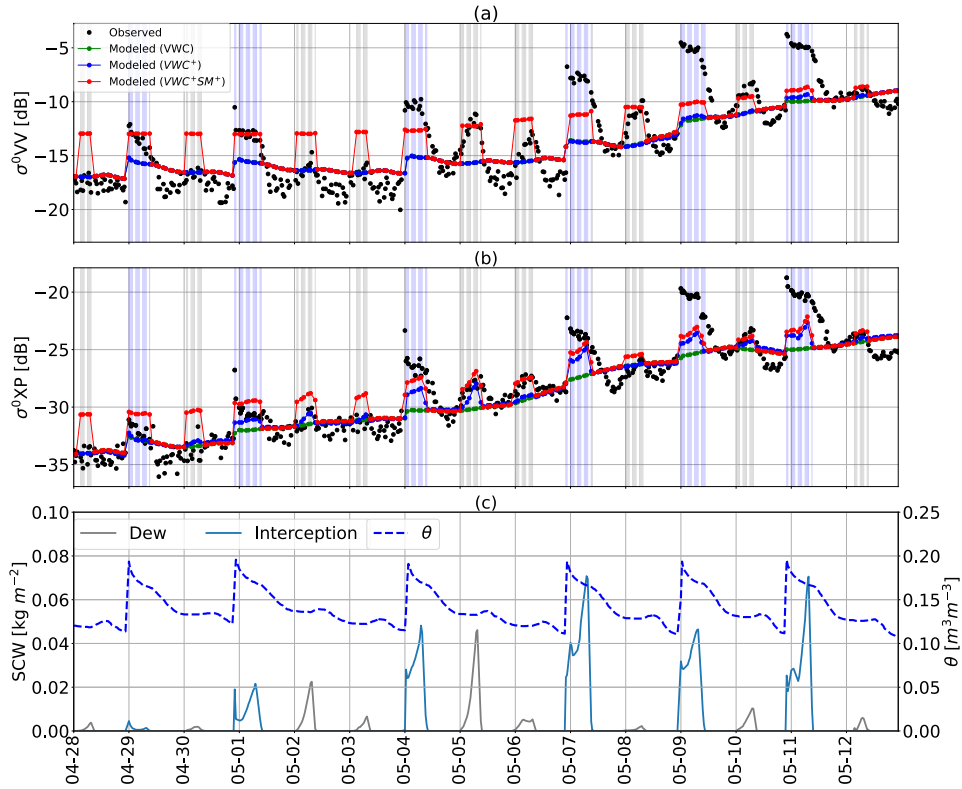


Figure 6.7.: Time series of observed backscatter and modeled backscatter for three implementations in (a) VV-polarization and (b) cross-polarized (XP). The vertical gray and blue lines indicate the presence of dew and interception during the radar acquisition respectively. (c) averaged volumetric soil moisture ( $\text{m}^3 \text{m}^{-3}$ ) profile at 5 cm, and SCW (dew/interception) amount ( $\text{kg m}^{-2}$ ) for 15 days during the early season.

magnitude of the decrease is around 1.3 dB in co-polarized C-band, and it is around 0.5 dB in cross-polarized C-band and all X-band polarizations. Comparing the VWC<sup>+</sup> (blue) to the VWC implementation (green), the presence of SCW only has an effect after 15 May, and in general it has more of an effect in C-band than in X-band. Results for VWC<sup>+</sup>SM<sup>+</sup> implementation show that considering the saturated soil level to represent the effect of dew on the soil surface highly affects the signal. This effect was highest on 28 April and its magnitude reduces by increasing biomass. In contrast, the VWC<sup>+</sup>SM<sup>+</sup> has a significant effect, up to 3 dB, at the start of the season. The difference between VWC<sup>+</sup>SM<sup>+</sup> and the standard VWC implementation decreases as biomass increases due to the loss of sensitivity to the surface. The two are virtually identical by 19 May.

Recall from Fig. 6.7 that the VWC<sup>+</sup>SM<sup>+</sup> implementation tended to overestimate

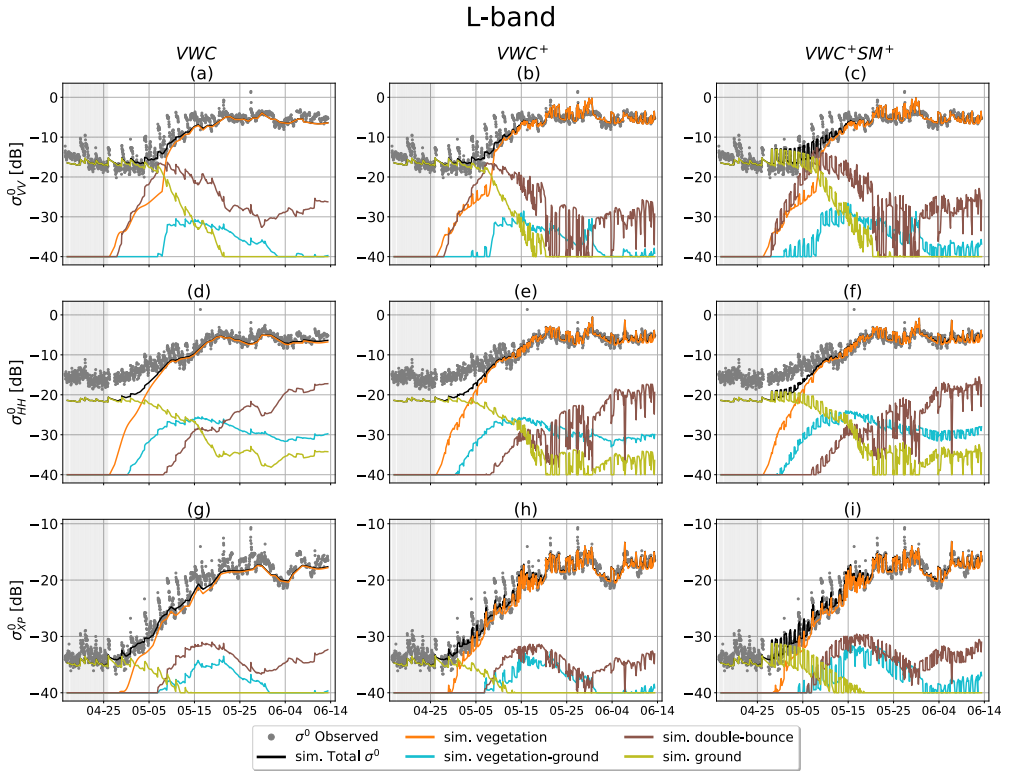


Figure 6.8.: Tor Vergata model simulations and observed backscatter in L-band for three polarization combinations and three implementations. Each column shows results for one implementation in VV, HH, and XP polarization from top to bottom. The gray background indicates period when no SCW was installed.

co-polarized backscatter during dew events, and underestimated during interception events, while providing reasonable estimates for both in cross-polarized backscatter. Therefore, we should consider the co-polarized backscatter in Fig. 6.9 as an upper limit for dew events and a lower limit for interception. Results from cross-polarized backscatter suggest that the total C- and X-band backscatter may vary by up to 3dB in the early season due to the presence of water on the soil.

Fig. 6.10 shows the contributions to C-band backscatter for each of the three Tor Vergata model implementations. In the VWC implementation (Fig. 6.10 left column) ground scattering dominates at the start of the season. However, vegetation scattering and vegetation-ground scattering increase in all polarizations as soon as the crop emerges on 22 April. By 5 May, vegetation scattering dominates, closely followed by vegetation-ground scattering. Double-bounce scattering has some seasonal variation in HH and VV but is low throughout the season and makes no

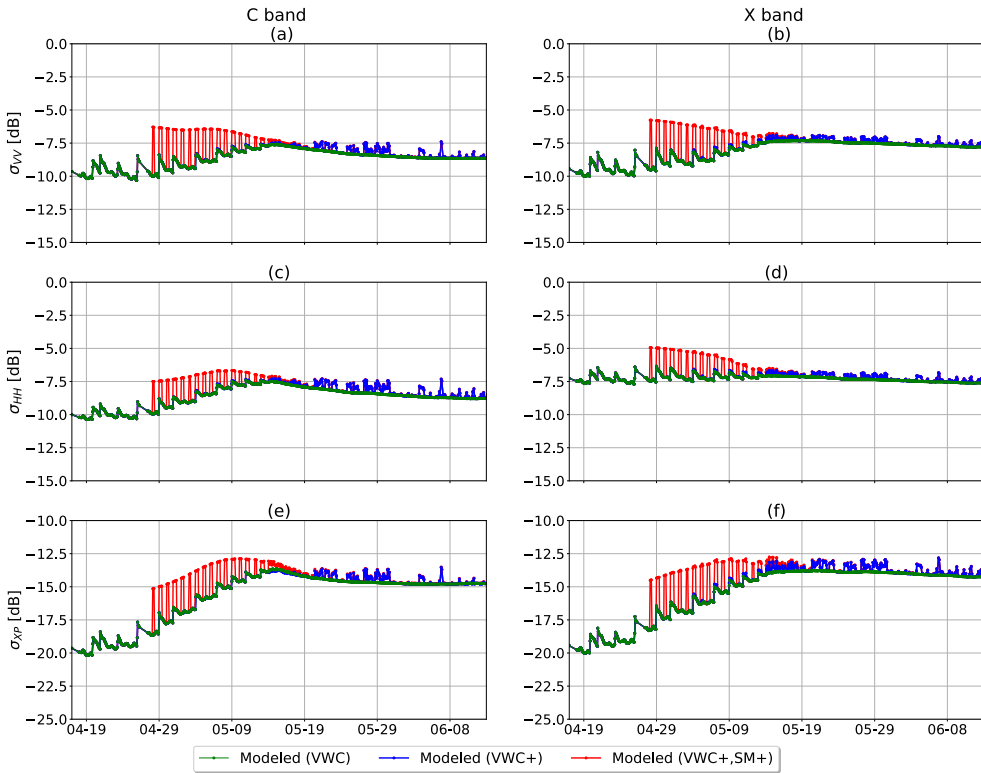


Figure 6.9.: Total simulated backscatter using Tor Vergata model for three implementations in C- and X-band and three polarization combinations for 20 days during the bare soil and early season.

contribution to cross-polarized backscatter at all.

Comparing the  $VWC^+$  implementation (Fig. 6.10 middle column) to the standard VWC implementation (left column), it is clear that the observed increase in total backscatter after 15 May comes from the effect of SCW on vegetation scattering. While SCW also has an effect on the vegetation-ground, and ground scattering, their contribution to total backscatter is not significant enough to have any impact.

When water on the soil surface is also included (Fig. 6.10 right column), it leads to transient increases in the ground scattering, vegetation-ground scattering, and double-bounce. The combination of the first two combine in the period prior to 15 May to produce the increase in total backscatter. As the vegetation scattering increases, reducing the importance of these two terms, the effect of the water on the soil also becomes less important.

Similar results were observed in X-band ((Fig. 6.11)). The main difference is that the double-bounce term is -40 dB throughout the season in X-band, compared to peak values of -30 dB in co-polarized C-band backscatter. The effect on total

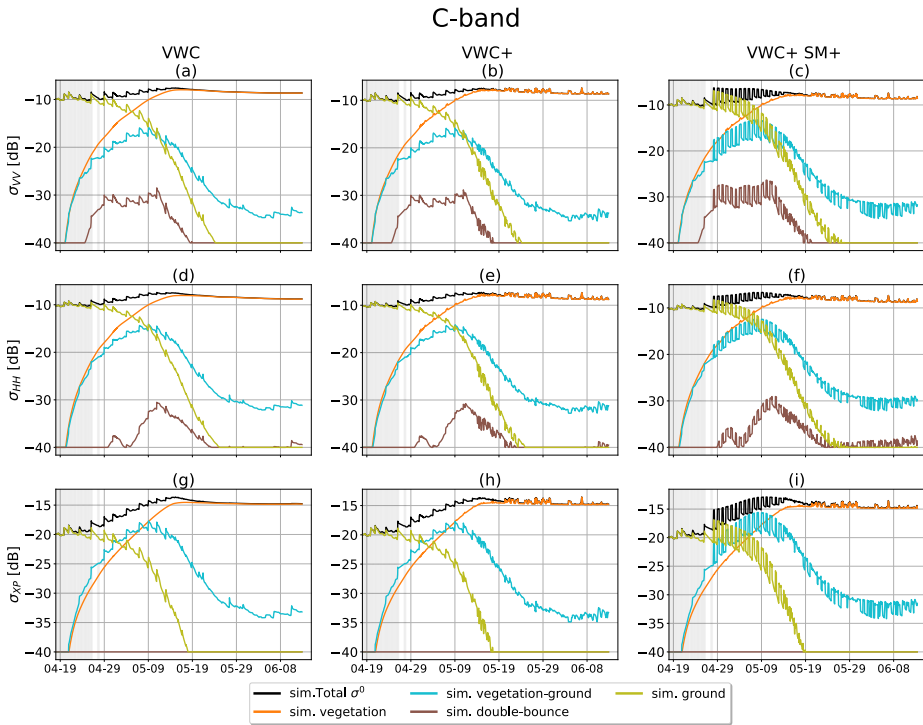


Figure 6.10.: Tor Vergata model simulations in C-band for three polarization combinations and three implementations. Each column shows results for one implementation in VV, HH, and XP polarization from top to bottom. The gray background indicates period when no SCW was installed.

backscatter is negligible though because in both frequencies, the total backscatter is dominated by ground and vegetation-ground scattering in the early season, and then vegetation scattering after 15 May.

### 6.3.5. THE EFFECT OF SCW ALONE ON BACKSCATTER AT L-, C-, AND X-BAND

In previous sections, the agreement between observations and simulations of the three implementations at L-band, as well as the contribution of scattering mechanisms was investigated. However, these simulations considered the combined effect of several factors simultaneously: change in internal vegetation water content caused by plant growth and diurnal cycle, soil moisture, SCW (modeled by adding the amount of SCW as internal water content of corn leaves, denoted as  $M_{g+}$ ), and dew on the soil surface (modeled by considering saturated soil moisture). It is important to clarify that the increase in the internal water content of corn leaves

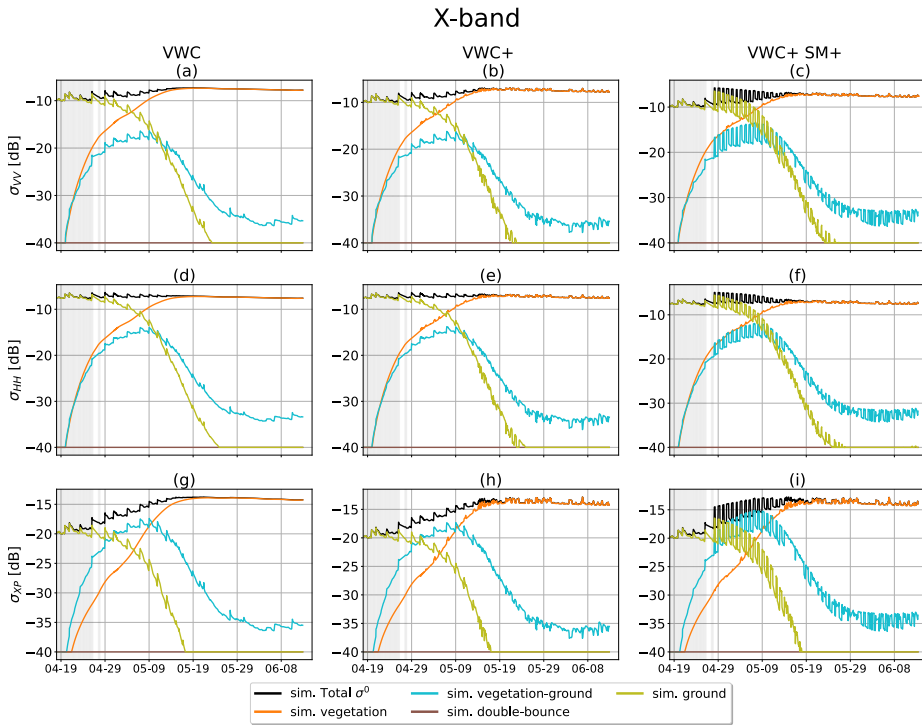


Figure 6.11.: Tor Vergata model simulations in X-band for three polarization combinations and three implementations. Each column shows results for one implementation in VV, HH, and XP polarization from top to bottom. The gray background indicates period when no SCW was installed.

( $M_{g+}$ ) in our simulations was solely to mimic the impact of SCW. This simulated increase should not be mistaken as an actual change in the internal water content of corn leaves. Therefore, to understand the influence of SCW alone, we need to compare observations where the only change is in SCW, while the change in soil moisture and internal vegetation water content is minimal.

Therefore, we will compare backscatter values for times at which we can be sure that the difference is only due to the presence and absence of SCW. Observations at 6 AM are used as representative of the presence of SCW, as this time coincides with the maximum SCW amount. It is also pre-sunrise, so the internal water content is at a maximum. [23] found that the VWC in corn can reach its maximum value around 10 PM, stay constant until 7 AM of the next day after which it can start to decrease.

To choose data for the absence of SCW or moisture on the soil surface, two times were considered: 10 PM on the previous day or 9 or 10 AM on the same day.

When morning SCW is due to solely to dew, the change in backscatter from 10 PM to 6 AM of the next day is only related to the accumulation of dew while the

VWC can be considered constant and the change in 5cm soil moisture negligible (Fig. 6.13 (c)). As shown in Fig. 2 (b), irrigation was applied on several dates, generally at night. During these interception events, the 5cm soil moisture changed considerably between 10 PM and 6 AM, having a significant effect on backscatter between these two times. Therefore, for interception events, the first acquisition after 9 AM was used as the observation without SCW to ensure that these are the first acquisitions after the SCW has fully dissipated. The soil moisture data in Fig. 6.13 (c) show that the 5cm soil moisture variations between 6 AM and 9 AM are negligible. Therefore the backscatter dynamics in Fig. 6.13 and 6.14 can mainly be attributed to the presence of water on the vegetation and soil alone. Since VWC may decrease between 6 AM and the first acquisition after 9 AM [23], the  $\Delta\sigma$  value due to SCW may be slightly lower than the values reported in these figures. Fig. 6.12 shows the amount of  $\Delta\text{SCW}$  on top of the corn leaves which is a difference in SCW amount over corn leaves between 6 AM and 10 PM of the day before for dew events and between early morning (6 AM) and late morning (after 9 AM) for interception events. The time series shows only days when the SCW amount on the acquisition of 10 PM or late morning was zero.

Fig. 6.13 shows  $\Delta\sigma$ , the difference between backscatter acquired during the presence and absence of SCW or moisture on the soil surface. Extracting the  $\Delta\sigma$  allows us to focus on the ability of the model to capture the  $\Delta\sigma$  rather than the absolute value of  $\sigma$ . Fig. 6.13 shows that there are strong variations in  $\Delta\sigma$  during the season.

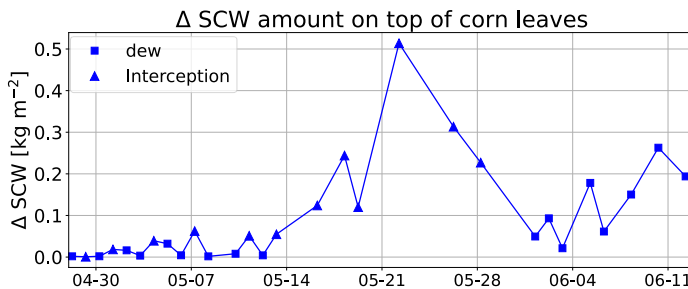


Figure 6.12.: Time series of difference in surface canopy water amount  $kg\ m^{-2}$  on top of corn leaves between 6 AM and 10 PM of a day before for dew events and between 6 AM and late morning (after 9 AM) for interception events.. The  $\Delta\text{SCW}$  was calculated only for days when the SCW amount on the acquisition of 10 PM or late morning was zero.

Fig. 6.13 shows that the  $\Delta\sigma$  values from the standard (VWC) model implementation are close to zero and that this implementation does not capture the observed  $\Delta\sigma$  values in L-band. For the period before 15 May, the  $VWC^+$  implementation does not capture the  $\Delta\sigma$  values in the observed VV or HH backscatter (Fig. 6.13 (a) and (b)). In VV, the  $VWC^+$  implementation is indistinguishable from the VWC implementation due to the lack of sensitivity to vegetation in the bare soil and early vegetative stages. This could be related to the fact that considering only

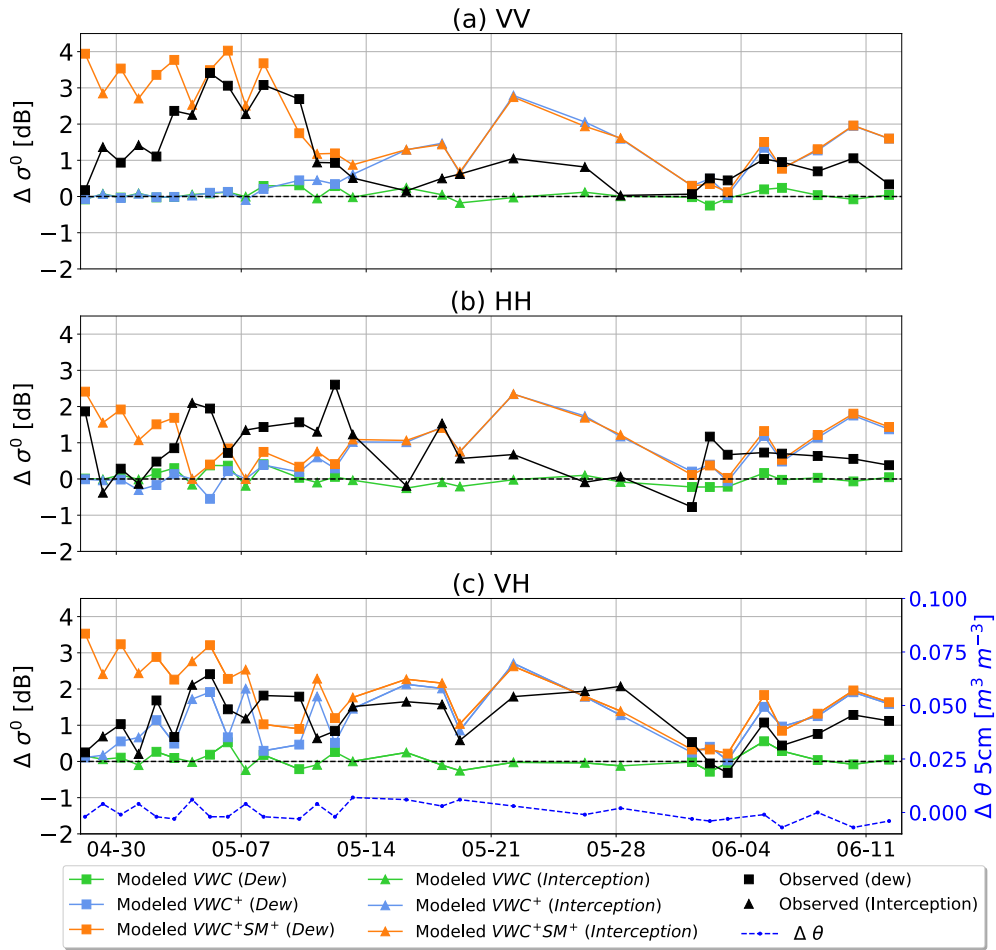


Figure 6.13.: Time series of difference in early morning observed and modeled backscatter for three implementations from wet and dry vegetation ( $\Delta\sigma$ ) in L-band and for (a) VV polarization, (b) HH polarization, and (c) cross-polarization (XP). The difference is calculated between 6 AM and 10 PM of a day before for dew events and between 6 AM and late morning (after 9 AM) for interception events. The difference in 5cm soil moisture values for the wet and dry canopy is shown in (c).

the water on the leaves mostly affects the direct vegetation term which is small at this time. Allowing for wet stems may lead to an increase vegetation-ground interaction.  $VWC^+$  introduces some dynamics in  $\Delta\sigma$  in HH, but it does not improve the estimate. Recall, however, that the characterization of roughness in IEM in HH-polarization resulted in poor simulations during this time. In XP, the  $VWC^+$  implementation improves the simulated  $\Delta\sigma$ .



Recall from Fig. 6.7 (a) that for the period before 15 May, the dynamic range of the model for  $VWC^+SM^+$  implementation was limited resulting in a maximum  $\sigma$  value (i.e. red data) higher than that observed during dew events but lower than observed during interception. However, in Fig. 6.13 (a) the  $\Delta\sigma$  estimated for  $VWC^+SM^+$  implementation during interception events (May 4 to May 15) from the models agrees well with the observed  $\Delta\sigma$ . Moreover, the  $VWC^+SM^+$  implementation produces a larger  $\Delta\sigma$  during dew events (squares) compared to interception events (triangles) for this period, while the observed data shows that the  $\Delta\sigma$  from interception is not always lower than those of the dew. This can be related to the fact that the dew on the soil surface does not penetrate to 5 cm depth. Therefore assuming the saturated soil moisture at 5 cm depth to model the effect of dew on the soil surface can cause an overestimation of the isolated effect of dew compared to interception, which can be an indication that dew on the soil surface is not represented in an optimal way. In XP, Fig. 6.13 (c) shows that the  $VWC^+$  implementation could model the  $\Delta\sigma$  from SCW and moisture on the soil surface before 15 May better than  $VWC^+SM^+$  implementation, while results in Fig. 6.7 showed the  $VWC^+SM^+$  implementation better captured the absolute values of the  $\sigma$  than  $VWC^+$  implementation.

For the period after 15 May, sensitivity to the soil surface is limited and the total backscatter is dominated by the vegetation scattering (Fig. 6.8), so the  $\Delta\sigma$  estimated using the  $VWC^+$  and  $VWC^+SM^+$  implementations are virtually identical. Between 15 May and 1 June, the  $\Delta\sigma$  from both implementations is higher than observed. Recalling Fig. 6.5 to 6.6, this is during the high biomass period ( $LAI > 1.5$ ) which was also very wet. The observed  $\sigma$  was close to saturation, however, the model  $VWC^+$  and  $VWC^+SM^+$  could still increase in the presence of SCW. After 1 June, results show that both implementations simulate the observed  $\Delta\sigma$  with higher accuracy except for the last two dates. The overestimation on these two dates could be related to the fact that the corn reached its maximum biomass after 25 May and the amount of SCW was very high on those dates (Fig. 6.12).

Fig. 6.14 shows simulated  $\Delta\sigma$  at L-, C-, and X-band using the  $VWC^+$  and the  $VWC^+SM^+$  implementations. Comparing the results in Fig. 6.14 left columns, it is clear that the magnitude of the difference due to water on the canopy varies considerably by frequency. The modeled  $\Delta\sigma$  can reach up to around 2.5 dB in L-band compared to 0.6 dB in C- and X-band. It should be noted that although the simulations in Fig. 6.13 could not capture  $\Delta\sigma$  dynamics perfectly, the simulations approximate the maximum and average magnitude of the change in  $\Delta\sigma$  during the season. During the interception events in the middle of the season, the  $\Delta\sigma$  values at C-band in various polarizations are comparable in magnitude. In X-band, the  $\Delta\sigma$  in XP is larger than that in co-polarized backscatter. Results also show that the effect of water on the vegetation is lower during the early season (especially in co-polarized channels) and reaches its maximum during the mid and high season as crop reaches its maximum biomass.

Fig. 6.15 shows the relationship between  $\Delta SCW$  and the modeled  $\Delta\sigma$  in L-, C-, and X-band from the  $VWC^+$  implementation. The Pearson correlation coefficients are relatively high for all frequencies and polarizations. Fig. 6.15 highlights the

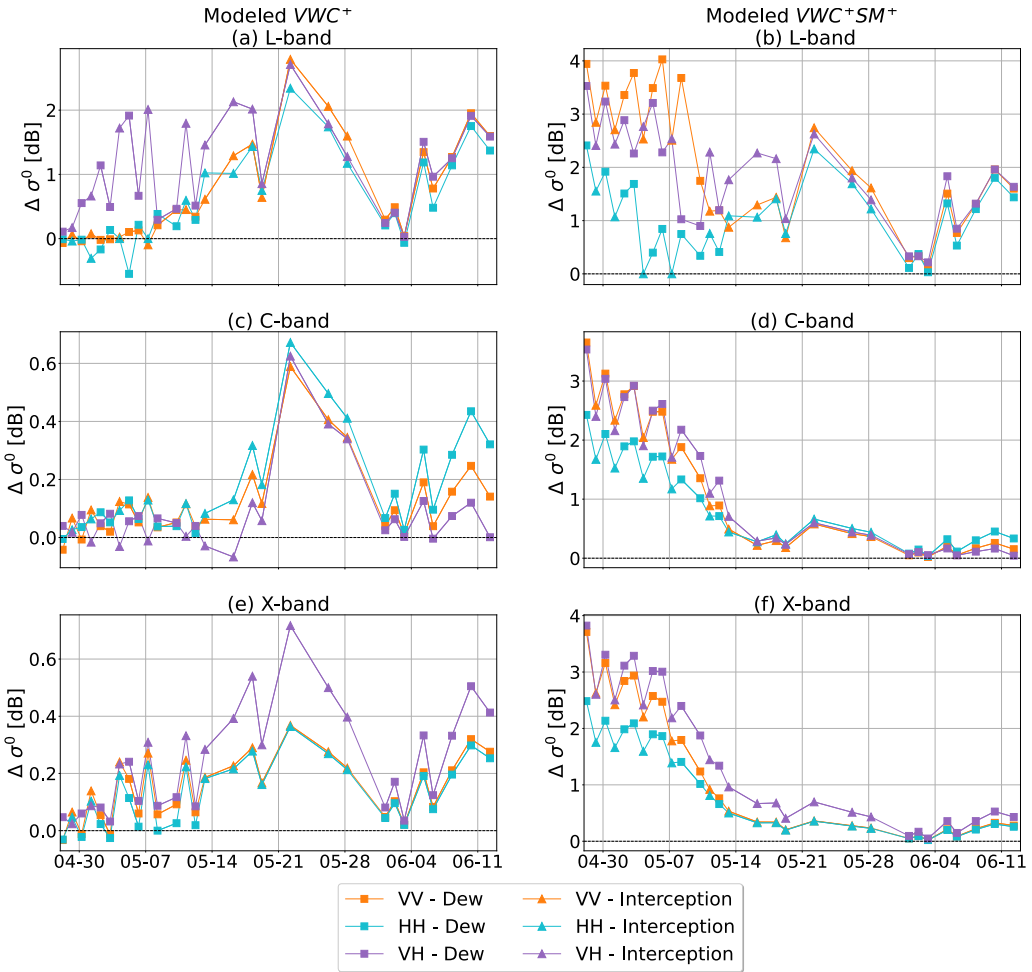


Figure 6.14.: Time series of difference in early morning simulated total backscatter from wet and dry vegetation ( $\Delta\sigma$ ) for three polarizations and L-, C-, and X-band for  $VWC^+$  implementation is shown in the left columns and for  $VWC^+SM^+$  implementation is shown in the right columns. Each row shows the results for one band.

contrast between frequencies in terms of sensitivity, and shows that the relationship between  $\Delta SCW$  and  $\Delta\sigma$  evolves with  $VWC$  as the contribution of direct scattering to total backscatter changes. The highest amount of  $SCW$  on 22 May ( $0.52 \text{ kg m}^{-2}$ ), caused by the heaviest rain event during the growing season (Fig. 6.1 (a) and (b)), resulted in a peak on  $\Delta\sigma$  at L-, C-, and X-band (Fig. 6.14 left columns). The reduction in the amount of  $\Delta SCW$  from 22 May until 4 June resulted in the reduction in modeled  $\Delta\sigma$  in all polarization at 3 bands. The rapid increase in  $\Delta SCW$

between 6 and 11 June happened due to the heavy rain event on 7 June and heavy dew event on 10 June. It should be noted that based on the L-band data from Fig. 6.13, the  $\Delta\sigma$  in this period could also overestimate the effect of dew on C- and X-band. In X-band, the effect of SCW was highest in XP polarization which can be explained by the scattering mechanisms. However, in this research due to the lack of experimental evidence on higher frequencies, the scattering mechanism was not investigated.

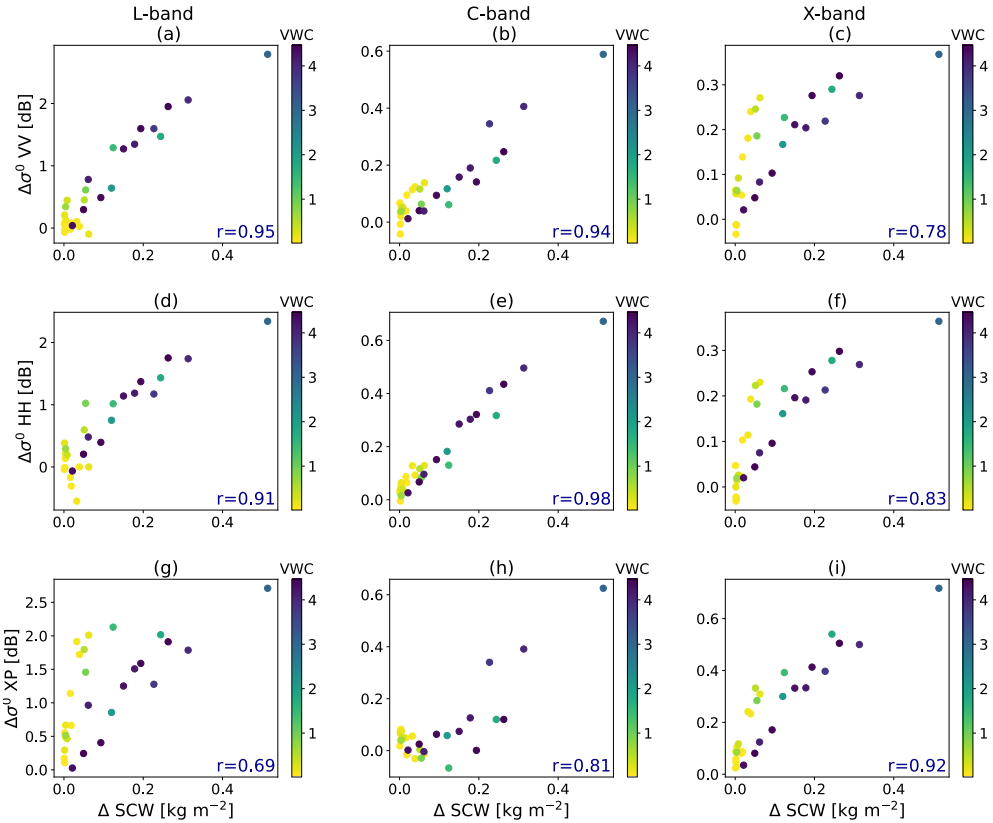


Figure 6.15.: The relationship between  $\Delta\sigma$  ( $VWC^+$  implementation) and the  $\Delta SCW$  for three polarizations and L-, C-, X-band is shown. The color for each data point shows the amount of VWC for the 6 AM acquisition. Pearson correlation coefficients are shown in the bottom right of each plot.

Fig 6.14 (b) shows that in L-band, the effect of water on the soil surface at the early season is as significant as the effect of water on the vegetation later in the season and both cases can affect the signal around 2.5-3.5 dB. However, in C- and X-band (Fig 6.14 (d) and (f)), accounting for the effect of dew on the soil surface during the bare soil and early vegetative stage could have a stronger effect than the presence of SCW during the mid and late season. Simulation results suggest that

dew on the soil surface during the bare soil and early season could affect the radar signal in C- and X-band for up to 3 dB, while the effect of SCW during the mid and late season can only affect the simulated signal for up to 0.6 dB. However, due to a lack of experimental evidence on these frequencies, further investigation is required to be able to make a firm conclusion.

The simulation results suggest that the water on the canopy could have a limited impact in C- and X-band but that water on the soil surface at the beginning of the season could have a comparatively large effect. Results in Fig 6.14 (d) and (f) also suggest that the effect of dew on the soil surface mostly decreases with the increase in crop biomass. The reduction in the sensitivity of backscatter to water on the soil surface diminishes earlier at higher frequencies. This finding is very relevant for applications such as soil moisture estimation over bare soil or sparsely-vegetated areas when the combined data from ascending and descending overpasses would be used at C- and X-band. If data from ascending and descending overpasses are combined without considering the effect of the presence of dew on the soil surface, it could lead to spurious soil moisture values.

## 6.4. CONCLUSIONS

The goal of this study was to improve our understanding of the influence of surface canopy water (SCW) on radar backscatter as a function of frequency and polarization. Observations were available from the UF LARS tower-based radar at L-band. In a previous study, these data had been analyzed against continuous leaf wetness sensor, soil moisture and crop geometry data to quantify the impact of SCW on observed L-band backscatter. Here, the L-band observations were compared to three implementations of the Tor Vergata model in which we attempted to account for the presence of SCW by increasing the vegetation and soil moisture contents. These L-band simulations provide insight into the contributions to total backscatter and how they may be affected by the presence of SCW. In addition, simulations with the same model at C- and X-band were used to explore the potential impact of SCW at higher frequencies.

The standard implementation of the Tor Vergata model accounts for internal vegetation water content, but does not explicitly consider the presence of SCW. One approach to account for the additional water present due to dew or interception would be to allow for a "cloud" of water droplets throughout the vegetation layer or specifically the leaf layer. However, SCW within the vegetation layer due to dew or interception is primarily concentrated on the leaves and so the additional water should be located at the leaves. Therefore, we accounted for the additional water present of SCW on the vegetation by augmenting the VWC, so that the additional water present as dew or interception is spatially distributed within the dielectric medium according to the geometry and architecture of the vegetation. In other words, the structural representation of the scatterers is the same, but they are wetter. Results at L-band show that this implementation ( $VWC^+$ ) improved the agreement between simulated and observed backscatter particularly when total backscatter was dominated by the impact of vegetation. However, while the bias was considerably

reduced, the agreement between model simulations and observations was far from perfect. Further improvements are necessary and could include, for example, the addition of a thin layer of droplets on the surface of the leaves. This would ensure that the spatial distribution was consistent with that of the vegetation elements, while representing the additional water as “free” water on the leaf surface.

Agreement between the  $VWC^+$  simulations and the L-band observations was comparatively poor during the bare soil and early vegetative stages. We hypothesized that this could be due to the presence of dew, in the form of water on top of the soil layer. We investigated if the effect on backscatter could be emulated by assuming the surface soil layer was saturated if the leaf wetness sensor indicated the presence of moisture on the field. This improved the agreement between the modeled and observed backscatter during the bare soil and early vegetative stages somewhat. However, the remaining mismatch suggests that this approach is less than optimal and should be improved. In past studies, the inclusion of a litter layer has proved beneficial in the simulation of emission and scattering from forest areas [196, 197]. So, one option could be to represent dew as a thin saturated litter layer. Alternatively, it may be physically more plausible to include an additional thin layer of water droplets on the surface above the soil when the leaf wetness sensors indicate the presence of moisture. Nonetheless, the comparison of simulated and observed L-band backscatter suggests that while there is scope for improvement, the  $VWC^+SM^+$  implementation provides better agreement with observations than the standard (VWC) or  $VWC^+$  implementations. It provides some insight into the importance of water on the soil surface during the bare and early growing stages.

Analysis of the contributions of the various scattering mechanisms at L-band shows that including the SCW as additional internal water content of leaves, in general, led to an increase in vegetation volume contribution and a reduction in the contribution from double bounce and direct scattering from the ground in all bands. This finding is consistent with Riedel *et al.* [82] and Riedel and Schmillius [83], who also observed an increase in volume scattering and a decrease in surface and double-bounce scattering based on use of the target decomposition theorem at L-band in the presence of SCW. Assuming a saturated surface soil layer to model the effect of dew on the soil surface has a significant effect on the scattering mechanisms during the bare soil and early season. This generally led to an increase in all contributions except the vegetation volume contribution. The influence of surface soil moisture or water at the soil surface is less important when the vegetation starts to dominate the total backscatter. Therefore, accounting for water on the soil surface is primarily important during the bare soil and early vegetative stages at L-band. While Wood *et al.* [75] also found that the presence of dew increases radar backscatter during dawn acquisitions, our study is the first to highlight the importance of considering the presence of dew on the soil surface at the beginning of the season for all frequencies, particularly for applications involving bare soil and low vegetation cover.

The TV model was also used to simulate backscatter at higher frequencies, to explore the potential sensitivity as a function of frequency and polarizations. Simulated results of  $\Delta\sigma$  due solely to SCW on backscatter were always low during

the early season and reached a maximum during the mid and late season. This effect varied with polarization and frequencies, with simulations suggesting that the impact of SCW alone on backscatter could reach up to 2.5 dB in L-band and up to 0.7 dB in C- and X-band. This is in contrast to the findings of Gillespie *et al.* [79], who observed a higher increase in radar backscatter at C-band than at L-band during dew events. However, the different conclusions may be due to the difference in crop type (wheat versus corn). Additionally, our findings differ from those reported by Riedel *et al.* [82] and Riedel and Schmullius [83], who observed no significant influence from dew events on VV-pol at L-band and X-band. While they studied a similar crop type as this study (corn), the different conclusions may be related to their comparatively sparse dataset (using data from 2 days and 3 times of the day: 6 AM, 9 AM, and 12 PM). They also used indirect measures, such as microclimatological data, to infer the presence of SCW. Again, while previous studies such as those by Herold, Pathe, and Schmullius [81], Riedel *et al.* [82] and Riedel and Schmullius [83] suggested a more pronounced effect at C-band and minimal impact at X-band, our finding indicate similar effect at both C- and X-band. These studies also relied on sparse datasets and the indirect measurements of interception. In contrast, our study could avail of high temporal resolution radar data combined with direct, continuous measurements of the SCW amount from leaf wetness sensors throughout the entire growing season.

Our results highlight a significant impact from SCW at L-band and a lower, but noticeable, effect at C- and X-band. This finding emphasizes the importance of considering SCW in low frequency data, in agreement with the findings of Wood *et al.* [75]. The divergence among previous studies underscores the complexities inherent in understanding the impact of SCW on radar observables.

Our finding suggests that considering the effect of SCW on the different applications is more important for lower frequency data. This is relevant for current SAR missions such as SAOCOM, and ALOS as well as future SAR missions, like NISAR and ROSE-L. Simulations showed that the isolated effect of dew on the soil surface during the early season on backscatter could reach up to 3.8 dB in all bands. These results suggest that while the presence of SCW has a limited impact at C- and X-band, the presence of dew on the soil surface at the beginning of the season should be considered during bare soil and low vegetation cover for all frequencies.

This study provides new insights into the effect of SCW on radar backscatter and various contribution to total backscatter. While the overall uncertainty of the UF-LARS was approximately 1.49 dB [107], the maximum impact of changes in soil moisture and the dynamic range in backscatter due to crop growth at L-band was around 5 dB and 10 dB, respectively. For comparison, the effect of SCW alone can reach up to 2.5 dB in L-band. In C- and X-band, modeling results indicate that the maximum effect of soil moisture during bare soil periods was around 2 dB, while the dynamic range in backscatter due to crop growth was approximately 2.7 dB in co-pol and 5 dB in cross-pol. For comparison, simulations suggest that the influence of SCW could reach up to 0.7 dB. Therefore, both observations and model simulations suggest that the presence of dew and intercepted precipitation is significant at microwave frequencies, warranting attention in the context of upcoming radar

missions such as Sentinel-1 NG, ROSE-L, and NISAR. In addition, this sensitivity of sub-daily SAR data to water on the canopy suggests that future sub-daily SAR data could be valuable in understanding the influence of interception on evaporation and evaporation partitioning. This is relevant in the context of Cosmo SkyMed, TerraSAR-X and TanDEM-X and data from commercial constellations such as those from Capella Space and ICEYE.

To our knowledge, this is the first study to consider the influence of dew on soil on backscatter which can have a particularly significant effect on backscatter during the early season. Measuring this quantity directly is challenging because, while some soil moisture sensors like Hydra Probes have large measurement volumes of around 30–40 cm<sup>3</sup>, most sensors designed for more localized soil moisture measurements such as EM-5 sensors need to be buried beneath the surface and typically measure a volume extending a few centimeters around the sensor. While the leaf wetness sensors could apparently detect the events, additional research is recommended to explore the potential to observe this more deliberately during field experiments using COTS sensors and providing a more direct method to quantify the amount of water on the soil surface.

Our exploration of C- and X-band is limited to model simulations due to the lack of observational data at these frequencies. Recall from Section 2.3 that the Tor Vergata model has been validated extensively at C- and X-band as well as L-band. The use of the UF LARS L-band data demonstrates the value and importance of tower-based radar experiments to improve our understanding of microwave interactions with vegetation and to guide model development to support future applications and exploitation of future satellite missions. Our simulated results provide valuable insights, but higher frequency observational data are essential to make these conclusions definitive. In addition, further ground-based studies and modeling experiments are recommended to extend the conclusions drawn here to a wider range of land cover types. In addition, this study highlights the need to develop realistic representations of dew and interception on the vegetation and soil surfaces in EM models. With the number of radar satellites, and novel applications of their data on the rise, these model developments are urgently needed to enable the use of SAR to model rapid water processes in the soil-vegetation-atmosphere continuum.

Finally, the impact of SCW extends beyond radar backscatter, influencing parameters like differential interferometry, phase differences, polarimetry, and interferometric coherence. Studies such as the TROPISCAT Experiment over tropical dense forests [198–201], and studies using the BorealScat on boreal forest areas [202–204] have explored the effect of SCW on interferometric coherence, particularly how rain and wind cause temporal decorrelation in tropical and boreal forests. Yet, the impact of dew accumulation, especially heavy dew, on interferometric coherence in temperate agricultural regions remains unclear. Future research should further investigate SCW effects using polarimetry, interferometry and backscatter across a range of cover types.

# 7

## CONCLUSION

*This dissertation aimed to expand our knowledge of the relationship between radar backscatter, vegetation dynamics, and surface canopy water (SCW) in agricultural monitoring, focusing on a range of frequencies and polarization. The research employed statistical analysis and radiative transfer modeling, utilizing fully polarimetric L-band data from a truck-mounted scatterometer and C-band data from Sentinel-1, along with extensive field data. The findings of this thesis have significant implications for current and future SAR missions and contribute to our understanding of how radar backscatter interacts with vegetation and soil. The results underscore the importance of the impact that daily patterns in surface canopy water can have on radar backscatter, and highlight the implications on agricultural monitoring.*



## 7.1. KNOWLEDGE GENERATED AND IMPLICATIONS

### 7.1.1. CROP MONITORING USING SENTINEL-1 SAR DATA

In line with studies by [13] and [45], the case study in the Flevopolder (Chapter3) highlights the significant potential of Sentinel-1 SAR backscatter and interferometric coherence for crop monitoring and the identification of key phenological stages such as crop emergence, closure, and harvest date. The findings illustrate that the SAR data can be used to ensure the real-time, reliable and continuous information on crop growth and development.

The results confirm that the cross-ratio (CR) of VH/VV proposed in previous research [13, 45] is valuable, with reduced sensitivity to soil moisture and stronger sensitive to changes in crop structure and biomass throughout the season than backscatter (in any polarization) alone. Key dates such as emergence and closure were successfully estimated using polynomial fitting on backscatter time series.

For harvest detection, backscatter data proves highly effective with crops such as maize and wheat. These crops generally exhibit short and swift harvest periods, often falling within a few weeks (e.g., between 2-3 Sentinel-1 acquisitions). This results in a consistent change in the areal average backscatter values, enabling more straightforward detection.

In contrast, the detection of harvest dates for crops like sugar beet and potato proves more challenging. While harvest in an individual potato or sugar beet field can be short and swift, the areal average values can be inconsistent. Potatoes and sugar beets can be left in the ground, leading to a varied harvest date for individual fields within a few months, resulting in no singular change in the areal average. Additionally, the process of haulming (killing the above-ground plant) prior to potato harvest and the senescence of sugar beets before harvest introduce complexities. In potatoes, several changes occur in a matter of weeks rather than a sudden change, as seen in crops like wheat. In sugar beets, the influence of above-ground biomass on backscatter around harvest time is limited due to senescence, with the main change being in surface roughness. Therefore, detecting harvest dates for these crops often requires the use of coherence data, taking into account the variations and particularities of their harvest processes.

The potential of interferometric coherence combined with the high temporal density of Sentinel-1 data, presents a promising path forward in agricultural monitoring practices. This research was among the earliest to leverage coherence data for detecting harvest times across diverse crops. Many subsequent studies have used coherence data both independently and in combination with backscatter data, to detect crucial dates in agricultural practices such as tillage, sowing, and harvesting. For example, Satalino *et al.* [206] developed a new classification algorithm using Sentinel-1 (SAR) and Sentinel-2 (optical) data to identify tillage over agricultural fields at a resolution of approximately 100 meter at the farm scale. In the same year, Van Tricht *et al.* [61] used both optical and SAR backscatter data to create a comprehensive crop map for Belgium.

Kavats *et al.* [207] proposed an algorithm to monitor harvesting events using time series of Sentinel-1 coherence and backscatter data on agricultural fields in northern Kazakhstan. Azzari *et al.* [208] combined Sentinel-1 and optical data (Landsat

5,7,8) with a random forest classifier to generate expansive maps of tillage intensity from 2005 to 2016. Ouaadi *et al.* [209] used the time series of the Sentinel-1 backscatter and the interferometric coherence to monitor the wheat across five growing seasons. Shang *et al.* [210], then developed a simple, yet effective algorithm using a set of physically-based rules for detecting crop seeding and harvest events using the Sentinel-1 data. [60] utilized both coherence and backscatter time series of Sentinel-1 data to detect the phenological stages of maize, sunflower, and wheat, finding a strong correlation between sowing, growth, and harvesting stages and radar coherence. Tampuu *et al.* [211] employed Sentinel-1 temporal median coherence data to detect harvest-related surface alterations over milled peats. Their use of the change detection method led to the detection of active peat extraction sites, peat extraction events, and partially harvested areas. Amherdt *et al.* [63] used both coherence and backscatter time series of Sentinel-1 data to apply a crop classification and a harvest date detection algorithm for corn and soybean fields. They discovered that changes in coherence data could be intrinsically linked to changes in the phenological stage of plants (from seeding to harvesting), alterations in surface structure induced by harvest operations, and the appearance of post-harvest crop stubble. More recently, Villarroya-Carpio, Lopez-Sanchez, and Engdahl [212] analyzed Sentinel-1 interferometric coherence data for crop monitoring in Sevilla, Spain, showcasing its high correlation with the NDVI and its efficiency in tracking crop growth stages across multiple crop species. The research, importantly, indicated that both coherence and backscattering data, derived directly from radar images, could be utilized for agricultural monitoring purposes since their temporal evolution fits well the main phenological stages of the different crops.

This trajectory of research underscores the increasing relevance and utility of coherence and backscatter data in agricultural monitoring, improving our ability to monitor and manage the cultivation of various crops.

### 7.1.2. INFLUENCE OF SCW ON THE RELATIONSHIP BETWEEN L-BAND BACKSCATTER AND BIOPHYSICAL VARIABLES

Comprehensive quantitative analysis of L-band data and SCW data (Chapters 4 and appendix-a) highlights the significant impact of SCW on radar backscatter and choice of overpass time. Results showed that the presence of dew can substantially affect radar backscatter. At the Florida study site, dew was present on the canopy for most days from 12 am to 10 am and L-band radar backscatter observations in the presence of dew were 2-3 dB higher than those made when the dew has dissipated. Moreover, commonly used metrics like cross-ratio and RVI, despite their role in mitigating soil moisture, were still influenced by dew and interception.

Furthermore, results showed that the presence of SCW affected the relationship between L-band observables and biophysical variables such as dry biomass, vegetation water content (VWC), plant height, and leaf area index (LAI) from radar data in all polarization and RVI and cross ratios (CR). This means that the parameters of the relationship between backscatter and biophysical variables of interest are different for dry and wet vegetation. The correlation coefficient between radar data and plant parameters was up to 0.33 higher in the absence

of dew. These findings illustrate that it is important to consider daily patterns in SCW when retrieving biophysical parameters. The choice of overpass time affects the probability of dew and consequently affects radar backscatter and biophysical parameter retrieval. Therefore, it is important to consider SCW in any vegetation applications when combining acquisitions from a single mission or multiple missions when the acquisitions are at different overpass times.

Vegetation optical depth (VOD) is often used as a proxy for vegetation water content (VWC) and is generally assumed to correlate linearly with VWC [164], regardless of Surface Canopy Water (SCW). The research in this thesis, however, suggests that while VOD and VWC are linearly related, the relationship between VOD and VWC changes markedly in the presence or absence of SCW. The linear regression coefficient parameters tend to be much higher when VOD is estimated in the presence of SCW. It is important to note that VOD is not a biophysical parameter, but a parameter of an electromagnetic model, in this case, the Water Cloud Model. Therefore, VOD should be interpreted as a measure of the degree to which the soil signal is attenuated by vegetation. Higher VOD values are typically seen as indicators of increased attenuation in soil moisture retrieval, but they might not be solely attributable to attenuation. We hypothesize that the presence of water on the canopy could lead to an increase in direct scattering from the vegetation, which may further reduce the signal that reaches the soil surface. Our modeling results from Chapter 6 have already shown that the presence of SCW can increase direct scattering from vegetation, suggesting that VOD increases in these situations are not solely due to attenuation. Although we did not use the Tor Vergata Model to simulate VOD directly in this research, our findings indicate that the presence of SCW increases the backscatter, potentially supporting this hypothesis.

The dependence of VOD estimation on SCW, a significant finding of this research, can be important for various applications and domains. For instance, it could lead to discrepancies in the interpretation and retrieval of soil moisture content and VWC from both passive and active microwave data. Thus, if VOD is to be utilized as a proxy for internal vegetation water content or for other applications, the effect of SCW must be carefully considered, particularly in areas with strong daily cycles of dew or interception. One approach may be to exclude the backscatter values affected by SCW. Alternatively, additional calibration or corrections may be applied to account for the effects of SCW. These could involve calibrating the linear regression coefficient parameters or developing models to simulate the scattering and emission characteristics of vegetation under varying surface moisture conditions. If these effects are not considered, it may be prudent to limit the estimation of VOD to satellite radar acquisitions at overpass times that are less likely to be affected by SCW.

### 7.1.3. MODELING THE INFLUENCE OF SCW ON L-, C-, AND X-BAND BACKSCATTER

In Chapter 6, the calibrated Tor Vergata Model was used to improve our understanding of the effect of SCW on backscatter as a function of frequency and polarization, and to better understand the underlying mechanisms. We examined

the impact of SCW on backscatter by utilizing L-band radar observations from the UF-LARS tower based scatterometer and implementing three versions of the Tor Vergata model. Results showed that representing SCW by the inclusion of additional water in the vegetation improved the correlation between simulated and observed backscatter at the L-band, especially when vegetation significantly influenced the total backscatter. While the agreement between simulated and observed data was suboptimal during bare soil and early vegetative stages even by considering the SCW, simulating the presence of water on the soil surface as saturated soil surface improved the correlation.

In case of the influence of SCW on L-band backscatter mechanisms, the presence of SCW led to an increase in the vegetation volume contribution and a reduction in contribution from double bounce and direct scattering from the ground. This result proved the hypothesis presented in Chapter 4 about the effect of SCW on VOD estimation. Moreover, simulating the presence of dew on the surface of soil layer affected scattering mechanisms predominantly during bare soil and early season stages, typically increasing all contributions except the vegetation volume contribution.

Comparing the effect of SCW on different frequencies revealed that the increase in total backscatter is higher at lower frequencies and it decreases with increasing frequency. Similar to results in Chapter 4, modeling results suggest that the impact of SCW on backscatter could reach up to 2.5 dB in L-band highlighting its relevance for low frequency data. The isolated effect of dew on backscatter could reach up to 3.8 dB across all bands, making its consideration vital during bare soil and low vegetation cover stages for all frequencies.

Our findings offer novel insights into the impact of SCW on radar backscatter, underscoring the significance of dew and interception at microwave frequencies. This research points out the potential value of current and future SAR missions including Sentinel-1, ROSE-L, NISAR, SAOCOM, ALOS, CosmoSkyMed and constellations such as those from ICEYE and Capella which have dawn/dusk overpasses or multiple overpasses per day for improving radar-based agricultural monitoring and enhancing understanding the influence of interception on evaporation and evaporation partitioning.

## 7.2. DIRECTIONS FOR FUTURE RESEARCH

### 7.2.1. USING SENTINEL-1 FOR AGRICULTURAL MONITORING

This thesis stands out as one of the initial efforts to use both backscatter and interferometric coherence time series for detecting phenological stages and monitoring crop growth. The current applications of interferometric coherence for observing changes in structural and fresh biomass is not fully explored, especially in the field of crop monitoring. It is therefore suggested that future studies utilize a combination of backscatter and interferometric coherence data, capitalizing on the strengths of both types of data simultaneously. To this end, [213, 214] demonstrated the synergistic use of combining backscatter and interferometric coherence for vegetation classification and crop growth modeling.

Results presented in Chapter 3 employed data from a single relative orbit (RO), providing a temporal resolution of 6 days, mirroring the common Sentinel-1 acquisition strategy. By integrating data from all relative orbits, nearly daily data could be obtained in the Netherlands and part of Europe, which would enhance the temporal resolution of emergence, closure, and harvest date estimates. Combining data from different relative orbits requires accounting for differences in acquisition parameters between the images. This necessitates more sophisticated calibration and normalization procedures [215–219]. To date, few studies have fully explored the methods for combining data with varying acquisition parameters, such as varying incidence angles [48, 61, 215, 217, 220, 221]. To mitigate the effects of these varying parameters, future studies should focus on their impact on both backscatter and interferometric coherence. One simple method to address this issue could involve analyzing data from each relative orbit separately, then combining the information from all separate time series to achieve more accurate results with higher temporal resolution.

One persistent barrier to the widespread use of SAR is the data volume, which presents substantial computational challenges in terms of storage and processing power. The emergence of cloud computing power, as exemplified by Google Earth Engine (GEE) [132] and Amazon Web Services (AWS) [222], affords opportunities for processing high volumes of data. However, the processing and analysis of coherence data are not currently available through GEE since they require the use of SLC data.

The temporal density of Sentinel-1 data, particularly in Europe, and the RADARSAT Constellation Mission (RCM) data (with a temporal density of 4 days) offers an opportunity to capitalize on the synergy between backscatter and coherence data for agricultural monitoring. However, increased temporal density introduces greater variety in the time series and magnifies the influence of environmental conditions on the backscatter, necessitating further research to fully comprehend and harness the full potential of these datasets. Furthermore, using data with higher temporal density increases the impact of SCW on the radar backscatter, which should be carefully considered.

To date, few researchers have focused on the effect of SCW on the interferometric coherence signal to understand the extent to which it can influence and decrease interferometric coherence over short periods. A series of the TROPISCAT EXPERIMENTs over tropical dense forests [198–201], and studies using the BorealScat on boreal forest areas [202–204] have investigated the temporal decorrelation of interferometric coherence due to rain and wind during daytime. However, the effect of the accumulation of dew, especially heavy dew, on interferometric coherence in temperate regions and specifically for agricultural areas is still not completely understood. This issue can be addressed in future studies by utilizing daily or very short period radar data for interferometric coherence analysis over agricultural areas.

In this thesis, the time series analysis was carried out using polynomial fitting and statistical analysis, providing accurate results about the type and timing of agricultural activities. However, the approach relied on simple rule or thresholds for detecting these activities. Given that time series data can be influenced by various factors, it would be beneficial to explore and compare more complex methods, such

as machine learning or deep learning, for detecting phenological stages and activity dates in future studies. Comparing these methods with time series analysis could shed light on their relative performance and possible increase in accuracy of the results. This could be more important when the study area would be very large (country level) and consist of different agricultural practice and dates and having different agroclimatic zones.

Looking further into the future, new satellite missions such as the NASA-ISRO SAR (NISAR) mission [223], the ROSE-L (Radar Observing System for Europe-L) mission [224], and the Next Generation Sentinel-1 (Sentinel-1 NG) mission [225] provide new opportunities for the application of SAR data in agricultural monitoring. These missions are designed to provide more capabilities than their predecessors. For instance, NISAR promises an unprecedented L-band SAR, facilitating better crop classification, and soil moisture estimation. ROSE-L, on the other hand, is designed to provide L-band SAR data at a global scale, with a 3-day revisit frequency. This will significantly enhance our capability to monitor crop growth and detect phenological stages. The Sentinel-1 NG will continue the legacy of the existing Sentinel-1 satellites, ensuring continuity of C-band SAR data.

Yet, as we go into this future, we must be mindful of the changing needs and demands of users. The agricultural sector, being a key stakeholder, requires solutions that are accessible and user-friendly. For example, initiatives, like the Agricultural Sandbox [226], aim to answer to this demand by providing the data in an accessible format so that users can interact with and analyze spaceborne radar data in an intuitive manner. These efforts parallel the work done by organizations like NASA [227], Alaska Satellite Facility [228], VITO [229] and Planet Labs[230], who are trying to simplify data analysis and interpretation for a broader audience.

However, the widespread adoption of SAR for agricultural monitoring is still a challenge. The primary hurdle lies in the complexity of SAR data, which often necessitates specialized knowledge for effective interpretation and usage. Addressing this concern, future studies should focus on bridging this knowledge gap. Future research could focus on making radar data more accessible and useful to a wide range of users, especially those in the agricultural sector. Additionally, as we approach the launch of upcoming missions it becomes crucial to prioritize research that will allow us to effectively utilize these new data sources. A thorough understanding of how to manage and analyze these high-volume datasets will be critical in avoiding wastage of such valuable resources. Furthermore, expanding the scope of future research to encompass diverse agricultural systems, with varied practices, crop types, and agroclimatic conditions, is essential for the successful adoption of radar data in agricultural monitoring at a global scale.

### 7.2.2. SURFACE CANOPY WATER VALIDATION DATA

Numerous studies from the nineties onwards have attempted to understand the influence of SCW on radar backscatter across various crop types and frequencies [68, 75, 76, 79, 81–83]. Unfortunately, many of these studies were constrained by having access only to limited and temporary sparse SCW data. In some instances, the presence of SCW was not measured directly but was estimated using meteorological

datasets. However, in our detailed experimental campaign in Florida, we collected the first extensive quantitative information about the SCW data with high temporal resolution (every 15 minutes during the whole growing season). It marked a key step in linking radar backscatter variations with continuous and simultaneous estimates of SCW.

Our data highlights consistent patterns between variations in the raw SCW data and dew and interception accumulation and dissipation. However, in this research, the monitoring was limited to three leaf wetness sensors at different heights in one location. This allowed us to monitor the duration and amount of SCW due to dew or interception events along the corn height, but it could not capture the distribution of dew across the field. There was also no sensor near the soil layer, which limited our understanding of dew presence at the bottom of the canopy and on the soil layer. Therefore, we highly recommend deployment of an increased number of leaf wetness sensors, which is crucial for future research campaigns. We propose installing more sensors not only along the plant height but also at different locations within the field. With a more densely distributed sensor network, we could potentially gain a more detailed perspective of spatial and vertical heterogeneity within the field. By having complete information about the accumulation and dissipation of dew and interception on a field scale over different canopy types a new avenue for future studies could focus on estimating and predicting the SCW amount and distribution on a field scale by considering weather data, having a small number of leaf wetness sensor and considering vegetation parameters such as LAI, plant height and biomass.

Given the proven utility of leaf wetness sensors, ease of operation, and cost-effectiveness, leaf wetness sensors can play an important role in future calibration and validation campaigns. The findings of this thesis suggest using these sensors in any field campaigns where the microwave data would be used. Therefore, the potential of these devices should be fully leveraged in the context of future research and broadly in agricultural monitoring using SAR data.

The findings of this research reveal that the presence of water on the top of the soil surface can significantly influence radar backscatter at all frequencies. This effect is especially pronounced during the bare soil and early growth stages and must be considered when monitoring agricultural activities during these periods, particularly for soil moisture estimation and retrieval applications.

However, despite the advancements in soil moisture sensor technology, accurate measurement of moisture at the surface or within the top millimeter of the soil remains a challenge. Particularly with the theta probe that operates around 100 MHz [110, 231], the necessity for full insertion into the soil arises from the sensor's methodology of measuring the real part of the permittivity [231, 232]. This property, closely related to the soil moisture content, requires the sensor electrodes to be fully embedded within the soil particles to ensure an accurate measurement of the dielectric constant. The complexity of soil mineral composition, the strong effect of water on the bulk permittivity of the soil, and the specific operating frequency of the theta probe further emphasize the need for complete immersion within the soil [233]. This design constraint inherently limits the sensor ability to precisely measure moisture content in the top 1 or 2 millimeters of the soil, a region

crucial for many applications but often misrepresented by the traditional sensing techniques. Consequently, there is no direct method to measure the soil moisture changes attributable to the accumulation and dissipation of dew on the top few millimeters of the soil. Therefore, it is highly recommended to either utilize other types of sensors such as thermal infrared sensors, or to develop new sensors that can measure the presence and amount of moisture in the very top layer (1 mm) of soil. This capability would considerably improve our understanding and ability to monitor soil moisture dynamics, particularly in the early stages of crop growth.

### 7.2.3. VALIDATION CAMPAIGNS FOR MICROWAVE REMOTE SENSING OF VEGETATION

This dissertation explored the impact of SCW on radar backscatter, largely based on experimental data gathered during a singular field experiment during three months in Florida, USA. This research was limited to a single crop type (i.e., sweet maize) and utilizes backscatter data acquired at a single frequency through the University of Florida L-band Automated Radar System (UF-LARS). The ground-based scatterometer experiments have long served as a foundation for fundamental research in active microwave remote sensing. For over 40 years, scholars like Ulaby [15, 16, 22, 36, 84, 234] and others [25, 79, 107, 166, 169, 198–204, 235, 236] have demonstrated how vital these studies are for advancing our understanding of radar and its potential application. Both previous research and this dissertation emphasize the value of tower-based radar experiments in enhancing our understanding of microwave interactions with vegetation. Such research also supports model development for future applications and paves the way for the future use of satellite missions.

However, the limitations of focusing on a single frequency and vegetation type mean that the conclusions may not entirely apply to all frequencies and vegetation types. Therefore, additional experiments are strongly recommended to examine the influence of SCW over a wider range of vegetation types and frequencies. This mainly relates to the fact that the capacity of various vegetation types to store water will depend on their structure and geometry (e.g., narrow-leaved or broad-leaved etc.). Furthermore, we need to understand how the presence of water droplets or films on vegetation might change microwave interactions. As demonstrated in Chapter 6 of this dissertation, the influence of SCW on backscatter strongly relates to the frequency. Therefore, data should be acquired across a broader range of frequencies in future studies for a more comprehensive understanding of SCW effects.

Interestingly, a recent study by Xu *et al.* [184] suggested that this dissertation's findings could extend beyond sweet maize to a broader range of cover types such as tropical forests and savanna sites in Brazil. However, recent studies have suggested that the influence of surface canopy water (SCW) on Vegetation Optical Depth (VOD) from passive microwave radiometry may be less pronounced than initially thought. In particular, research by Holtzman *et al.* [237] found that the presence of dew in the oak forest did not significantly alter the VOD from L-band radiometer on a tower above the forest. This is consistent with other studies that found minimal effect of dew on observed brightness temperatures at the L-band over grasslands and corn fields [238, 239]. These findings indicate that the impact of leaf surface wetness



on VOD may depend strongly on the canopy type and droplet amount, suggesting that the relationship between SCW and radar backscatter might be more nuanced than previously understood. However, the studies were limited to certain types of vegetation and certain frequencies, and other research has indicated that leaf surface water can significantly influence observed X-band brightness temperatures at a tropical forest [240].

Hence, while these studies provide valuable insights, it is clear that more research is still required. First, a deeper understanding is required to explore how external water content influences crop biophysical parameters. Second, it is vital to explore how the sensitivity of Vegetation Optical Depth (VOD) estimation varies with water both inside and outside the canopy. This variation occurs across different crop types, land cover types, and frequencies, making the issue complex. Understanding these relationships could lead to more accurate interpretations of how surface canopy water (SCW) affects the retrieval of soil and vegetation parameters from both active and passive microwave remote sensing. Therefore, additional research across multiple locations and crop types is necessary. This not only underscores the conclusions of this dissertation but also defines the future direction of this research area.

#### 7.2.4. RADIATIVE TRANSFER MODELING

Results and findings in Chapter 4 of this thesis highlighted an urgent need for improved understanding of microwave interactions with vegetation in the presence of SCW. Therefore, in Chapters 5 and 6 of this thesis the Tor Vergata model has been used to improve our understanding of the interaction processes between microwave backscatter and corn crops especially in the presence of SCW over different frequencies and polarization. The Tor Vergata model was originally developed to simulate the seasonal evolution of the radar backscatter due to crop growth with high accuracy. The results of Vermunt *et al.* [119] showed that this model was not able to capture the sub-daily dynamics in observed backscatter for data from a canopy without SCW. Additionally, the standard version of the Tor Vergata model does not explicitly account for the presence of SCW.

Therefore, in Chapter 5, we introduced a technique to enhance the model capacity to simulate the high-temporal dynamics that occur due to changes in soil moisture and, importantly, internal vegetation water dynamics. This improvement was achieved by allowing the small cylinder radius size to vary during the season rather than relying on a fixed value for the entire growing season. This improved our ability to capture sub-daily dynamics observed in backscatter. However, this method necessitates the availability of high-temporal observation data for calibration. In general, these results suggest that as we start to use radiative transfer models to simulate variations at finer temporal resolutions, we need to pay increased attention to the representation of vegetation structural dynamics and their role in weighing the various contributions to the total backscatter.

In a parallel study using the same experimental dataset, Vermunt *et al.* [23] showed significant diurnal water dynamics within corn stems and leaves. In addition, they showed that the total backscatter was primarily sensitive to dynamics in specific

layers of the vegetation. Combined, these could have a significant influence on the diurnal cycle of backscatter on dry days. Allowing for a more detailed representation of the vertical distribution of internal water content by height as well as constituent could improve our ability to capture diurnal variations in backscatter.

To address the sub-daily variations in observed backscatter driven by the presence of SCW and dew on the soil surface, we propose two implementations of the Tor Vergata model (discussed in Chapter 6). These implementations seek to account for impact of SCW on both vegetation and the soil surface in the simulated backscatter. In order to include the influence of dew on the canopy, we adjusted the vegetation water content (VWC) to account for the additional water from SCW. This augmentation means that any extra water from dew or intercepted rain is distributed spatially within the dielectric medium in accordance with the geometry and structure of the vegetation. This method led to improved agreement between simulated and observed backscatter when the total backscatter was predominantly influenced by vegetation. Although the bias was substantially reduced, the model simulations and observations were still not in perfect agreement. One possible reason for this discrepancy could be that the scattering from free water droplets or a water layer on top of the canopy could be different from the scattering of additional water inside the vegetation tissue. This could be explored in future studies. In particular, it could be helpful to allow for an additional thin layer of droplets on leaf surfaces in radiative transfer models to account for the effect of free water on the leaf surface. Furthermore, during dew and rain interception events, all parts of a crop experience increased wetness. However, in this research, we focused solely on the wetness of corn leaves. Future studies should extend this focus to consider the presence of water on stems and all other constituents.

In this research we encountered a relatively poor agreement between observed data and the  $VWC^+$  implementation during bare soil and early vegetative stages. We hypothesized that this discrepancy could arise from the presence of dew in the form of water on top of the soil layer. To test this, we attempted to mimic the effect of dew on top of the soil layer on backscatter by assuming the surface soil layer as saturated if the leaf wetness sensor indicated the presence of moisture. This adjustment somewhat improved the agreement between the modeled and observed backscatter during bare soil and early vegetative stages. However, the remaining mismatch suggests that this approach is less than optimal and requires further refinement. We suggest for future work to consider updating the radiative transfer models and soil moisture estimation models to consider an additional thin layer of water droplets on the soil surface when the leaf wetness sensors detect moisture. This is an important consideration for many application since the presence of dew on top soil can affect the radar backscatter considerably. Alternatively, dew could be represented as a thin saturated litter layer similar to previous research on the inclusion of a litter layer which has proved beneficial in the simulation of emission and scattering from forest areas [196, 197].

Our research can be considered among the first studies that investigate and simulate the influence of dew on soil on backscatter. Our results proved that this can have a significant effect on backscatter over bare soil and during the early season.

The findings underscore the necessity to refine electromagnetic models used for soil moisture retrieval and crop monitoring for more realistic representations of dew and interception on vegetation and soil surfaces. Given the increasing number of radar satellites and innovative applications for their data, these model enhancements are urgently needed. With these advancements, the use of Synthetic Aperture Radar (SAR) could be effectively harnessed to model rapid water processes within the soil-vegetation-atmosphere continuum.

### 7.3. CONCLUDING REMARKS

This research represents a significant improvement in understanding the interaction of radar backscatter with vegetation, particularly focusing on the influence of surface canopy water (SCW) and internal vegetation water content. We have discovered how important these factors are for accurately modeling electromagnetic behavior, with potential implications for various applications like agricultural parameter retrieval, monitoring droughts, and agricultural management.

By studying the relationships between L-band backscatter, biophysical variables, and SCW, as well as the effects of SCW on modeled L-, C-, and X-Band backscatter, we have established a new benchmark for understanding and utilizing radar data for vegetation monitoring. This is especially exciting because it opens up many possibilities for current and future SAR missions such as NiSAR, ROSE-L, and Sentinel-1 NG and also the constellations such as ICEYE, and Capella which have dawn/dusk overpasses or multiple overpasses per day.

However, despite the considerable advances made in this thesis, it has also underlined areas demanding further exploration. Future research should focus on investigating the influence of SCW on backscatter and other radar observables across diverse land cover types, as well as refining representations of dew and interception effects on vegetation and soil surfaces in electromagnetic models. This will give us a better understanding of how radar backscatter interacts with vegetation and soil, benefiting future SAR missions and their applications.

While we have gained valuable knowledge from field experiments and models developed in the past, we need to constantly reassess and update these models to account for the detailed dynamics of vegetation water. Field experiments can be costly, but they are essential for fully realizing the potential of radar remote sensing.

In conclusion, this thesis emphasizes the significance of accurately representing SCW to improve our understanding of electromagnetic models and radar interactions with vegetation and soil. This work is just a step towards more advanced remote sensing techniques for precise, timely, and relevant information on agricultural monitoring and management. The findings in this research pave the way for the continued exploration, innovation, and development in this exciting field.

# BIBLIOGRAPHY

- [1] A. Kross, H. McNairn, D. Lapen, M. Sunohara, and C. Champagne. “Assessment of RapidEye vegetation indices for estimation of leaf area index and biomass in corn and soybean crops”. In: *International Journal of Applied Earth Observation and Geoinformation* 34 (2015), pp. 235–248. ISSN: 0303-2434.
- [2] C. Georgi, D. Spengler, S. Itzerott, and B. Kleinschmit. “Automatic delineation algorithm for site-specific management zones based on satellite remote sensing data”. In: *Precision Agriculture* 19.4 (2018), pp. 684–707. ISSN: 1573-1618.
- [3] M. Vizzari, F. Santaga, and P. Benincasa. “Sentinel 2-Based Nitrogen VRT Fertilization in Wheat: Comparison between Traditional and Simple Precision Practices”. In: *Agronomy* 9.6 (2019), p. 278.
- [4] R. Houborg and M. F. McCabe. “Daily Retrieval of NDVI and LAI at 3 m Resolution via the Fusion of CubeSat, Landsat, and MODIS Data”. In: *Remote Sensing* 10.6 (2018), p. 890.
- [5] S. C. Steele-Dunne, H. McNairn, A. Monsivais-Huertero, J. Judge, P.-W. Liu, and K. Papathanassiou. “Radar remote sensing of agricultural canopies: A review”. In: *IEEE Journal of Selected Topics in Applied Earth Observations and Remote Sensing* 10.5 (2017), pp. 2249–2273.
- [6] H. McNairn and J. Shang. “A review of multitemporal synthetic aperture radar (SAR) for crop monitoring”. In: *Multitemporal Remote Sensing: Methods and Applications* (2016), pp. 317–340.
- [7] M. H. et al. “Using multi-polarization C- and L-band synthetic aperture radar to estimate biomass and soil moisture of wheat fields”. In: *INT J APPL EARTH OBS* 58 (2017). ISSN: 0303-2434.
- [8] C. Atzberger. “Advances in remote sensing of agriculture: context description, existing operational monitoring systems and major information needs”. In: *Remote Sensing* 5.2 (2013), pp. 949–981.
- [9] D. J. Mulla. “Twenty five years of remote sensing in precision agriculture: Key advances and remaining knowledge gaps”. In: *Biosystems Engineering* 114.4 (2013), pp. 358–371.
- [10] B. Brisco and R. J. Brown. “Agricultural applications with radar”. In: *Manual of Remote Sensing: Principles and Applications of Imaging Radar*. John Wiley & Sons, 1998, pp. 381–406.
- [11] P. Berkhout and C. van Bruchem. *The food puzzle: Pathways to securing food for all*. Wageningen Academic Publishers, 2015.

- [12] T. van der Wal, B. Abma, A. Viguria, E. Prévinaire, P. J. Zarco-Tejada, P. Serruys, E. van Valkengoed, and P. van der Voet. “Fieldcopter: unmanned aerial systems for crop monitoring services”. In: *Precision agriculture'13*. Springer. 2013, pp. 169–175.
- [13] A. Veloso, S. Mermoz, A. Bouvet, T. Le Toan, M. Planells, J.-F. Dejoux, and E. Ceschia. “Understanding the temporal behavior of crops using Sentinel-1 and Sentinel-2-like data for agricultural applications”. In: *Remote sensing of environment* 199 (2017), pp. 415–426.
- [14] T. F. Bush and F. T. Ulaby. “An evaluation of radar as a crop classifier”. In: *Remote Sensing of Environment* 7.1 (1978), pp. 15–36. ISSN: 0034-4257.
- [15] F. Ulaby, T. Bush, and P. Batlivala. “Radar response to vegetation II: 8-18 GHz band”. In: *IEEE Transactions on Antennas and Propagation* 23.5 (1975), pp. 608–618. ISSN: 0018-926X.
- [16] F. Ulaby, R. Moore, and A. Fung. *Microwave remote sensing: Active and passive. Volume 2-Radar remote sensing and surface scattering and emission theory*. 1982.
- [17] H. McNairn and B. Brisco. “The application of C-band polarimetric SAR for agriculture: A review”. In: *Canadian Journal of Remote Sensing* 30.3 (2004), pp. 525–542.
- [18] M. Link, D. Entekhabi, T. Jagdhuber, P. Ferrazzoli, L. Guerriero, M. Baur, and R. Ludwig. “Simulating L/L-band and C/L-band active-passive microwave covariation of crops with the Tor Vergata scattering and emission model for a SMAP-Sentinel 1 combination”. In: *2017 IEEE International Geoscience and Remote Sensing Symposium (IGARSS)*. IEEE. 2017, pp. 4143–4146.
- [19] D. Entekhabi, E. G. Njoku, P. E. O’Neill, K. H. Kellogg, W. T. Crow, W. N. Edelstein, J. K. Entin, S. D. Goodman, T. J. Jackson, J. Johnson, J. Kimball, J. R. Piepmeier, R. D. Koster, N. Martin, K. C. McDonald, M. Moghaddam, S. Moran, R. Reichle, J. Shi, M. W. Spencer, S. W. Thurman, L. Tsang, and J. Van Zyl. “The Soil Moisture Active Passive (SMAP) Mission”. In: *Proceedings of the IEEE* 98.5 (2010), pp. 704–716.
- [20] A. G. Konings, Y. Yu, L. Xu, Y. Yang, D. S. Schimel, and S. S. Saatchi. “Active microwave observations of diurnal and seasonal variations of canopy water content across the humid African tropical forests”. In: *Geophysical Research Letters* 44.5 (2017), pp. 2290–2299.
- [21] S. C. Steele-Dunne, H. McNairn, A. Monsivais-Huertero, J. Judge, P.-W. Liu, and K. Papathanassiou. “Radar Remote Sensing of Agricultural Canopies: A Review”. In: *IEEE Journal of Selected Topics in Applied Earth Observations and Remote Sensing* 10.5 (2017), pp. 2249–2273. ISSN: 1939-1404, 2151-1535.
- [22] F. T. Ulaby, R. K. Moore, and A. K. Fung. *Microwave remote sensing: Active and passive. volume 1-microwave remote sensing fundamentals and radiometry*. 1981.

- [23] P. C. Vermunt, S. C. Steele-Dunne, S. Khabbazan, V. Kumar, and J. Judge. “Towards Understanding the Influence of Vertical Water Distribution on Radar Backscatter from Vegetation Using a Multi-Layer Water Cloud Model”. In: *Remote Sensing* 14.16 (2022), p. 3867.
- [24] J. Judge, P.-W. Liu, A. Monsiváis-Huertero, T. Bongiovanni, S. Chakrabarti, S. C. Steele-Dunne, D. Preston, S. Allen, J. P. Bermejo, P. Rush, *et al.* “Impact of vegetation water content information on soil moisture retrievals in agricultural regions: An analysis based on the SMAPVEX16-MicroWEX dataset”. In: *Remote Sensing of Environment* 265 (2021), p. 112623.
- [25] B. A. M. Bouman and H. W. J. van Kasteren. “Ground-based X-band (3-cm wave) radar backscattering of agricultural crops. II. Wheat, barley, and oats; the impact of canopy structure”. In: *Remote Sensing of Environment* 34.2 (1990), pp. 107–119. ISSN: 0034-4257.
- [26] X. Jiao, H. McNairn, J. Shang, E. Pattey, J. Liu, and C. Champagne. “The sensitivity of RADARSAT-2 quad-polarization SAR data to crop LAI”. In: *Remote Sensing and Modeling of Ecosystems for Sustainability VI*. Vol. 7454. SPIE. 2009, pp. 136–146.
- [27] M. Jia, L. Tong, Y. Zhang, and Y. Chen. “Multitemporal radar backscattering measurement of wheat fields using multifrequency (L, S, C, and X) and full-polarization”. In: *Radio Science* 48.5 (2013), pp. 471–481. ISSN: 1944-799X.
- [28] M. El Hajj, N. Baghdadi, H. Bazzi, and M. Zribi. “Penetration Analysis of SAR Signals in the C and L Bands for Wheat, Maize, and Grasslands”. In: *Remote Sensing* 11.1 (2018), p. 31. ISSN: 2072-4292.
- [29] P. Kumar, R. Prasad, D. K. Gupta, V. N. Mishra, A. K. Vishwakarma, V. P. Yadav, R. Bala, A. Choudhary, and R. Avtar. “Estimation of winter wheat crop growth parameters using time series Sentinel-1A SAR data”. In: *Geocarto International* 33.9 (2018), pp. 942–956. ISSN: 1010-6049, 1752-0762.
- [30] M. El Hajj, N. Baghdadi, J.-P. Wigneron, M. Zribi, C. Albergel, J.-C. Calvet, and I. Fayad. “First Vegetation Optical Depth Mapping from Sentinel-1 C-band SAR Data over Crop Fields”. In: *Remote Sensing* 11.23 (2019), p. 2769. ISSN: 2072-4292.
- [31] G. Picard, T. L. Toan, and F. Mattia. “Understanding C-band radar backscatter from wheat canopy using a multiple-scattering coherent model”. In: *IEEE Transactions on Geoscience and Remote Sensing* 41.7 (2003), pp. 1583–1591. ISSN: 0196-2892.
- [32] J. Friesen *et al.* “Diurnal Differences in Global ERS Scatterometer Backscatter Observations of the Land Surface”. In: *IEEE TGARS* 50.7 (2012), pp. 2595–2602. ISSN: 0196-2892, 1558-0644.
- [33] M. Vreugdenhil, W. A. Dorigo, W. Wagner, R. A. De Jeu, S. Hahn, and M. J. Van Marle. “Analyzing the vegetation parameterization in the TU-Wien ASCAT soil moisture retrieval”. In: *IEEE Transactions on Geoscience and Remote Sensing* 54.6 (2016), pp. 3513–3531.

- [34] S. C. Steele-Dunne et al. “Investigating vegetation water dynamics and drought using Metop ASCAT over the North American Grasslands”. In: *Remote Sensing of Environment* (2019).
- [35] *Copernicus Open Access Hub*. English. <https://scihub.copernicus.eu/>.
- [36] F. T. Ulaby, K. Sarabandi, K. McDONALD, M. Whitt, and M. C. Dobson. “Michigan Microwave Canopy Scattering Model”. In: *International Journal of Remote Sensing* 11.7 (1990), pp. 1223–1253. ISSN: 0143-1161, 1366-5901.
- [37] M. Mahdianpari, F. Mohammadimanesh, H. McNairn, A. Davidson, M. Rezaee, B. Salehi, and S. Homayouni. “Mid-season Crop Classification Using Dual-, Compact-, and Full-Polarization in Preparation for the radarsat Constellation Mission (RCM)”. In: *Remote Sensing* 11.13 (2019), p. 1582.
- [38] R. Bindlish and A. P. Barros. “Parameterization of vegetation backscatter in radar-based, soil moisture estimation”. In: *Remote Sensing of Environment* 76.1 (2001), pp. 130–137. ISSN: 00344257.
- [39] D. Mandal, V. Kumar, D. Ratha, J. M. Lopez-Sanchez, A. Bhattacharya, H. McNairn, Y. Rao, and K. Ramana. “Assessment of rice growth conditions in a semi-arid region of India using the Generalized Radar Vegetation Index derived from RADARSAT-2 polarimetric SAR data”. In: *Remote Sensing of Environment* 237 (2020), p. 111561.
- [40] F. Mattia, G. Satalino, A. Balenzano, M. Rinaldi, P. Steduto, and J. Moreno. “Sentinel-1 for wheat mapping and soil moisture retrieval”. In: *2015 IEEE International Geoscience and Remote Sensing Symposium (IGARSS)*. 2015, pp. 2832–2835.
- [41] G. Satalino, A. Balenzano, F. Mattia, and M. Davidson. “Sentinel-1 SAR data for mapping agricultural crops not dominated by volume scattering”. In: *2012 IEEE International Geoscience and Remote Sensing Symposium*. 2012, pp. 6801–6804.
- [42] R. Fieuzal, F. Baup, and C. Marais-Sicre. “Sensitivity of TerraSAR-X, RADARSAT-2 and ALOS satellite radar data to crop variables”. In: *2012 IEEE International Geoscience and Remote Sensing Symposium*. IEEE, 2012, pp. 3740–3743. ISBN: 978-1-4673-1159-5.
- [43] S. Gao, Z. Niu, N. Huang, and X. Hou. “Estimating the Leaf Area Index, height and biomass of maize using HJ-1 and RADARSAT-2”. In: *International Journal of Applied Earth Observation and Geoinformation* 24 (2013), pp. 1–8. ISSN: 03032434.
- [44] D. Han, H. Yang, G. Yang, and C. Qiu. “Monitoring model of corn lodging based on Sentinel-1 radar image”. In: *2017 SAR in Big Data Era: Models, Methods and Applications (BIGSAR DATA)*. IEEE, 2017, pp. 1–5. ISBN: 978-1-5386-4519-2.
- [45] M. Vreugdenhil, W. Wagner, B. Bauer-Marschallinger, I. Pfeil, I. Teubner, C. Rüdiger, and P. Strauss. “Sensitivity of Sentinel-1 backscatter to vegetation dynamics: An Austrian case study”. In: *Remote Sensing* 10.9 (2018), p. 1396.

- [46] N. Ouaadi, L. Jarlan, J. Ezzahar, S. Khabba, V. L. Dantec, Z. Rafi, M. Zribi, and P.-L. Frison. "Water Stress Detection Over Irrigated Wheat Crops in Semi-Arid Areas using the Diurnal Differences of Sentinel-1 Backscatter". In: *2020 Mediterranean and Middle-East Geoscience and Remote Sensing Symposium (M2GARSS)*. IEEE, 2020, pp. 306–309. ISBN: 978-1-72812-190-1.
- [47] D. Wood, H. McNairn, R. J. Brown, and R. Dixon. "The effect of dew on the use of RADARSAT-1 for crop monitoring: Choosing between ascending and descending orbits". In: *Remote Sensing of Environment* 80.2 (2002), pp. 241–247. ISSN: 0034-4257.
- [48] S. Schaufler, B. Bauer-Marschallinger, S. Hochstöger, and W. Wagner. "Modelling and correcting azimuthal anisotropy in Sentinel-1 backscatter data". In: *Remote Sensing Letters* 9.8 (2018), pp. 799–808. ISSN: 2150-704X, 2150-7058.
- [49] M. Rüetschi, M. Schaepman, D. Small, M. Rüetschi, M. E. Schaepman, and D. Small. "Using Multitemporal Sentinel-1 C-band Backscatter to Monitor Phenology and Classify Deciduous and Coniferous Forests in Northern Switzerland". In: *Remote Sensing* 10.1 (2017), p. 55.
- [50] Q. Gao, M. Zribi, M. Escorihuela, N. Baghdadi, P. Segui, Q. Gao, M. Zribi, M. J. Escorihuela, N. Baghdadi, and P. Q. Segui. "Irrigation Mapping Using Sentinel-1 Time Series at Field Scale". In: *Remote Sensing* 10.9 (2018), p. 1495.
- [51] S. Paloscia, S. Pettinato, E. Santi, C. Notarnicola, L. Pasolli, and A. Reppucci. "Soil moisture mapping using Sentinel-1 images: Algorithm and preliminary validation". In: *Remote Sensing of Environment* 134 (2013), pp. 234–248. ISSN: 0034-4257.
- [52] B. Bauer-Marschallinger, V. Freeman, S. Cao, C. Paulik, S. Schaufler, T. Stachl, S. Modanesi, C. Massari, L. Ciabatta, L. Brocca, and W. Wagner. "Toward Global Soil Moisture Monitoring With Sentinel-1: Harnessing Assets and Overcoming Obstacles". In: *IEEE Transactions on Geoscience and Remote Sensing* (2018), pp. 1–20. ISSN: 0196-2892.
- [53] H. Bazzi, N. Baghdadi, M. El Hajj, M. Zribi, D. H. T. Minh, E. Ndikumana, D. Courault, and H. Belhouchette. "Mapping Paddy Rice Using Sentinel-1 SAR Time Series in Camargue, France". In: *Remote Sensing* 11.7 (2019), p. 887.
- [54] N. Torbick, D. Chowdhury, W. Salas, and J. Qi. "Monitoring Rice Agriculture across Myanmar Using Time Series Sentinel-1 Assisted by Landsat-8 and PALSAR-2". In: *Remote Sensing* 9.2 (2017), p. 119.
- [55] E. Ndikumana, D. Ho Tong Minh, N. Baghdadi, D. Courault, and L. Hossard. "Deep Recurrent Neural Network for Agricultural Classification using multitemporal SAR Sentinel-1 for Camargue, France". In: *Remote Sensing* 10.8 (2018), p. 1217.
- [56] M. Arias, M. A. Campo-Bescós, and J. Álvarez-Mozos. "Crop Type Mapping Based on Sentinel-1 Backscatter Time Series". In: *IGARSS 2018 - 2018 IEEE International Geoscience and Remote Sensing Symposium*. 2018, pp. 6623–6626.



- [57] M. Haagsma. “Crop monitoring with Radar”. English. MA thesis. TUDelft, 2015.
- [58] N. Baghdadi, H. Bazzi, M. El Hajj, and M. Zribi. “Detection of Frozen Soil Using Sentinel-1 SAR Data”. In: *Remote Sensing* 10.8 (2018), p. 1182.
- [59] R. Nasirzadehdizaji, F. Balik Sanli, S. Abdikan, Z. Cakir, A. Sekertekin, and M. Ustuner. “Sensitivity analysis of multi-temporal Sentinel-1 SAR parameters to crop height and canopy coverage”. In: *Applied Sciences* 9.4 (2019), p. 655.
- [60] R. Nasirzadehdizaji, Z. Cakir, F. B. Sanli, S. Abdikan, A. Pepe, and F. Calo. “Sentinel-1 interferometric coherence and backscattering analysis for crop monitoring”. In: *Computers and Electronics in Agriculture* 185 (2021), p. 106118.
- [61] K. Van Tricht, A. Gobin, S. Gilliams, and I. Piccard. “Synergistic use of radar Sentinel-1 and optical Sentinel-2 imagery for crop mapping: A case study for Belgium”. In: *Remote Sensing* 10.10 (2018), p. 1642.
- [62] N. den Besten, S. S. Dunne, A. Mahmud, D. Jackson, B. Aouizerats, R. de Jeu, R. Burger, R. Houborg, M. McGlinchey, and P. van der Zaag. “Understanding Sentinel-1 backscatter response to sugarcane yield variability and waterlogging”. In: *Remote Sensing of Environment* 290 (2023), p. 113555.
- [63] S. Amherdt, N. C. Di Leo, S. Balbarani, A. Pereira, C. Cornero, and M. C. Pacino. “Exploiting Sentinel-1 data time-series for crop classification and harvest date detection”. In: *International Journal of Remote Sensing* 42.19 (2021), pp. 7313–7331.
- [64] D. Mandal, V. Kumar, D. Ratha, S. Dey, A. Bhattacharya, J. M. Lopez-Sanchez, H. McNairn, and Y. S. Rao. “Dual polarimetric radar vegetation index for crop growth monitoring using Sentinel-1 SAR data”. In: *Remote Sensing of Environment* 247 (2020), p. 111954. ISSN: 00344257.
- [65] A. Willis. “Dune water and nutrient regimes—their ecological relevance”. In: *Sand Dunes and Their Management: Report of a Meeting, Swansea*. Vol. 13. Focus on Nature Conservation. 1984, pp. 159–174.
- [66] E. D. Kabela, B. K. Hornbuckle, M. H. Cosh, M. C. Anderson, and M. L. Gleason. “Dew frequency, duration, amount, and distribution in corn and soybean during SMEX05”. In: *Agricultural and forest meteorology* 149.1 (2009), pp. 11–24.
- [67] B. K. Hornbuckle, T. L. Rowlandson, E. Russell, A. Kaleita, S. Logsdon, A. Kruger, S. Yueh, and R. D. De Roo. “How does dew affect L-band backscatter? analysis of PALS data at the Iowa validation site and implications for SMAP”. In: *2010 IEEE International Geoscience and Remote Sensing Symposium*. IEEE. 2010, pp. 4835–4838.
- [68] M. Tanase, R. Panciera, K. Lowell, and C. Aponte. “Monitoring live fuel moisture in semiarid environments using L-band radar data”. In: *International Journal of Wildland Fire* 24.4 (2015), pp. 560–572.

- [69] S. Heffernan and B. M. Strimbu. “Estimation of Surface Canopy Water in Pacific Northwest Forests by Fusing Radar, Lidar, and Meteorological Data”. In: *Forests* 12.3 (2021), p. 339.
- [70] N. Agam and P. R. Berliner. “Dew formation and water vapor adsorption in semi-arid environments—a review”. In: *Journal of Arid Environments* 65.4 (2006), pp. 572–590.
- [71] J. R. Wallin. “Agrometeorological aspects of dew”. In: *Agricultural Meteorology* 4.2 (1967), pp. 85–102.
- [72] R. O. Slatyer and D. K. Markus. “Plant-water relationships”. In: *Soil Science* 106.6 (1968), p. 478.
- [73] T. E. Dawson and G. R. Goldsmith. “The value of wet leaves”. In: *New Phytologist* 219.4 (2018), pp. 1156–1169.
- [74] L. Huber and T. Gillespie. “Modeling leaf wetness in relation to plant disease epidemiology”. In: *Annual review of phytopathology* 30.1 (1992), pp. 553–577.
- [75] D. Wood, H. McNairn, R. Brown, and R. Dixon. “Erratum to The effect of dew on the use of RADARSAT-1 for crop monitoring: Choosing between ascending and descending orbits [Remote Sensing of Environment 80/2 (2002 241–247)]”. In: *Remote Sensing of Environment* 81.2-3 (2002), p. 456.
- [76] T. Riedel and C. Schmullius. “Impact of interception on the thematic analyses of SAR data in agricultural areas”. In: *IGARSS 2003. 2003 IEEE International Geoscience and Remote Sensing Symposium. Proceedings (IEEE Cat. No. 03CH37477)*. Vol. 4. IEEE. 2003, pp. 2218–2220.
- [77] R. A. De Jeu, B. G. Heusinkveld, H. Vugts, T. R. Holmes, and M. Owe. “Remote sensing techniques to measure dew: The detection of canopy water with an L-band passive microwave radiometer and a spectral reflectance sensor”. In: *Remote Sensing for Agriculture, Ecosystems, and Hydrology VI*. Vol. 5568. SPIE. 2004, pp. 225–235.
- [78] C. T. Allen and F. T. Ulaby. *Modeling the backscattering and transmission properties of vegetation canopies*. Tech. rep. 1984.
- [79] T. Gillespie, B. Brisco, R. Brown, and G. Sofko. “Radar detection of a dew event in wheat”. In: *Remote sensing of environment* 33.3 (1990), pp. 151–156.
- [80] B. K. Hornbuckle, A. W. England, M. C. Anderson, and B. J. Viner. “The effect of free water in a maize canopy on microwave emission at 1.4GHz”. In: *Agricultural and Forest Meteorology* 138.1 (2006), pp. 180–191. ISSN: 0168-1923.
- [81] M. Herold, C. Pathe, and C. Schmullius. “The effect of free vegetation water on the multi-frequency and polarimetric radar backscatter—first results from the TerraDew 2000 campaign”. In: *IGARSS 2001. Scanning the Present and Resolving the Future. Proceedings. IEEE 2001 International Geoscience and Remote Sensing Symposium (Cat. No. 01CH37217)*. Vol. 5. IEEE. 2001, pp. 2445–2447.

- [82] T. Riedel, C. Pathe, C. Thiel, M. Herold, and C. Schmullius. “Systematic investigation on the effect of dew and interception on multifrequency and multipolarimetric radar backscatter signals”. In: *Retrieval of Bio-and Geo-Physical Parameters from SAR Data for Land Applications*. Vol. 475. 2002, pp. 99–104.
- [83] T. Riedel and C. Schmullius. “Effect of Interception on the Backscattering Behaviour of Crops”. In: *Applications of SAR Polarimetry and Polarimetric Interferometry*. Vol. 529. 2003.
- [84] E. Attema and F. T. Ulaby. “Vegetation modeled as a water cloud”. In: *Radio science* 13.2 (1978), pp. 357–364.
- [85] M. Bracaglia, P. Ferrazzoli, and L. Guerriero. “A fully polarimetric multiple scattering model for crops”. In: *Remote Sensing of Environment* 54.3 (1995), pp. 170–179.
- [86] A. Monsivais-Huertero, P.-W. Liu, and J. Judge. “Phenology-based backscattering model for corn at L-band”. In: *IEEE Transactions on Geoscience and Remote Sensing* 56.9 (2018), pp. 4989–5005.
- [87] L. Villard and P. Borderies. “Backscattering border effects for forests at C-Band”. In: *Piers Online* 3.5 (2007), pp. 731–735.
- [88] P. Ferrazzoli and L. Guerriero. “Radar sensitivity to tree geometry and woody volume: A model analysis”. In: *IEEE Transactions on Geoscience and Remote Sensing* 33.2 (1995), pp. 360–371.
- [89] A. Della Vecchia, P. Ferrazzoli, L. Guerriero, L. Ninivaggi, T. Strozzi, and U. Wegmuller. “Observing and modeling multifrequency scattering of maize during the whole growth cycle”. In: *IEEE Transactions on Geoscience and Remote Sensing* 46.11 (2008), pp. 3709–3718.
- [90] L. Guerriero, N. Pierdicca, L. Pulvirenti, and P. Ferrazzoli. “Use of satellite radar bistatic measurements for crop monitoring: A simulation study on corn fields”. In: *Remote Sensing* 5.2 (2013), pp. 864–890.
- [91] J. Stamenkovic, P. Ferrazzoli, L. Guerriero, D. Tuia, J.-P. Thiran, and M. Borgeaud. “Crop backscatter modeling and soil moisture estimation with support vector regression”. In: *2014 IEEE Geoscience and Remote Sensing Symposium*. Ieee. 2014, pp. 3228–3231.
- [92] L. Guerriero, P. Ferrazzoli, C. Vittucci, R. Rahmoune, M. Aurizzi, and A. Mattioni. “L-band passive and active signatures of vegetated soil: Simulations with a unified model”. In: *IEEE Journal of Selected Topics in Applied Earth Observations and Remote Sensing* 9.6 (2016), pp. 2520–2531.
- [93] M. Acuña, P. Ferrazzoli, and L. Guerriero. “Modeling L-and X-band backscattering of wheat and tests over fields of Pampas”. In: *European Journal of Remote Sensing* 52.sup4 (2019), pp. 84–101.
- [94] P. Ferrazzoli and L. Guerriero. “Emissivity of vegetation: theory and computational aspects”. In: *Journal of Electromagnetic Waves and Applications* 10.5 (1996), pp. 609–628.

- [95] P. Ferrazzoli, L. Guerriero, A. Quesney, O. Taconet, and J.-P. Wigneron. “Investigating the capability of C-band radar to monitor wheat characteristics”. In: *IEEE 1999 International Geoscience and Remote Sensing Symposium. IGARSS'99 (Cat. No. 99CH36293)*. Vol. 2. IEEE. 1999, pp. 723–725.
- [96] P. Ferrazzoli, L. Guerriero, and G. Schiavon. “Experimental and model investigation on radar classification capability”. In: *IEEE transactions on Geoscience and remote sensing* 37.2 (1999), pp. 960–968.
- [97] A. Della Vecchia, I. Bruni, P. Ferrazzoli, and L. Guerriero. “Recent advances in crop modeling: The curved leaf and the hollow stem”. In: *IGARSS 2004. 2004 IEEE International Geoscience and Remote Sensing Symposium*. Vol. 2. IEEE. 2004, pp. 895–898.
- [98] A. Della Vecchia, P. Ferrazzoli, L. Guerriero, X. Blaes, P. Defourny, L. Dente, F. Mattia, G. Satalino, T. Strozzi, and U. Wegmuller. “Influence of geometrical factors on crop backscattering at C-band”. In: *IEEE transactions on geoscience and remote sensing* 44.4 (2006), pp. 778–790.
- [99] A. D. Vecchia, L. Guerriero, I. Bruni, and P. Ferrazzoli. “Hollow cylinder microwave model for stems”. In: *Journal of electromagnetic waves and applications* 20.3 (2006), pp. 301–318.
- [100] X. Blaes, P. Defourny, U. Wegmuller, A. Della Vecchia, L. Guerriero, and P. Ferrazzoli. “C-band polarimetric indexes for maize monitoring based on a validated radiative transfer model”. In: *IEEE transactions on geoscience and remote sensing* 44.4 (2006), pp. 791–800.
- [101] A. Della Vecchia, P. Ferrazzoli, L. Guerriero, T. Strozzi, and U. Wegmuller. “A statistical and theoretical study about radar sensitivity to crop growth from S to X band”. In: *2007 IEEE International Geoscience and Remote Sensing Symposium*. IEEE. 2007, pp. 1424–1427.
- [102] S. Khabbazan, S. Steele-Dunne, P. Vermunt, J. Judge, M. Vreugdenhil, and G. Gao. “The influence of surface canopy water on the relationship between L-band backscatter and biophysical variables in agricultural monitoring”. In: *Remote Sensing of Environment* 268 (2022), p. 112789.
- [103] M. C. Peel, B. L. Finlayson, and T. A. McMahon. “Updated world map of the Köppen-Geiger climate classification”. In: *Hydrology and earth system sciences* 11.5 (2007), pp. 1633–1644.
- [104] R. J. Black. *Florida Climate Data 1*. 1993.
- [105] T. Bongiovanni, P.-W. Liu, K. Nagarajan, D. Preston, P. Rush, T. H. van Emmerik, R. Terwilleger, A. Monsivais-Huertero, J. Judge, S. Steele-Dunne, *et al.* “Field Observations during the Eleventh Microwave Water and Energy Balance Experiment (MicroWEX-11): from April 25, 2012, through December 6, 2012: AE514/AE514, 7/2015”. In: *EDIS* 2015.6 (2015), pp. 96–96.

- [106] K. Nagarajan, P.-W. Liu, R. DeRoo, J. Judge, R. Akbar, P. Rush, S. Feagle, D. Preston, and R. Terwilleger. “Automated L-band radar system for sensing soil moisture at high temporal resolution”. In: *IEEE Geoscience and Remote Sensing Letters* 11.2 (2013), pp. 504–508.
- [107] P.-W. Liu, J. Judge, R. D. DeRoo, A. W. England, T. Bongiovanni, and A. Luke. “Dominant backscattering mechanisms at L-band during dynamic soil moisture conditions for sandy soils”. In: *Remote Sensing of Environment* 178 (2016), pp. 104–112. ISSN: 00344257.
- [108] T. F. Bush and F. T. Ulaby. “Fading characteristics of panchromatic radar backscatter from selected agricultural targets”. In: *IEEE Transactions on Geoscience Electronics* 13.4 (1975), pp. 149–157.
- [109] K. Sarabandi and F. T. Ulaby. “A convenient technique for polarimetric calibration of single-antenna radar systems”. In: *IEEE Transactions on Geoscience and Remote Sensing* 28.6 (1990), pp. 1022–1033.
- [110] METER Group. *ECH2O EC-5 Moisture Sensor*. 2021. URL: <https://www.metergroup.com/environment/products/ec-5-soil-moisture-sensor>.
- [111] M.-y. Jang, K.-J. C. Tien, J. Casanova, and J. Judge. “Measurements of soil surface roughness during the fourth microwave water and energy balance experiment: April 18 through June 13, 2005”. In: *Technical Report*. Citeseer, 2005.
- [112] J. Álvarez-Mozos, M. González-Audicana, J. Casali, and A. Larranaga. “Effective versus measured correlation length for radar-based surface soil moisture retrieval”. In: *International Journal of Remote Sensing* 29.17-18 (2008), pp. 5397–5408.
- [113] N. Baghdadi, I. Gherboudj, M. Zribi, M. Sahebi, C. King, and F. Bonn. “Semi-empirical calibration of the IEM backscattering model using radar images and moisture and roughness field measurements”. In: *International Journal of Remote Sensing* 25.18 (2004), pp. 3593–3623.
- [114] N. Baghdadi, N. Holah, and M. Zribi. “Calibration of the integral equation model for SAR data in C-band and HH and VV polarizations”. In: *International Journal of Remote Sensing* 27.4 (2006), pp. 805–816.
- [115] METER Group. *PHYTOS 31 Dielectric Leaf Wetness Sensor*. 2021. URL: <https://www.metergroup.com/en/meter-environment/products/phytos-31-leaf-wetness-sensor>.
- [116] METER Group. *Em50® series data loggers from METER Group*. 2019. URL: <https://www.metergroup.com/en/meter-environment/products/phytos-31-leaf-wetness-sensor>.
- [117] METER Group. *PREDICTING THE AMOUNT OF WATER ON THE SURFACE OF THE PHYTOS 31 DIELECTRIC LEAF WETNESS SENSOR*. 2021. URL: <https://publications.metergroup.com/Sales%5C%20and%5C%20Support/METER%5C%20Environment/Website%5C%20Articles/predicting-amount-water-surface-lws-leaf-wetness-sensor.pdf>.

- [118] D. R. Cobos. “Predicting the amount of water on the surface of the LWS dielectric leaf wetness sensor”. In: (2008).
- [119] P. C. Vermunt, S. Khabbazan, S. C. Steele-Dunne, J. Judge, A. Monsivais-Huertero, L. Guerriero, and P.-W. Liu. “Response of Subdaily L-Band Backscatter to Internal and Surface Canopy Water Dynamics”. In: *IEEE Transactions on Geoscience and Remote Sensing* 59.9 (2021), pp. 7322–7337.
- [120] W. Meier, H. Bleiholder, L. Buhr, C. Feller, H. Hack, M. Heß, P.D. Lancashire, U. Schnock, R. Stauß, T. Van den Boom, E. Weber, and P. Zwerger. “The BBCH System to Coding the Phenological Growth Stages of Plants – History and Publications –”. In: *Journal für Kulturpflanzen* 61.2 (2009), pp. 41–52.
- [121] S. Khabbazan, P. Vermunt, S. Steele-Dunne, L. Ratering Arntz, C. Marinetti, D. van der Valk, L. Iannini, R. Molijn, K. Westerdijk, and C. van der Sande. “Crop monitoring using Sentinel-1 data: A case study from The Netherlands”. In: *Remote Sensing* 11.16 (2019), p. 1887.
- [122] P. Berkhout. *Agricultural Economic Report 2015 Summary*. English. SUMMARY Report 2015-092. The Hague, Agricultural Economics Research Institute (LEI), 2015, p. 30.
- [123] *The Netherlands in 2030*. Tech. rep. Rotterdam: ECORYS, 2014, p. 106. URL: <https://www.ecorys.nl/sites/default/files/Nederland%20in%202030.pdf>.
- [124] B. Brisco, R. Brown, T. Hirose, H. McNairn, and K. Staenz. “Precision agriculture and the role of remote sensing: a review”. In: *Canadian Journal of Remote Sensing* 24.3 (1998), pp. 315–327.
- [125] D. J. Mulla. “Twenty five years of remote sensing in precision agriculture: Key advances and remaining knowledge gaps”. In: *Biosystems Engineering*. Special Issue: Sensing Technologies for Sustainable Agriculture 114.4 (2013), pp. 358–371. ISSN: 1537-5110.
- [126] *Introductie - PDOK*. <https://www.pdok.nl/introductie/-/article/basisregistratie-gewaspercelen-brp->.
- [127] KNMI. *Dagwaarden Neerslagstations*. <https://www.knmi.nl/nederland-nu/klimatologie/monv/reeksen>. 2017.
- [128] E. S. Russell. “Effect of Dew and Intercepted Precipitation on Radar Backscatter of a Soybean Canopy”. M.Sc. Thesis. Ames, Iowa, USA: Iowa State University, 2011.
- [129] *Soil-specific calibrations for METER soil moisture sensors | METER Environment*. <https://www.metergroup.com/environment/articles/how-calibrate-soil-moisture-sensors/>.
- [130] *ML3 ThetaProbe Soil Moisture Sensor - Soil Moisture Measurement - Soil Moisture Meter*. <https://www.delta-t.co.uk/product/ml3/>.
- [131] U. Meier. “Growth Stages of Mono-and Dicotyledonous Plants”. In: Federal Biological Research Centre for Agriculture and Forestry.2 (2001), p. 158.

- [132] N. Gorelick, M. Hancher, M. Dixon, S. Ilyushchenko, D. Thau, and R. Moore. “Google Earth Engine: Planetary-scale geospatial analysis for everyone”. In: *Remote Sensing of Environment* (2017).
- [133] *Sentinel-1 Algorithms | Google Earth Engine API*. <https://developers.google.com/earth-engine/sentinel1>.
- [134] *SNAP - ESA Sentinel Application Platform v6.0.0, Download | STEP*. <https://step.esa.int/main/download/snap-download/>. 2018.
- [135] *SNAP Documentation | STEP*. <https://step.esa.int/main/doc/>.
- [136] *7.2 Opbrengstprognose | Teelthandleiding | Stichting IRS*. <https://www.irs.nl/alle/teelthandleiding/7.2-opbrengstprognose>.
- [137] N. van Swaaij. *Groei en ontwikkeling van de suikerbiet*. Dutch. [https://www.irs.nl/userfiles/testhandleiding\\_render/7.1-groei-en-ontwikkeling-van-de-suikerbiet.pdf](https://www.irs.nl/userfiles/testhandleiding_render/7.1-groei-en-ontwikkeling-van-de-suikerbiet.pdf). 2011.
- [138] J. Bronswijk and J. Evers-Vermeer. *KRIMPKARAKTERISTIEKEN VAN KLEIGRONDEN IN NEDERLAND*. Dutch. Tech. rep. 22. WAGENINGEN: INSTITUUT VOOR CULTUURTECHNIEK EN WATERHUISHOUDUNG (ICW), 1987, p. 59.
- [139] C. Liu, J. Shang, P. W. Vachon, and H. McNairn. “Multiyear Crop Monitoring Using Polarimetric RADARSAT-2 Data”. In: *IEEE Transactions on Geoscience and Remote Sensing* 51.4 (2013), pp. 2227–2240. ISSN: 0196-2892.
- [140] G. Wiseman, H. McNairn, S. Homayouni, and J. Shang. “RADARSAT-2 Polarimetric SAR Response to Crop Biomass for Agricultural Production Monitoring”. In: *IEEE Journal of Selected Topics in Applied Earth Observations and Remote Sensing* 7.11 (2014), pp. 4461–4471. ISSN: 1939-1404, 2151-1535.
- [141] M. S. Moran, L. Alonso, J. F. Moreno, and M. P. C. Mateo. “A RADARSAT-2 Quad-Polarized Time Series for Monitoring Crop and Soil Conditions in Barrax, Spain”. In: *IEEE TRANSACTIONS ON GEOSCIENCE AND REMOTE SENSING* 50.4 (2012), p. 14.
- [142] H. McNairn, C. Duguay, B. Brisco, and T. J. Pultz. “The effect of soil and crop residue characteristics on polarimetric radar response”. In: *Remote sensing of environment* 80.2 (2002), pp. 308–320.
- [143] X. Jiao, H. McNairn, J. Shang, E. Pattey, J. Liu, and C. Champagne. “The sensitivity of RADARSAT-2 polarimetric SAR data to corn and soybean leaf area index”. In: *Canadian Journal of Remote Sensing* 37.1 (2011), p. 14.
- [144] P. Ferrazzoli, S. Paloscia, P. Pampaloni, G. Schiavon, D. Solimini, and P. Coppo. “Sensitivity of microwave measurements to vegetation biomass and soil moisture content: a case study”. In: *IEEE Transactions on Geoscience and Remote Sensing* 30.4 (1992), pp. 750–756. ISSN: 0196-2892.
- [145] C. S. T. DAUGHTRY, K. J. RANSON, and L. L. BIEHL. “C-band backscattering from corn canopies”. In: *International Journal of Remote Sensing* 12.5 (1991), pp. 1097–1109. ISSN: 0143-1161.

- [146] S. C. M. Brown, S. Quegan, K. Morrison, J. C. Bennett, and G. Cookmartin. “High-resolution measurements of scattering in wheat canopies-implications for crop parameter retrieval”. In: *IEEE Transactions on Geoscience and Remote Sensing* 41.7 (2003), pp. 1602–1610. ISSN: 0196-2892.
- [147] F. Mattia, T. L. Toan, G. Picard, F. I. Posa, A. D’Alessio, C. Notarnicola, A. M. Gatti, M. Rinaldi, G. Satalino, and G. Pasquariello. “Multitemporal C-band radar measurements on wheat fields”. In: *IEEE Transactions on Geoscience and Remote Sensing* 41.7 (2003), pp. 1551–1560. ISSN: 0196-2892.
- [148] G. Macelloni, S. Paloscia, P. Pampaloni, F. Marliani, and M. Gai. “The relationship between the backscattering coefficient and the biomass of narrow and broad leaf crops”. In: *IEEE Transactions on Geoscience and Remote Sensing* 39.4 (2001), pp. 873–884.
- [149] A. Larrañaga, J. Álvarez-Mozos, L. Albizua, and J. Peters. “Backscattering Behavior of Rain-Fed Crops Along the Growing Season”. In: *IEEE GEOSCIENCE AND REMOTE SENSING LETTERS* 10.2 (2013), p. 5.
- [150] W. Devos, D. Fasbender, P. Griffiths, G. Lemoine, P. Loudjani, P. Milenov, A. Sima, C. Wirthardt, European Commission, and Joint Research Centre. *Second discussion document on the introduction of monitoring to substitute OTSC: rules for processing applications in 2018-2019*. OCLC: 1111215521. 2017. ISBN: 978-92-79-94171-9. URL: [http://publications.europa.eu/publication/manifestation\\_identifier/PUB\\_KJNA29369ENN](http://publications.europa.eu/publication/manifestation_identifier/PUB_KJNA29369ENN).
- [151] T. W. Brakke, E. T. Kanemasu, J. L. Steiner, F. T. Ulaby, and E. Wilson. “Microwave radar response to canopy moisture, leaf-area index, and dry weight of wheat, corn, and sorghum”. In: *Remote Sensing of Environment* 11 (1981), pp. 207–220.
- [152] M. Hosseini, H. McNairn, A. Merzouki, and A. Pacheco. “Estimation of Leaf Area Index (LAI) in corn and soybeans using multi-polarization C- and L-band radar data”. In: *Remote Sensing of Environment* 170 (2015), pp. 77–89. ISSN: 00344257.
- [153] Q. Chang. “Mapping shrub biomass, Leaf Area Index and rainfall interception capacities in the Arctic tundra using L-band SAR”. PhD thesis. 2020.
- [154] C. Liao, J. Wang, J. Shang, X. Huang, J. Liu, and T. Huffman. “Sensitivity study of Radarsat-2 polarimetric SAR to crop height and fractional vegetation cover of corn and wheat”. In: *International Journal of Remote Sensing* 39.5 (2018), pp. 1475–1490. ISSN: 0143-1161, 1366-5901.
- [155] S. Paloscia and P. Pampaloni. “Microwave vegetation indexes for detecting biomass and water conditions of agricultural crops”. In: *Remote Sensing of Environment* 40.1 (1992), pp. 15–26. ISSN: 00344257.
- [156] S. S. Saatchi, J. J. van Zyl, and G. Asrar. “Estimation of canopy water content in Konza Prairie grasslands using synthetic aperture radar measurements during FIFE”. In: *Journal of Geophysical Research: Atmospheres* 100.D12 (1995), pp. 25481–25496.



- [157] S.-B. Kim, H. Huang, T.-H. Liao, and A. Colliander. “Estimating vegetation water content and soil surface roughness using physical models of L-band radar scattering for soil moisture retrieval”. In: *Remote Sensing* 10.4 (2018), p. 556.
- [158] R. A. Molijn, L. Iannini, A. Mousivand, and R. F. Hanssen. “Analyzing C-band SAR polarimetric information for LAI and crop yield estimations”. In: *Remote Sensing for Agriculture, Ecosystems, and Hydrology XVI*. Vol. 9239. International Society for Optics and Photonics. 2014, p. 92390V.
- [159] S. Dzikiti, J. Verreyne, J. Stuckens, A. Strever, W. Verstraeten, R. Swennen, and P. Coppin. “Determining the water status of Satsuma mandarin trees [Citrus Unshiu Marcovitch] using spectral indices and by combining hyperspectral and physiological data”. In: *Agricultural and Forest Meteorology* 150.3 (2010), pp. 369–379. ISSN: 0168-1923.
- [160] P. S. Thenkabail and J. G. Lyon. *Hyperspectral remote sensing of vegetation*. CRC press, 2016.
- [161] C. J. Tucker. “Remote sensing of leaf water content in the near infrared”. In: *Remote sensing of Environment* 10.1 (1980), pp. 23–32.
- [162] J. Penuelas, I. Filella, C. Biel, L. Serrano, and R. Save. “The reflectance at the 950–970 nm region as an indicator of plant water status”. In: *International Journal of Remote Sensing* 14.10 (1993), pp. 1887–1905.
- [163] B. Barrett, E. Dwyer, and P. Whelan. “Soil Moisture Retrieval from Active Spaceborne Microwave Observations: An Evaluation of Current Techniques”. In: *Remote Sensing* 1.3 (2009), pp. 210–242. ISSN: 2072-4292.
- [164] A. G. Konings, K. Rao, and S. C. Steele-Dunne. “Macro to micro: microwave remote sensing of plant water content for physiology and ecology”. In: *New Phytologist* 223.3 (2019), pp. 1166–1172.
- [165] F. Frappart, J.-P. Wigneron, X. Li, X. Liu, A. Al-Yaari, L. Fan, M. Wang, C. Moisy, E. Le Masson, Z. A. Lafkih, *et al.* “Global monitoring of the vegetation dynamics from the Vegetation Optical Depth (VOD): A review”. In: *Remote Sensing* 12.18 (2020), p. 2915.
- [166] Y. Inoue, T. Kurosu, H. Maeno, S. Uratsuka, T. Kozu, K. Dabrowska-Zielinska, and J. Qi. “Season-long daily measurements of multifrequency (Ka, Ku, X, C, and L) and full-polarization backscatter signatures over paddy rice field and their relationship with biological variables”. In: *Remote Sensing of Environment* 81.2 (2002), pp. 194–204. ISSN: 0034-4257.
- [167] Y. Kim, T. Jackson, R. Bindlish, H. Lee, and S. Hong. “Radar vegetation index for estimating the vegetation water content of rice and soybean”. In: *IEEE Geoscience and Remote Sensing Letters* 9.4 (2011), pp. 564–568.
- [168] Y. Kim, S. Hong, K. Lee, T. Jackson, R. Bindlish, G. Jung, S. Jang, Na, and Sangil. “Estimating wheat growth for radar vegetation indices”. In: *2013 IEEE International Geoscience and Remote Sensing Symposium - IGARSS*. IEEE, 2013, pp. 3219–3222. ISBN: 978-1-4799-1114-1.

- [169] P. K. Srivastava, P. O'Neill, M. Cosh, R. Lang, and A. Joseph. "Evaluation of radar vegetation indices for vegetation water content estimation using data from a ground-based SMAP simulator". In: *2015 IEEE International Geoscience and Remote Sensing Symposium (IGARSS)*. IEEE, 2015, pp. 1296–1299.
- [170] J. Ma, S. Huang, J. Li, X. Li, X. Song, P. Leng, and Y. Sun. "Estimating Vegetation Water Content of Corn and Soybean Using Different Polarization Ratios Based on L- and S-band Radar Data". In: *IEEE Geoscience and Remote Sensing Letters* 14.3 (2017), pp. 364–368. ISSN: 1545-598X, 1558-0571.
- [171] Y.-h. Kim, S. Y. Hong, and H. Lee. "Radar Backscattering Measurement of a Paddy Rice Field using Multi-frequency (L, C and X) and Full-polarization". In: *IGARSS 2008 - 2008 IEEE International Geoscience and Remote Sensing Symposium*. IEEE, 2008, pp. IV-553-IV-556. ISBN: 978-1-4244-2807-6.
- [172] X. Jiao, H. McNairn, J. Shang, and J. Liu. "The sensitivity of multi-frequency (X, C and L-band) radar backscatter signatures to bio-physical variables (LAI) over corn and soybean fields". In: *ISPRS TC VII Symposium—100 Years ISPRS*. 2010, pp. 317–325.
- [173] P. A. Rosen, Y. Kim, R. Kumar, T. Misra, R. Bhan, and V. R. Sagi. "Global persistent SAR sampling with the NASA-ISRO SAR (NISAR) mission". In: *2017 IEEE Radar Conference (RadarConf)*. IEEE, 2017, pp. 0410–0414.
- [174] N. Pierdicca, M. Davidson, M. Chini, W. Dierking, S. Djavidnia, J. Haarpaintner, G. Hajduch, G. V. Laurin, M. Lavalley, C. López-Martinez, *et al.* "The copernicus L-band SAR mission ROSE-L (Radar Observing System for Europe)(conference presentation)". In: *Active and Passive Microwave Remote Sensing for Environmental Monitoring III*. Vol. 11154. International Society for Optics and Photonics. 2019, 111540E.
- [175] Y. Kim and J. J. van Zyl. "A time-series approach to estimate soil moisture using polarimetric radar data". In: *IEEE Transactions on Geoscience and Remote Sensing* 47.8 (2009), pp. 2519–2527.
- [176] Y. Kim, T. Jackson, R. Bindlish, S. Hong, G. Jung, and K. Lee. "Retrieval of wheat growth parameters with radar vegetation indices". In: *IEEE Geoscience and Remote Sensing Letters* 11.4 (2013), pp. 808–812.
- [177] D. Haldar, V. Dave, A. Misra, and B. Bhattacharya. "Radar Vegetation Index for assessing cotton crop condition using RISAT-1 data". In: *Geocarto International* 35.4 (2020), pp. 364–375.
- [178] Y. Huang, J. P. Walker, Y. Gao, X. Wu, and A. Moneris. "Estimation of Vegetation Water Content From the Radar Vegetation Index at L-Band". In: *IEEE Transactions on Geoscience and Remote Sensing* 54.2 (2016), pp. 981–989. ISSN: 0196-2892, 1558-0644.
- [179] C. Szigarski, T. Jagdhuber, M. Baur, C. Thiel, M. Parrens, J.-P. Wigneron, M. Piles, and D. Entekhabi. "Analysis of the radar vegetation index and potential improvements". In: *Remote Sensing* 10.11 (2018), p. 1776.

- [180] W. Wagner, G. Lemoine, and H. Rott. “A method for estimating soil moisture from ERS scatterometer and soil data”. In: *Remote sensing of environment* 70.2 (1999), pp. 191–207.
- [181] A. Sharma, R. H. Lang, M. Kurum, P. E. O’Neill, and M. H. Cosh. “L-band Radar Experiment and Modeling of a Corn Canopy Over a Full Growing Season”. In: *IEEE Transactions on Geoscience and Remote Sensing* (2020).
- [182] A. Monsivais-Huertero and J. Judge. “Comparison of backscattering models at L-band for growing corn”. In: *IEEE Geoscience and Remote Sensing Letters* 8.1 (2010), pp. 24–28.
- [183] R. A. Molijn, L. Iannini, P. López Dekker, P. S. Magalhães, and R. F. Hanssen. “Vegetation characterization through the use of precipitation-affected SAR signals”. In: *Remote Sensing* 10.10 (2018), p. 1647.
- [184] X. Xu, A. G. Konings, M. Longo, A. Feldman, L. Xu, S. Saatchi, D. Wu, J. Wu, and P. Moorcroft. “Leaf surface water, not plant water stress, drives diurnal variation in tropical forest canopy water content”. In: *New Phytologist* (2021).
- [185] S. T. Allen, D. P. Aubrey, M. Y. Bader, M. Coenders-Gerrits, J. Friesen, E. D. Gutmann, F. Guillemette, C. Jiménez-Rodríguez, R. F. Keim, A. Klamerus-Iwan, *et al.* “Key questions on the evaporation and transport of intercepted precipitation”. In: *Precipitation Partitioning by Vegetation*. Springer, 2020, pp. 269–280.
- [186] V. L. Mironov, M. C. Dobson, V. H. Kaupp, S. A. Komarov, and V. N. Kleshchenko. “Generalized refractive mixing dielectric model for moist soils”. In: *IEEE transactions on Geoscience and Remote sensing* 42.4 (2004), pp. 773–785.
- [187] V. L. Mironov and S. V. Fomin. “Temperature and mineralogy dependable model for microwave dielectric spectra of moist soils”. In: *Piers online* 5.5 (2009), pp. 411–415.
- [188] A. K. Fung, K.-S. Chen, and K. Chen. *Microwave scattering and emission models for users*. Artech house, 2010.
- [189] H. J. Eom and A. Fung. “A scatter model for vegetation up to Ku-band”. In: *Remote Sensing of Environment* 15.3 (1984), pp. 185–200.
- [190] M. Karam and A. Fung. “Electromagnetic scattering from a layer of finite length, randomly oriented, dielectric, circular cylinders over a rough interface with application to vegetation”. In: *International Journal of Remote Sensing* 9.6 (1988), pp. 1109–1134.
- [191] P. Silva, A. Damasceno, K. Silva, O. Oliveira, and R. Queiroga. “Growth and yield of corn grain and green ear in competition with weeds”. In: *Planta Daninha* 27.SPE (2009), pp. 947–955.
- [192] K. Sprangers, S. Thys, D. Van Dusschoten, and G. T. Beemster. “Gibberellin enhances the anisotropy of cell expansion in the growth zone of the maize leaf”. In: *Frontiers in plant science* (2020), p. 1163.

- [193] D. C. Montgomery, E. A. Peck, and G. G. Vining. “An Introduction to Linear Regression Analysis”. In: *Wiley Series in Probability and Statistics* (2012).
- [194] S. Khabbazan, P. C. Vermunt, S. C. Steele-Dunne, and J. Judge. “The Importance of Overpass Time in Agricultural Applications of Radar”. In: *2021 IEEE International Geoscience and Remote Sensing Symposium IGARSS*. IEEE, 2021, pp. 6084–6087.
- [195] C. Matzler. “Microwave (1-100 GHz) dielectric model of leaves”. In: *IEEE Transactions on Geoscience and Remote Sensing* 32.4 (1994), pp. 947–949.
- [196] A. Della Vecchia, P. Ferrazzoli, J.-P. Wigneron, and J. P. Grant. “Modeling forest emissivity at L-band and a comparison with multitemporal measurements”. In: *IEEE Geoscience and Remote Sensing Letters* 4.4 (2007), pp. 508–512.
- [197] L. Dente, P. Ferrazzoli, Z. Su, R. Van Der Velde, and L. Guerriero. “Combined use of active and passive microwave satellite data to constrain a discrete scattering model”. In: *Remote sensing of environment* 155 (2014), pp. 222–238.
- [198] S. E. I. Essebtey, L. Villard, P. Borderies, T. Kolečk, J.-P. Monvoisin, B. Burban, and T. Le Toan. “Temporal decorrelation of tropical dense forest at C-band: First insights from the TropiScat-2 experiment”. In: *IEEE Geoscience and Remote Sensing Letters* 17.6 (2019), pp. 928–932.
- [199] D. H. T. Minh, S. Tebaldini, F. Rocca, T. Le Toan, P. Borderies, T. Kolečk, C. Albinet, A. Hamadi, and L. Villard. “Vertical structure of P-Band temporal decorrelation at the Paracou forest: Results from TropiScat”. In: *IEEE Geoscience and Remote Sensing Letters* 11.8 (2014), pp. 1438–1442.
- [200] S. E. I. Essebtey, L. Villard, P. Borderies, T. Kolečk, B. Burban, and T. Le Toan. “Long-term trends of P-Band temporal decorrelation over a tropical dense forest-experimental results for the BIOMASS mission”. In: *IEEE Transactions on Geoscience and Remote Sensing* 60 (2021), pp. 1–15.
- [201] A. Hamadi, L. Villard, P. Borderies, C. Albinet, T. Kolečk, and T. Le Toan. “Comparative analysis of temporal decorrelation at P-band and low L-band frequencies using a tower-based scatterometer over a tropical forest”. In: *IEEE Geoscience and Remote Sensing Letters* 14.11 (2017), pp. 1918–1922.
- [202] A. R. Monteith and L. M. Ulander. “Temporal characteristics of P-band tomographic radar backscatter of a boreal forest”. In: *IEEE Journal of Selected Topics in Applied Earth Observations and Remote Sensing* 14 (2021), pp. 1967–1984.
- [203] L. M. Ulander, A. R. Monteith, M. J. Soja, and L. E. Eriksson. “Multiport vector network analyzer radar for tomographic forest scattering measurements”. In: *IEEE Geoscience and Remote Sensing Letters* 15.12 (2018), pp. 1897–1901.
- [204] A. R. Monteith and L. M. Ulander. “A tower-based radar study of temporal coherence of a boreal forest at P-, L-, and C-bands and linear cross polarization”. In: *IEEE Transactions on Geoscience and Remote Sensing* 60 (2021), pp. 1–15.

- [205] V. Brancato, F. Liebisch, and I. Hajnsek. “Impact of plant surface moisture on differential interferometric observables: A controlled electromagnetic experiment”. In: *IEEE Transactions on Geoscience and Remote Sensing* 55.7 (2017), pp. 3949–3964.
- [206] G. Satalino, F. Mattia, A. Balenzano, F. P. Lovergine, M. Rinaldi, A. P. De Santis, S. Ruggieri, D. N. Garcia, V. P. Gómez, E. Ceschia, *et al.* “Sentinel-1 & Sentinel-2 data for soil tillage change detection”. In: *IGARSS 2018-2018 IEEE International Geoscience and Remote Sensing Symposium*. IEEE. 2018, pp. 6627–6630.
- [207] O. Kavats, D. Khramov, K. Sergieieva, and V. Vasyliov. “Monitoring harvesting by time series of Sentinel-1 SAR data”. In: *Remote Sensing* 11.21 (2019), p. 2496.
- [208] G. Azzari, P. Grassini, J. I. R. Edreira, S. Conley, S. Mourtzinis, and D. B. Lobell. “Satellite mapping of tillage practices in the North Central US region from 2005 to 2016”. In: *Remote Sensing of Environment* 221 (2019), pp. 417–429.
- [209] N. Ouaadi, L. Jarlan, J. Ezzahar, S. Khabba, V. Le Dantec, Z. Rafi, M. Zribi, and P.-L. Frison. “Water stress detection over irrigated wheat crops in semi-arid areas using the diurnal differences of Sentinel-1 backscatter”. In: *2020 Mediterranean and Middle-East Geoscience and Remote Sensing Symposium (M2GARSS)*. IEEE. 2020, pp. 306–309.
- [210] J. Shang, J. Liu, V. Poncos, X. Geng, B. Qian, Q. Chen, T. Dong, D. Macdonald, T. Martin, J. Kovacs, *et al.* “Detection of crop seeding and harvest through analysis of time-series Sentinel-1 interferometric SAR data”. In: *Remote Sensing* 12.10 (2020), p. 1551.
- [211] T. Tampuu, J. Praks, A. Kull, R. Uiboupin, T. Tamm, and K. Voormansik. “Detecting peat extraction related activity with multi-temporal Sentinel-1 InSAR coherence time series”. In: *International Journal of Applied Earth Observation and Geoinformation* 98 (2021), p. 102309.
- [212] A. Villarroya-Carpio, J. M. Lopez-Sanchez, and M. E. Engdahl. “Sentinel-1 interferometric coherence as a vegetation index for agriculture”. In: *Remote Sensing of Environment* 280 (2022), p. 113208.
- [213] T. Nikaein, L. Iannini, R. A. Molijn, and P. Lopez-Dekker. “On the value of sentinel-1 insar coherence time-series for vegetation classification”. In: *Remote Sensing* 13.16 (2021), p. 3300.
- [214] T. Nikaein, P. Lopez-Dekker, S. Steele-Dunne, V. Kumar, and M. Huber. “Modeling SAR Observables with Combining a Crop-Growth Model and a Machine-Learning”. In: *IEEE Journal of Selected Topics in Applied Earth Observations and Remote Sensing* (2023).
- [215] G. Kaplan, L. Fine, V. Lukyanov, V. Manivasagam, J. Tanny, and O. Rozenstein. “Normalizing the local incidence angle in sentinel-1 imagery to improve leaf area index, vegetation height, and crop coefficient estimations”. In: *Land* 10.7 (2021), p. 680.

- [216] D. Small. “Flattening gamma: Radiometric terrain correction for SAR imagery”. In: *IEEE Transactions on Geoscience and Remote Sensing* 49.8 (2011), pp. 3081–3093.
- [217] B. Bauer-Marschallinger, S. Cao, C. Navacchi, V. Freeman, F. Reuß, D. Geudtner, B. Rommen, F. C. Vega, P. Snoeij, E. Attema, *et al.* “The normalised Sentinel-1 Global Backscatter Model, mapping Earth’s land surface with C-band microwaves”. In: *Scientific Data* 8.1 (2021), p. 277.
- [218] C. Navacchi, S. Cao, B. Bauer-Marschallinger, P. Snoeij, D. Small, and W. Wagner. “Utilising Sentinel-1’s Orbital Stability for Efficient Pre-Processing of Radiometric Terrain Corrected Gamma Nought Backscatter”. In: *Sensors* 23.13 (2023), p. 6072.
- [219] S. Modanesi, C. Massari, A. Gruber, H. Lievens, A. Tarpanelli, R. Morbidelli, and G. J. De Lannoy. “Optimizing a backscatter forward operator using Sentinel-1 data over irrigated land”. In: *Hydrology and Earth System Sciences* 25.12 (2021), pp. 6283–6307.
- [220] B. Widhalm, A. Bartsch, and R. Goler. “Simplified normalization of C-band synthetic aperture radar data for terrestrial applications in high latitude environments”. In: *Remote Sensing* 10.4 (2018), p. 551.
- [221] D. Mengen, T. Jagdhuber, A. Balenzano, F. Mattia, H. Vereecken, and C. Montzka. “High Spatial and Temporal Soil Moisture Retrieval in Agricultural Areas Using Multi-Orbit and Vegetation Adapted Sentinel-1 SAR Time Series”. In: *Remote Sensing* 15.9 (2023), p. 2282.
- [222] Amazon. *Amazon Web Services, Inc.* Accessed: 2023-08-04. 2023. URL: <https://aws.amazon.com>.
- [223] NASA-ISRO Synthetic Aperture Radar (NISAR). 2023. URL: <https://nisar.jpl.nasa.gov/>.
- [224] *Radar Observing System for Europe- L-band (ROSE-L)*. 2023. URL: [https://www.esa.int/Applications/Observing\\_the\\_Earth/The\\_Living\\_Planet\\_Programme/Earth\\_Explorers/Future\\_Missions](https://www.esa.int/Applications/Observing_the_Earth/The_Living_Planet_Programme/Earth_Explorers/Future_Missions).
- [225] *Sentinel-1 Next Generation*. 2023. URL: <https://sentinels.copernicus.eu/web/sentinel/missions/sentinel-1>.
- [226] V. Kumar, M. Huber, B. Rommen, and S. C. Steele-Dunne. “Agricultural SandboxNL: A national-scale database of parcel-level processed Sentinel-1 SAR data”. In: *Scientific Data* 9.1 (2022), p. 402.
- [227] *National Aeronautics and Space Administration (NASA)*. 2023. URL: <https://www.nasa.gov/>.
- [228] *Alaska Satellite Facility*. 2023. URL: <https://www.asf.alaska.edu/>.
- [229] *Flemish Institute for Technological Research (VITO)*. 2023. URL: <https://www.vito.be/en>.
- [230] *Planet Labs Inc.* 2023. URL: <https://www.planet.com/>.

- [231] D. A. Robinson, C. S. Campbell, J. W. Hopmans, B. K. Hornbuckle, S. B. Jones, R. Knight, F. Ogden, J. Selker, and O. Wendroth. "Soil moisture measurement for ecological and hydrological watershed-scale observatories: A review". In: *Vadose zone journal* 7.1 (2008), pp. 358–389.
- [232] G. Topp, J. Davis, and A. Annan. "Electromagnetic determination of soil water content: Measurements in coaxial transmission lines: Water Resources Research WRERAQ 0043-1397, 16, 574–582". In: *Crossref Web of Science* (1980).
- [233] I. Paltineanu and J. Starr. "Real-time soil water dynamics using multisensor capacitance probes: Laboratory calibration". In: *Soil Science Society of America Journal* 61.6 (1997), pp. 1576–1585.
- [234] C. Allen and F. Ulaby. "Characterization of the microwave extinction properties of vegetation canopies". In: *Radiation Laboratory, Dept. of Electrical Engineering and Computer Science, The University of Michigan, Ann Arbor, MI 48109* (1984).
- [235] G. P. De Loor, P. Hoogeboom, and E. W. Attema. "The dutch ROVE program". In: *IEEE Transactions on Geoscience and Remote Sensing* 1 (1982), pp. 3–11.
- [236] P. E. O'Neill, R. H. Lang, M. Kurum, C. Utku, and K. R. Carver. "Multi-Sensor microwave soil moisture remote sensing: NASA's Combined Radar/Radiometer (ComRAD) system". In: *2006 IEEE MicroRad*. IEEE. 2006, pp. 50–54.
- [237] N. M. Holtzman, L. D. Anderegg, S. Kraatz, A. Mavrovic, O. Sonnentag, C. Pappas, M. H. Cosh, A. Langlois, T. Lakhankar, D. Tesser, *et al.* "L-band vegetation optical depth as an indicator of plant water potential in a temperate deciduous forest stand". In: *Biogeosciences* 18.2 (2021), pp. 739–753.
- [238] M. J. Escorihuela, Y. H. Kerr, P. De Rosnay, K. Saleh, J.-P. Wigneron, and J. C. Calvet. "Effects of dew on the radiometric signal of a grass field at L-band". In: *IEEE Geoscience and Remote Sensing Letters* 6.1 (2008), pp. 67–71.
- [239] T. L. Rowlandson, B. K. Hornbuckle, L. M. Bramer, J. C. Patton, and S. D. Logsdon. "Comparisons of evening and morning SMOS passes over the Midwest United States". In: *IEEE transactions on geoscience and remote sensing* 50.5 (2012), pp. 1544–1555.
- [240] M. Schneebeli, S. Wolf, N. Kunert, W. Eugster, and C. Mätzler. "Relating the X-band opacity of a tropical tree canopy to sapflow, rain interception and dew formation". In: *Remote sensing of environment* 115.8 (2011), pp. 2116–2125.
- [241] P. Vermunt *et al.* "Reconstructing Diurnal Cycles of Vegetation Water Content To Understand Subdaily Patterns In Radar Backscatter". In: *In prep* (2021).

# A

## APPENDIX-A: THE IMPORTANCE OF OVERPASS TIME IN AGRICULTURAL APPLICATIONS OF RADAR

*Chapter 4 illustrates that the presence of SCW can significantly affect radar backscatter and the retrieval of crop biophysical variables. Most current and future SAR missions have sun-synchronized orbits, implying they have dawn/dusk overpasses or multiple overpasses per day. Since the probability of SCW is much higher before dawn than later in the morning, this chapter investigates the effect of diurnal variation in internal and surface canopy water on L-band backscatter, with regard to the influence of overpass time on agricultural applications. The findings underscore the importance of taking overpass timing into account for agricultural monitoring, whether when selecting times for a single mission, integrating data from multiple missions, or planning acquisition times for future missions.*

---

This chapter is based on:

Khabbazan, Saeed et al., "The Importance of Overpass Time in Agricultural Applications of Radar."  
2021 IEEE International Geoscience and Remote Sensing Symposium IGARSS. IEEE, 2021.[194]



## A.1. INTRODUCTION

Several studies have used sun-synchronized satellite data (ascending and descending observation) to demonstrate the capability of radar data to detect diurnal variation in internal vegetation water content[32, 34]. They reported differences between evening and morning observations that were attributed to a change in internal vegetation water content. In addition, several studies have demonstrated that the presence of surface canopy water increases the radar backscatter[66–68, 75, 76, 79, 81–83].

However, the limited radar datasets (using ascending and descending overpass) in previous studies leave open questions in terms of sub-daily pattern in backscatter and the sensitivity of backscatter to both variation in surface and internal water content. Moreover, the limited ground validation datasets on surface canopy water limit quantitative analysis. The main goal of this study is to investigate the possible influence of overpass time on backscatter variations due to surface canopy water, and its effect on the retrieval of biophysical parameters.

## A.2. DATA AND METHODS

### A.2.1. STUDY AREA

The study was conducted at UF/IFAS Extension Plant Science Research and Education Unit (PRSEU), Citra, Florida, USA. Sweet corn (*Zea mays* L. var. *rugosa*) was planted with an average density of 7.9 plants  $m^{-2}$  on 13 April 2018 and harvested on 18 June 2018. The corn field was around 250 m by 150 m and the soil consisted of >90% by volume fine sand. The study area has a humid subtropical climate and midnight irrigation was necessary at the beginning of the season to control the soil moisture content.

### A.2.2. HYDROMETEOROLOGY

Meteorological data were obtained from the Florida Automated Weather Network (FAWN) weather station located 600 m east of the corn field. Rainfall, relative humidity, temperature, solar radiation, and wind speed were obtained every 15 minutes. The presence and duration of surface canopy water (SCW) were monitored using three Phytos31 dielectric leaf wetness sensors. These sensors were installed at different heights in the canopy and the heights of the sensors were adjusted as the corn grew. Surface canopy water was classified as precipitation, irrigation or dew using the precipitation and irrigation data. Soil moisture was observed every 15 minutes at 5, 10, 20, 40, and 80 cm depth in two pits near the radar footprint. A site calibration was applied and the average of two locations is presented here. Vegetation water content (VWC) and dry biomass were measured by predawn destructive vegetation sampling every 2-3 days. More details on hydrometeorology and vegetation sampling during this experiment can be found in Vermunt et al. [119].

### A.2.3. MICROWAVE SCATTERING SYSTEM

The University of Florida L-band Automated Radar System (UF-LARS) was used to acquire radar backscatter ( $\sigma^0$ ). The system operates at a central frequency of 1.25 GHz and has a dual-polarization horn antenna, which allows us to acquire data at four polarization combinations (VV, HH, VH, and HV) simultaneously. The UF-LARS was installed on a Genie platform and scanned the corn field with an antenna height of 14 meters and a fixed elevation angle of 40°. The ground range and azimuth resolution were measured using 3dB antenna beamwidth and are provided in Table A.1 and a full description of the system can be found in [106]. The UF-LARS system was programmed automatically to acquire 32 measurements per day during the growing season and the internal calibration was applied during each acquisition [119]. The external calibration was conducted using a trihedral corner reflector several times during the growing season. The Single Target Calibration Technique (STCT) was used to calculate backscatter coefficient  $\sigma^0$  from the received signal and the total systematic and random error were estimated as 1.49 and 0.85 dB respectively.

Table A.1.: UF-LARS specifications

Parameter		UF-LARS
Range resolution (m)	HH / VV / cross-pol	8.5 / 6.2 / 6.2
Azimuth resolution (m)	HH / VV / cross-pol	4.7 / 6.4 / 4.7

## A.3. RESULTS

### A.3.1. METEOROLOGICAL DATA

The first three weeks of the season were dry and warm. Therefore midnight irrigation was applied on 8 occasions to control soil moisture content. The resultant rapid increase in 5 and 10 cm soil moisture after irrigation can be seen in Fig. A.1. Three heavy rain events on 21, 27 and 30 May led to sharp increases in root zone soil moisture content Fig. A.1. A dry period with few rain events and high humidity between June 1 and June 10 resulted in a rapid decrease in soil moisture at all depths. The mid-season was frequently rainy with very high humidity, which resulted in the presence of water on the canopy surface for long periods during the day. Fig. A.2 illustrates that the SCW (dew/interception) was present on most days from midnight until around 10 am. In terms of overpass times note, for example, that SCW was present on 95% of days at 6 am and just 25% of days at 6 pm.

### A.3.2. FACTORS INFLUENCING L-BAND BACKSCATTER

Fig. A.3 (a-c) shows that there are slow changes in radar backscatter due to crop growth, and more rapid changes associated with vegetation water dynamics. The increasing trend in all polarizations is due to crop growth, as this time series is during the leaf development growth stage [119, 120]. The daily cycles superimposed

A

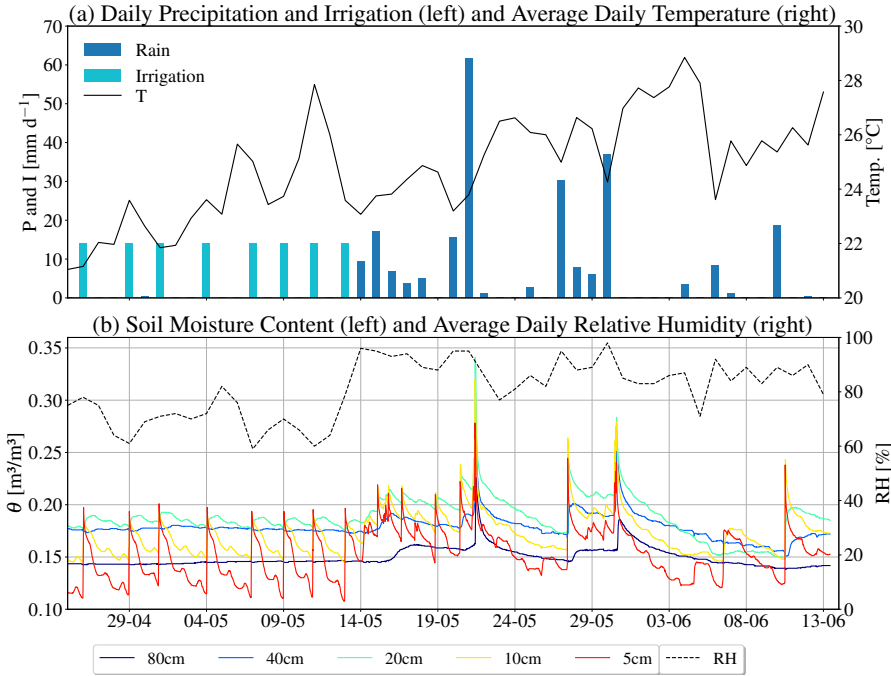


Figure A.1.: Time series of meteorological data collected by FAWN and averaged volumetric soil moisture from two pits on different depth

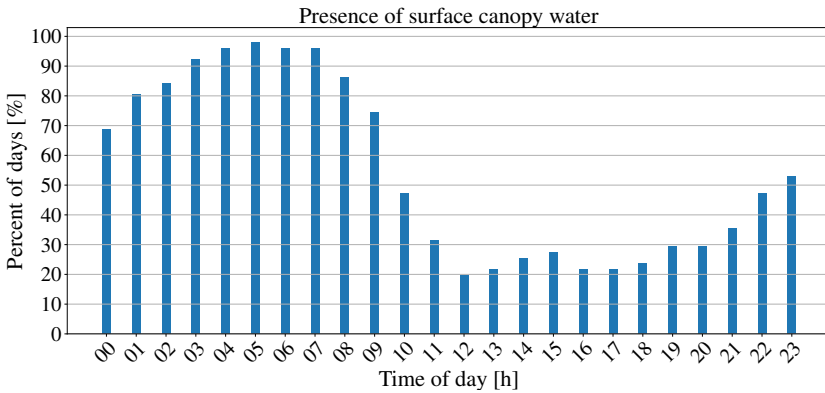


Figure A.2.: The percent of days that surface canopy water was presented at each hour of the day

on this upward trend are due to dynamics in surface and internal water content and soil moisture. Fig. A.3 (d) shows the soil moisture and surface canopy water variations during this time. Interception of irrigation events at midnight on May 7, 9

and 11 led to rapid increase in surface soil moisture. In addition, dew accumulation leads to an increase in backscatter during the night.

The backscatter data in Fig. A.3 have been colored to indicate if the observations were acquired in the presence of dew and/or interception. This illustrates that the sharp increase in interception and soil moisture following irrigation can result in an increase of more than 5 dB in VV and VH. Results are less convincing in HH due to noise in the observations. During the night, the decrease in backscatter due to soil moisture is inhibited by the presence of interception and the accumulation of dew.

On nights without irrigation, the accumulation of dew from midnight until sunrise led to a gradual increase in backscatter of up to 2-3 dB, even though soil moisture was decreasing. Dew and interception dissipate rapidly after sunrise, so the backscatter variations (highlighted in black) are due to variations in internal water content and surface soil moisture. As the daily radiation cycle drives evapotranspiration, the backscatter in all polarization is found to decrease from 10 am to a minimum in the late afternoon in response to moisture losses.

### A.3.3. DIURNAL CYCLES OF WATER CONTENT AND BACKSCATTER

The clear daily cycle in radar backscatter in response to accumulation and dissipation of dew and variations in internal water content (VWC) can be seen in Fig. A.4. These data were collected during the flowering and fruit development stages [120], so the corn has reached maximum biomass and L-band backscatter is dominated by the vegetation contribution [119]. [119] Continuous internal canopy water content were estimated using a water balance approach combining sparse destructive sampling with continuous records of evapotranspiration and sap flow [241]. The diurnal change in VWC is around  $0.38 \text{ kg m}^{-2}$  which is about 9.1 % of total VWC, and is comparable in magnitude to the variation in SCW. The range of the mean daily cycle in backscatter at this time is 1.64, 2.43, and 1.96 dB in HH, VV and cross-pol respectively. The maximum value is observed at the acquisition of 7:30 am in VV and cross-pol, and the minimum occurs in the late afternoon in all polarizations when the VWC reaches its minimum value.

### A.3.4. IMPACT OF SCW ON L-BAND BACKSCATTER

Fig. A.5 provides insight into the quantitative change in backscatter due to surface canopy water. The  $\Delta\sigma$  indicates the difference in backscatter between 6 am, when the vegetation is covered in dew (red) or dew and interception (yellow) and 9 am when the dew/interception has dissipated. Internal water content is mostly constant during this period as the presence of SCW suppresses transpiration, and the difference in soil moisture,  $\Delta\theta$ , is negligible ( $< 0.01 \text{ m}^3/\text{m}^3$ ). Therefore, any difference in backscatter can be attributed to surface canopy water content. The presence of SCW generally leads to an increase in backscatter, so  $\Delta\sigma$  is generally positive. The average value of  $\Delta\sigma$  is 1.02 dB for co-pol and 1.27 dB for cross-pol but can reach up to 3-4 dB. This is consistent with values observed in other studies [79]. Considerable variability is observed due to variability in SCW, as well as variation in the relative contribution of vegetation to total backscatter during the growing season. The

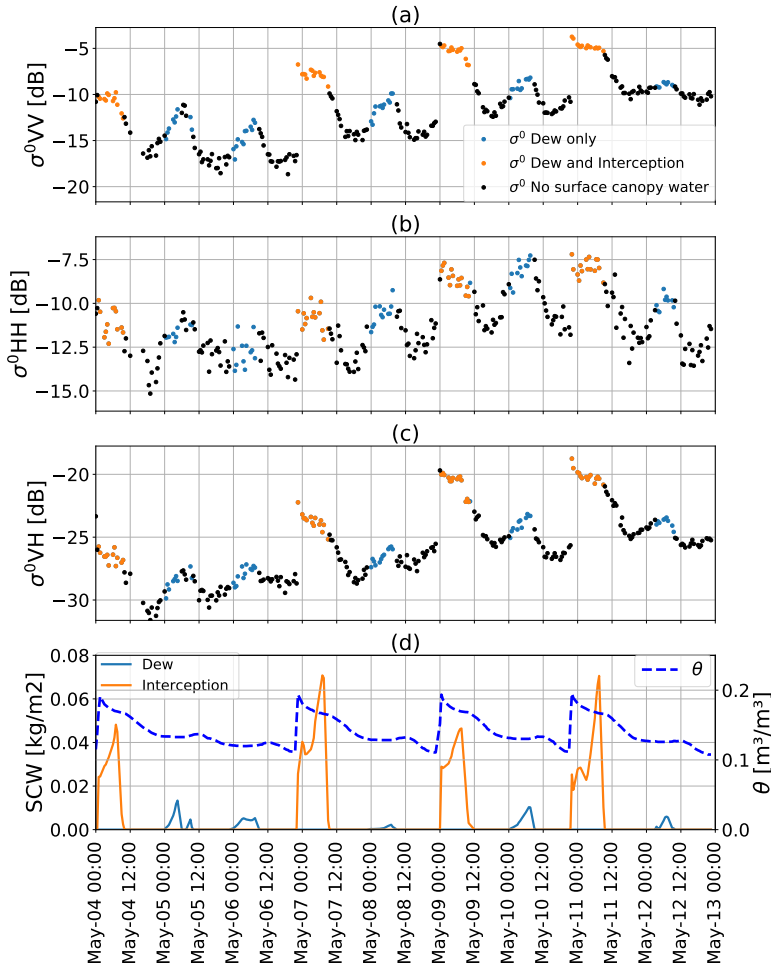


Figure A.3.: Time series of co- and cross-polarized backscatter divided to three situations based on presence and absent of SCW (three upper rows), soil moisture profile at 5 cm, and SCW (dew/interception) content (lower row) for 9 days during the early season

decreasing trend in  $\Delta\sigma$  from May 23 to June 1 is due to a decreasing trend in 6 am SCW. The amount of SCW on 23, 26, 28 and 31 May was 0.6, 0.31, 0.2, and 0.058  $kg\ m^{-2}$  respectively.

### A.3.5. EFFECT OF SURFACE CANOPY WATER ON RELATIONSHIP BETWEEN BACKSCATTER AND BIOPHYSICAL VARIABLES

Given that the probability of SCW is much higher before dawn than later in the morning (Fig. A.2), and that the presence of SCW influences backscatter (Fig. A.3), it

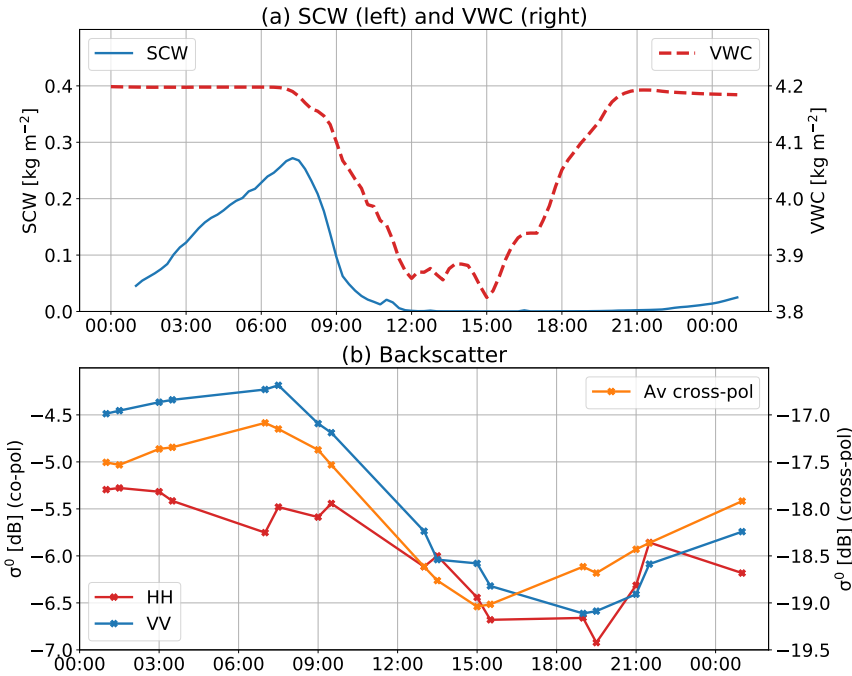


Figure A.4.: Mean daily cycle of (a) surface canopy water (dew) and modeled VWC and (b) co- and cross-polarized backscatter for just 3 days without precipitation between June 2 and June 13.

is hypothesized that acquisition time is an important consideration for the retrieval of biophysical parameters in agricultural monitoring. Fig. A.6 shows the relationship between backscatter and three biophysical variables. Blue points correspond to data collected at 6 am, while red points correspond to the first backscatter data collected after dew had dissipated (generally between 10 am and 12 pm). Note that the Spearman correlation coefficient is always higher (up to 0.33) when the radar data are collected in the absence of SCW. The relationship between radar data and the biophysical variable of interest depends on whether or not SCW was present. Among the crop biophysical variables, the impact of SCW is greatest in LAI. Among the polarizations, HH is least influenced by SCW. Therefore, the presence of surface canopy water has a confounding effect on the retrieval of biophysical variables. For the retrieval of VWC, dry biomass and LAI, acquisitions in the late morning are more strongly correlated with the biophysical variables. The difference in variability is likely due to the varying amount of dew and its influence on backscatter.

### A.4. CONCLUSION

Surface canopy water and internal VWC have daily cycles that are driven by local hydrometeorological conditions and root zone soil moisture availability. Backscatter

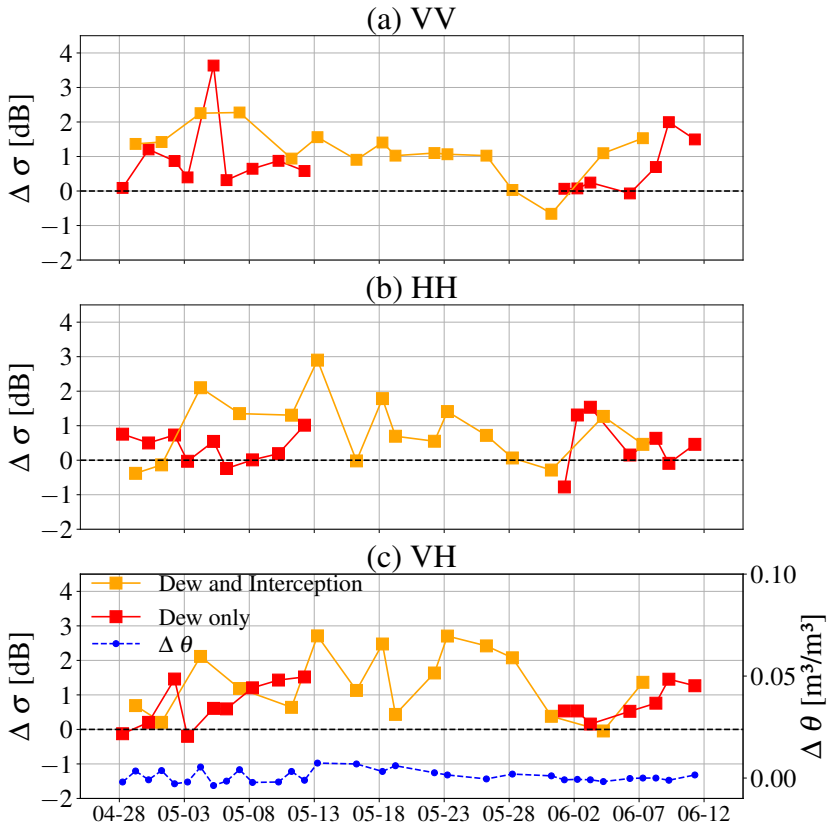


Figure A.5.: Time series of difference in radar backscatter between wet and dry vegetation for (a) VV, (b) HH, and (c) VH polarization. Difference was computed by using radar data at 6 am (wet vegetation) and first radar data after 9 am when the surface of canopy was dry (dry vegetation). The blue dashed line shows the difference in surface soil moisture value between wet and dry vegetation.

in all polarizations is highly affected by these daily cycles. In the morning, L-band radar backscatter observations in the presence of dew are 2-3 dB higher than those made when the dew has dissipated and the internal water dynamics in fully grown corn can change a radar backscatter around 2 dB. The parameters of the relationship between backscatter and biophysical variables of interest are different for dry and wet vegetation and the correlation coefficient between radar data and plant parameters is up to 0.33 higher in the absence of dew. Choice of overpass time affects the probability of dew, and the strength of the relationship between backscatter and biophysical variables in agricultural monitoring. This should be taken into account in any vegetation applications when combining overpass times for a single mission, combining overpasses from multiple missions or selecting an

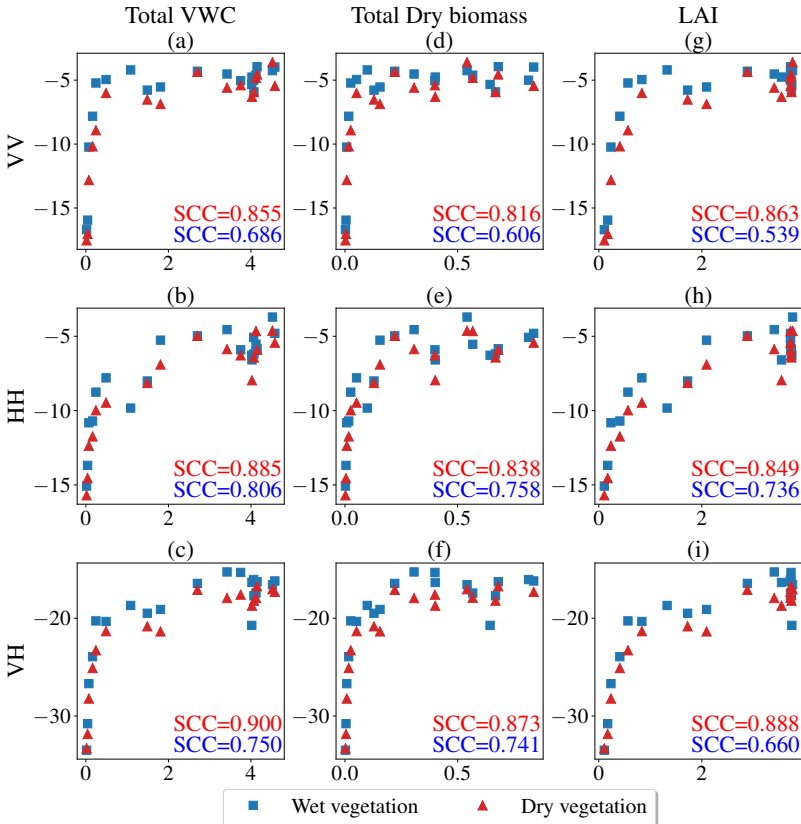


Figure A.6.: The relationship between radar backscatter and measured total VWC, total dry biomass and LAI in the presence (red) or absence (blue) of surface canopy water. The corresponding Spearman Correlation Coefficients (SCC) are in the lower right corner.

acquisition time for future missions.



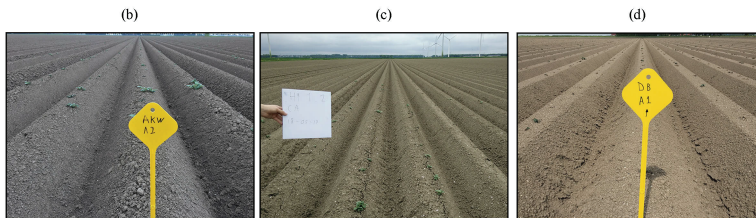
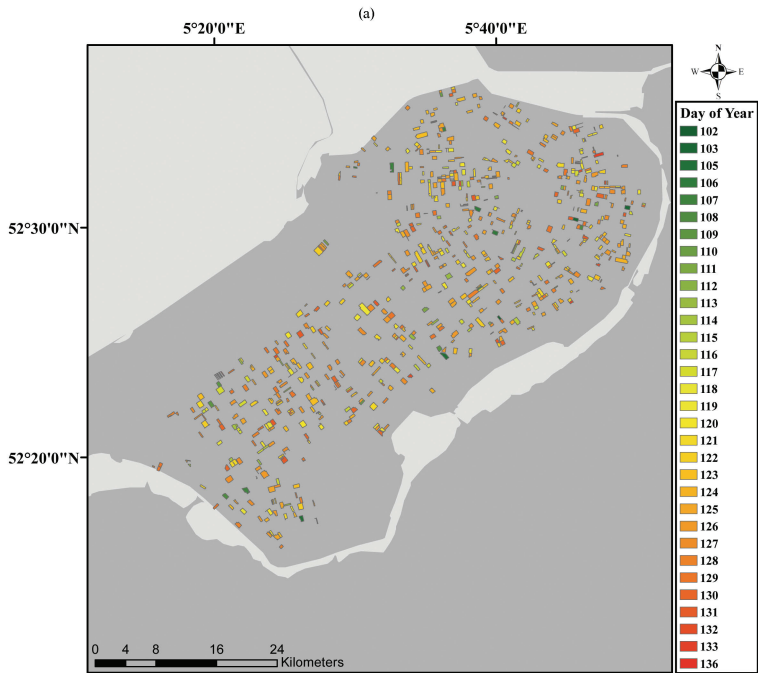


# B

## APPENDIX-B: SUPPLEMENTARY MATERIAL

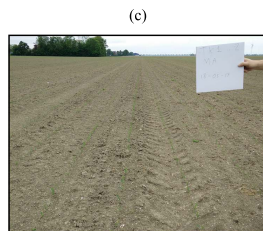
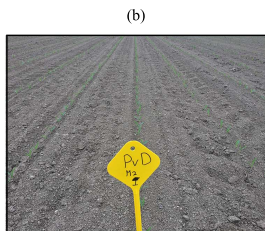
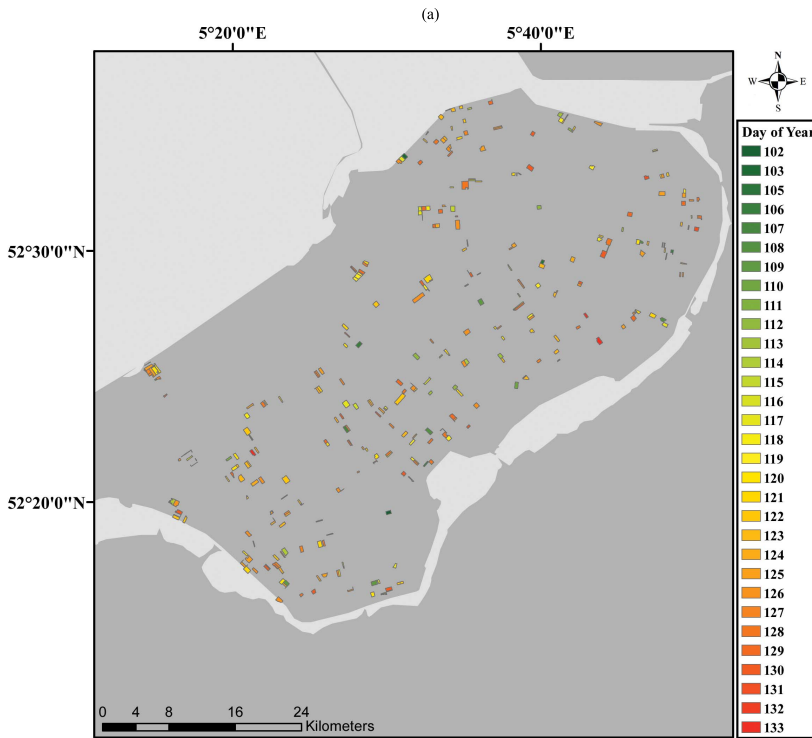
## B.1. SUPPLEMENTARY MATERIAL FOR CHAPTER 3

B



Field Name:	AKW	HF	DB
Photo Date:	18/5/2017	18/5/2017	17/5/2017
Estimated Date:	4/5/2017	5/5/2017	7/5/2017

Figure B.1.: Estimated emergence date for potato parcels in Flevopolder; (a) Map of emergence date; (b-e) Photos from monitored parcels in the closest time to emergence date.



<b>Field Name:</b>	PVD	TK1
<b>Photo Date:</b>	18/05/2017	18/05/2017
<b>Estimated Date:</b>	14/05/2017	14/05/2017

Figure B.2.: Estimated emergence date for maize parcels in Flevopolder; (a) Map of emergence date; (b-c) Photos from monitored parcels in the closest time to emergence date.

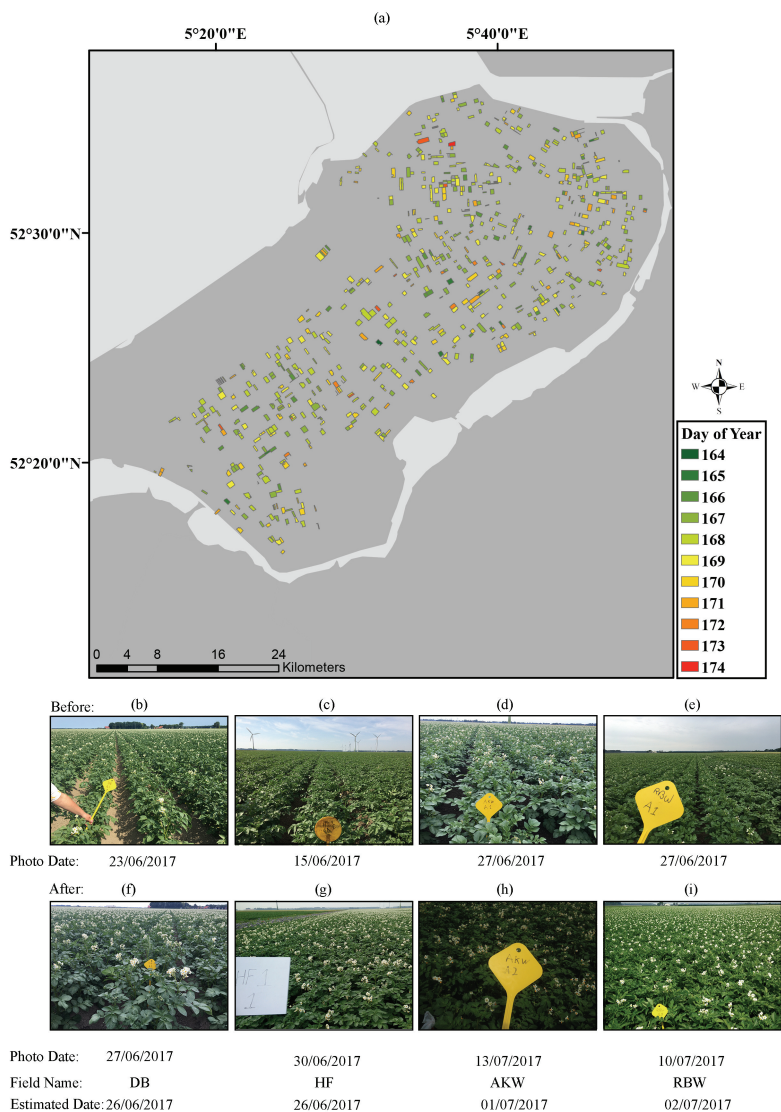


Figure B.3.: Estimated closure date for potato parcels in Flevopolder; (a) Map of closure date; (b-e) Photos from monitored parcels in the closest time before closure date; (f-i) Photos from monitored parcels in the closest time after closure date.

## **B.2. SUPPLEMENTARY MATERIAL FOR CHAPTER 5**

B

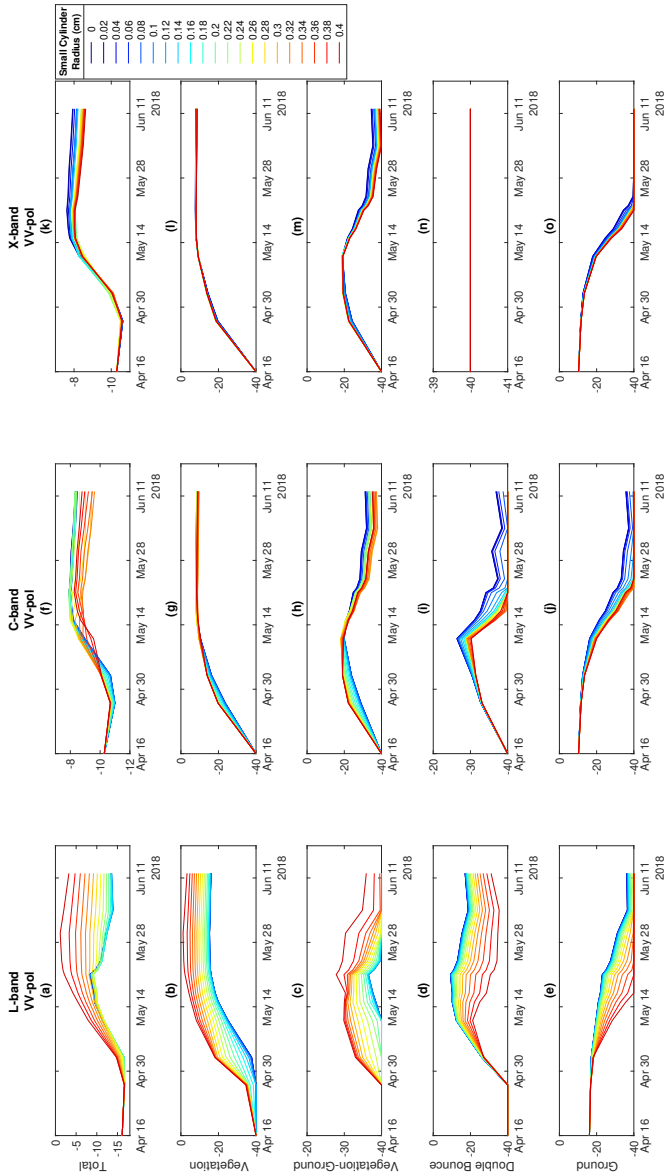
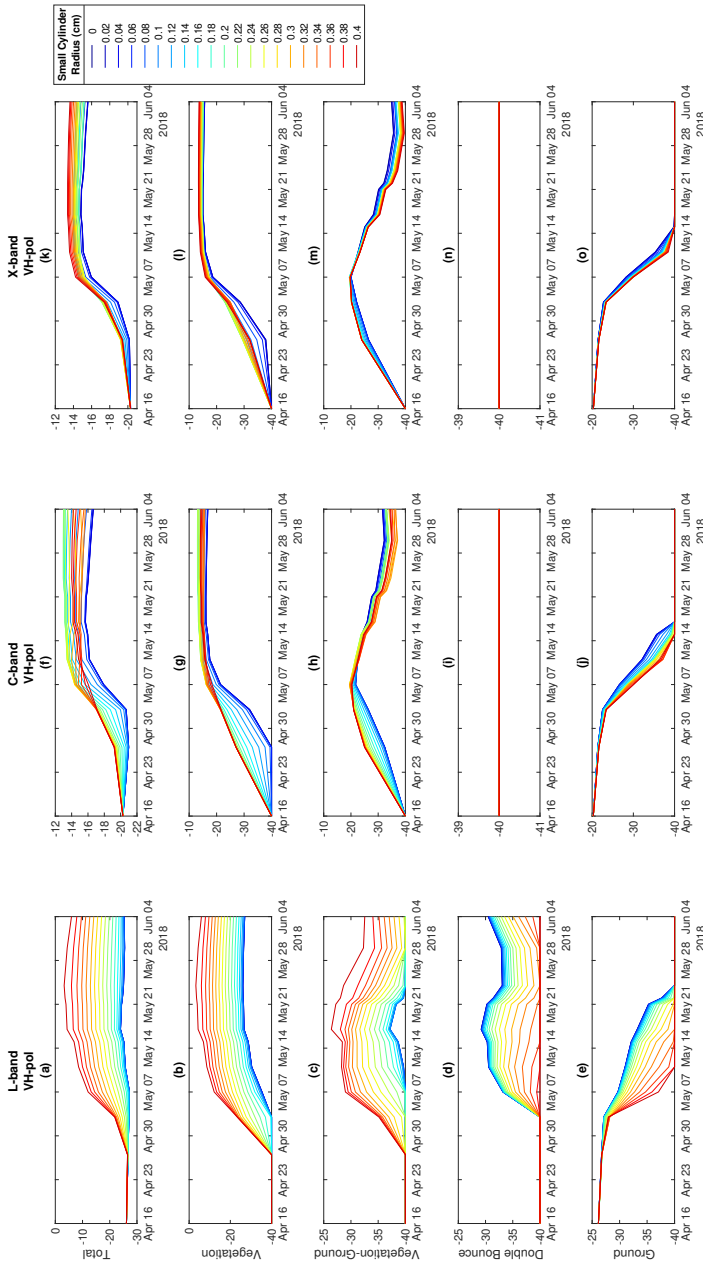


Figure B.4.: Time series of all scattering mechanisms for RT model simulations using different small cylinder radius (SCR) sizes for VV pol in L-band(left column), C-band (middle column), and X-band (right column) for whole growing season of a corn. Each colored line shows simulation using one SCR. Dark blue corresponds to the smallest SCR and dark red corresponds to the largest SCR. SCR was chosen from 0 to 0.4 cm by an interval of 0.02 cm.



B

Figure B.5.: Time series of all scattering mechanisms for RT model simulations using different small cylinder radius (SCR) sizes for XP pol in L-band(left column), C-band (middle column), and X-band (right column) for whole growing season of a corn. Each colored line shows simulation using one SCR. Dark blue corresponds to the smallest SCR and dark red corresponds to the smallest SCR. SCR was chosen from 0 to 0.4 cm by an interval of 0.02 cm.



**B.3. SUPPLEMENTARY MATERIAL FOR CHAPTER 6**

B

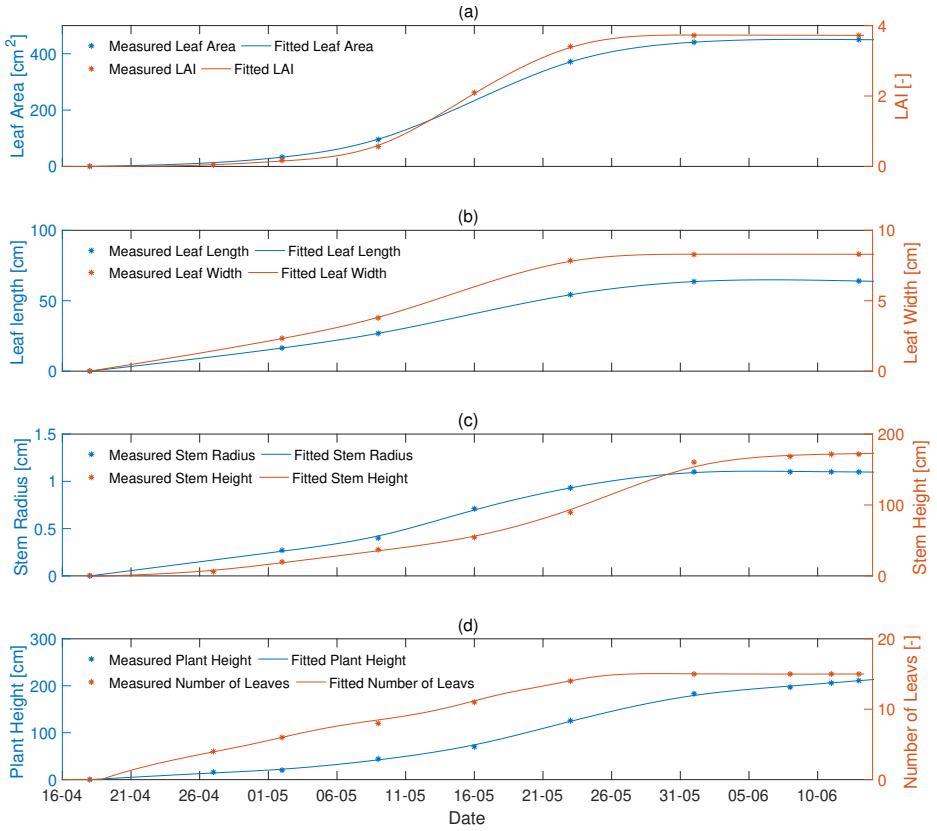


Figure B.6.: Measured data (stars) and fitted relationships (blue and orange curves) for vegetation descriptors.

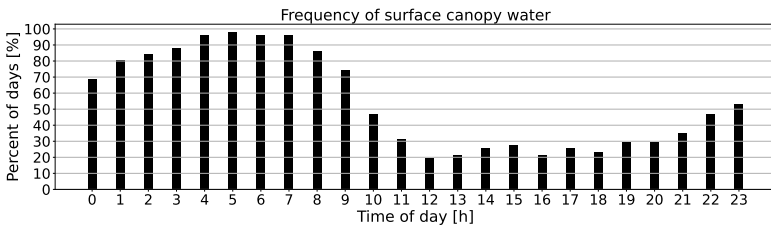


Figure B.7.: The percentage of days on which SCW was present for each hour of the day.

# ACKNOWLEDGEMENTS

At this important point in my academic journey, I take a moment to reflect on the incredible journey that has led me here, filled with gratitude for those who supported, inspired, and believed in me.

I would like to express my heartfelt gratitude to my supervisor, Prof. Susan Steele-Dunne, for her unwavering support and encouragement throughout my PhD journey. Your profound insights into the nature of research have consistently inspired me, and our discussions on SAR remote sensing of agriculture have sparked numerous research ideas. Your expertise in physical modeling and fieldwork experiments has been invaluable, providing a concrete foundation on which I could construct my research. More than that, you have nurtured my scientific thinking, helping me to understand not only the 'how' but also the 'why' of our inquiries. This has been instrumental in guiding me during these years, giving me the tools to approach research with a critical and discerning eye. Your mentorship went beyond academia. You helped shape me as a person, setting a high standard for hard work, honesty, and love of discovery. I can't thank you enough for believing in me and supporting me every step of the way.

I am also indebted to my co-promotor, Dr. Paco Lopez-Dekker, for his invaluable counsel and wisdom, especially when it came to addressing issues with our scatterometer system.

I owe a special debt of gratitude to my PhD colleague, Dr. Paul Vermunt, with whom I collaborated on our shared project and conducted extensive field campaigns. Paul, I deeply admire your dedication during our fieldwork and cherish the memories of our challenging yet rewarding experiences together. Through our joint efforts, we conducted groundbreaking fieldworks. Thank you for your support and guidance throughout my journey.

I am also very grateful to Prof. Jasmeet Judge from the University of Florida for dedicating significant time, offering her expertise during our field campaign in Florida, and providing constructive feedback for our papers. I would like to express my appreciation to Patrick Rush, Daniel Preston, and Eduardo Carrascal for their technical expertise during the fieldwork in Florida. Without their support, particularly with the L-band data from the UF-LARS system, this research would not have been possible. Many thanks to everyone at the UF Center for Remote Sensing.

My thanks go to Professor Leila Gurriero for granting access to the Tor Vergata model and guiding its utilization and further development. I would also like to thank Dr. Mariette Vreugdenhil for her insights into VOD modeling. The knowledge and support from both of you paved the way for me and helped me conduct the modeling analysis.

I would like to thank Xu Shan, Lexy Ratering Arntz, Caterina Marinetti, Karin

Bremer, Ge Gao, and Xuemeng Tian for their collaboration during our fieldwork in the Netherlands. I also extend my thanks to Jacob van den Borne, Paul van Zoggel, Dieter Bergez and everyone on their team, who offered unconditional technical assistance during our fieldwork in the Netherlands.

Dr. Vineet Kumar, I am thankful for the insights you shared during our fieldwork in the Netherlands and our enlightening discussions throughout my PhD journey.

I would like to extend my heartfelt appreciation to Dr. Nadja Den Besten, a remarkable friend and colleague. As a former student of my supervisor, our paths have crossed both academically and professionally. From engaging discussions to shared conference experiences, our collaboration has been both enriching and inspiring. Her expertise has extended beyond our academic pursuits, as she graciously took on the role of translating my summaries into Dutch, reflecting her dedication and proficiency. Nadja's friendship and support have been invaluable to me, and I cherish the good times we have shared.

To my dear friends Bahareh Kianfar, Elaheh Jamalinia, Yang Lu, Saeed Mahmoudi Motlagh and Ali Haseltalab at TU Delft, I express my gratitude for the joyful moments we have shared over the past years.

I am truly grateful to the secretary team of the GRS group for their unconditional support during the final steps of my PhD. They provided me with a very pleasant space to finish my thesis. They helped me at a critical time when my backpack was stolen, particularly providing me with a laptop to enable me to finish my journey. I sincerely appreciate your kindness and support.

I would like to convey my heartfelt appreciation to the members of the examination board for their time, effort, and insightful feedback on my research, as well as their meticulous evaluation of this thesis.

Last but not least, my heart swells with eternal gratitude and love for my beloved family, the unwavering backbone of my life and this academic journey. Your constant love, encouragement, understanding, and sacrifice have been the pillars of my strength, shaping me into the person and researcher I have become.

To my parents, whose selfless love, enduring faith, and nurturing guidance have molded me, I extend my deepest appreciation. Your lessons and values resonate in everything I do, and your pride in me has been a motivating force that propelled me forward. To my brother, my comrade in life, your support and friendship mean more than words can express. Your belief in me and the shared memories have been a source of joy and inspiration.

And to Sepideh, the love of my life and my best friend, words fall short to convey the depth of my gratitude. Your unwavering support, profound love, patience, and trust have been my greatest source of strength. Through every triumph and trial, your presence has been a constant, your encouragement a soothing balm, and your faith in me a guiding star. Your sacrifices, wisdom, and kindness not only supported my academic pursuits but enriched my life in immeasurable ways. You are not only my partner in life but in all the dreams and successes we share. Your love is the heartbeat of my life, and I am forever thankful for you.

*Saeed  
Delft, June 2023*

# CURRICULUM VITÆ

## Saeed Khabbazan

1989/07/05 Born in Mashhad, Iran

### EDUCATION

2017 - 2023 Ph.D. in Geoscience and Remote Sensing

Delft University of Technology, the Netherlands

Thesis: Quantifying and modeling the effect of external and internal vegetation water dynamics on radar data

promotor: Prof. dr. ir. Susan C. Steele-Dunne

co-promotor: dr. ir. Paco F. Lopez Dekker 2011 - 2014 M.Sc. in Remote Sensing  
University of Tehran, Iran

Thesis: Soil moisture estimation over bare soil agricultural fields using active microwave remote sensing data

Supervisor: Dr. Mahdi Motagh 2007 - 2011 B.Sc. in Geodesy and Geomatics  
Engineering

University of Tabriz, Iran

### AWARDS

2016 National Talents award from Iran's National Elites Foundation

2014 Top student award in M.Sc. program of Remote Sensing Engineering at  
University of Tehran, Iran

2011 Full M.Sc. degree Scholarship at University of KNT (Khaje Nasir Toosi), Iran

### CONFERENCES AND ORAL PRESENTATIONS

**Saeed Khabbazan**, Susan Steele-Dunne, Paul Vermunt, Mariette Vreugdenhil, Jasmeet Judge. "The Importance of Surface Canopy Water on Agricultural Monitoring using SAR". In European Space Agency (ESA) Living planet symposium, Bone, Germany, 23-27 May 2022.

**Saeed Khabbazan**, Paul Vermunt, Susan Steele-Dunne, Jasmeet Judge. "Investigating the Effect of Surface Canopy Water on Agricultural Monitoring using Fully Polarimetric L-band backscatter". In XXXIVth General Assembly and Scientific Symposium of the International Union of Radio Science (URSI GASS), IEEE, 2021.

**Saeed Khabbazan**, Paul Vermunt, Susan Steele-Dunne, Jasmeet Judge. "The Importance of Overpass Time in Agricultural Applications of Radar". IEEE International Geoscience and Remote Sensing Symposium IGARSS, 2021.

**Saeed Khabbazan**, Paul C Vermunt, Susan C. Steele-Dunne, Ge Gao, Mariette Vreugdenhil, Jasmeet Judge. "Inferring the effects of surface canopy water on VOD estimation from L-band backscatter". EGU General Assembly Conference, Vienna, Austria, 2021.

**Saeed Khabbazan**, Ge Gao, Paul Vermunt, Susan Steele-Dunne, Jasmeet Judge, and Mariette Vreugdenhil. "Interpreting Vegetation Optical Depth (VOD) using detailed destructive vegetation sampling of a corn canopy." EGU General Assembly Conference, Vienna, Austria, 2020.

**Saeed Khabbazan**, Paul Vermunt, Susan Steele-Dunne, Lorenzo Iannini, Dirk van der Valk, Kees Westerdijk, and Corn e van der Sande. "Using Sentinel-1 time series for monitoring crop phenology in the Netherlands"; European Space Agency (ESA) Living planet symposium, Milan, Italy, 13-17 May 2019.

Susan C. Steele-Dunne, **Saeed Khabbazan**, Paul C. Vermunt, Lexy Ratering Arntz, Caterina Marinetti, Lorenzo Iannini, Kees Westerdijk, and Corné van der Sande. "Monitoring Key Agricultural CROPS in the Netherlands using Sentinel-1." IEEE International Geoscience and Remote Sensing Symposium IGARSS, 2018.

**Saeed Khabbazan**, Mahdi Motagh, and Mehdi Hosseini. "Evaluation of Radar Backscattering Models IEM, OH, and Dubois using L and C-Bands SAR Data over different vegetation canopy covers and soil depths." Int. Arch. Photogramm. Remote Sens., 2013.

# LIST OF PUBLICATIONS

7. **Saeed Khabbazan**, Susan C. Steele-Dunne, Paul C Vermunt, Leila Guerriero, Jasmeet Judge, 2023. "The Influence of Surface Canopy Water on L, C and X-bands Backscatter: A study combining detailed in-situ data and the Tor Vergata Radiative Transfer Model". Science of Remote Sensing, in review.
6. **Saeed Khabbazan**, Susan C. Steele-Dunne, Paul C Vermunt, Jasmeet Judge, Mariette Vreugdenhil, and Ge Gao, 2021. "The influence of surface canopy water on the relationship between L-band backscatter and biophysical variables in agricultural monitoring". Remote Sensing of Environment, 268, p.112789
5. **Saeed Khabbazan**, Paul Vermunt, Susan Steele-Dunne, Lexy Ratering Arntz, Caterina Marinetti, Dirk van der Valk, Lorenzo Iannini, Ramses Molijn, Kees Westerdijk, and Corne van der Sande. "Crop monitoring using sentinel-1 data: a case study from the Netherlands". Remote Sensing, 11(16):1887, 2019
4. Paul C Vermunt, Susan C. Steele-Dunne, **Saeed Khabbazan**, Vineet Kumar, and Jasmeet Judge, 2022. "Towards Understanding the Influence of Vertical Water Distribution on Radar Backscatter from Vegetation Using a Multi-Layer Water Cloud Model." 2022, Remote Sensing 14, no. 16 (2022): 3867.
3. Paul C Vermunt, Susan C. Steele-Dunne, **Saeed Khabbazan**, Nick van de Giesen, and Jasmeet Judge. "Reconstructing Continuous Vegetation Water Content To Understand Sub-daily Backscatter Variations". Hydrology and Earth System Sciences Discussions, 2021, pp.1-26
2. Paul C Vermunt, **Saeed Khabbazan**, Susan C. Steele-Dunne, Jasmeet Judge, Alejandro Monsivais-Huertero, Leila Guerriero, and Pang-Wei Liu. "Response of Subdaily L-Band Backscatter to Internal and Surface Canopy Water Dynamics." IEEE Transactions on Geoscience and Remote Sensing 2020
1. **Saeed Khabbazan**, Mehdi Hosseini, Mohammad Reza Saradjian, Mahdi Motagh, and Ramata Magagi. "Accuracy Assessment of IWCM Soil Moisture Estimation Model in Different Frequency and Polarization Bands." Journal of the Indian Society of Remote Sensing 43, no. 4 2015

